

Role of oxidative stress in the pathogenesis of triple A syndrome and familial glucocorticoid deficiency

Prasad, Rathi

The copyright of this thesis rests with the author and no quotation from it or information derived from it may be published without the prior written consent of the author

For additional information about this publication click this link.

<http://qmro.qmul.ac.uk/jspui/handle/123456789/8850>

Information about this research object was correct at the time of download; we occasionally make corrections to records, please therefore check the published record when citing. For more information contact scholarlycommunications@qmul.ac.uk

**Role of oxidative stress in the pathogenesis of triple A syndrome and familial glucocorticoid
deficiency**

Dr Rathi Prasad

BSc, MBBS, MRCPCH

Submitted in partial fulfillment of the requirements of the Degree of Doctor of Philosophy

Centre for Endocrinology

William Harvey Research Institute

Barts and the London School of Medicine and Dentistry

Queen Mary University of London

Statement of Originality


I, Rathi Prasad, confirm that the research included within this thesis is my own work or that where it has been carried out in collaboration with, or supported by others, that this is duly acknowledged below and my contribution indicated. Previously published material is also acknowledged below.

I attest that I have exercised reasonable care to ensure that the work is original, and does not to the best of my knowledge break any UK law, infringe any third party's copyright or other Intellectual Property Right, or contain any confidential material.

I accept that the College has the right to use plagiarism detection software to check the electronic version of the thesis.

I confirm that this thesis has not been previously submitted for the award of a degree by this or any other university.

The copyright of this thesis rests with the author and no quotation from it or information derived from it may be published without the prior written consent of the author.

Signature: 

Date: 15/09/2014

Publications arising from this thesis

Prasad R., Metherell L.A., Clark A.J., Storr H.L. (2013) Deficiency of ALADIN impairs redox homeostasis in adrenal cells and inhibits steroidogenesis. *Endocrinology*, 154 (9): 3209-18

Prasad R., Chan L.F., Hughes C.R., Kaski J.P., Kowalczyk J., Savage M.O., Peters C.J., Nathwani N., Clark A.J.L., Storr H.L., Metherell L.A. (2014) Thioredoxin reductase 2 (*TXNRD2*) mutation associated with familial glucocorticoid deficiency (FGD). *Journal of Clinical Endocrinology and Metabolism*, 99 (8): E1556-63.

Prasad R., Kowalczyk J., Meimaridou E., Storr H.L., Metherell L.A. (2014) Oxidative Stress and adrenocortical insufficiency. *Journal of Endocrinology*, 221 (3): R63-67

Acknowledgements

I would like to thank:

My supervisors Helen Storr, Adrian Clark and Lou Metherell for their encouragement and support. They have provided an inspiring environment within which to work and learn, enabling me to develop as a scientist.

The patients and their families, without whom, this work would not have been possible.

Dr Banerjee and Dr Nisha Nathwani (Luton and Dunstable University Hospital), Dr Catherine Peters and Dr Juan Kaski (Great Ormond Street Hospital for Children, London) for their help in attaining clinical information.

Guglielmo Rosignoli and Will Day (Flow Cytometry Core Facility, William Harvey Research Institute) for their assistance in obtaining and analysing flow cytometry data, and Felix Norman-Williams (Clinical Biochemistry, Royal London Hospital) for his assistance in obtaining cortisol measurements for the study.

Eamonn Maher, Richard Durbin, Shane McCarthy, Richard Trembath, David van Heel for access to exome sequence data on subjects funded by the Wellcome Trust Strategic Award WT102627 and sequenced at the Wellcome Trust Sanger Institute (Wellcome Trust Award WT098051).

My colleagues and friends in the lab for their advice and support, with particular thanks to Julia Kowalczyk.

My funding bodies; this work was supported by a Clinical Training Fellowship from Barts and the London Charity and a Research Training Fellowship from the Wellcome Trust (Clinical Research Training Fellowship Grant WT095984AIA).

Finally, I would like to thank my family and my husband, Andrew, for their support in everything that I do and their forbearance particularly during the writing up of this thesis.

Abstract

Maintaining redox homeostasis is crucial for normal cellular functions. Electron leak by the cytochrome P450 enzymes renders steroidogenic tissues acutely vulnerable to redox imbalance and oxidative stress is implicated in several potentially lethal adrenal disorders. This thesis aims to further delineate the role of oxidative stress in triple A syndrome and familial glucocorticoid deficiency (FGD).

Triple A syndrome incorporates adrenal failure and progressive neurodegenerative disease. The *AAAS* gene product is the nuclear pore complex protein ALADIN, of unknown function. Patient dermal fibroblasts are sensitive to oxidative stress, with failure of nuclear import of DNA repair proteins and ferritin heavy chain protein. To provide an adrenal and neuronal-specific disease model, I established *AAAS*-knockdown in H295R human adrenocortical tumour cells and SH-SY5Y human neuroblastoma cells. This had effects on cell viability, exacerbated by hydrogen peroxide treatment. Redox homeostasis was impaired in *AAAS*-knockdown H295R cells, with depletion of key components of the steroidogenic pathway and a significant reduction in cortisol production, with partial reversal following treatment with N-acetylcysteine.

Mutations in the mitochondrial antioxidant, nicotinamide nucleotide transhydrogenase (NNT), causing FGD, have recently highlighted the importance of redox regulation in steroidogenesis. I investigated seven individuals from a consanguineous Kashmiri kindred, mutation negative for known causes of FGD. A stop gain mutation, p.Y447* in *TXNRD2*, encoding the mitochondrial selenoprotein thioredoxin reductase 2 segregated with the disease trait; with complete absence of the 56 kDa *TXNRD2* protein in patients homozygous for the mutation. *TXNRD2*-knockdown led to impaired redox homeostasis in H295R cells. This is the first report of a homozygous mutation in any component of the thioredoxin antioxidant system leading to inherited disease in humans.

Antioxidant defence within the adrenal gland warrants further investigation and abnormalities of other components within these pathways may prove to be causative in as yet unaccounted for cases of primary adrenal insufficiency.

Table of Contents

Title	1	
Statement of Originality	2	
Publications arising from this thesis	3	
Acknowledgements	4	
Abstract	5	
Table of Contents	7	
List of Figures	14	
List of Tables	16	
List of abbreviations	17	
Chapter 1	Introduction	21
1.1	Hypothalamic-pituitary-adrenal axis	21
1.2	Cortisol production	21
1.3	Androgen production	23
1.4	Aldosterone production	24
1.5	Inherited primary adrenal insufficiency	25
1.6	The triple A syndrome	30
1.6.1	Epidemiology of triple A syndrome	30
1.6.2	Clinical manifestations of triple A syndrome and current management of triple A syndrome patients	30
1.6.2.1	Alacrima	30
1.6.2.2	Achalasia	31
1.6.2.3	Adrenal Insufficiency	31
1.6.2.4	Neurodegenerative dysfunction	32
1.6.2.5	Other clinical features	33

1.6.3	Genetics of triple A syndrome	33
1.6.4	Genotype-phenotype correlation	34
1.6.5	<i>GMPAA</i> mutations causing achalasia, alacrima and neurological deficits	34
1.6.6	Expression of <i>AAAS</i>	35
1.6.7	Triple A syndrome gene product, ALADIN	35
1.6.7.1	Structure of ALADIN and WD family of proteins	35
1.6.7.2	WD proteins and disease	36
1.6.7.3	ALADIN in the nuclear pore complex (NPC)	37
1.6.7.4	Nuclear pore complex structure	38
1.6.7.5	Nuclear pore complex and nuclear-cytoplasmic transport	39
1.6.7.6	Transport independent roles of the nuclear pore complex	40
1.6.7.7	ALADIN localisation to the nuclear pore complex	41
1.6.7.8	The nuclear pore complex and human disease	42
1.6.8	Proteins interacting with the triple A syndrome gene product	43
1.6.8.1	ALADIN and NDC1	43
1.6.8.2	ALADIN and Ferritin Heavy Chain (FTH1)	44
1.6.8.3	Ferritin Heavy Chain: Structure and function	44
1.6.8.4	Evidence for nuclear ferritin heavy chain	45
1.6.8.5	Ferritin Heavy Chain in disease	46
1.6.8.6	Localisation of FTH1 in triple A syndrome patient dermal fibroblasts	47
1.6.9	Oxidative stress and the triple A syndrome	48
1.6.10	Other research to date	50
1.6.10.1	<i>AAAS</i> -knockout mouse	50
1.6.11	Triple A syndrome summary	51
1.7	Familial glucocorticoid deficiency (FGD)	52

1.7.1	FGD clinical features and patient management	52
1.7.2	FGD type 1; <i>MC2R</i> gene mutations	53
1.7.3	FGD type 2; <i>MRAP</i> gene mutations	56
1.7.4	FGD type 3; Non-classical lipid congenital adrenal hyperplasia	58
1.7.5	FGD type 4; defects in DNA replication	60
1.7.6	FGD type 5; defects in antioxidant pathways	62
1.7.7	Familial glucocorticoid deficiency summary	66
1.8	Steroidogenesis and reactive oxygen species (ROS) production	66
1.9	Reactive oxygen species generation in mitochondria	64
1.10	Adrenal cortex antioxidant defence mechanisms	70
1.11	Thesis Rationale	73
Chapter 2	Materials and Methods	74
2.1	Cell culture	74
2.1.1	Cell culture conditions	74
2.1.1.1	Freezing cells for future use	76
2.1.2	Lentiviral shRNA transduction	76
2.1.2.1	Transformation of chemically competent bacterial cells	78
2.1.2.2	Preparation of LB agar plates and LB broth	78
2.1.2.3	Midi-prep preparation	79
2.1.2.4	Transient Transfection with Lipofectamine-2000	80
2.1.2.5	Transfection of HEK293T cells followed by lentiviral shRNA transduction of H295R/SH-SY5Y cells	81
2.1.2.6	Generation of puromycin kill curve	82
2.2	Western blotting	83
2.2.1	Cell lysate preparation	83

2.2.2	Bradford Assay	83
2.2.3	SDS-Page	84
2.2.4	Immunoblotting	84
2.3	RNA extraction and reverse transcription	84
2.3.1	RNA extraction from animal cells	84
2.3.2	DNase treatment of RNA	86
2.3.3	RNA extraction from whole blood	86
2.3.4	Phenol extraction and RNA precipitation	88
2.3.5	Reverse transcription	88
2.4	DNA extraction from whole blood	89
2.5	Polymerase Chain Reaction (PCR) and sequencing	90
2.5.1	Oligonucleotide design	90
2.5.2	Polymerase Chain Reaction (PCR)	91
2.5.3	Sequencing	92
2.5.4	Sequencing analysis	92
2.6	Whole exome sequencing	93
2.6.1	Sample preparation	93
2.6.2	Sequence capture array and sequencing	93
2.7	Quantitative RT-PCR	94
2.7.1	Gel extraction	94
2.7.2	Standard curves for quantitative RT-PCR	94
2.7.3	Quantitative RT-PCR (qPCR)	95
2.8	Cell viability	97
2.8.1	Cell counting using haemocytometer	98
2.8.2	Cell viability assay	98

2.8.3	PARP (Poly-ADP-ribose polymerase) cleavage	99
2.9	Analysis of cell GSH/GSSG ratio	99
2.10	Cortisol analysis	100
2.11	Thioredoxin Reductase assay	101
2.12	Leukocyte separation	102
2.13	Flow cytometry	104
2.13.1	Cell cycle analysis by flow cytometry	104
2.13.2	Mitochondrial superoxide production (MitoSox Red)	105
Chapter 3	Deficiency of ALADIN impairs redox homeostasis in human adrenal cells and inhibits steroidogenesis	108
3.1	Triple A syndrome and oxidative stress	108
3.2	Failure of nuclear import of specific cargo-(es) leads to increased oxidative stress in triple A syndrome patient dermal fibroblasts	109
3.3	Aims of the study	110
3.4	AAAS-knockdown in H295R adrenocortical tumour cells and SH-SY5Y neuroblastoma cells	111
3.5	AAAS-knockdown results in a reduction in cell viability in H295R cells	112
3.6	AAAS-knockdown cells are hypersensitive to oxidative stress	113
3.7	AAAS-knockdown in H295R cells results in cell cycle arrest and an increase in cell death by apoptosis	114
3.8	AAAS-knockdown in H295R cells results in an imbalance of redox homeostasis	115
3.9	Treatment with the anti-oxidant N-acetylcysteine, improves cell viability in AAAS-knockdown cells	116
3.10	AAAS-knockdown affects key components of the steroidogenic pathway	

	including a reduction of steroidogenic acute regulatory protein (STAR) and P450c11 β protein expression	118
3.11	AAAS-knockdown in H295R cells results in a significant reduction in cortisol production, which is partially rescued by N-acetylcysteine treatment	120
3.12	Discussion	120
Chapter 4	Mutation in the mitochondrial antioxidant, thioredoxin reductase 2 (TXNRD2) is associated with familial glucocorticoid deficiency (FGD)	127
4.1	Aetiology and molecular genetics of FGD	127
4.2	Aims of the study	129
4.3	Study approval	130
4.4	Clinical Case Reports	130
4.5	A stop gain mutation in <i>TXNRD2</i> is associated with disease in the kindred	133
4.6	Expression of <i>TXNRD2</i> in affected individuals	137
4.7	Discussion	138
Chapter 5	<i>TXNRD2</i>-knockdown in human adrenocortical cells causes an imbalance in redox homeostasis	145
5.1	Mitochondrial <i>TXNRD2</i>	145
5.2	Aims of the study	146
5.3	<i>TXNRD2</i> is highly expressed in the human adrenal cortex	147
5.4	<i>TXNRD2</i> -knockdown in H295R adrenocortical tumour cells	148
5.5	<i>TXNRD2</i> -knockdown in H295R adrenocortical cells results in an imbalance of redox homeostasis	149
5.6	Steroidogenesis in <i>TXNRD2</i> -deficient H295R cells	152
5.7	Discussion	153

Chapter 6	General discussion and future work	161
6.1	Oxidative stress and adrenocortical insufficiency	161
6.2	Models of disease	167
6.2.1	<i>In vitro</i> models of disease	167
6.2.2	<i>In vivo</i> models of disease	168
6.3	Conclusion	171
	Uniform Resource Locator (URL)	172
	References	172
	Appendices	206
Appendix 1	cDNA primer sequences	206
Appendix 2	Genomic primer sequences	207
Appendix 3	shRNA sequences	210
Appendix 4	Vector maps	212
Appendix 5	Details of antibodies used in western blotting	215
Appendix 6	Details of candidate variants remaining following penultimate filtration step applied to WES data	217
Appendix 7	Details of candidate variants following final filtration step applied to WES data	219
Appendix 8	General buffers and solutions	220
Appendix 9	Commercial assays used and composition of reagents	221
Appendix 10	Presentations	225

List of Figures

Figure 1.1	Schematic overview of the HPA axis	22
Figure 1.2	The adrenal steroidogenesis pathway	25
Figure 1.3	FTH1-V5-His localises to the nucleus in cotransfected SK-N-SH cells	47
Figure 1.4	FTH1 and ALADIN are protective against oxidative stress	49
Figure 1.5	Schematic diagram demonstrating all mutations in <i>MC2R</i> associated with FGD type 1	54
Figure 1.6	Schematic diagram demonstrating mutations in <i>STAR</i> associated with adrenal insufficiency	58
Figure 1.7	Schematic diagram demonstrating <i>NNT</i> mutations identified so far	63
Figure 1.8	Detoxification of mitochondrial superoxide species produced during electron leak from the mitochondrial electron transport chain	64
Figure 1.9	Reactive oxygen species production during steroidogenesis	69
Figure 1.10	Maintenance of reduced peroxiredoxin 3 (PRDX3-SH) by thioredoxin 2 (TXN2) and sulfiredoxin (SRX)	72
Figure 2.1	Achieving target gene knockdown using a lentiviral transduction system	77
Figure 2.2	Puromycin kill curve generated for H295R cells	82
Figure 2.3	Representative images for standards generated during quantitative RT-PCR	96
Figure 2.4	Haemocytometer grid	98
Figure 2.5	Leucocyte separation using Histopaque solution 1077	103
Figure 2.6	Cell cycle arrest in <i>AAAS</i> -knockdown H295R cells	105
Figure 2.7	Determination of mitochondrial superoxide production, steps used in Gating	107
Figure 3.1	Lentiviral shRNA knockdown of the <i>AAAS</i> gene in (A) H295R and (B) SH-SY5Y cells	111

Figure 3.2	A reduction in cell viability of AAAS-KD cells	112
Figure 3.3	Cell cycle arrest and increased apoptosis is observed in AAAS-KD H295R adrenal cells	115
Figure 3.4	An imbalance in redox homeostasis is observed in AAAS-KD adrenal cells	116
Figure 3.5	Treatment with the anti-oxidant N-acetylcysteine (NAC) improves AAAS-KD cell viability	117
Figure 3.6	The expression of three key enzymes in cortisol production was studied	118
Figure 3.7	STAR and P450c11 β (CYP11B1) expression are reduced in AAAS-KD H295R cells with a subsequent reduction in cortisol production	119
Figure 4.1	Aetiology of disease within the FGD cohort, comprising more than 250 patients	128
Figure 4.2	Pedigree of the affected kindred	130
Figure 4.3	Whole exome sequencing filtering strategy	134
Figure 4.4	Segregation of the p.Y447* <i>TXNRD2</i> mutation in the pedigree	135
Figure 4.5	Identification of p.Y447* <i>TXNRD2</i> mutation	136
Figure 4.6	p.Y447* <i>TXNRD2</i> mutation leads to loss of TXNRD2 protein	137
Figure 4.7	RT-PCR of <i>TXNRD2</i>	138
Figure 4.8	Selenoprotein biosynthesis with incorporation of Sec at UGA codons	140
Figure 5.1	The thioredoxin and glutathione systems maintain mitochondrial redox Homeostasis	146
Figure 5.2	TXNRD2 is expressed in all human tissues investigated, with highest <i>TXNRD2</i> mRNA levels in the adrenal cortex	147
Figure 5.3	Lentiviral shRNA knockdown of the <i>TXNRD2</i> gene in H295R cells	149
Figure 5.4	TXNRD2 deficiency in H295R cells leads to increased pressure on the glutathione system	150

Figure 5.5	<i>TXNRD2</i> -KD in H295R cells leads to impaired mitochondrial redox homeostasis	151
Figure 5.6	There is no significant impact on steroidogenesis in <i>TXNRD2</i> -deficient H295R cells compared with controls	153
Figure 5.7	Ribbon representation of the overall structure of the mouse <i>Txnrd2</i> Homodimer	155
Figure 5.8	Maintenance of reduced peroxiredoxin 3 (PRDX3-SH) by thioredoxin 2 (TXN2) and sulfiredoxin (SRX)	157

List of Tables

Table 1.1	Genetic causes of primary adrenal insufficiency	27
Table 2.1	Transfection with lipofectamine-2000 according to culture vessel type	80
Table 4.1	Clinical details of the members of the kindred	132

List of abbreviations

μM	micromolar
ABC	ATP binding cassette
ACTH	adrenocorticotropic hormone
Ago2	Argonaute 2
ALADIN	Alacrima Achalasia aDrenal Insufficiency Neurologic disorder
ALD	adrenoleukodystrophy
ALDP	adrenoleukodystrophy protein
ALS	amyotrophic lateral sclerosis
AMN	Adrenomyeloneuropathy
ARE	antioxidant responsive element
ATP	adenosine triphosphate
AVP	arginine vasopressin
BSO	L-buthionine-(S,R)- sulfoximine
CAC	chromatin assembly complex
cAMP	cyclic adenosine monophosphate
CNS	central nervous system
CRE	cAMP responsive element
CREB	cAMP response element binding protein
CRH	corticotropin-releasing hormone
Ct	threshold cycle
Cu	copper
Cys	cysteine
DHEA	dehydroepiandrosterone
DHEAS	sulphur ester of dehydroepiandrosterone
DMEM	Dulbecco's Modified Eagle Medium
DMSO	Dimethylsulfoxide
DNA	Deoxyribonucleic acid
dNTPs	deoxynucleotidetriphosphates
DTNB	5, 5'-dithiobis (2-nitrobenzoic) acid
E Coli	<i>Escherichia coli</i>
EDTA	Trypsin/Ethylenediaminetetraacetic acid
ER	endoplasmic reticulum

FAD	flavin adenine dinucleotide
FG	Phenylalanine-Glycine
FGD	familial glucocorticoid deficiency
FTH1	Ferritin Heavy Chain
FTL	ferritin light chain
GDP	guanosine diphosphate
GFP	green fluorescent protein
GH	glycine-histidine
GLRX	glutaredoxin
GPX	glutathione peroxidase
GSH	glutathione (reduced)
GSR	glutathione reductase
GSSG	glutathione disulphide
H ₂ O ₂	hydrogen peroxide
HPA	hypothalamic-pituitary-adrenal
IGF	insulin-like growth factor
iMFI	integrated median fluorescence intensity
IMM	inner mitochondrial membrane
IRE	iron regulatory element
IRP	iron responsive proteins
Kb	kilobase pairs
KD	knockdown
kDa	kilodalton
LCAH	lipoid congenital adrenal hyperplasia
M	molar
MAP	mitogen-activated protein
Mbp	mega base pairs
MC1R	melanocortin 1 receptor
MC2R	melanocortin 2 receptor
MC3R	melanocortin 3 receptor
MC4R	melanocortin 4 receptor
MC5R	melanocortin 5 receptor
MCM4	mini chromosome maintenance-deficient 4
mM	millimolar

MnSOD	manganese superoxide dismutase
MRAP	melanocortin receptor 2 accessory protein
mRNA	messenger RNA
MTS	3-(4,5-dimethylthiazol-2-yl)-5-(3-carboxymethoxyphenyl)-2-(4-sulfophenyl)-2H-tetrazolium
Na ₂ EDTA	disodium ethylenediaminetetraacetate
NADPH	reduced nicotinamide adenine dinucleotide phosphate
NNT	nicotinamide nucleotide transhydrogenase
NOS	nitric oxide synthases
NOX	NADPH-dependent oxidases
NPC	nuclear pore complex
NTC	no template control
Nups	nucleoporins
O ₂	oxygen
O ₂ ⁻	superoxide anions
·OH	hydroxyl radicals
OMIM	online mendelian inheritance in man
OMM	outer mitochondrial membrane
Paraquat	1-1'-diethyl-4,4'-bipyridylium dichloride
PARP	poly-ADP-ribose polymerase
PCR	polymerase chain reaction
PMS	phenazine methosulphate
POMC	proopiomelanocortin
PRDX	peroxiredoxin
PRDX3-SH	reduced peroxiredoxin 3
PRDX3-SO ₂ ⁻	peroxiredoxin 3 sulfinic form
PVN	paraventricular nucleus
qPCR	quantitative RT-PCR
RLU	relative light units
RISC	RNA-induced silencing complex
RNA	Ribonucleic acid
RNase	Ribonuclease
RNS	reactive nitrogen species
ROS	reactive oxygen species

rpm	rotations per minute
SD	standard deviation of the mean
SDS	standard deviation score
SDS-Page	Sodium dodecyl sulphate polyacrylamide gel electrophoresis
Se	selenium
shRNA	small hairpin RNA
siRNA	small interfering RNA
SNP	single nucleotide polymorphism
SOD	superoxide dismutase
SRX	sulfiredoxin
STAR	steroidogenic acute regulatory protein
TCA	tricarboxylic acid
Tm	melting temperature
TNB ²⁻	5-thio-2-nitrobenzoic acid
TSPO	translocator protein
TXN	thioredoxin
TXNRD	thioredoxin reductase
VLCFA	very long chain fatty acid
WD	tryptophan-aspartic acid
WES	whole exome sequencing
WT	wild-type
Zn	zinc

Chapter 1 Introduction

1.1 Hypothalamic-pituitary-adrenal axis

The adrenal glands are responsible for the production of several classes of steroids. The central adrenal medulla contains neural crest-derived chromaffin cells that release catecholamines in response to stimulation by the sympathetic nervous system. The outer part of the gland, the cortex, is further subdivided into 3 functionally distinct sections comprising the outer zona glomerulosa which produces aldosterone, the middle zona fasciculata which secretes glucocorticoids and the inner zona reticularis which produces adrenal androgens. The hypothalamus and pituitary tightly regulate the production of glucocorticoids enabling an appropriate stress response and the maintenance of a diurnal rhythm of cortisol secretion. Emotional and physical stresses excite brainstem catecholamine producing circuits which in turn stimulate parvocellular neurons of the hypothalamic paraventricular nucleus. These secrete corticotropin-releasing hormone (CRH) and arginine vasopressin (AVP) into the hypophyseal portal circulation. CRH and AVP synergistically trigger secretion of adrenocorticotrophic hormone (ACTH) from the anterior pituitary. ACTH is formed by cleavage of proopiomelanocortin (POMC), from which α -, β - and γ -melanocyte-stimulating hormones are also produced. ACTH has physiological actions in several peripheral sites, namely the adrenal glands where it stimulates glucocorticoid release. Glucocorticoids exert their effects in a range of tissues. Furthermore they exert negative feedback, regulating the release of CRH and AVP from the hypothalamus and ACTH from the anterior pituitary. This constitutes the hypothalamic-pituitary-adrenal pathway (Figure 1.1).

1.2 Cortisol production

ACTH exerts its effects in the adrenal zona fasciculata by binding to the melanocortin 2 receptor, MC2R. This stimulates production of intracellular cyclic adenosine monophosphate (cAMP) which in turn stimulates cAMP-dependent protein kinase (protein kinase A). This process induces the import of cholesterol esters into the cell, by the scavenger receptor B1, which are hydrolysed by hormone

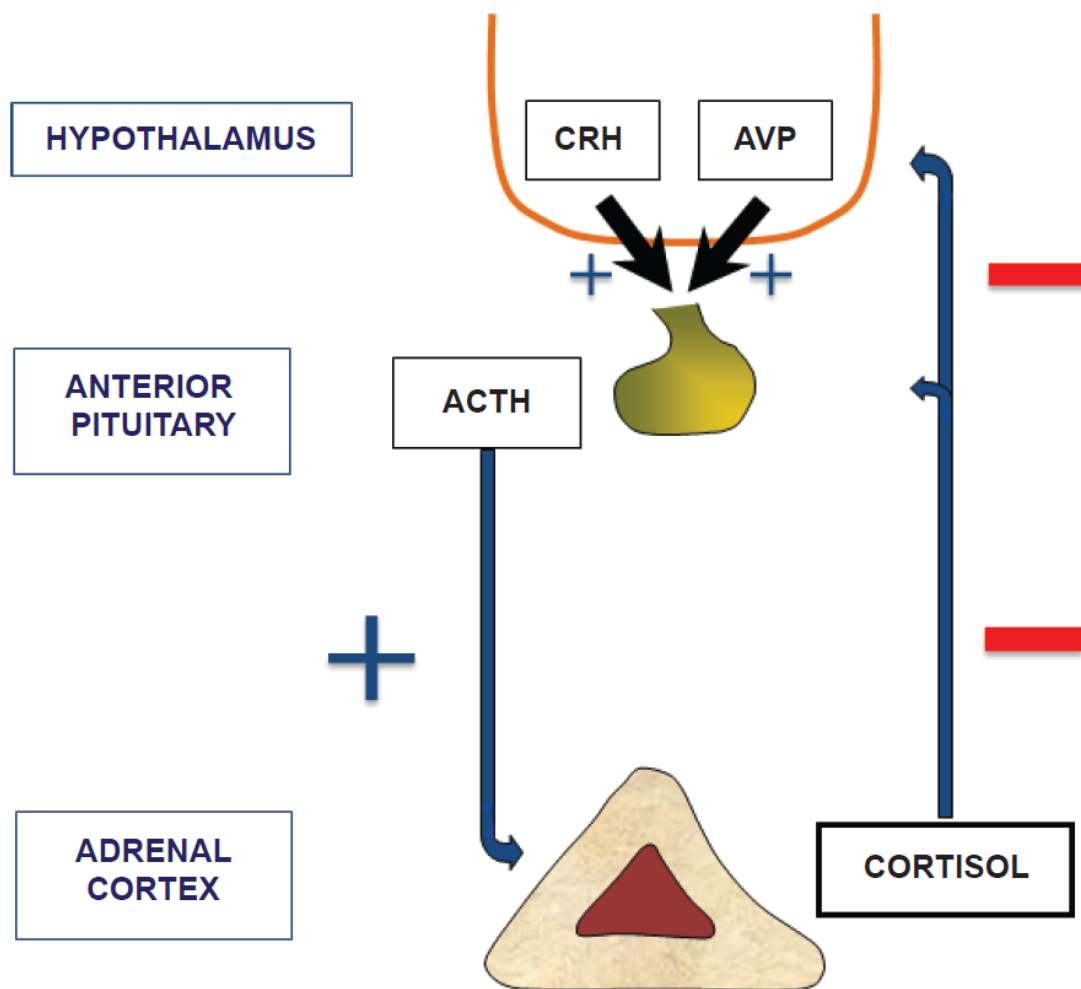


Figure 1.1. Schematic overview of the HPA axis. CRH and AVP at the hypothalamus stimulate ACTH production in the anterior pituitary gland. ACTH released into the circulation acts on the adrenal cortex to produce glucocorticoids (cortisol in humans and corticosterone in rodents). Glucocorticoids negatively feedback to regulate the release of CRH and AVP at the hypothalamus and ACTH at the pituitary.

sensitive lipase. Cholesterol is then taken up into the mitochondrion, a process activated by steroidogenic acute regulatory protein (STAR) and mediated by the translocator protein (TSPO)-associated multi-component complex [1]. This is the first and rate limiting step in cortisol synthesis. ACTH stimulates the synthesis of several steroidogenic enzymes, including STAR, via a variety of mechanisms. These include activation of the cAMP response element binding protein (CREB) and

furthermore ACTH induces *STAR* transcription by cAMP inhibition of salt induced kinase (SIK), which allows phosphorylation of the transducer of regulated CREB activity (TORC), which in turn activates CREB thereby inducing *STAR* transcription [2]. Plasma cortisol increases almost within minutes of the adrenal cortex being stimulated by ACTH, largely dependent on pre-existing *STAR* stores [3]. Following the acute response a longer term response to ACTH involves maintenance of steroidogenic enzyme level, including *STAR*, regulated by cAMP [4]. The biosynthesis of glucocorticoid from cholesterol involves the sequential actions of the cytochrome P450 enzymes in the mitochondria and smooth endoplasmic reticulum and the hydroxysteroid dehydrogenases (Figure 1.2). The cytochrome P450 enzymes are divided into the Type I mitochondrial enzymes (P450_{scc}, P450_{c11β}, and P450_{c11AS}) and Type II microsomal enzymes (P450_{c17} and P450_{c21}) [5]. Both sets of enzymes require the transfer of electrons from reduced NADP (NADPH) for activity; for the Type I enzymes this occurs via ferredoxin and ferredoxin reductase, and for the Type II enzymes, via P450 oxidoreductase.

In healthy individuals cortisol secretion is pulsatile with circulating cortisol concentrations fluctuating in a circadian fashion, with highest levels in the early morning, between 0600h and 0800h and lowest around midnight. Whilst there is diurnal variation in cortisol synthesis, levels tend to remain similar through all stages of life.

1.3 Androgen production

The adrenal androgens, androstenedione, dehydroepiandrosterone (DHEA) and the sulphur ester of dehydroepiandrosterone (DHEAS) are produced in the zona reticularis, under the regulation of ACTH (Figure 1.2). The precise mechanisms responsible for the control of androgen synthesis and the development of the zona reticularis remain unclear. Unlike cortisol production, androgen production varies through life. Typically high levels are seen in the neonatal period with a decline during the first few months of life. Thereafter there is a steady increase during adrenarche between the ages of 6

and 10 years. Peak levels are found during the 3rd decade of life followed by a steady decline from the 5th decade.

1.4 Aldosterone production

The regulation of aldosterone production is a separate entity to the ACTH-induced production of glucocorticoids and androgens. Instead aldosterone production is predominantly controlled by the renin-angiotensin-aldosterone system.

The juxtaglomerular cells of the kidney produce renin in response to a number of stimuli, including hyponatraemia, hyperkalaemia, low renal arteriolar pressure, upright position, vasodilatory drugs and β -adrenergic stimulation. Renin cleaves Angiotensinogen to Angiotensin I, which is converted to Angiotensin II by the angiotensinogen converting enzyme. Angiotensin II causes an increase in blood pressure via actions mediated through the AT₁ receptor. In the first instance Angiotensin II stimulates arteriolar vasoconstriction, a process that occurs within seconds. Secondly, Angiotensin II stimulates increased transcription of *CYP11B2* encoding the cytochrome P450 enzyme, P450c11AS, within the zona glomerulosa, thereby increasing aldosterone synthesis. Increased plasma potassium also stimulates aldosterone production through membrane depolarisation and calcium channel alteration leading to *CYP11B2* transcription. Aldosterone causes renal sodium retention and potassium loss, increasing intravascular volume and therefore blood pressure.

As regulation of aldosterone synthesis is not ACTH-induced, certain disorders of adrenal insufficiency, such as classical familial glucocorticoid deficiency involving disrupted ACTH signalling, may occur in the absence of hypoaldosteronism. Other conditions involving adrenal hypoplasia or destruction can affect both systems.

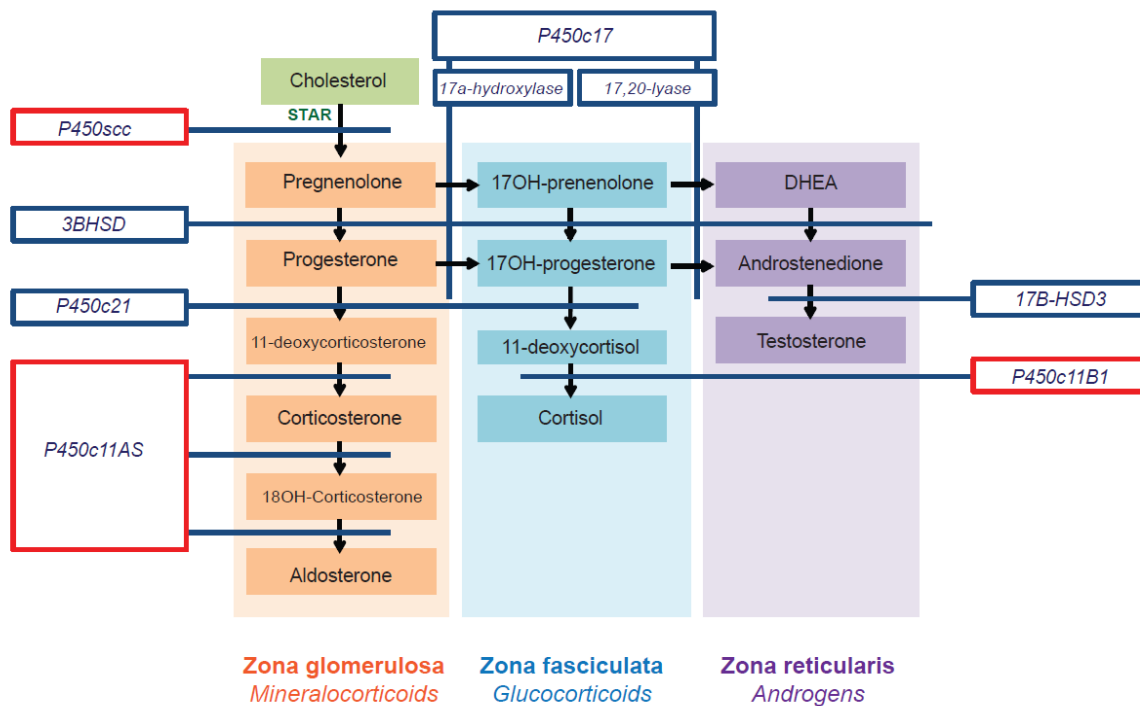


Figure 1.2. The adrenal steroidogenesis pathway. Enzymes required for steroidogenesis are shown in italics. Those requiring electron transfer by ferredoxin reductase and ferredoxin are outlined in red (Type I mitochondrial enzymes). The microsomal enzymes are outlined in blue, these include the Type II microsomal P450 enzymes (P450c17 and P450c21) which accept electrons from P450 oxidoreductase, and the hydroxysteroid dehydrogenases (3βHSD, 17β-HSD3).

1.5 Inherited primary adrenal insufficiency

Perturbations in the hypothalamic-pituitary-adrenal (HPA) axis can be caused by several physiological mechanisms and pathological conditions. Adrenal insufficiency is classified according to the underlying mechanism; with primary relating to disease at the level of the adrenal glands, secondary relating to pituitary disease impairing the release of ACTH and tertiary caused by impaired synthesis or action of CRH and/or AVP from the hypothalamus.

The prevalence of primary adrenal insufficiency is increasing, with autoimmune adrenal insufficiency as the primary cause accounting for 80-90% of cases in the developed world, of which 40% are isolated and 60% occur in the context of autoimmune polyendocrinopathy syndrome [6]. In

idiopathic autoimmune adrenal disease, cell-mediated immune mechanisms lead to destruction of the adrenal cortex and may involve antibodies against 21-hydroxylase and other autoantigens [7]. Additionally, increased susceptibility to autoimmune Addison's disease has been identified in association with the MHC haplotypes DR3-DQ2 and DR4-DQ8, protein tyrosine-phosphatase non-receptor type 22, cytotoxic T lymphocyte antigen 4 and MHC class II transactivator. Autoimmune adrenal insufficiency is also described in the context of autoimmune polyendocrinopathy syndromes: Type 1 (APECED; autoimmune polyendocrinopathy, candidiasis, ectodermal dystrophy), Type 2 (autoimmune adrenal insufficiency, autoimmune thyroid disease, with or without type 1 diabetes mellitus) and Type 4 (autoimmune adrenal insufficiency with one or more minor component autoimmune disease) [8]. Both Types 1 and 2 have a strong genetic component with Addison's disease as a prominent feature of the disorder. Additionally, 40-50% of patients with Addison's disease will go on to develop an associated endocrinopathy. Aetiologies of acquired primary adrenal insufficiency include infection, haemorrhage and drug-induced disease. Infectious causes include tuberculosis-associated adrenalitis which was once the most prevalent cause of primary adrenal insufficiency.

In childhood, genetic causes of primary adrenal insufficiency are the most common. Most frequently seen is congenital adrenal hyperplasia, which in the main is caused by mutations in *CYP21A2* leading to 21-hydroxylase deficiency and more rarely by deficiency in 11 β -hydroxylase, 17 α -hydroxylase, 17, 20-lyase, 3 β -hydroxysteroid dehydrogenase or P450 oxidoreductase. Classic 21-hydroxylase deficiency is characterised by glucocorticoid deficiency but a large proportion also have mineralocorticoid deficiency and adrenal hyperandrogenism leading to virilisation. Impaired development and activity of the adrenal medulla can also occur. Several other inherited causes of primary adrenal insufficiency are described including X-linked adrenoleukodystrophy (ALD). ALD is an inherited neurometabolic disorder incorporating progressive demyelination in the central nervous system, axonopathy in the spinal cord and adrenal insufficiency [9]. The disease is caused by

mutations in the *ABCD1* gene on Xq28, encoding the adrenoleukodystrophy protein (ALDP), a member of the peroxisomal ATP-binding cassette (ABC) transporters. The clinical phenotype is variable, from a late onset, slowly progressive disease adrenomyeloneuropathy (AMN) to cerebral inflammatory demyelinating forms which can be fatal [9]. Adrenal insufficiency occurs in approximately two thirds of patients with AMN, presenting with both hypocortisolism and a reduction in adrenal androgen production [10]. Other causes of inherited primary adrenal insufficiency are listed below in Table 1.1.

Genetic Disorder	Clinical features in addition to adrenal insufficiency	Pathogenetic mechanism
Adrenoleukodystrophy or adrenomyeloneuropathy	Weakness, spasticity, dementia, blindness, quadriparesis	<i>ABCD1</i> and <i>ABCD2</i> mutations
Congenital adrenal hyperplasia		
21-hydroxylase deficiency	Hyperandrogenism	<i>CYP21A2</i> mutations
11 β -hydroxylase deficiency	Hyperandrogenism, hypertension	<i>CYP11B1</i> mutations
3 β -hydroxysteroid dehydrogenase type 2 deficiency	Ambiguous genitalia in boys, postnatal virilisation in girls	<i>HSD3B2</i> mutations
17 α -hydroxylase deficiency	Pubertal delay in both sexes, hypertension	<i>CYP17A1</i> mutations
P450 oxidoreductase deficiency	Skeletal malformation (Antley-Bixler syndrome), abnormal genitalia	<i>POR</i> mutations
P450 side-chain cleavage	XY sex reversal	<i>CYP11A1</i> mutations

deficiency		
Congenital lipoid adrenal hyperplasia	XY sex reversal	<i>STAR</i> mutations
Smith-Lemli-Opitz syndrome	Craniofacial malformations, mental retardation, growth failure, hyponatraemia, hyperkalaemia, cholesterol deficiency	<i>DHCR7</i> mutations
Adrenal hypoplasia congenita		
X-linked	Hypogonadotropic hypogonadism in boys	<i>NROB1</i> mutations
Xp21 contiguous gene syndrome	Duchenne muscular dystrophy, glycerol kinase deficiency, psychomotor retardation	Deletions of genes for muscular dystrophy (<i>DMD</i>), glycerol kinase (<i>GK</i>), <i>NROB1</i>
SF-1 linked	XY sex reversal	<i>NR5A1</i> mutations
IMAGe syndrome	Intrauterine growth retardation, metaphyseal dysplasia, adrenal hypoplasia congenital, genital abnormalities	<i>CDKN1C</i> mutations
Kearns-Sayre syndrome	External ophthalmoplegia, retinal degeneration, cardiac conduction defects, other endocrine disorders	Mitochondrial DNA deletions
Wolman's disease	Bilateral adrenal calcification, hepatosplenomegaly	<i>LIPA</i> mutations
Sitosterolaemia	Xanthomata, arthritis, premature coronary artery disease, short stature, gonadal and adrenal failure	<i>ABCG5</i> and <i>ABCG8</i> mutations

Familial glucocorticoid deficiency		
Type 1	Hyperpigmentation, tall stature, characteristic facial features such as hypertelorism and frontal bossing, lethargy and muscle weakness but normal blood pressure	<i>MC2R</i> mutations
Type 2	Hyperpigmentation, normal height, hypoglycaemia, lethargy and muscle weakness, but normal blood pressure	<i>MRAP</i> mutations
FGD variant: <i>MCM4</i>	Growth failure, increased chromosomal breakage, natural killer cell deficiency	<i>MCM4</i> mutations
FGD variant: <i>NNT</i>	Hyperpigmentation	<i>NNT</i> mutations
Triple A syndrome	Achalasia, alacrima, deafness, mental retardation, hyperkeratosis	<i>AAAS</i> mutations

Table 1.1. Genetic causes of primary adrenal insufficiency adapted from Charmandari et al, Lancet, 2014 [6].

The contents of this thesis relate to triple A syndrome and familial glucocorticoid deficiency (FGD). ACTH resistance occurs in both conditions causing glucocorticoid deficiency. Both conditions are inherited in an autosomal recessive manner. Clinical features in triple A syndrome can be variable and neurodegenerative features can arise together with adrenal insufficiency, similar to ALD. Classically in FGD, isolated glucocorticoid deficiency is seen, however in the newly described FGD variants due to *MCM4* mutation, extra-adrenal manifestations are described. In both triple A syndrome and more recently FGD, oxidative stress is implicated in the pathogenesis.

1.6 The triple A syndrome

Triple A syndrome (OMIM #231550) was initially described in two pairs of siblings by Allgrove and colleagues in 1978 [11]. It is classically characterised by a triad of alacrima (an inability to produce tears), achalasia of the oesophageal cardia and adrenal failure. In approximately 70% of patients a highly disabling neurodegenerative process ensues. It is an autosomal recessive disorder linked to a mutation in *AAAS* (Achalasia-Addisonianism-Alacrima Syndrome) encoding the protein ALADIN (**A**lacrima **A**chalasia **a**Drenal Insufficiency **N**eurologic disorder) of unknown function. Mutations of *AAAS* have also been identified in patients presenting with just one of the classical features. In fact, only 58% of patients described in the largest case series to date (215 patients in 173 families from 37 countries) present with all three 'A's: alacrima, achalasia, adrenal insufficiency (Huebner, personal communication).

1.6.1 Epidemiology of triple A syndrome

Triple A syndrome is a rare condition with just over 200 cases reported worldwide from over 30 different countries. Families reported in the literature have been of European, Asian, North African, Arab and North American origin [12-14]. Consanguinity is described in 30% of families and the age of presentation is relatively heterogeneous (Huebner, personal communication). Male to female ratios are approximately equal. There are no founder effects for triple A syndrome.

1.6.2 Clinical manifestations of triple A syndrome and current management of triple A syndrome patients

1.6.2.1 Alacrima

The earliest and most consistent manifestation of triple A syndrome is alacrima, an inability to produce tears, which affects the majority of patients. This is often described retrospectively following diagnosis, and is reported to develop in the first year of life [13, 15]. Alacrima is confirmed

by Schirmer's test in which the deficiency of tear production is observed. Small lacrimal ducts have been observed on MRI scanning in one case and autonomic dysfunction at the level of the lacrimal glands has also been suggested as the cause of the failure of tear production [16].

Additional ophthalmic features described include optic atrophy, identified by pathological visual evoked responses, and optical coherence tomography [17]. Normal electroretinograms suggest that the retina is not involved. Interfamilial variability relating to the extent of optic atrophy is described.

1.6.2.2 Achalasia

Approximately 80% of triple A patients present with achalasia of the oesophageal cardia. Symptoms include dysphagia, vomiting and failure to thrive [13, 18]. Management includes repeated endoscopic balloon dilatation with some patients requiring surgical intervention, for instance Heller cardiomyectomy combined with Nissen fundoplication.

The pathophysiology of the achalasia is unclear. The absence of ganglion cells and nerve fibres was described following necropsy in one adult with triple A syndrome [11]. A recent study of myomectomy specimens from ten children with triple A syndrome revealed fibrosis of the intermuscular plane (between the circular and longitudinal musculature) in all patients [19]. This was postulated to impair the mechanical properties together with electrical coupling between the two muscle layers, contributing to the pathogenesis. In addition, there was a marked reduction of the number of myentric ganglia and myentric neurons suggesting a lack of intrinsic innervation. Similar to achalasia of other causes, a lack of nitrergic inhibition with preservation of cholinergic excitation is observed, contributing to the sphincter hypertonicity seen in the disease [19].

1.6.2.3 Adrenal Insufficiency

The adrenal failure observed in triple A syndrome is ACTH-resistant. It most commonly occurs in the first decade of life, although the age at presentation can vary from birth to 35 years of age. Adrenal insufficiency can manifest as hypoglycaemic seizures, frequent fainting and in some patients, when

the cortisol deficiency is unrecognised, death as a result of acute adrenal crisis [20]. Hyperpigmentation as a consequence of raised POMC products is also observed. The adrenal insufficiency is predominantly glucocorticoid deficiency (75% patients) however mineralocorticoid deficiency also occurs in 27% of these patients (Huebner, personal communication).

Glucocorticoid insufficiency is diagnosed by a failed response (inability to show an appropriate rise in cortisol) to a low dose synacthen (ACTH) test [13]. A high baseline ACTH in the face of normal cortisol is also characteristic. Given the devastating consequences of adrenal insufficiency, glucocorticoid deficiency should be screened for in all patients with a potential diagnosis of triple A syndrome. Those patients with glucocorticoid deficiency are commenced on physiological replacement therapy, with some also requiring additional mineralocorticoid replacement.

Necropsy carried out in one of the pairs of original siblings published revealed atrophy of the adrenal cortical zona fasciculata and zona reticularis, suggesting a degenerative process [11].

1.6.2.4 Neurodegenerative dysfunction

The neurological features of triple A syndrome are highly variable, even amongst members of the same kindred [12]. Pathology often occurs in a patchy distribution and can encompass autonomic neuropathy with or without central and peripheral nervous system involvement. The most commonly associated features are that of a pyramidal syndrome, peripheral neuropathy and bulbar dysfunction [15].

Autonomic neuropathy symptoms include impotence, postural hypotension and bladder dysfunction [12, 15]. The alacrims commonly seen in the disease may also be related to a lack of parasympathetic innervation of the tear glands [12]. Upper and lower motor neuron abnormalities are also observed with hyper-reflexia presenting in the first decade [13]. The neuropathy predominantly involves motor fibres with a few patients also exhibiting sensory deficits. Some patients can present with Parkinsonian features and others may have dementia [12, 15].

The pathophysiology of the neurodegenerative aspects of the disease is unclear. MRI images of the brain and spinal cord of five families presenting with significant neurodegenerative disease have been reported as normal [12]. There have been no consistent histological features reported; some reports describe normal sural nerve biopsies whilst others describe changes suggestive of axonal degeneration with loss of both myelinated and unmyelinated fibres [12, 21].

The neurodegenerative aspects of the disease are progressive and can be highly disabling with little room for therapeutic intervention. Those patients presenting late with the triple A syndrome often have predominantly neurodegenerative features and the syndrome should be considered in patients with a multisystem neurological disorder [15, 21].

1.6.2.5 Other clinical features

Several dermatological features are also described and these include xerostomia, palmo-plantar and punctate hyperkeratosis [15]. Other features such as microcephaly and short stature are also reported [22]. Additionally, 27.5% of patients are reported to have delayed puberty, particularly amongst male patients (Huebner, personal communication). For some this was demonstrated to be secondary to hypogonadotropic hypogonadism. Amenorrhoea is reported in 4.1% of female patients and impotence in 13.2% of male patients (Huebner, personal communication).

1.6.3 Genetics of triple A syndrome

A systematic genome linkage scan in eight triple A families, of whom three were consanguineous, showed evidence for linkage of the triple A syndrome to markers on chromosome 12q13, with no evidence of genetic heterogeneity in these families. Haplotype and multipoint analyses suggested that the gene was located on a chromosomal segment flanked by the markers D12S1629 and DS12S312 (6cM apart) [23]. The novel gene, named *AAAS*, encoding a 547 amino acid protein was subsequently identified using fine-mapping based on linkage disequilibrium in 8 North African inbred families, with homozygous mutations in affected individuals [24]. This was corroborated by a second

group who also identified mutations in *AAAS* following refinement of the critical region on chromosome 12q13 and a positional genomics approach [25].

Since then, over 60 different mutations have been described in the literature in *AAAS*, scattered throughout the gene. In the majority of patients these are frameshift and nonsense mutations. In the largest case series to date which encompasses 175 families and 215 patients, 31 of these families do not have mutations in the *AAAS* gene suggesting that genetic heterogeneity exists (Huebner, personal communication). This finding has also previously been reported in the literature [12, 26, 27].

1.6.4 Genotype-phenotype correlation

Three mutations have recently been identified as most commonly causing the disease; p.G14fs (c.43C>A), p.S263P (c.787T>C), c.1331+1G>A. Genotype-phenotype correlation has been investigated in these and other mutations [12, 13, 28] (Huebner, personal communication). Interestingly there is a lack of correlation, indicating that modifying factors related to other genes or the environment could be important. Triple A syndrome patients with *AAAS* mutations are reported to present with a higher frequency of adrenal insufficiency in comparison to those without identified *AAAS* mutations.

1.6.5 *GMPAA* mutations causing achalasia, alacrima and neurological deficits

Mutations in guanosine diphosphate (GDP)-mannose pyrophosphorylase A (*GMPPA*) have recently been described in a cohort of patients with a disease characterised by achalasia, alacrima and neurological deficits [29]. The condition, inherited in an autosomal recessive manner, shows many similarities to triple A syndrome. Importantly, none of the individuals with *GMPPA* mutations have adrenal insufficiency. *GMPPA* is thought to serve as a regulatory unit of *GMPPB* which catalyses the formation of GDP-mannose, an essential precursor of glycan moieties of glycoproteins and glycolipids, associated with congenital and limb-girdle muscular dystrophies with hypoglycosylation of α -dystroglycan. The authors propose that individuals presenting with a triple A syndrome-like

phenotype in the absence of adrenal insufficiency should primarily be investigated for mutations in *GMPPA*.

1.6.6 Expression of AAAS

AAAS expression has been investigated using a multiple human tissue expression array. Abundant AAAS expression was demonstrated in the adrenal gland, gastrointestinal structures, pituitary gland, cerebellum and foetal lung [25]. Expressed sequence tags or ESTs homologous to AAAS were also identified in cDNA libraries of a diverse range of adult human tissues (Hs 125262) and whole embryo (AA330197), suggesting ubiquitous expression of AAAS [25].

In situ hybridisation studies in the adult rat reveal high levels of AAAS mRNA in the adrenal cortex, peripheral and central nervous systems [30]. CNS expression was found to be the highest in neurons of the cerebral cortex, cerebellum, hippocampus, motor-associated nuclei of the brainstem and the ventral horn of the spinal cord. Non-neuronal cells such as fibrous astrocytes also expressed high levels of AAAS mRNA. Relatively little or no detectable AAAS mRNA was seen in the hepatocytes, enteric smooth muscle and fibroblasts. The highest level of expression in the developing embryo was found in the neural tissues [30].

1.6.7 Triple A syndrome gene product, ALADIN

The triple A syndrome gene product is the protein ALADIN (**A**lacrima **A**chalasia **a**Drenal Insufficiency **N**eurologic disorder) of unknown function.

1.6.7.1 Structure of ALADIN and WD family of proteins

ALADIN's sequence predicts a central domain composed of four WD-repeats producing a β -propeller structure [24, 25]. WD repeats comprise a domain of approximately 40-60 amino acids, initiated by a glycine-histidine (GH) dipeptide 11-24 residues from the N-terminus ending with a tryptophan-aspartic acid (WD) peptide at the C terminus [31].

The repeating unit is referred to as the GH-WD repeat or WD-40 repeat. Most proteins belonging to this family have between 4 (the minimum number of repeats reported) and 16 repeats [32]. The crystal structure of this repeat unit has been studied in the β -subunit of the GTP-binding protein transducin, in which this domain was originally described [33]. The G protein β -subunit adopts a β -propeller fold made up of WD-repeats, which is highly symmetrical. These folds act as stable platforms for protein-protein interactions, the residues on the top and bottom of the propeller forming interacting surfaces, together with a circumferential surface available for binding. Given the conservation of the WD-repeat domain, it is likely that all WD-repeat proteins adopt a similar structure [31]. There are over 136 WD-repeat proteins described in humans [32]. These are thought to differ in the variable region within the WD-repeat, by the number of repeats and by the sequence outside the WD-repeat domain. Localisation signals can sometimes be found external to the WD-repeat domain.

The WD-repeat domain has no catalytic activity, therefore, the function of this family of proteins are dependent on the interactions achieved with other proteins/protein complexes [34]. The cellular functions of WD-repeat proteins described are extremely diverse [32]. $G\beta$ protein and LIS1 are examples of proteins that are involved in signal transduction. Intracellular vesicular trafficking is conducted by another group of WD-repeat proteins, the α and β -CoP proteins, which comprise the Golgi-derived coated vesicles. These are involved in vesicular budding, translocation and fusion with target membranes [35]. Dynein intermediate chains, responsible for targeting various dyneins to the specific cell organelles to which they associate, are WD-repeat proteins and play a part in cytoskeletal assembly [36, 37]. WD-repeat proteins also have roles to play in the *de novo* nucleosome assembly pathway as part of the chromatin assembly complex (CAC) [38]. Additionally, other key roles including gene regulation, cell cycle regulation are described together with roles in programmed cell death [39-44].

Thus the WD-repeat family of proteins are involved in several key cellular pathways. The functions of several of these proteins, including ALADIN, are yet to be determined [32].

1.6.7.2 WD proteins and disease

Several other human diseases, in addition to triple A syndrome, arise as a consequence of mutations in WD-repeat proteins. Whilst triple A syndrome is alone in causing adrenal insufficiency, mutations in several WD-repeat proteins are associated with neurological conditions. Mutations in *LIS1* have segregated with lissencephaly (absence of convolutions or gyri in the brain) [45, 46]. Autosomal recessive primary microcephaly with cortical malformations is caused by mutations in *WDR62* which results in disordered cerebral cortical development [47, 48]. Mutations in *WDR36* have been associated with primary open-angle glaucoma, one of the leading causes of blindness worldwide [49, 50]. The *WDR36* null mouse shows defects in axonal growth with progressive degeneration at the peripheral retina [51].

Suboptimal response to oxidative stress is associated with mutations in other WD-repeat proteins. A subtype of the premature aging syndrome Cockayne syndrome, in which patients also present with dwarfism, mental retardation, optic atrophy, deafness, pigmentary retinopathy and skeletal abnormalities, is caused by mutations in the CSB protein. This WD-repeat protein is involved in several biological processes including DNA repair and transcription, regulating several genes post oxidative stress [52].

All the WD-repeat proteins described above exert their role as members of macro-molecular complexes with mutations impacting on various key biological processes.

1.6.7.3 ALADIN in the nuclear pore complex (NPC)

ALADIN was identified as one of 30 nucleoporins of the mammalian nuclear pore complex (NPC) by detailed proteomic analysis in 2002. A fractionation procedure was used to enrich the NPC fraction of rat liver, and the supernatant for analysis identified by a panel of anti-nucleoporin antibodies [53].

Characterisation of the nucleoporins in this fraction was then undertaken by mass spectrometry analysis.

NPCs are present throughout the nuclear envelope and are the sole site of nuclear–cytoplasmic transport. They are relatively well conserved between species [54]. ALADIN is not present in yeast but is observed in all higher eukaryotes [55].

1.6.7.4 Nuclear pore complex structure

The vertebrate NPC is postulated to form an 8 fold symmetrical structure creating a transport channel across the nuclear envelope, with a molecular mass of 60-90 mDa [53, 55]. The NPC comprises a nuclear basket, central core and asymmetrically arranged cytoplasmic fibrils [56-58].

The nucleoporins that form this structure can roughly be divided into 3 categories: the transmembrane proteins, the scaffold proteins and finally the nucleoporins residing at the nuclear basket. The nucleoporins POM121 and gp210, are transmembrane proteins important in nuclear pore formation in the nuclear pore complex [59, 60]. NDC1 has been shown to be integral to the formation of the NPC in yeast has alternately been described as a transmembrane and a scaffold nucleoporin [61]. All these nucleoporins are postulated to be involved in the early phase of NPC development [60, 62]. Interestingly studies also suggest that these proteins are not absolutely essential for NPC formation implying that NPC formation is a relatively fault tolerant process [63, 64]. The scaffold proteins, of which ALADIN is believed to be a member, constitute the second category of nucleoporins providing the stable structure of the NPC in 2 large sub-complexes; the Nup107-160 and the Nup 93-205 [65]. These are WD- and α - solenoid protein rich, with β propeller platforms, important for their role in establishing macro-molecular complexes. These proteins are postulated to be relatively stable in their residence time at the nuclear pore complex with very low turnover rates [57, 65, 66]. A study using GFP-tagged ALADIN demonstrated that ALADIN was present at the NPC for approximately 57 hours, with other nucleoporin residence times at the NPC varying between a few seconds and several days [66]. This suggests relatively stable expression of

ALADIN at the NPC. Interestingly absence of ALADIN at the NPC has minimal or no effect on NPC structure [67, 68].

The third category of nucleoporins comprise the FG repeat-(repetitive stretches of Phe-Gly residues) containing Nups residing at the nuclear basket, that mediate selectivity and permeability of the nuclear pore [69]. The non-FG domains of these Nups have β -propeller, coiled-coil and β sandwich structures, presumably allowing them to assemble onto the β -propeller and α -solenoid platforms of the scaffold nucleoporins [70, 71]. These FG Nups are believed to provide low affinity binding sites for transport receptors and mediate the passage of these receptors and their cargo through the nuclear pore [72, 73]. Some only spend a few seconds at the NPC, shuttling between the cytoplasm and nucleoplasm [66].

1.6.7.5 Nuclear pore complex and nuclear-cytoplasmic transport

Whilst small molecules (less than 40 kDa) are capable of traversing the nuclear pore by passive diffusion, the transport mechanisms of larger macro-molecular complexes remain controversial. In contrast to the initial theories that NPC proteins provide stable docking sites for rapidly trafficking transport receptors, current concepts are moving towards a more dynamic model. Active NPC transport involves interactions directly with the NPC or association with several types of transport receptors. The karyopherins comprise the largest class of these transport receptors and include importins, exportins and transportins which are highly specialised for import or export. Directionality at the NPC is maintained by the small GTPase Ran which organises cargo binding and release in a compartment specific manner [57]. Certain FG Nups, for instance Nup98 and Nup50, have active roles in establishing disassembly of transport receptor-cargo complexes [74-76]. Several members of the NPC are also involved in mRNA export [77].

Selectivity across the NPC is believed to be maintained by the dynamic FG Nups which bind to specific transport receptors [78]. Differential expression of various transport receptors have been

demonstrated in different cell types. Each FG Nup may interact with only a subset of transport receptors allowing for selective pathways across the NPC [79-81]. Interestingly, depletion of nearly half the FG mass of the NPC does not affect cell viability or impact on NPC active transport suggesting an importance of the core/scaffold Nups in maintaining the permeability barrier [79]. Consistent with this, several tissue-specific diseases related to human mutations of nucleoporins involve core / scaffold components of the NPC [78, 82].

Variation in NPC conformation between cell types is postulated given the differential tissue expression of several Nups [78, 82]. Enrichment of certain Nups, including ALADIN, in specific tissues may occur depending on tissue-specific requirements. The Mlp1 and Mlp2 proteins, which bind to ribonucleoproteins and associate with the nuclear pore complex, are not equally distributed along the nuclear envelope [83]. These proteins bind preferentially to some NPCs, mainly those associated with active chromatin, suggesting that NPCs are not identical even within an individual cell. Furthermore, within each cell type, conformational changes in the NPC are thought to occur during transport [84]. This suggests that the NPC is a dynamic system, able to model depending on the requirements of the cell.

1.6.7.6 Transport independent roles of the nuclear pore complex

Conformational changes in the NPC are thought to occur during the various stages of the cell cycle [84]. During mitosis the nuclear envelope breaks down and the NPCs divide into several sub-complexes which serve as NPC building blocks during telophase [84]. Several Nups localise to kinetochores during mitosis, including members of the Nup 107-160 subcomplex and Nup358; these steps are thought to be integral to entry into mitosis [85]. Depletion of certain Nups also lead to defects in spindle formation [86].

The NPC is proposed to be involved in chromatin organisation, also suggesting a role in transport independent gene regulation. A ChIP approach in yeast demonstrates the NPC binding to the 3' end

of genes whilst other studies suggest NPC binding to the promoter and 5' ends [87, 88]. A model of chromatin looping has been proposed, in which active chromatin localises to nuclear pore structures. [89]. High resolution images of the NPC show heterochromatin interspersed by NPC pores in a periodic manner [78]. Therefore, the NPC could act as boundary elements which prevent communication between active and silent chromatin and the stable core component of the NPC could be integral in this function [90].

NPCs may also have a more dynamic involvement in gene regulation as suggested by the transcription dependent mobility of Nup153 and Nup98, which can move away from the NPC to interact with transcribing genes and mRNA [91]. Efficient coordination of transcription and mRNA export may, thus, be achieved by these dynamic nucleoporins.

1.6.7.7 ALADIN localisation to the nuclear pore complex

ALADIN does not have a nuclear localisation signal (NLS). Immunocytochemistry has demonstrated that ALADIN co-localises with the nucleoporin Nup358 (RanBP2) to the cytoplasmic face of the NPC [68]. Interaction of ALADIN with the scaffold nucleoporin NDC1 has also been demonstrated [92, 93]. ALADIN appears to require the presence of NDC1 for appropriate docking onto the NPC, with depletion of NDC1 resulting in mislocalisation of ALADIN to the cytoplasm [92]. In contrast, depletion of the other core Nups, POM 121 and GP210, have no effect on the localisation of ALADIN [92].

The effect of naturally occurring AAAS mutations on ALADIN subcellular localisation has been investigated by transiently transfecting wild-type and several GFP-tagged mutant AAAS constructs into HeLa cells. These mutants are demonstrated to predominantly mislocalise to the cytoplasm suggesting that localisation of ALADIN to the nuclear pore complex is necessary for its function [68, 94].

1.6.7.8 The nuclear pore complex and human disease

Tissue specific requirements for Nups are supported by human mutations that lead to tissue-specific human pathologies [82]. A missense mutation in human *NUP155*, which forms part of the scaffold complex, has been associated with an inherited form of atrial fibrillation [95]. Homozygous mice carrying the knockout *Nup155* allele die in mid-embryogenesis whilst heterozygous mice show an atrial fibrillation specific phenotype [95]. Interestingly the drosophila homologue of NUP 155, *Nup154*, has been shown to be involved in gametogenesis demonstrating both tissue-specific and species-specific roles of the Nups [96, 97].

The NPC is implicated in the regulation of gene expression and this is supported by multiple genomic translocations of *NUP98* and *NUP214* genes which result in fusions of the Nups to 'partner genes' leading to the generation of leukemogenic fusion proteins. For instance, the oncogenic fusion of *NUP98* to the transcription factor *HOXA9* induces aberrant expression of *HOXA9* target genes leading to acute myelogenous leukaemia [98]. Fusion of *NUP98* to PHD-finger proteins, containing nuclear protein interaction-domains, similarly lock target genes to an aberrant state leading to leukaemic transformation [99]. Furthermore, fusion of *NUP214* to the tyrosine kinase *ABL1* is seen in a proportion of acute lymphoblastic leukaemia [100, 101].

Aside from triple A syndrome, two other diseases involving the central nervous system have been associated with mutations in nucleoporins. A missense mutation of human *Nup358/RANBP2* was identified in familial cases of infection triggered acute necrotizing encephalopathy [102]. *RANBP2* has been described to have several roles in mitosis and nucleocytoplasmic transport. More recently it has been identified as a SUMO E3 ligase interacting with *RanGAP1/SUMO1* complex and *Ubc9*. This complex is described to have multiple roles in nucleocytoplasmic transport, cell-cycle progression, and protein sumoylation [103]. Additionally, it has been detected with mitochondria and microtubules in primary neurons with a potential role in intracellular trafficking, implying a role outside the NPC [104]. Missense mutations in the FG-repeat containing nucleoporin, *Nup62*, cause

degeneration of the basal ganglia in the autosomal recessive infantile bilateral striatal necrosis. This mutation does not affect localisation of the mutant protein to NPCs, and the precise mechanism by which basal ganglia disease is caused is unclear [105]. Furthermore, antibodies against nucleoporins have also been associated with human disease. These include antibodies against human Nup62 and human Gp210 which have been demonstrated in approximately 50% of patients with primary biliary cirrhosis [106].

All current known human mutations in nucleoporins display tissue specific pathology, yet the precise pathological mechanisms in some, including triple a syndrome, remain elusive.

1.6.8 Proteins interacting with the triple A syndrome gene product

As a WD-repeat protein at the nuclear pore, ALADIN would be predicted to be involved in several protein-protein interactions. Identifying protein partners of ALADIN is crucial for further understanding the function of ALADIN and mutations of genes encoding these proteins may account for the genetic heterogeneity observed in the disease.

1.6.8.1 ALADIN and NDC1

ALADIN has been shown to interact with the NPC protein NDC1 which is described as a 'scaffold' NPC protein [92, 93]. ALADIN's localisation appears to be dependent on the presence of NDC1 in the NPC; depletion of NDC1 by siRNA results in the mislocalisation of ALADIN to the cytoplasm [92]. Interestingly, the presence of ALADIN at the NPC appears to be required for NDC1 to localise appropriately. Fluorescence resonance energy transfer (FRET) measurements demonstrate the association between NDC1 and ALADIN. GFP-tagged ALADIN has also been demonstrated to co-immunoprecipitate with NDC1 [93]. No human mutations have been identified in *NDC1* however in yeast, NDC1 has been demonstrated to be necessary to establish the biosynthesis and the integrity of the NPC [61].

1.6.8.2 ALADIN and Ferritin Heavy Chain (FTH1)

Ferritin Heavy Chain (FTH1) was identified as an interacting protein partner of ALADIN from 2 separate human cDNA libraries (HeLa cell and cerebellar cDNA libraries) using the full length human ALADIN sequence as bait in bacterial two-hybrid screening [107]. This interaction was validated by co-immunoprecipitation following transfection of tagged FTH1 and ALADIN. Additionally, GFP-tagged ALADIN was found to co-immunoprecipitate with endogenous FTH1. FRET studies confirmed this interaction *in vivo* [107].

1.6.8.3 Ferritin Heavy Chain: Structure and function

The 24 unit ferritin heteropolymer is described as a hollow protein shell capable of sequestering free iron. Ferritin is comprised of ferritin light chain, a 19 kDa protein of 175 amino acids (encoded by *FTL*, on chromosome 19) and the 21 kDa ferritin heavy chain of 183 amino acids (encoded by *FTH*, on chromosome 11) [108]. The ferritin light and heavy chains are multi-helical and share a 55% identical sequence. However, they are functionally distinct with the light chain playing an important role in iron storage and heavy chain having potent ferroxidase activity [109, 110]. The ratio of heavy to light chain in the intracellular environment is dependent on the cell type, with those tissues more abundant in free iron having a greater heavy chain component whilst those that have an iron storage role have a higher light chain ratio [108, 111]. Intracellularly, both FTH1 and ferritin light chain localise mainly to the cytoplasm. Both *FTH* and *FTL* possess IREs (iron regulatory element) in the 5' UTR region. These IREs bind iron responsive proteins (IRP), which act as transcription repressors [111, 112]. Intracellular levels of iron and variations in redox haemostasis modulate IRP binding and subsequent transcription of the ferritin subunits. *FTL* is more tightly regulated by intracellular iron than *FTH* [113]. Both *FTH* and *FTL* also have upstream antioxidant responsive element (ARE) and are upregulated by the transcription factors NRF2 and JunD in conditions of oxidative stress [114]. Hence cytosolic FTH and FTL levels are tightly controlled.

In 2001, a novel member of the ferritin family was described: mitochondrial ferritin [115]. This is encoded by the intronless *FTMT* gene on chromosome 5. This is highly similar to ferritin heavy chain and can also be incorporated into a homopolymer ferritin shell and functionally has potent ferroxidase activity. It has a specific leader sequence for targeting to the mitochondria which is cleaved on entry into the mitochondria, reducing the 30kDa precursor to 22kDa. It is postulated to have a role in iron homeostasis in this organelle. Approximately, 79% of the coding regions overlap with FTH (with conservation of the amino acids required for ferroxidase activity) and 63% overlap with FTL [115, 116]. However, unlike FTH and FTL, mitochondrial ferritin does not have an IRE.

1.6.8.4 Evidence for nuclear localisation of ferritin heavy chain

Nuclear FTH1 has been observed in avian corneal epithelial cells in response to ultraviolet-induced damage [117, 118]. In addition, the presence of nuclear FTH1 has been described in human hepatocytes and astrocytoma cells in response to oxidative stress, with a dose related increase response seen in the latter cell type [119]. The bulk of nuclear ferritin in human astrocytoma cells is within the soluble nuclear fraction with some associating with the nuclear matrix [120]. In avian corneal epithelial cells nuclear ferritin is found throughout the nucleus but not in the nucleolus [118].

Only FTH1 has been observed in the nucleus. Studies using a variety of constructs for FTH1 and light chain describe only the FTH1 constructs localising to the nucleus [120]. This preferential translocation is postulated to be related to the presence of O-glycosylation sites in FTH1 and alloxan blocking of these sites in astrocytoma cells reduced the presence of nuclear ferritin heavy chain [120]. It is not clear whether the heteropolymer is able to pass through the nuclear pore or whether it is broken into its constituent parts and then translocated. The intact ferritin complex would be of approximately 450kDa with an estimated external diameter of 13 nm. Although the resting nuclear pore diameter is an estimated 9nm, during active transport a diameter of approximately 39 nm can

be achieved [121]. siRNAs targeting FTH1 deplete both cytoplasmic and nuclear FTH1 indicating that nuclear FTH1 is not distinct from that observed in the cytoplasm [120].

FTH1 was demonstrated to be transported into the nucleus via the nuclear pore; wheat germ agglutinin (which blocks the nuclear pore) prevents nuclear translocation of FTH1 [119]. This translocation is an energy dependent process as apyrase ATP-depletion prevents the nuclear translocation of FTH1 [119]. FTH1 does not have a nuclear localisation signal and translocation into the nucleus is an importin-independent process [122]. In the avian corneal epithelium a nuclear transport molecule named ferritoid (which contains a *SV40-type* nuclear localisation signal and a second region similar to ferritin heavy chain) has been identified [117, 123]. SV40 nuclear localisation signals are classic nuclear localisation signals, named after their initial description in the SV40 large T antigen. Ferritoid is highly specific to avian corneal epithelium and no other chaperone proteins have been identified in human cells.

Supercoil relaxation assays in human astrocytoma cells demonstrate that nuclear FTH1 protects against DNA fragmentation in response to oxidative stress [119]. Similarly, avian corneal epithelial cells with nuclear ferritin had significantly less DNA breakage than the other cells types examined [117].

1.6.8.5 Ferritin Heavy Chain in disease

There have been no identified conditions associated with human mutations in ferritin heavy chain. A knockout mouse model results in lethality in the embryonic stage [124]. Heterozygous mice are healthy and do not differ significantly from their litter mates. Studies have been conducted on a conditional *Fth*-knockout mouse using a Cre-inducible system [125]. Complete loss of ferritin heavy chain was achieved in the liver, spleen and bone marrow (adrenal and neural tissue were not studied). On an iron-rich diet, irreversible hepatocyte damage was observed associated with significant DNA strand breaks demonstrated on TUNEL assays. Furthermore, *Fth*-knockout mouse

embryonic fibroblasts demonstrated a significant increase in the free iron pool and reactive oxygen species (ROS). The mitochondrial depolarisation which preceded cell death in this model appeared to occur as direct consequence of iron-mediated ROS formation [125].

Hereditary ferritinopathy in humans is associated with mutations in ferritin light chain [126]. The associated clinical phenotype includes a severe movement disorder and histopathology reveals the presence of nuclear and cytoplasmic inclusion bodies in glia and neurons.

1.6.8.6 Localisation of FTH1 in triple A syndrome patient dermal fibroblasts

Unlike control cells, no nuclear FTH1 is apparent in triple A syndrome patient dermal fibroblasts or lymphocytes [107]. Additionally, when cells are transfected with His-tagged FTH1, very little nuclear immunofluorescence was seen. However, when SK-N-SH neuronal cells (which express very low levels of endogenous AAAS mRNA) are co-transfected with both FTH1 and ALADIN, FTH1 is readily visible in the nucleus, implicating ALADIN in the nuclear localisation of FTH1 (Figure 1.3).

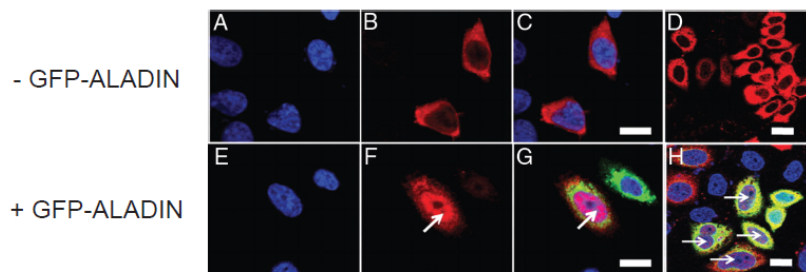


Figure 1.3. FTH1-V5-His localises to the nucleus in cotransfected SK-N-SH cells. SK-N-SH cells were either transfected with the pcDNA3.1-FTH1-V5-His vector alone (A–D) or cotransfected with the pcDNA3.1-FTH1-V5-His and pEGFP-AAAS vectors (E–H). Images show the localisation of DAPI nuclear stain (blue, A and E) and localisation of the V5-His-tagged FTH1 (red, B and F). The V5-His-tagged FTH1 has a mainly cytoplasmic localisation when transfected alone (B–D) but is clearly visualised in the nucleus when coexpressed with GFP-ALADIN (F–H) (arrows). Images are $73.1 \times 73.1 \mu\text{m}$. Scale bars, $10 \mu\text{m}$. *Images reproduced with authors' permission (Storr et al, 2009).*

1.6.9 Oxidative stress and the triple A syndrome

Several studies to date indicate that oxidative stress may be involved in the pathogenesis of triple A syndrome. The first of these involves study of cultured dermal fibroblasts from a triple A syndrome patient with the mutation, 1482Sf, by Hirano and colleagues [127]. The mutant protein failed to target appropriately to the NPC. The patient fibroblasts were demonstrated to be hypersensitive to oxidative stress (treatment with L-buthionine-(S,R)- sulfoximine) with increased frequency of DNA single-strand breaks [127]. Additionally, decreased nuclear accumulations of aprataxin (DNA repair protein for DNA single strand breaks) and DNA ligase I were noted in the 1482Sf fibroblasts. Transfection of wild-type *AAAS* restored the nuclear import of these DNA repair proteins [127]. Fusion of classic nuclear localisation signals (SV40 nuclear localisation signals) to these DNA repair proteins also allowed successful nuclear import of these proteins in patient dermal fibroblasts with reduced oxidative stress-induced cell death [128]. However, successful nuclear import of both aprataxin and DNA ligase I did not fully restore the survival of patient fibroblasts to the level of the positive control of wild-type ALADIN suggesting the presence of other proteins that may be selectively imported by ALADIN.

A lack of FTH1, which has potent ferroxidase activity, was noted in the nuclear fractions of triple A syndrome patient dermal fibroblasts suggesting ALADIN-dependent nuclear import of FTH1 [107]. Co-transfection of human neuronal cells with *AAAS* and *FTH1* allowed successful nuclear import of FTH1 (Figure 1.3). Protection against oxidative stress was demonstrated in this neuronal cell line with transfection of *AAAS* or *FTH1*, with maximal protection conferred with transfection of both proteins [107] (Figure 1.4).

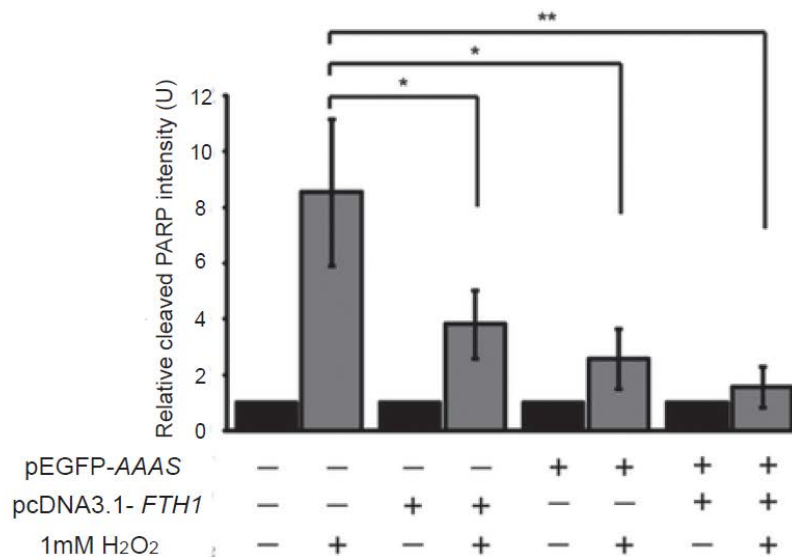


Figure 1.4. FTH1 and ALADIN are protective against oxidative stress. Densitometric analysis of Western blot of SH-SY5Y cells transfected with pEGFP-AAAS, pcDNA3.1-FTH1, or pEGFP-AAAS and pcDNA3.1-FTH1 and treated with or without hydrogen peroxide (H₂O₂). H₂O₂ treatment causes an increase in PARP cleavage relative to untreated controls, and cotransfection of pEGFP-AAAS and pcDNA3.1-FTH1 reduces the amount of PARP cleavage relative to untransfected cells. Analysis showed a significant ($p = 0.01$) decrease in cleaved PARP between untransfected cells and cells cotransfected with pEGFP-AAAS and pcDNA3.1-FTH1. Values are intensities of cleaved PARP relative to GAPDH relative to untreated controls (dark bars). *, $p < 0.05$; **, $p < 0.01$; $n = 4$. Images reproduced with authors' permission (Storr et al, 2009).

Triple A syndrome dermal fibroblasts have a significant baseline increase in reactive oxygen species (ROS) in comparison to wild-type fibroblasts [129]. This is further exacerbated by the inducer of oxidative stress paraquat. Mitochondrial networks were found to be more extensive in triple A syndrome fibroblasts, though the metabolic activity and maximum ATP synthesis were unchanged. The importance of this change in mitochondrial morphology is unclear. The mRNA expression of several well-known anti-oxidant enzymes was also studied with equivocal results [129]. A significant increase in superoxide dismutase 1 was seen in comparison to wild type fibroblasts, whilst catalase levels were decreased in triple A patient fibroblasts. There were no clear differences observed in superoxide dismutase 2 or glutathione reductase levels compared with controls. Triple A syndrome

patient fibroblasts exhibited features of senescent cells suggesting they may undergo stress-induced premature senescence [129].

1.6.10 Other research to date

1.6.10.1 *Aaas*-knockout mouse

Aaas-knockout (*Aaas*^{-/-}) mice have been established by Angela Huebner's group using standard homologous recombination in mice from a 129/01a-C57Bl/6 mixed background [67]. *Aaas* was inactivated by integration of a neomycin resistant cassette replacing the start codon by homologous recombination.

With regards to phenotype, the *Aaas*^{-/-} mutants were largely indistinguishable from wild-type. The knockout mice were observed to have a slightly lower body weight at 10 weeks postnatally in the males and 8 weeks postnatally in the females. Achalasia was not observed in the knockout animals. The development appeared normal with the oldest male *Aaas*^{-/-} mutant being 2.9 years and the oldest female 2.7 years. Neurological observations were made in those mice above 7.5 months. Reflexes were described as the same as wild type with no significant difference in motor coordination. The *Aaas*^{-/-} null mutants were observed to be slightly less active than wild-type, spending more time resting. Interestingly, the female *Aaas*^{-/-} mice were infertile.

Hormonal analysis conducted included baseline ACTH and corticosterone measurements in both *Aaas*^{-/-} and wild type mice at 11 months, with no significant difference observed. Histology revealed no gross abnormality of any of the organs studied. The adrenals, ovary, testes, oesophagus, pituitary and peripheral nerves had similar features to the wild-type. Infertility in the female *Aaas*^{-/-} mice was postulated to be related to problems with the maturation of oocytes. Ultra structurally, there were no observable differences to the NPC (using kidney and liver tissue). In addition, no NPC structural differences were seen by immunocytochemistry of embryonic dermal fibroblasts.

In summary, the *Aaas*^{-/-} mice failed to show a phenotype analogous to triple A syndrome patients. Possibilities to consider include functional redundancy of ALADIN in mice. ALADIN's function at the NPC may be species-specific, certainly species-specific function(s) of nucleoporins have been demonstrated with other Nups [96, 97]. One also needs to consider that these mice were maintained in pathogen-free conditions and it is possible that phenotypic features could emerge with stress particularly if oxidative stress is imposed. Finally, complete absence of ALADIN, as would be the case in the *Aaas*^{-/-} mouse model, may be less harmful than the presence of a mutant, mislocalised protein. This could potentially be tested using 'knock-in' approaches where mutations are inserted in the mouse *Aaas* gene, allowing for a more faithful genetic model of the human condition. However, two naturally occurring mutations leading to triple A syndrome suggest that a toxic gain of function is unlikely; 43C>A in exon 1, leads to aberrant splicing and hence a predicted complete absence of the protein and L25P which leads to normal localisation of the protein to the NPC, still cause the disease phenotype and [94].

1.6.11 Triple A syndrome summary

Triple A syndrome is a rare autosomal recessive condition incorporating adrenal insufficiency with neurodegenerative disease. In the main, the condition is caused by mutations in *AAAS*, encoding the nuclear pore complex protein ALADIN, of which relatively little is known. The expression of *AAAS* is enriched in the tissues affected by the disease. Interestingly, the *Aaas*^{-/-} mouse does not recapitulate the human phenotype, suggesting functional redundancy in the mouse model and perhaps a species-specific role for this nucleoporin. *In vitro* studies using patient dermal fibroblasts suggest nuclear import of specific cargo-(es) may be defective, rendering ALADIN deficient cells susceptible to oxidative stress. The precise impact of ALADIN loss of function in the adrenocortical and neuronal environment, tissue types affected by the disease, is not known.

1.7 Familial glucocorticoid deficiency (FGD)

Familial glucocorticoid deficiency was first described in 1959, in a report of 2 sisters with Addison's disease without hypoaldosteronism, and involves a hereditary unresponsiveness to ACTH [130]. This rare autosomal recessive disorder manifests in most cases as glucocorticoid and adrenal androgen deficiency.

1.7.1 FGD clinical features, diagnosis and patient management

Affected individuals in the case of FGD type 1, 2 and 3 commonly present in the first 2 to 3 years of life [131]. Typically they have deficient production of cortisol in the presence of high ACTH levels. Adrenal androgen production is also affected. Mineralocorticoid production is relatively unaffected and renin and aldosterone levels are normal as patients have an intact renin-angiotensin axis.

Clinical features are reflective of the low cortisol and raised ACTH levels. Hypoglycaemia is a common feature, which, if untreated, can lead to neurological sequelae [132, 133]. Clinical presentation includes failure to thrive in the neonatal or early childhood periods and an increased susceptibility to infections. This disorder can lead to significant morbidity and is potentially fatal if untreated. Patients commonly present with hyperpigmentation, a consequence of overstimulation of melanocortin 1 receptor (MC1R) by proopiomelanocortin products. This hyperpigmentation may be present at birth or may develop over time. Interestingly, lack of hyperpigmentation was seen in a recent case of FGD involving the coexistence of a homozygous, inactivating *MC1R* variant which has previously been associated with red hair and fair skin [134]. Indeed genetic variants in *MC1R* are detected in over 80% of individuals with red hair and fair skin who tan poorly [135]. Thus one must consider that hyperpigmentation seen in FGD may be less common in affected individuals from white ethnicities more predisposed to mutations in *MC1R*. A lack of adrenarche in affected individuals is seen as a consequence of adrenal androgen deficiency, although puberty and fertility are unaffected as the hypothalamic-pituitary-gonadal axis remains intact [136]. Other clinical

features can be specific to a particular FGD subtype depending on the underlying aetiology. These are described further below.

At diagnosis, ACTH levels are extremely high, often greater than 1000 pg/ml (normal range <80 pg/ml). A standard ACTH stimulation test will confirm an impaired cortisol response (<500 nmol/l) and verify adrenal insufficiency. Treatment involves glucocorticoid replacement usually with hydrocortisone. In children doses of 8 to 10 mg/m²/day and in adults 20 mg hydrocortisone are given daily in three to four divided doses. Importantly, ACTH levels often remain high during the treatment of FGD and it is essential that only physiological replacement doses are given rather than higher doses in an attempt to suppress ACTH. Overzealous replacement can have adverse effects particularly in children, where the impact of steroid therapy on growth needs to be considered. It is also essential that hydrocortisone dosing is increased 2 to 3-fold during times of stress. It is crucial to ensure the patient and their family have adequate education about when and how to increase hydrocortisone doses and in the administration of emergency intramuscular hydrocortisone or hydrocortisone suppositories.

1.7.2 FGD type 1; *MC2R* gene mutations

The isolated nature of the adrenal defect in FGD, appearing to predominantly affect the ACTH dependant zones of the adrenal, indicated that a receptor defect was responsible. Cloning of the ACTH receptor gene (melanocortin 2 receptor, *MC2R*), in 1992, allowed this theory to be addressed [137]. In 1993, the first mutation in *MC2R* was discovered in two siblings with FGD, by direct sequencing of the gene [138]. A single base change causing an amino acid substitution (p.S74I) in the receptor was associated with the disease. Since this initial discovery, over forty mutations in *MC2R* have been described [139] (Figure 1.5). The *MC2R* mutations, identified in cases of FGD, result in loss of receptor function. Only one activating mutation of *MC2R* has been reported (p.F278C); a rare mutation discovered in an individual with cyclical Cushing's syndrome [140].

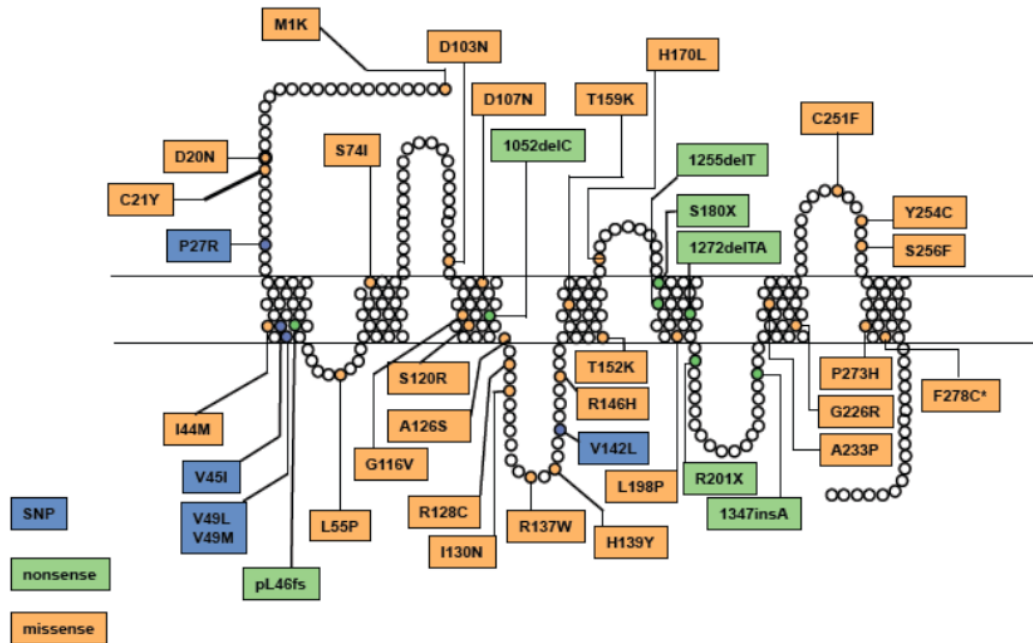


Figure 1.5. Schematic diagram demonstrating all mutations in *MC2R* associated with FGD type 1. These comprise missense mutations (in orange), likely benign polymorphisms (in blue) and nonsense or frameshift mutations (in green). *Image reproduced with authors' permission [141].*

MC2R, together with the other melanocortin receptors (1, 3, 4 and 5), form a distinct subfamily of transmembrane G-protein coupled receptors. These mediate the signalling of hormones derived from the cleavage of proopiomelanocortin (POMC). Five MCRs with varying roles have so far been described. MC1R is found in the skin and hair where it is an important regulator of pigmentation, responsible for the production of dark eumelanin pigment and the tanning response [135]. MC3R and MC4R contribute significantly to the regulation of food intake and energy homeostasis [142-144] and MC5R, whilst highly expressed in embryogenesis, is thought to be involved in exocrine function in adults [145, 146]. MC1, 3, 4, 5R respond to all POMC products (ACTH, α -, β - and γ -MSH) with varying preference. MC2R however responds to ACTH alone [147].

MC2R is the smallest member of the family, encoded by an intron-less gene mapped to the distal end of chromosome 18 and comprising 297 amino acids. *MC2R* mRNA is present in all three adrenocortical zones but ACTH predominantly activates receptors in the zona fasciculata [137]. In

response to ACTH binding, MC2R becomes active and in turn activates the heterotrimeric G-protein complex which activates adenylase cyclase. This in turn catalyses cAMP generation with subsequent activation of protein kinase A, required for expression of steroidogenic enzymes and consequently cortisol production in the zona fasciculata. ACTH activation in the zona reticularis results in the production of adrenal androgens [136]. Several cAMP responsive element (CRE)-like sequences are found in the promoter region of *MC2R* and ACTH is thus able to upregulate its own receptor, increasing receptor numbers in the zona fasciculata and reticularis. Interestingly some studies suggest a rare involvement of MC2R in cortisol-secreting adrenal tumours [148].

Postmortem histological analysis of adrenal glands of affected individuals reveals atrophy of the ACTH-dependant zona fasciculata and reticularis. Where these zones normally comprise 90% of the adrenal cortex, only a narrow band of fibrous tissue remains [149, 150]. This is unsurprising given the important trophic effect ACTH has on the adrenal cortices. The angiotensin II-dependent zona glomerulosa is relatively well preserved. Similar histological findings are seen in the *Mc2r*^{-/-} mouse [151]. Knockout resulted in neonatal lethality in three quarters of the mice, thought to be a consequence of hypoglycaemia. Similar to affected human patients, knockout of *Mc2r* in mice leads to high levels of ACTH, unresponsiveness to ACTH, and hypoglycaemia after prolonged fasting. However in contrast to the human phenotype, these mice are also found to be aldosterone deficient. A mild salt-losing phenotype has been described in patients with severe loss of function mutations in MC2R, however this tends to be a transitory phenomenon [152, 153].

An additional feature seen in the FGD 1 phenotype is tall stature, the mechanism for which is unclear [154]. It is possible that either ACTH or cortisol deficiency is responsible for excessive growth. It has been suggested that excess ACTH stimulates melanocortin receptors in the growth plate, stimulating growth [155]. Hypertelorism, marked epicanthic folds and frontal bossing are also noted [154]. Another proposal is that cortisol inhibits the synthesis of IGF (insulin-like growth factor) binding protein 6 (IGFBP6), which binds to and prevents the actions of IGF II in the osteoblast [156]. Thus it is

possible that cortisol deficiency could result in a lack of IGFBP6 inhibition and hence increased growth. Early diagnosis and glucocorticoid replacement in patients appears to prevent excess growth.

Mutations in *MC2R* account for 25% of cases of FGD, indicating that the condition is genetically heterogeneous [131]. The majority of *MC2R* mutations lead to defective trafficking of the receptor from the endoplasmic reticulum to the plasma membrane [157].

1.7.3 FGD type 2; *MRAP* gene mutations

Defective trafficking of *MC2R* to the cell surface results in disrupted ACTH signalling and it became apparent that a further factor was required for this process, as evidenced by the difficulty in expressing *MC2R* in cells of a non-adrenal origin (heterologous cells) [158]. These studies implied that an adrenal-specific factor was required. To identify this factor a whole genome scan by single nucleotide polymorphism (SNP) array genotyping was carried out in one consanguineous FGD family and mapped a locus to chromosome 21q22.1 [159]. RT-PCR of candidate genes within the region identified a single adrenal specific gene, *C21ORF61*. Further genetic screening of an FGD patient cohort who did not carry *MC2R* mutations identified several nonsense and splice site mutations in *C21ORF61* [159]. These mutations were predicted to result in complete absence or a short truncated version of the gene product. This protein, named fat tissue-specific low molecular weight protein, of unknown function, had previously been identified in differentiating adipocyte cells [160]. It was seen to be predominantly expressed in the adrenal and to a lesser extent expression was also seen in other tissues including the brain, thyroid, ovary, testis and breast [159]. It was demonstrated to interact with *MC2R* and furthermore its co-expression with *MC2R* in heterologous cells allowed for delivery of a significant proportion of the ACTH receptor to the cell membrane [159]. This protein was renamed melanocortin receptor 2 accessory protein (*MRAP*) and mutations in *MRAP* account for a further 20% of cases in FGD, FGD type 2 [131]. Patients with FGD 2 tend to present with disease in early infancy. Clinically, unlike FGD 1 patients, FGD 2 patients do not have tall stature and this is

thought to be related to the earlier diagnosis and earlier institution of replacement glucocorticoids. The first missense mutations, p.V26A and p.Y59D, in *MRAP* have also been described leading to a later onset, milder form of the disease [131]. Altogether twelve mutations in *MRAP* have been described [131].

MRAP comprises 172 amino acids and forms a stable anti-parallel homodimer at the plasma membrane and endoplasmic reticulum (ER) [161]. It is a small single transmembrane protein which forms a stable heterodimer with *MC2R* at the plasma membrane [162]. Further functional analysis has demonstrated that this dual topology of *MRAP* is essential to its function since deletion of the residues responsible for the antiparallel dimerization result in failure of trafficking of *MC2R* to the cell surface. *MRAP* directly interacts with *MC2R* at the ER and is responsible for correct folding or trafficking of the receptor to the plasma membrane. mRNA levels of *MC2R* and *MRAP* are regulated by ACTH [163, 164]. Two isoforms of *MRAP* (*MRAP-α* and *MRAP-β*) have been described with differing C terminals. Exons 3, 4 and 5 encode the 172 amino acid *MRAP-α* with alternative splicing of exons 3, 4 and 6 resulting in the 102 amino acid *MRAP-β* isoform. The importance of the variation in C terminal and the precise role of the two isoforms remains unclear. It has been suggested that the C-terminus may determine the localisation of *MRAP*; the α -isoform localising mainly to the ER and the β isoform exhibiting strong localisation to the plasma membrane [165]. An *MRAP*-knockout mouse model has yet to be described in the literature. A homologue of *MRAP* has recently been described, *MRAP 2*, sharing 39% sequence identity within the N-terminus [166]. *MRAP 2* is seen in the developing adrenal but in very low levels in adulthood, as demonstrated in rodents [167]. It also forms a heterodimer with *MC2R* [166], although the role of this heterodimer needs to be fully elucidated and its importance in the adrenal has yet to be determined.

The predominant mechanism of disease in FGD, causing 50% of cases, is therefore related to defective ACTH signalling in the adrenal, a consequence of mutations of *MC2R* or its accessory protein encoded by *MRAP*.

1.7.4 FGD type 3; Non-classical lipid congenital adrenal hyperplasia

A locus on chromosome 8 had previously been linked to the FGD-disease phenotype in 3 families who were mutation negative for *MC2R* and *MRAP* mutations. Analysis by single-nucleotide polymorphism array of the genotype of one of these individuals revealed a large region of homozygosity encompassing the steroidogenic acute regulatory protein gene, *STAR*. A homozygous *STAR* mutation, p.R192C, was identified in this patient and his 3 siblings [168]. Screening of 79 families within the FGD cohort revealed the presence of a previously described homozygous p.R188C *STAR* mutation in a further nine individuals from four other families [168]. *STAR* mutations have accounted for approximately 10% of cases within our FGD cohort [131].

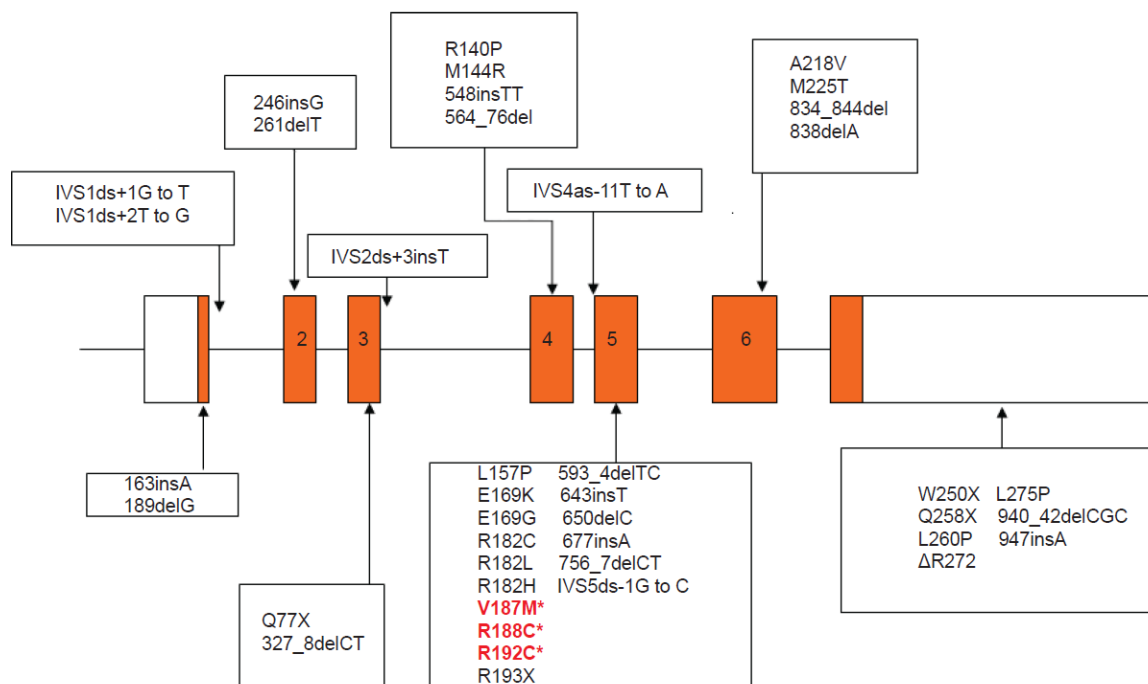


Figure 1.6. Schematic diagram demonstrating mutations in *STAR* associated with adrenal insufficiency. The mutations in red are those that have been identified in association with FGD.

STAR in conjunction with a multi-component complex facilitates the transport of cholesterol across the inner mitochondrial membrane, following which cholesterol is metabolised along the steroidogenic pathways [1]. Over 40 mutations have been described in *STAR*, mainly located in the C terminal domain of the protein encoded by exons 5, 6 and 7 (Figure 1.6). These mutations cause

lipoid congenital adrenal hyperplasia (LCAH; OMIM #201701), an autosomal recessive disorder characterised by adrenal insufficiency in early infancy together with gonadal insufficiency. The absence of foetal testosterone/ dihydrotestosterone production can lead to a failure of androgenisation and a female phenotype in 46, XY individuals. Whilst affected females can undergo normal puberty, they develop a progressive hypergonadotropic hypogonadism. With regards to pathological mechanism, Miller's two hit hypothesis describes mutations in *STAR* ablating the acute steroidogenic response, leading to low circulatory steroid levels and a compensatory increase in ACTH, angiotensin II and LH [169]. This in turn leads to increased cellular uptake of LDL cholesterol and *de novo* lipid deposition in steroidogenic cells which gradually have an impact on normal cell function over time [169]. The zona glomerulosa and fasciculata accumulate cholesterol esters after birth and the foetal testis is affected early in gestation due to chorionic gonadotropin stimulation. In contrast, the foetal and childhood ovary are relatively protected until after puberty when cholesterol deposits accumulate with LH and FSH stimulation of steroidogenesis. Investigation of *Star*^{-/-} mice demonstrates the hierarchy of involvement of the different steroidogenic organs and pathological findings recapitulate the human phenotype [170]. Newborn knockout mice lack normal adrenal gland architecture with abundant lipid deposits although they still demonstrate some residual capacity for corticosteroid production. Progressive changes are seen and the zona fasciculata and glomerulosa are particularly affected, with relative preservation of the zona reticularis. By 16 weeks, adrenocortical hyperplasia akin to the human phenotype is seen. Whilst ovaries are normal at birth, worsening histopathology is seen with age, beginning at the time of puberty with stromal cells particularly affected. In males, residual biosynthesis of androgens is suggested with normal appearances of the epididymis and vas deferens (both derived from the wolffian ducts) and mature spermatids within the epididymis. However at 4 weeks of age, delayed germ cell maturation is seen with increased apoptosis in developing spermatocytes. In contrast, the seminal vesicles and prostate are markedly hypoplastic with absence of virilisation of the external genitalia; suggesting a more

significant impairment of the endocrine actions of the androgens compared to the paracrine actions in the structures closer to the testes.

The p.R192C and previously described p.V187M and p.R188C mutations in humans confer a milder isolated adrenal phenotype, specifically involving glucocorticoid deficiency [168, 171]. The relative sparing of mineralocorticoid production is believed to reflect the lower rate of production of aldosterone in comparison with cortisol, thereby sparing the zona glomerulosa from excessive lipid accumulation. Whilst preserved gonadal function has allowed for normal male and female pubertal development in the patients, some of the adults have progressed to compromised fertility. The Val187 and Arg188 contribute to the sterol-binding pocket of the protein and modelling suggests a steric inhibition of cholesterol binding in the case of the p.V187M mutation [172]. With regards to the p.R188C mutation, the formation of the normal salt bridge present between residues R188 and E169 is prevented, instead a weaker bond between residues T167 and C188 is formed. This may be sufficient to preserve the shape of the binding pocket for cholesterol transport and functional analysis of the p.R188C and p.V187M mutants revealed preservation of greater than 20% normal cholesterol binding activity [172].

STAR mutations associated with the FGD-like phenotype demonstrate the spectrum of clinical phenotype associated with *STAR* mutations, ranging from LCAH through to a phenotype of adrenal dysfunction, similar to FGD, with or without disorders of sexual development.

1.7.5 FGD type 4; defects in DNA replication

A variant of FGD has recently been described in a genetically isolated Irish traveller population by Hughes and colleagues [173]. Affected individuals, seven children from three kindreds, had the characteristic finding of isolated glucocorticoid deficiency with normal renin and aldosterone levels. Patients however appeared to have a period of normal adrenal function, with onset of disease in childhood rather than infancy as is classical in FGD. Additional features described included low birth

weight and short stature (short for mid-parental height standard deviation score (SDS)) in association with an intact growth hormone/IGF1 axis. In addition, a specific natural killer cell deficiency is described, with one individual demonstrating an increased susceptibility to infection, in particular respiratory infections. Chromosomal fragility is also described. Patients were mutation negative for known causes of FGD. In common with other inherited causes of FGD, an autosomal recessive pattern of inheritance was seen. SNP genotyping in 8 patients followed by targeted exome sequencing in 1 patient identified a variant (c.71-1insG) in minichromosome maintenance-deficient 4 (*MCM4*) that segregated with the disease. MCM4 is a DNA replicase and forms a highly conserved hexameric complex with MCM2, MCM3, MCM5, MCM6 and MCM7. This complex, known as the minichromosome maintenance complex, is required for the initiation and elongation phases of eukaryotic DNA replication. The mutation identified was predicted to result in a severely truncated protein (p.Pro24ArgfsX4), however western blotting of patient lymphocytes revealed conservation of the minor 86 kDa form of the protein with absence of the major 96 kDa isoform [173]. Further investigation suggested that this smaller isoform may be produced by an alternative translation start site, the third in frame ATG, leading to absence of the N terminus of the full length protein, but leaving essential conserved C-terminal domains intact. Independently, Gineau and colleagues also identified the same mutation in six other related patients from the Irish traveller population who presented with a similar clinical phenotype; the patients described in this study were however all immune compromised [174]. Their work demonstrated conservation of formation of the MCM2-7 complex, indicating that the N terminal domain is not necessary for formation of the MCM2-7 complex and DNA binding. However SV40-immortalised human fibroblasts from controls and patients demonstrated an effect on DNA replication with an impact on the mitotic phase. Furthermore with compromise of replication, DNA becomes more prone to breakage and increased genomic instability was demonstrated in patient-derived cells (as determined by the assessment of chromatid breaks and chromosomal exchanges).

Interestingly, genetic knockout of *Mcm4* in mice is embryonically lethal [175]. It is proposed that the relatively mild phenotype seen in humans is a consequence of preservation of the smaller isoform of MCM4. For further interrogation of the adrenal phenotype a viable *Mcm4* depleted mouse model was used; mice with a hypomorphic *Chaos3* mutation [176]. The F345I mutation in this model affects a well conserved amino acid located close to the zinc finger motif, important for interactions between MCMs but represents a viable, defective allele of *Mcm4*. This *Mcm4* depleted mouse model, demonstrated abnormal adrenal morphology with atypical spindle shaped cells populating the zona fasciculata with reduced expression of steroidogenic cells [173]. These spindle shaped cells were positive for GATA-4 (a transcription factor not usually present in the adult adrenal) and Gli1 (characteristic of cells from the mesenchymal adrenal capsule). The normal architecture of the capsule was lost and it is hypothesised that these cells are of capsular origin, entering the cortex but failing to differentiate into steroidogenic cells instead activating GATA-4 expression. This population of cells displace normal steroidogenic cells thus compromising steroidogenic output. The *Mcm4* depleted mice demonstrate severe growth failure and increased susceptibility to the development of mammary tumours, histiocytic sarcomas and lymphomas [176]. So far no form of cancer has been detected in patients.

MCM4 may therefore play a role in adrenal stem cell differentiation and defective function may prevent adrenal capsular cells from differentiating into steroidogenic cells. This cohort of patients presenting with an FGD-like phenotype has highlighted the potential role of replicative stress on primary adrenal insufficiency.

1.7.6 FGD type 5; defects in antioxidant pathways

In 2012, linkage to a locus on chromosome 5 was identified in 3 consanguineous families by SNP genotyping with discovery of a mutation in nicotinamide nucleotide transhydrogenase (*NNT*, OMIM #614736) [177]. *NNT* encodes nicotinamide nucleotide transhydrogenase, a proton pump located in

the inner mitochondrial membrane [177]. Mutations in *NNT* are estimated to account for 10% of disease within our FGD cohort (Figure 1.7).

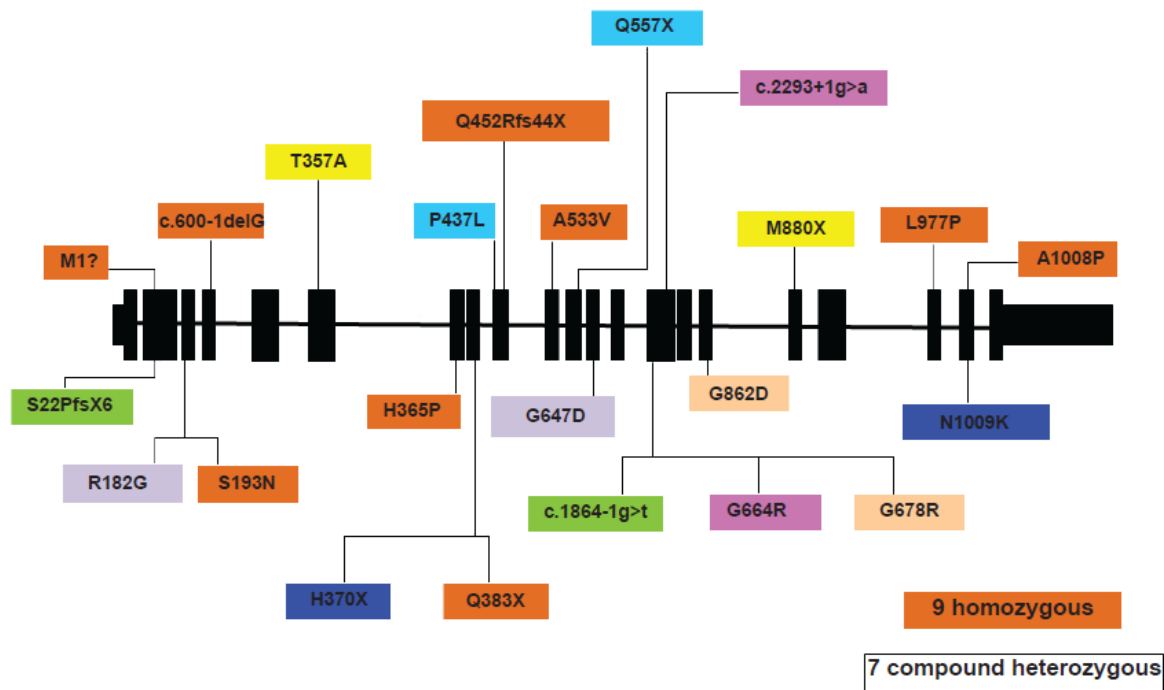


Figure 1.7. Schematic diagram demonstrating *NNT* mutations identified so far; 9 homozygous (in orange) and 7 compound heterozygous (delineated by matching colours). Image reproduced with authors' permission[131].

NNT uses energy from the mitochondrial proton gradient to regenerate NADPH from NADP⁺, using NADH produced in the tricarboxylic acid (TCA) cycle. *NNT* couples the production of NADPH to the rate of mitochondrial metabolism and the production of ROS generated by the electron transport chain. High concentrations of NADPH are required by both the glutathione (GSH) and thioredoxin (TXN) systems for detoxification of mitochondrial ROS (Figure 1.8; this system is discussed in further detail in section 1.9 and 1.10). NADPH is also utilised by the electron transfer proteins ferredoxin reductase and ferredoxin, critical for the reduction of the P450 enzymes in steroidogenesis [178]. Thus there are several mechanisms by which *NNT* deficiency may impact on steroidogenesis. *NNT* is widely expressed with high levels apparent in the adrenal glands of both humans and mice [177].

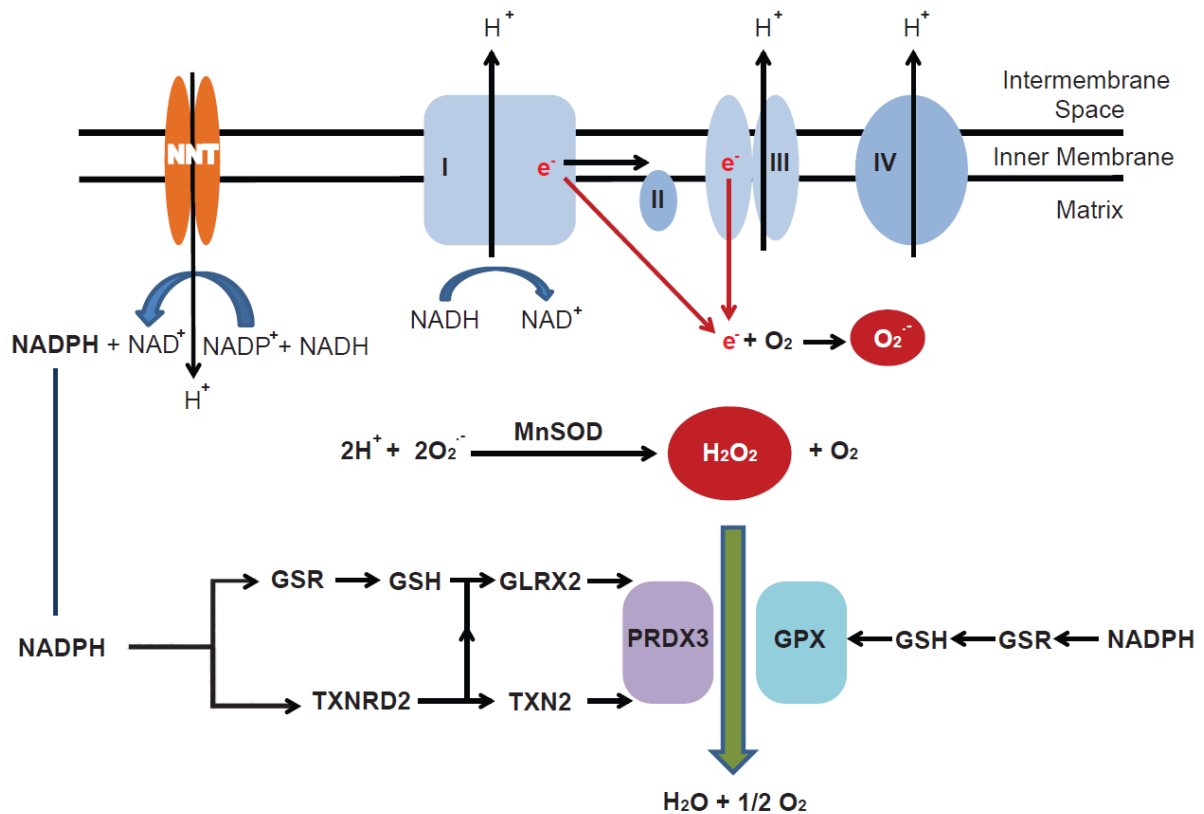


Figure 1.8. Detoxification of mitochondrial superoxide species produced during electron leak from the mitochondrial electron transport chain. The superoxide radical $O_2^{\cdot-}$, produced from electrons (e^-) leaked at complex I and III of the mitochondrial electron transport chain, can be protonated to form H_2O_2 , this process of dismutation is catalysed by MnSOD (manganese superoxide dismutase). Mitochondrial H_2O_2 is detoxified by the thioredoxin and glutathione systems, which require high concentrations of NADPH (reduced nicotinamide adenine dinucleotide phosphate) provided by NNT (nicotinamide nucleotide transhydrogenase). The flow of electron transfer from NADPH to peroxiredoxin 3 (PRDX3) and glutathione peroxidase (GPX), through the various components of the thioredoxin and glutathione systems are shown in the figure. GSR, glutathione reductase; GSH, reduced glutathione; TXNRD2, thioredoxin reductase 2; TXN2, thioredoxin 2; GLRX2, glutaredoxin 2.

A substrain of C57BL6/J mice carries a spontaneous *Nnt* mutation leading to a 5-exon deletion; partial-deletion of the first domain of NNT, which binds NADH, and four of the fourteen transmembrane domains which comprise the proton channel [179]. This substrain of C57BL6/J mice show an increased sensitivity to $O_2^{\cdot-}/H_2O_2$ particularly in the absence of mitochondrial MnSOD (SOD2) and a deficiency in both antioxidants results in death within 1 to 2 days [180] due to dilated

cardiomyopathy. Introduction of a normal copy of *Nnt* in the *Sod2*^{-/-} mice with the C57BL/6J background confers improved cardiovascular function during foetal development [181]. Adrenals from the *Nnt*-mutant substrain are noted to have slightly disorganised zonae fasciculata with higher levels of apoptosis than wild-types [177]. No differences in P450_{scc} (CYP11A1) and P450_{c11β} (CYP11B1) distribution were seen between the two substrains, however the mutant mice had lower basal and stimulated levels of corticosterone, though the deficiency was not as marked as that seen in the human disease [177]. Lentiviral shRNA-knockdown of *NNT* in the human adrenocortical H295R cell line leads to increased levels of mitochondrial ROS, a decrease in the reduced to oxidised glutathione (GSH/GSSG) ratio and increased apoptosis [177].

Extra-adrenal features have also been demonstrated in this substrain of mice. *Nnt*-mutant mice have impaired glucose tolerance with loss of glucose dependent insulin secretion and ATP production in isolated pancreatic islet cells, reminiscent of a type 2 diabetes mellitus model [179, 182]. When fed on a high fat diet, C57BL/6J mice develop obesity, hyperglycaemia and insulin resistance [183]. Interestingly, it has been demonstrated that the C57BL/6J mice expressing the truncated protein have comparable insulin secretion and glucose tolerance to the C57BL/6N mice expressing the full length wild type protein, but lower levels than other strains (C3H/HeH and DBA/2) with higher expression of *Nnt* [184]. This suggests that it is low levels of NNT rather than the specific 5 exon deletion that has the impact. This also raises the possibility that another enzyme is able to functionally compensate for the loss of NNT in the C57BL/6J mice, this could explain the relative preservation of steroidogenesis in this strain in comparison to the human phenotype. C57BL/6J mice have also been shown to have a higher sensitivity to neurotoxic agents [185]. There are currently no published reports of extra adrenal clinical manifestations in patients with *NNT* mutations, however careful clinical surveillance is required for these patients given the ubiquitous expression of NNT.

1.7.7 Familial glucocorticoid deficiency summary

FGD is a rare autosomal recessive disorder of primary adrenal insufficiency leading to ACTH resistance, glucocorticoid and adrenal androgen deficiency. Mutations in the ACTH receptor *MC2R* have been associated with disease. Further study of aetiology within the patient cohort, negative for *MC2R* mutations, led to the discovery of the melanocortin receptor accessory protein (*MRAP*) providing further valuable understanding of the mechanism of ACTH signalling in the adrenal cortex. Mutations of *MC2R* and *MRAP* account for half of the disease, therefore, classically FGD involves disruption of ACTH signalling in the adrenal. More recently novel pathways have been implicated, including defective DNA replication and mitochondrial antioxidant defence, widening the spectrum of causative mechanisms.

1.8 Steroidogenesis and reactive oxygen species (ROS) production

Reactive oxygen species (ROS) are derived from O_2 and comprise molecules with varying oxidant properties. At low concentrations ROS modulate many cellular processes through redox dependent signalling, including proliferation, differentiation, apoptosis, immune regulation and cellular adaptation to stress [186, 187]. A critical balance in redox status needs to be maintained and this is achieved by numerous interacting antioxidant pathways. Oxidative stress occurs when this balance is disturbed. ROS can then have deleterious effects on proteins, lipids, and nucleic acids, ultimately leading to cell damage and death. Oxidative stress is implicated in a plethora of conditions including neurodegenerative disorders, diabetes mellitus, cardiovascular disease and aging. Antioxidant defence mechanisms are complex and can be specific to cell type and furthermore to sub-cellular compartment. In comparison to many other tissues, including those with high metabolic demand such as the liver and brain, the adrenal cortex has high levels of several antioxidants, both enzymatic and non-enzymatic [188]. This investment is necessary given the high turnover of lipid within the mitochondria and ROS production during steroidogenesis. Disturbances in redox homeostasis within

the adrenocortical environment could therefore have an impact on steroidogenesis. This is corroborated by several disorders of adrenal insufficiency, including most recently FGD.

1.9 Reactive oxygen species generation in mitochondria

Mitochondria are responsible for the majority of cellular ROS production secondary to electron leak as a consequence of respiration. During respiration, electrons are transferred across to molecular oxygen to generate water via the four complexes of the electron transport chain. The electron proton gradient established during this process is used to generate energy in the form of adenosine triphosphate (ATP). As a result of electron leak at complexes I (NADH dehydrogenase) and III (cytochrome c reductase) a small percentage of the molecular oxygen is converted to superoxide anions ($O_2^{\cdot-}$) (Figure 1.8). These superoxide anions can be protonated to form strongly oxidant hydroxyl radicals ($\cdot OH$) which can cause oxidative modification of proteins and membrane lipids. ROS can also modify key components of the electron transport chain thereby further exacerbating electron leak and superoxide production. Dismutation, catalysed by the superoxide dismutases (SODs), reduces superoxide ions to hydrogen peroxide (H_2O_2). H_2O_2 can also contribute to oxidative stress by reacting with free metals to form $\cdot OH$. Additionally, in comparison to $O_2^{\cdot-}$ which tends to remain at the site of production, H_2O_2 readily traverses membranes into other subcellular compartments where it may impact on signalling pathways.

Several compartment specific antioxidant mechanisms are in place to target superoxide production. Cytoplasmic copper/zinc dependent SOD1 (CuZnSOD), mutations of which are associated with the neurodegenerative disorder amyotrophic lateral sclerosis (ALS) and mitochondrial matrix manganese dependent SOD2 (MnSOD) catalyse the conversion of superoxide anions into H_2O_2 (Figure 1.8). H_2O_2 has preferential reactivity towards (seleno) cysteine residues in target proteins and is detoxified by members of the glutathione peroxidase (GPX) and peroxiredoxin (PRDX) families, discussed later in section 1.10. The relative contribution of each of these enzymes may be tissue and compartment specific and determined by the source of H_2O_2 and the expression levels of each individual enzyme.

In addition to electron leak during respiration, other sources of superoxide production within the mitochondria include reactions catalysed by xanthine/xanthine oxidase, uncoupled nitric oxide synthases (NOS), NADPH-dependent oxidases (NOXs) and most pertinent to the adrenal cortex, cytochrome P450 isoforms. The P450 enzymes are involved in the biosynthesis of cholesterol derived steroidal compounds [5]. In steroidogenic tissues, the expression of P450 enzymes are approximately ten times higher than other electron transport chain proteins and electron leak in the P450 system can also contribute to ROS production [178, 189]. P450 groups are represented by microsomal cytochrome P450s present in the endoplasmic reticulum, and mitochondrial cytochrome P450s, present in the inner mitochondrial membrane. Type 1 P450 isoforms present in the mitochondria include P450_{scc} (side chain cleavage; CYP11A1), which catalyses the conversion of cholesterol to pregnenolone, and P450_{c11β} responsible for the β-hydroxylation of 11-deoxycorticosterone to cortisol (Figure 1.9). The reactions catalysed by these P450 enzymes require NADPH as a reducing agent, in addition to molecular oxygen. NADPH donates two electrons which are transferred to P450 enzymes via 2 electron transfer proteins, ferredoxin reductase (adrenodoxin reductase) and then ferredoxin (adrenodoxin) [190, 191]. Ferredoxin reductase is a FAD (flavin adenine dinucleotide) containing flavoenzyme and is able to accept both electrons from NADPH. These are then passed one at a time to ferredoxin and finally to the P450 enzymes for hydroxylation of substrates, the order of electron transfer as seen below (Hanukoglu 2006):



In a tightly coupled system, all electrons from NADPH are used in substrate hydroxylation however electron transfer within the P450 system can be relatively 'uncoupled' or 'leaky,' with the rate of electron leak variable depending on P450 subtype [178]. Up to 40% of total electron flow in the P450_{c11β} system, catalysing the final step in cortisol synthesis, are directed to ROS formation in

comparison to the 15% in the P450_{scc} system [192]. Thus steroidogenesis, particularly glucocorticoid production, contributes significantly to cellular ROS production (Figure 1.9). Type 2 microsomal P450 isoforms, catalysing all the other steps in steroidogenesis, are present in the endoplasmic reticulum and are reliant on P450 oxidoreductase and NADPH for reduction [5].

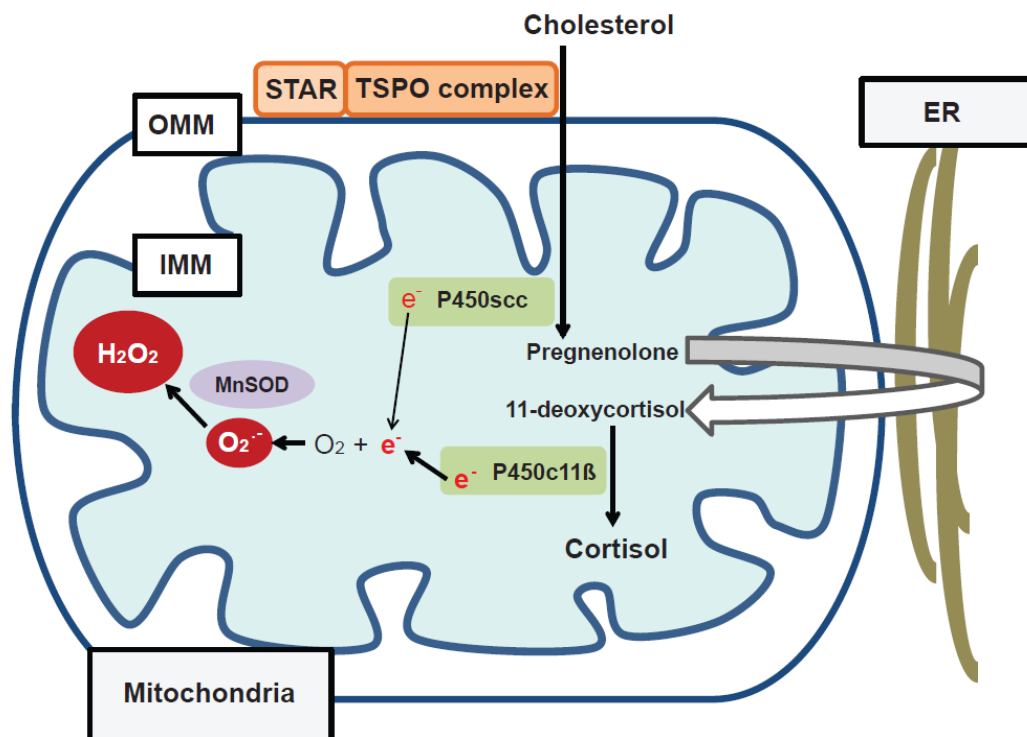


Figure 1.9. Reactive oxygen species production during steroidogenesis. The import of cholesterol from the outer mitochondrial membrane (OMM) to the inner mitochondrial membrane (IMM) is activated by STAR and mediated by the translocator protein (TSPO)-associated multi-component complex. This is followed by cholesterol side chain cleavage to pregnenolone by P450_{scc} (CYP11A1). The other steps in the steroidogenic pathway are catalysed by P450 cytochrome isoforms in the endoplasmic reticulum (ER). The final step in cortisol synthesis is catalysed by P450_{c11β} (CYP11B1) in the mitochondria, converting 11-deoxycortisol to cortisol. Electron leak during this process results in reactive oxygen species production.

1.10 Adrenal cortex antioxidant defence mechanisms

The adrenal cortex is particularly equipped to handle the increased risk of oxidative stress. Several antioxidants, both enzymatic and non-enzymatic, are highly expressed in comparison to other tissues. Ascorbic acid (vitamin C), which recycles α -tocopherol (vitamin A) radicals, is present at the highest levels in the adrenal cortex [188], indeed endogenous ascorbic acid was first isolated from adrenal tissue [193, 194]. Depletion of ascorbic acid secondary to vitamin A deficiency in rats leads to adrenocortical degeneration [195]. Other non-enzymatic antioxidants present in high levels within the adrenal cortex include vitamin A and vitamin E [196].

As previously described $O_2^{\cdot-}$ radicals are converted by SODs to H_2O_2 . Mitochondrial H_2O_2 is further reduced by two major thiol antioxidant systems dependent on reduced glutathione (GSH) and the small protein thioredoxin 2 (TXN2), each system having several associated proteins (Figure 1.8). Reduced GSH and components of the TXN2 system are seen in abundance in the adrenal cortex [196, 197]. Both TXN2 and GSH systems are dependent on the reducing power of NADPH. NADPH supply within the mitochondria is maintained by the proton pump NNT, mutations of which have recently been associated with FGD [177]. Mitochondrial NADPH stores can also be restored by mitochondrial dehydrogenases including malate dehydrogenase and isocitrate dehydrogenase.

GSH contributes significantly to maintaining a reduced cellular environment. In physiological conditions a high reduced (GSH) to oxidised glutathione (GSSG, glutathione disulphide) ratio is maintained. GSH, synthesised in the cytosol, is transported into the mitochondria by dicarboxylate and 2-oxoglutarate carriers [198]. Within the mitochondria, GSH is regenerated from GSSG by the enzyme glutathione reductase with NADPH as a cofactor. GSH acts as an electron donor for the glutathione peroxidases (GPXs), members of the selenoprotein family, which incorporate selenocysteine in their enzymatic catalytic site. These selenocysteine residues are highly redox reactive and GPXs play an important role in reducing H_2O_2 to water. Selenium (Se) content in the adrenal is high and Se is preferentially retained in this organ during selenium deficiency [199]. Se

deficiency results in a significant depletion of GPX activity and a reduction in steroidogenesis in an adrenal cell line [200]. Eight GPX isoforms have been identified in humans, GPX1 being the major isoform in most tissues, present primarily in the cytosol but also in small amounts in the mitochondria. Our unpublished data shows particularly high expression in the adrenal cortex. In the testes and spermatozoa, the mitochondrial isoform of GPX4 is the most prevalent form with depletion causing male infertility in mice [201].

Mammalian peroxiredoxins (PRDXs) also catalyse the reduction of H_2O_2 and lipid peroxides, albeit less efficiently than the GPXs. They comprise a family of 6 members, most of which (PRDX 1 to 5) use TXN as an electron donor. PRDX 3 and 5 are present within the mitochondria; PRDX3 is mitochondrial-specific and is seen in particular abundance within the adrenal cortex, with a significant role in H_2O_2 detoxification within the mitochondrial matrix. It is estimated that PRDX3 is the target for up to 90% of H_2O_2 generated within the matrix [202]. During H_2O_2 elimination, two reduced PRDX3 subunits are converted to an oxidised disulphide-linked dimer that is reduced again by the mitochondrial TXN2 system [203] (Figure 1.8 & 1.10). TXN2 in turn is maintained in reduced form by the mitochondrial selenoprotein, thioredoxin reductase 2 (TXNRD2) (Figure 1.8). In parallel, GSH can work together with glutaredoxin 2 (GLRX2) in the mitochondria to also reduce peroxiredoxins [204] (Figure 1.8).

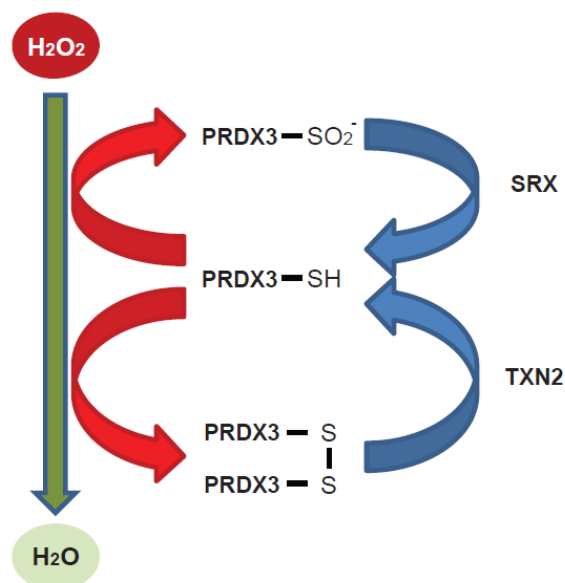


Figure 1.10. Maintenance of reduced peroxiredoxin 3 (PRDX3-SH) by thioredoxin 2 (TXN2) and sulfiredoxin (SRX). PRDX3, in its reduced form, detoxifies H_2O_2 in the mitochondria. This process induces the formation of disulphide PRDX3 which in turn is reduced back to PRDX3-SH by TXN2. With excessive H_2O_2 PRDX3 is hyper oxidised to an inactive sulfinic form ($PRDX3-SO_2^-$) and this hyper oxidation is reversed by SRX.

The catalytic cysteine (Cys) in the mammalian 2-Cys PRDX enzymes (PRDX 1 to 4) can undergo hyperoxidation to cysteine sulfinic acid ($Cys-SO_2^-$), inactivating peroxidase function [205]. This inactive sulfinic form can be reduced back to the active form by sulfiredoxin (SRX), also seen most abundantly within the adrenal gland [206] (Figure 1.10). The only PRDX to be seen in sulfinic form within the adrenal cortex is PRDX3 and this inactivation of PRDX3 has recently been demonstrated to trigger a series of events within the adrenocortical environment [206]. In both the murine and bovine models, ACTH stimulation increases inactivated sulfinic PRDX3, an effect that is prevented by metyrapone treatment, a $P450c11\beta$ inhibitor. This suggests that H_2O_2 produced in this final step of cortisol synthesis is in the main responsible for this hyperoxidation of PRDX3. Inactivation of PRDX3 results in accumulation of H_2O_2 which can diffuse into the cytosol, activating p38 mitogen-activated protein (MAP) kinase signalling pathways with subsequent suppression of STAR protein synthesis and inhibition of steroidogenesis [206]. It is proposed that this mechanism of redox signalling exerts

physiological control over steroidogenesis at the level of the adrenal gland, in addition to the well characterised negative feedback exerted by cortisol on the HPA axis.

1.11 Thesis Rationale

Triple A syndrome and FGD are disorders of primary adrenal insufficiency, characterised by ACTH resistance. Oxidative stress has been implied in the pathogenic mechanism of several conditions of primary adrenal insufficiency including ALD, triple A syndrome and most recently the FGD subtype related to *NNT* mutations.

Triple A syndrome is tissue specific and progressive, characterised by adrenal failure, alacrima, achalasia and neurodegenerative disease. Similarities between the neurological features of triple A syndrome and amyotrophic lateral sclerosis (ALS) have been recognised. The first section, aims to investigate ALADIN, the *AAAS* gene product's role in cellular defence against oxidative stress. To date, models of the disease include the *AAAS*^{-/-} mouse, which does not bear a similar phenotype to the human disease and triple A syndrome patient dermal fibroblasts. To establish an adrenal and neuronal model for the disease, representative of the major tissue types involved in the disease, I have induced shRNA lentiviral *AAAS*-knockdown in adrenal and neuronal cell lines. Detailed functional studies on these cells included investigating the effects of oxidative stress on cell growth, survival, and apoptosis. Using this *in vitro* adrenal model I interrogated specific effects of ALADIN deficiency on steroidogenesis.

In the second part of the thesis I investigated several individuals, within a consanguineous Kashmiri family with glucocorticoid deficiency, who were demonstrated to be mutation negative for the known causes of FGD to date. An autosomal recessive pattern of inheritance is suggested within this consanguineous kindred and I hypothesised that, in keeping with previous causes of FGD, a novel non-synonymous homozygous mutation would be associated with disease in this family. Whilst most cases of FGD are caused by defective ACTH signaling, newly identified mechanisms of disease

indicate an important role for replicative and oxidative stress in the pathogenesis of FGD. It is possible that other candidates within these biological pathways could be associated with disease in this family. Whole exome sequencing was utilised together with direct sequencing of potential candidate genes within this extended family.

Ultimately, I hoped to provide insights into the pathogenesis of triple A syndrome and FGD and identify potential therapeutic targets. This work could give insights into the understanding of disease mechanisms in additional cases of primary adrenal insufficiency and other neurodegenerative disorders.

Chapter 2 Materials and Methods

2.1 Cell culture

2.1.1 Cell culture conditions

H295R human adrenocortical tumour cells were obtained from Ian Mason, University of Edinburgh; HEK293T human embryonic kidney cells from the European Collection of Cell Cultures (ECACC) at the Health Protection Agency (HPA; Salisbury, UK) and SH-SY5Y human neuroblastoma cells from European Collection of Cell Cultures (ECACC) at the Health Protection Agency (HPA; Salisbury, UK).

H295R cells were cultured in GIBCO Dulbecco's Modified Eagle Medium/ F12-Ham (1:1) + GlutaMAX™-I (Sigma Aldrich, Poole, UK), supplemented with 5% NuSerum (BD Biosciences, Oxford, UK), 1% penicillin/streptomycin solution (Pen/Strep; Invitrogen, Paisley, UK) and 1% insulin-transferrin-selenium (ITS; 6.25µg/ml Insulin, 6.25µg/ml Transferrin, and 6.25ng/ml Selenous Acid; BD Biosciences, Oxford, UK). SH-SY5Y neuroblastoma cells were cultured in Dulbecco's Modified Eagle Medium/ F12-Ham (1:1) (Sigma Aldrich, Poole, UK), supplemented with 10% foetal calf serum (FCS; Invitrogen, Paisley, UK) and 1% Pen/Strep solution. HEK293T cells were maintained in DMEM (Sigma Aldrich, Poole, UK) with 10% FCS and 1% Pen/Strep. All cells were incubated in a humidified incubator at 37°C and 5% CO₂.

Harvesting of cells was carried out as follows: cells were cultured to 90% confluency in a 75 cm² (T75) flask, cells were washed twice in 5 ml of Phosphate Buffered Saline (PBS) solution (Sigma Aldrich, Poole, UK) prior to incubation with 3 ml of Trypsin/Ethylenediaminetetraacetic acid (EDTA, Invitrogen, Paisley, UK) until detachment of cells was achieved. Neutralisation of TE buffer was achieved by addition of 7 ml of media and cells were then divided into separate flasks or spun gently at 1000 rpm for 5 minutes (mins) until a cell pellet was formed and the supernatant is discarded.

2.1.1.1 Freezing cells for future use

Cell pellets from individual T75 flasks were obtained as described above. A solution of 2.7 ml FCS together with 0.3 ml Dimethylsulfoxide (DMSO; Sigma, Poole, UK) was prepared. DMSO acts as a cryoprotectant preventing cell death during the freezing process. The prepared solution was poured over the cell pellet and the pellet resuspended and the suspension divided into 2 vials for freezing. The vials were wrapped in bubble wrap and placed in a -80°C freezer overnight. The following day the vials were placed in liquid nitrogen storage.

Following recovery from storage, cell vials were placed in a water bath at 37°C for a few minutes until thawed. 5 ml of media was added to the cell suspension and transferred to a 15 ml falcon tube for centrifugation at 1000 rpm for 5 mins. The cell pellet was subsequently resuspended in fresh media for plating.

2.1.2 Lentiviral shRNA transduction

To establish AAAS-knockdown, *TXNRD2*-knockdown and scrambled control cells commercially produced puromycin-resistant synthetic shRNA (Sigma Aldrich, Poole, UK; OpenBiosystems, ThermoScientific, Leicestershire, UK; for sequences and vector maps see appendices 3 and 4) were used together with packaging vectors PMDG.2 plasmid (packaging plasmid) and the pCMV 8.74 plasmid (envelope plasmid for producing viral particles).

Introduction of small double-stranded synthetic RNA can induce sequence-specific gene silencing in mammalian systems and small hairpin shRNAs are used to achieve longer term gene-silencing. These are produced as single-stranded molecules of 50-70 nucleotides in length comprising a 5-10 nucleotide loop connecting 2 complementary 19-29 nucleotide long RNA fragments that create a double stranded stem by base pairing. This forms a stem loop or 'hairpin' structure *in vivo*. The shRNA are subsequently ligated into a vector (plasmid, lenti- or retroviral) for transfection; the shRNA used in my investigations were incorporated into a lentiviral vector. Lentiviral vectors allow

for effective transduction of non-dividing cells and lentiviruses integrate into the host genome and their genomic backbone and with life-long expression of a transgene of interest.

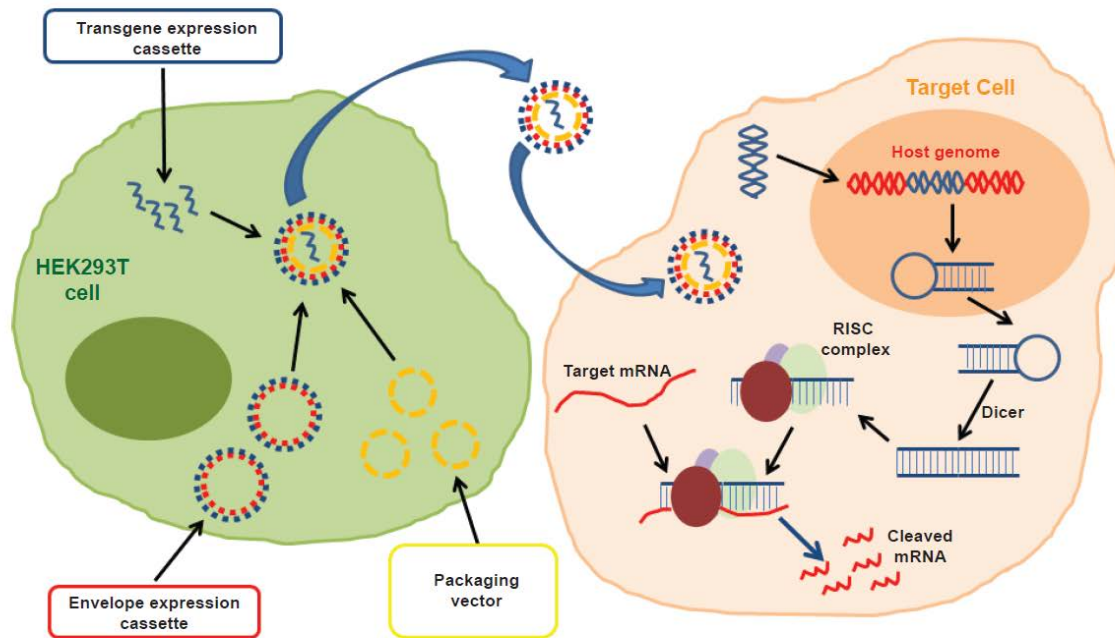


Figure 2.1. Achieving target gene knockdown using a lentiviral transduction system. Packaging of 3 plasmids into a functional lentiviral vector, used to transduce the target cell and integrate into the host genome. Once transcribed shRNA can be further processed and exported into the cytoplasm for gene silencing.

The initial transduction also requires packaging plasmids containing the viral structural genes, a vector plasmid containing the transgene and cis elements needed for integration and packaging and finally a heterologous viral (usually VZV-G) envelope encoding plasmid (Figure 2.1). This ensures that a replication incompetent virus is subsequently released which is then used to transduce the target cells for transgene expression. In the cytoplasm the shRNA are converted, by cellular nucleases and the multidomain ribonuclease DICER, into small fragments (siRNAs). DICER then loads these small RNA products (siRNA) into a large multiprotein complex called the RNA-induced silencing complex (RISC) during which the passenger strand is cleaved by the enzyme Argonaute 2 (Ago2). The

antisense strand then guides the RISC to the corresponding mRNA as a result of sequence homology and the same Ago2 nuclease cleaves the target mRNA achieving sequence specific gene silencing. With continual expression of siRNAs toxic effects can occur. To account for these controls are generated using a shRNA insert that does not target human genes. Following successful transfection of target cells I massively expanded cell lines for freezing and I endeavored to conduct experiments using cells within 8 passages of the initial transfection.

2.1.2.1 Transformation of chemically competent bacterial cells

NEB 5-alpha Competent E. Coli (High Efficiency) (New England Biolabs, Hertfordshire, UK) were used for high efficiency transformation. Competent cells were stored at -80°C. For use, one tube of NEB 5-alpha Competent E. Coli cells was thawed on ice for 5 mins. The contents of a single tube were then divided into five 1.5ml microcentrifuge tubes for use. 1-5 µl containing 50 ng of plasmid DNA was added to the cell mixture. The tube was flicked carefully 4 to 5 times to mix cells and DNA. The mixture was then placed on ice for 2 mins following which the mixture was heat shocked at exactly 42°C for exactly 30 seconds. The microcentrifuge tube was then placed on ice for 2 mins following which 950 µl of room temperature SOC Outgrowth Medium (New England Biolabs, Hertfordshire, UK) was added to the mixture. The cell mixture was centrifuged at 4000g for 4 mins following which 850 µl of supernatant was discarded. The remaining 100 µl of the cell mixture was spread onto pre-prepared LB agar plates containing 100 µg/ml ampicillin inverted and incubated overnight at 37°C for colony formation.

2.1.2.2 Preparation of LB agar plates and LB broth

LB broth (10g LB Broth (Sigma Aldrich, Poole, UK) and 500 ml distilled H₂O) and LB Agar (10g LB Broth, 10g Agar (Sigma Aldrich, Poole, UK) and 500 ml distilled H₂O) were both autoclaved prior to use. To prepare LB agar plates LB agar was simmered for 10 minutes and allowed to cool. Once cool to touch 50 ml LB agar was poured into a 50 ml falcon tube and 50 µl of 100 mg/ml Ampicillin (Sigma

Aldrich, Poole, UK) was added. 25 ml of the above was poured evenly into each plate and allowed to set with a lit Bunsen burner kept in close vicinity to help maintain a sterile environment.

2.1.2.3 Midi-prep preparation

A single colony was picked from a freshly streaked (overnight incubation) LB agar ampicillin selection plate and used to inoculate a starter culture of 3 ml LB broth containing 100 µg/ml ampicillin. This was incubated for approximately 8 hours at 37°C with vigorous shaking (300 rpm). The starter culture was then diluted 1/500 into 50 ml ampicillin selective LB broth. This was grown at 37°C for 16 hours with vigorous shaking (300 rpm). Bacterial cells were harvested by centrifugation at 4000g for 30 mins at 4°C. The supernatant was discarded and all traces of supernatant removed by inverting the open centrifuge tube until all medium had been drained. Midi-prep preparation was carried out using the Qiagen HI SPEED Plasmid Midi Kit (Qiagen, Crawley, UK). The Qiagen Tips in the kit contain an anion-exchange resin, allowing for an anion-exchange-based plasmid DNA preparation. During the procedure impurities such as RNA, protein, carbohydrates, and small metabolites are washed from QIAGEN resin with medium-salt buffers, while plasmid DNA remains bound until eluted with a high-salt buffer. For details of the composition of each of the buffers see Appendix 9.

The bacterial pellet was resuspended in 6 ml of Buffer P1 (with LyseBlue added to achieve a 1:1000 dilution) before adding 6 ml of Buffer P2. The suspension was mixed thoroughly by vigorously inverting the sealed tube 4 to 6 times and incubating at room temperature for 5 mins. Following the addition of Buffer P2 the suspension turns blue with mixing resulting in a homogeneously coloured suspension. 6 ml of chilled Buffer 3 was added to the lysate and mixed thoroughly by inverting 4 to 6 times. The lysate was subsequently poured into the prepared QIAfilter Cartridge and incubated at room temperature for 10 mins. A HiSpeed Midi Tip was equilibrated by applying 4 ml of Buffer QBT and allowing the column to empty by gravity flow. The cap was removed from the QIAfilter outlet nozzle and the plunger gently inserted into the cartridge to filter the cell lysate into the equilibrated HiSpeed Tip. The cleared lysate was allowed to enter the resin by gravity flow. The HiSpeed Tip was

subsequently washed with 20 ml Buffer QC allowed through by gravity flow. The DNA was eluted with 5 ml Buffer QF into a 15 ml falcon tube. The DNA was precipitated by adding 3.5 ml room temperature isopropanol and kept overnight at -20°C. This was then spun for 30 minutes at 4000g. The supernatant was discarded and 3 ml 70% ethanol was added followed by a further spin for 30 minutes. This step was repeated before resuspending the DNA pellet in 50 µl sterile water.

2.1.2.4 Transient Transfection with Lipofectamine-2000

Lipofectamine-2000 reagent (Invitrogen, Paisley, UK) was used for transient transfection. For a standard 6-well plate, 3 µg plasmid DNA was diluted in 100 µl Opti-MEM (Invitrogen, Paisley, UK), mixed gently by pipetting and incubated at room temperature for 5 minutes. During incubation, a master mix of Opti-MEM (100 µl/well) and Lipofectamine-2000 (5 µl/well) was prepared. The Lipofectamine-2000/ Opti-MEM solution was mixed slowly with the DNA/ Opti-MEM solution, and incubated for a further 20 minutes at room temperature. Media was removed from wells and replaced with 1.3 ml fresh cell culture media. The solutions of DNA/ Lipofectamine-2000 were added to wells, and cells were incubated overnight at 37°C with 5% CO₂. Media was replaced the following morning. Depending on the size of the culture vessel, transfections were scaled up or down as follows:

Culture Vessel	Opti-MEM (µl)	DNA (µg)	Lipofectamine-2000 (µl)	Opti-MEM (µl)
6 well plate	100	3	5	100
T25 flask	250	8	15	250
T75 flask	1500	24	40	1500

Table 2.1. Transfection with lipofectamine-2000 according to culture vessel type

2.1.2.5 Transfection of HEK293T cells followed by lentiviral shRNA transduction of H295R/SH-SY5Y cells

HEK293T cells were used at 60% confluency on the day of transfection in 6 well plates. In each well, packaging vectors PMDG.2 plasmid (0.75 µg) and the pCMV 8.74 plasmid (1.0 µg), together with a combination of 2 commercially produced puromycin-resistant synthetic shRNA (0.625 µg each) (Sigma Aldrich, # TRCN0000118924 and TRCN0000118926, for AAAS-knockdown) were transfected using Lipofectamine-2000. A commercially available lentivirus plasmid vector containing a shRNA insert that does not target human and mouse genes was used to generate controls (Sigma Aldrich, Poole, UK). A total of 3 µg of DNA was transfected into each well of HEK293T cells in 1.5 ml of media. Cells were incubated for 48 hours in a humidified incubator at 37°C and 5% CO₂. 48 hours post transfection, 1.5 ml of viral media from each well of the HEK293T cells was filtered using 0.22 µm Millex-GP filter units and used to transduce 1 well of H295R or SH-SY5Y cells. Viral media was left on the cells for 24 hours and then replaced with fresh media. Cells were left to grow for 5 days before application of a selection antibiotic, puromycin at a concentration of 5 µg/ml. AAAS-knockdown cell lines were generated in 3 biological replicates. All subsequent experiments were conducted on cultured cells in which AAAS-knockdown was achieved by the combination of the 2 shRNAs together and following a minimum of 10 days puromycin selection.

Stable knockdown of *TXNRD2* was established in H295R human adrenocortical cells again by lentiviral shRNA transduction. Lentiviral plasmids (V3LHS_354173; OpenBiosystems, ThermoScientific, Leicestershire, UK) were obtained in a p.GIPZ backbone and contained shRNA specific for human *TXNRD2* (NM 10587) under the control of the CMV promoter, plus the puromycin resistance and green fluorescence protein (GFP) genes. Techniques for transduction and selection were as described above. Transduction efficiency was determined by fluorescence microscopy. A control cell line was generated using a lentiviral plasmid vector containing a shRNA insert that does not target human and mouse genes (Open Biosystems, ThermoScientific, Leicestershire, UK).

2.1.2.5 Generation of puromycin kill curve

A puromycin kill curve was generated to identify the optimum concentration of puromycin (Sigma Aldrich, Poole, UK) required for selection of cells transduced with puromycin-resistant vectors. To do this cells were plated at 20,000 cells per well in a 24 well plate on day 0. Cells were plated in triplicate for 6 different concentrations of puromycin (0, 1, 2.5, 5, 7.5, 10 $\mu\text{g/ml}$). The antibiotic-containing media was added to the wells on day 1 (cells 10% confluent at this time). Cell viability was examined every day and cells were cultured for 10 days. The media containing puromycin was replaced every 3 days. The optimum concentration of puromycin for each cell type was determined by the minimum concentration of puromycin that caused complete cell death after 3 to 5 days (Figure 2.2). For both the H295R and SH-SY5Y cells 5 $\mu\text{g/ml}$ puromycin was found to be optimal.

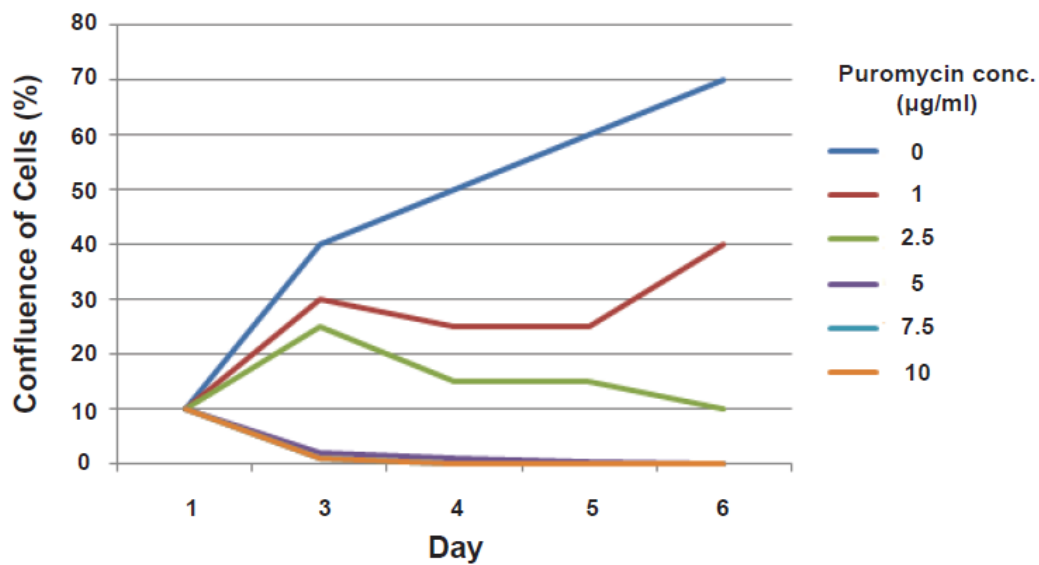


Figure 2.2. Puromycin kill curve generated for H295R cells. 5 $\mu\text{g/ml}$ puromycin provides the minimum concentration of puromycin to cause complete cell death after 3 days.

2.2 Western blotting

2.2.1 Cell lysate preparation

Cells were lysed with RIPA buffer (50 mM Tris-HCL, pH8.0, with 150 mM sodium chloride, 1% IGEPAL CA-630 [NP-40], 0.5% sodium deoxycholate, and 0.1% sodium dodecyl sulphate) (Sigma Aldrich, Poole, UK). 150 µl of RIPA buffer was used per well of a 6 well plate, supplemented with complete, Mini, EDTA-free Protease Inhibitor Cocktail tablets (Roche Diagnostics Ltd, West Sussex, UK), placed on ice for 30 minutes and centrifuged at 15,000g for 12 minutes at 4°C. The supernatant was subsequently added to an equal volume of Laemmli loading buffer (Sigma Aldrich, Poole, UK) and stored at -80°C for later use. To obtain lysates in non-reducing conditions, the supernatant was added to a non-reducing buffer (250 mM Tris HCl, pH 6.8, with 8% SDS, 40% glycerol, 0.02% bromophenol blue) and stored at -80°C for later use.

2.2.2 Bradford Assay

To determine the protein concentration of cell lysates a Bradford Assay was used prior to addition of Laemmli buffer to the samples. The assay is based on the maximum absorbance shift from 465nm to 595nm of Coomassie Brilliant Blue G-250 when bound to a protein. The protein assay dye (Coomassie Brilliant Blue G-250(5x); Bio-Rad, Hemel Hempstead, UK) was diluted 1 in 5 with PBS (Sigma-Aldrich, Poole, UK) prior to the assay. For protein standards, I used serial dilutions of BSA (Bovine serum albumin; Sigma-Aldrich, Poole, UK) ranging from 0 to 1 mg/ml in concentration. 10 µl of standard or test sample were added in triplicate to each well of a 96-well plate, plus 200 µl protein assay dye. The samples were left to incubate at room temperature for 5 minutes, then absorbance was read using a standard plate reader. A standard curve was produced by plotting OD595 against concentration of the BSA standard, and the protein concentration of each sample was determined by extrapolating from the linear equation.

2.2.3 SDS-PAGE

Samples were heated to 95-100°C for 5 mins and 10 µg of protein loaded on pre-cast 4-12% polyacrylamide NuPage BisTris gels (Invitrogen, Paisley, UK). The gels were run in 1 x3 3-(N-morpholino)propanesulfonic acid (MOPS) running buffer (50 mM MOPS, 50 mM Tris, 0.1% SDS, 1 mM EDTA, pH 7.7) for 60 mins at 170 volts. Novex sharp pre-stained protein standard (Life Technologies, Paisley, UK) was loaded alongside the samples.

2.2.4 Immunoblotting

Following electrophoretic transfer, the proteins were transferred for 30 mins at 15 volts to a nitrocellulose membrane by semi-dry transfer using the Trans-Blot SD semi-dry transfer cell (Bio-Rad, Hemel Hempstead, UK). The transfer buffer consisted of 20 mM Tris, 120 mM glycine and 10% methanol. Blots were blocked with 5 ml of 5% milk powder in PBS with 0.05% Tween (PBST). All incubations, unless otherwise stated, were performed for 1 hour at room temperature in blocking buffer. The membranes were subsequently incubated in 5 ml of 5% milk in PBST containing the appropriate antibody (antibody dilution and incubation period specific to each antibody). For antibody dilutions and incubation periods see Appendix 5. Following incubation with the primary antibody, membranes were washed three times in PBST, each wash lasting 20 mins. Membranes were subsequently incubated in appropriate species-specific infra-red secondary antibodies (Licor, Cambridge, UK) at a dilution of 1:5000 for 1 hour. After three 15 min washes in PBST, membranes were imaged using the Licor Odyssey infrared scanner.

2.3 RNA extraction and reverse transcription

2.3.1 RNA extraction from animal cells

RNA extraction from H295R/ SH-SY5Y cells was performed using the Qiagen RNeasy mini kit (Qiagen, Crawley, UK). The kit relies on a specialised high-salt buffer system allowing RNA to bind to the

RNeasy silica-gel membrane of the RNeasy mini column. Details of the buffers can be found in Appendix 9.

Cells were washed in PBS twice. For each well of a 6 well plate 350 μ l of Buffer RLT was added together with 3.5 μ l 2- β mercaptoethanol. Buffer RLT contains guanidine isothiocyanate which is highly denaturing and inactivates RNases, ensuring isolation of intact RNA. Cells were agitated using a cell scraper and the cell suspension pipetted into a 1.5 ml microcentrifuge tube. To homogenise the sample a syringe with a 20 gauge needle was used to withdraw and release the sample 5 times. One volume of 70% ethanol was added to the homogenised lysate and mixed by pipetting. The 700 μ l sample was applied to an RNeasy mini column placed in a 2 ml collection tube, this was then centrifuged at 13,000 rpm for 15 seconds. The flow-through was discarded and 700 μ l of Buffer RW1 was added to the RNeasy column for a wash step. Again the sample was spun for 15 seconds at 13,000 rpm and the flow through discarded. The RNeasy column was transferred to a fresh 2 ml collection tube and 500 μ l of Buffer RPE (supplemented with ethanol as per manufacturer's protocol) was added to the column followed by a further spin at 13,000 rpm for 15 seconds. This step was repeated with a longer spin for 2 mins at 13,000 rpm to dry the RNeasy silica-gel membrane. To elute the RNeasy column was transferred to a 1.5 ml microcentrifuge tube and 30 μ l RNase free water added directly to the RNeasy silica-gel membrane with a final spin step for 1 min at 13,000 rpm. The flow through in this step contains the required RNA. Absorbance of the RNA was measured using the NanoDrop ND-1000 spectrophotometer; good quality RNA having an OD 260/280 ratio of 1.8 to 2.0 or an OD 260/230 of > 1.8; indicating RNA devoid of contaminants. The quality of the RNA could be further assessed by electrophoresis on a denaturing agarose gel. Ribosomal RNA should be sharp and intense with an upper 28S rRNA band being twice as intense as a lower 18S rRNA band.

2.3.2 DNase treatment of RNA

DNase treatment of RNA from cell lysates was carried out to cleave and remove genomic DNA. Each reaction mixture contained 1µg RNA, 5µl DNase Turbo buffer (Ambion, Life Technologies, Paisley, UK), 0.5µl RNase inhibitor (RNasin, Promega, Southampton, UK) to prevent RNA degradation and 1 µl DNase 1 (Deoxyribonuclease 1, 10,000 units/ml, Sigma-Aldrich), made up to a volume of 50 µl with RNase free water (Sigma Aldrich, Poole, UK). Reactions were incubated at 37°C for 15 minutes and then transferred to ice. RNA was purified and precipitated as detailed in section 2.3.4.

2.3.3 RNA extraction from whole blood

RNA extraction from whole blood was conducted using the PAXgene Blood RNA kit, details of the buffers in the kit can be found in Appendix 9.

A small amount of blood was drawn into a 'discard' tube prior to drawing blood into the PAXgene Blood RNA tube (Qiagen, Crawley, UK). The tube contains a reagent which protects RNA molecules from degradation by RNAses. Following blood collection the PAXgene Blood RNA tube was inverted 8 to 10 times with subsequent storage at 4°C in an upright position for up to 5 days. Prior to the RNA extraction procedure the RNA tube was incubated at room temperature to achieve complete lysis of blood cells. The PAXgene Blood RNA tube was centrifuged for 10 mins at 3000xg using a swing out rotor. The supernatant was removed by pipetting. 4 ml of RNase-free water was added to the remaining pellet and the tube using a fresh secondary BD Hemogard closure. The pellet was dissolved by vortexing and then centrifuged for 10 mins at 3000xg using a swing out rotor. The supernatant was then discarded. 350 µl resuspension buffer (BR1) was added and again the sample vortexed until the pellet dissolved. The sample was pipetted into a 1.5 ml microcentrifuge tube; 300 µl binding buffer (BR2) and 40 µl proteinase K were added and the sample mixed by vortexing for 5 seconds. This was then incubated for 10 mins at 55 °C using a Grant OLS200 shaking waterbath (Cambridge, UK) at 200 rpm. After use the incubator was set at 65 °C for use in a later step of the protocol. The lysate was pipetted directly into a PAXgene Shredder spin column and placed in a 2 ml

processing tube then centrifuged for 3 mins at maximum speed to homogenise the cell lysate and remove any cell debris. The entire supernatant of the flow through fraction was transferred into a fresh 1.5 ml microcentrifuge tube without disturbing the pellet left in the processing tube. 350 μ l of 100% ethanol was added, to adjust binding conditions, and the sample mixed by vortexing and centrifuging briefly (1 to 2 seconds at 1000 x g). The 700 μ l sample was pipetted into the PAXgene RNA spin column (PRC), placed in a 2 ml processing tube and centrifuged for 1 min at 10,000 x g and the flow-through discarded. The spin column was then placed in a new processing tube. Any remaining sample was pipetted into a PAXgene RNA spin column and centrifuged for 1 min at 10,000 x g. RNA selectively binds to the Paxgene silica membrane in the spin column whilst contaminants pass through during centrifugation. The PRC was placed in a new 2ml processing tube.

A series of wash steps were carried out, to remove any remaining contaminants, and include treatment with DNase I to remove any traces of bound DNA. Wash buffer I, BR3 (350 μ l), was pipetted into the PRC and centrifuged for 1 minute at 10,000 x g. The flow through was discarded and the spin column was placed into a new 2 ml processing tube. 10 μ l DNase I stock solution was added to 70 μ l DNA digestion buffer in a 1.5 ml microcentrifuge tube. The contents of tube were gently fixed and centrifuged briefly to collect residual liquid from the sides of the tube. The DNase I incubation mix (80 μ l) was pipetted directly onto the PAXgene RNA spin column (PRC) membrane and was left at room temperature for 15 mins. Wash buffer I, BR3 (350 μ l), was pipetted into the PRC and centrifuged for 1 min at 10,000 x g. The flow through was discarded and the spin column was placed into a new 2 ml processing tube. Wash buffer 2, BR4 (500 μ l), was added to the spin column and the centrifuge step repeated and again the flow-through discarded. A further 500 μ l of wash buffer 2 was added to the PRC and the sample centrifuged for 3 mins at 10,000 x g. The flow through and processing tube were discarded and the PRC placed in a new processing tube followed by further centrifugation for 1 min at 10,000 x g. The flow through was discarded and the PRC placed in a 1.5 ml microcentrifuge tube. 40 μ l of elution buffer (BR5) was pipetted directly onto the PRC

membrane and centrifuged for 1 min at 10,000 x g to elute the RNA. The elution step was repeated using a further 40 µl of elution buffer and the same microcentrifuge tube. The eluate was incubated for 5 mins at 65 °C in a water bath (without shaking); this step denatures the RNA. After incubation the sample was chilled immediately on ice. RNA samples were then stored at -80 °C if not being used immediately.

2.3.4 Phenol extraction and RNA precipitation

The organic solvent phenol was used to remove protein contaminants from nucleic acids. RNA samples were vortexed with an equal volume (50 µl) of pH 7.8 phenol (Sigma-Aldrich, Poole, UK). The samples were centrifuged at 14,000 rpm for 1.5 minutes to separate the layers. The top aqueous layer containing purified RNA was transferred to a fresh microcentrifuge tube and precipitated by ethanol precipitation. For this a mixture of 5 µl 3M sodium acetate pH 5.3 (BDH Chemicals), 4 µl 5 mg/ml glycogen (Ambion, Life Technologies, Paisley, UK) and 125 µl absolute ethanol (Fisher-Scientific, UK) was added to the purified RNA sample for overnight incubation at 80°C.

Precipitated RNA was collected the next day by centrifugation at 14,000 rpm for 10 minutes at 4°C, with removal of supernatant. The RNA pellet was washed with 70% ethanol, spun for a further 5 minutes at 14,000 rpm at 4°C, with removal of the supernatant. The RNA pellet was resuspended in RNase-free water for reverse transcription as detailed below.

2.3.5 Reverse transcription

For cDNA production via reverse transcription, 2 µl of 2 mg/ml RNA in 15 µl RNase-free water (Sigma-Aldrich, Poole, UK) was incubated with 2 µl random primers (hexadeoxynucleotides, 500µl/ml; Promega, Southampton, UK) at 70°C for 5 mins, followed by incubation on ice for 2 mins. A 1 µl aliquot was taken as a pre-reverse transcription negative control which should not contain cDNA or genomic DNA if DNase treatment was successful. 1 µl reverse transcriptase enzyme (MMLV-RT enzyme, Promega, Southampton, UK) was added, with 5 µl 5x reverse transcriptase buffer (50

mM Tris-HCl (pH8.3), 75 mM KCl, 3 mM MgCl₂ and 10 mM DTT; 5x MMLV RT-buffer, Promega, Southampton, UK), 1.25 µl dNTPs (deoxynucleotidetriphosphates ; consisting of 10 mM dATP, 10 mM dCTP, 10 mM dGTP, 10 mM dTTP; Promega, Southampton, UK) and 0.75 µl RNase inhibitor (RNasin; Promega, Southampton,UK). The entire mixture was incubated at 37°C for 60 mins. The resulting cDNA was used as a template for PCR amplification.

2.4 DNA extraction from whole blood

The illustra Nucleon Genomic DNA Extraction Kit (GE Healthcare, Buckinghamshire, UK) was used to extract genomic DNA from patient whole blood. The procedure involves initial cell lysis, deproteinisation with sodium perchlorate, extraction with chloroform treatment and nucleon resin and finally DNA recovery and DNA washing. Details of the buffers used in the kit can be found in Appendix 9.

3-5 ml of patient blood was collected in sodium EDTA tubes. Blood stored at 4°C should ideally be extracted within 24 hours of collection alternatively samples can be stored at -20°C. For cell lysis, using an aseptic procedure 4 times the volume of provided Reagent A (10 mM Tris-HCl, 320 mM sucrose, 5 mM MgCl₂ 1% (v/v) Triton X-100, pH8.0) was added to the blood sample and placed on a rotary mix for 4 mins at room temperature. Samples were then centrifuged at 1300x g for 5 minutes and the supernatant discarded. The pellet was resuspended in 2 ml of Reagent B (detergent for nucleic lysis) and vortexed. The suspension was then transferred to a 15 ml falcon tube following which 500 µl of sodium perchlorate solution was added for deproteinisation. The suspension was mixed by inversion, seven times. To extract DNA 2 ml of chloroform was added and the suspension was mixed again by inversion. Without remixing the phases 300 µl of Nucleon resin was added and the sample was centrifuged at 1300x g for 3 minutes. Two phases separated by the brown Nucleon resin layer were evident and the upper phase (approximately 2.5 ml) was transferred to a fresh 15 ml falcon tube. To precipitate the DNA 2 volumes of cold absolute ethanol were added and the sample mixed by inversion until a precipitate was evident. This precipitated DNA was hooked out

using a heat-sealed Pasteur pipette and placed directly into 50 µl of sterile water. If no precipitate was evident the DNA was pelleted by centrifugation at 4000x g for 5 mins. For DNA washing 2 ml of cold 70% (v/v) ethanol was added and the sample re-centrifuged. This step was repeated and the supernatant discarded. The DNA pellet was then air-dried for 10 mins before adding 100 µl of sterile water. The sample was subsequently rotary mixed for 2 hours to dissolve the DNA.

2.5 Polymerase chain reaction (PCR) and sequencing

2.5.1 Oligonucleotide design

The relevant sequence of the gene of interest was established using Ensembl (see URL). Primer sequences for genomic DNA correspond to sequences within the intronic regions whilst primer sequences for cDNA traverse intronic regions. The following guidelines were then used for PCR primer pair design:

- Oligonucleotide length of between 18 to 30 nucleotides
- GC content should be between 40-60%
- Primer pairs should have similar T_m (melting temperature) values, where the T_m can be estimated as follows; $T_m = 2^\circ\text{C} \times (\text{number of A and T residues}) + 4^\circ\text{C} \times (\text{number of G and C residues})$.
- Complementary sequences within a primer sequence and between pairs should be avoided.
- Runs of 3 or more Gs or Cs should be avoided at the 3' end.
- Complementarity of 2 or 3 bases at the 3' ends of primer pairs should be avoided to reduce primer-dimer formation.

The stock primer solution was stored at -20°C . To avoid repeat freeze-thawing small working aliquots of 10 µM were prepared.

2.5.2 Polymerase Chain Reaction (PCR)

Each exon of genes of interest including intronic boundaries was amplified by PCR using specific primers (primer sequences, appendix 1). The reaction mixture made up to a volume of 25 μ l contained the following reagents:

- 100 ng DNA template
- 2.5 μ l 10 x Standard *Taq* polymerase Buffer (10 mM Tris-HCl, 50 mM KCl, 1.5 mM MgCl₂, pH8.3) (New England Biolabs, Hertfordshire, UK)
- 0.5 μ l, 200 μ M each dNTP (dATP, dTTP, dCTP, dGTP; Promega, Southampton, UK)
- 200 nM each primer (forward and reverse, for primer sequences see Appendices 1 and 2)
- 0.125 μ l *Taq* polymerase (5000 u/ml) (New England Biolabs, Hertfordshire, UK)
- Nuclease-free water (Sigma Aldrich, Poole, UK) to make up total PCR reaction volume to 25 μ l

Cycling conditions were: 95°C for 5 mins (1 cycle); 95°C for 30 seconds, 55°C for 30 seconds, and 72°C for 30 seconds (30 cycles); and 72°C for 5 mins.

PCR products were then separated and visualized using agarose gel electrophoresis. This technique involves application of an electric field across an agarose gel which induces the nucleic acids loaded into it to migrate towards the anode due to the net negative charge of the sugar-phosphate backbone of the nucleic acid chain. Molecules traverse the gel at different speeds depending on their size, with longer molecules moving more slowly as they experience more resistance. The PCR products were visualized on 1-2% agarose gel made in 1x TAE buffer (40mM Tris-acetate, 2mM disodium ethylenediaminetetraacetate (Na₂EDTA), pH 8.3; National Diagnostics, UK) with GelRed (Biotium, Cambridge BioScience, Cambridge, UK) staining, alongside DNA markers (GeneRuler™ DNA Ladder Mix, 0.5 mg DNA/ml, Fermentas). Prior to loading into the gel wells 5 μ l of each reaction was mixed with 1 μ l of loading dye solution (40% w/v sucrose, 0.25% w/v bromophenol blue or Orange G, 1mmol EDTA pH 8.0). Electrophoresis was carried out at approximately 120 V for 30 minutes or

until clear separation of products was obtained. GelRed intercalated into DNA fluoresces under UV light at 300 nm allowing the DNA and therefore the PCR product to be visualized. A Uvitec transilluminator was used to visualize the bands and capture an image of the gel. The approximate size of the PCR product can be determined by comparison with the DNA markers on the agarose gel.

2.5.3 Sequencing

PCR products were sequenced using the ABI Prism Big Dye sequencing kit and an ABI 3730 automated DNA sequencer (Applied Biosystems, Foster City, CA), carried out by the Genome Centre in Bart's and the London, QMUL. This is based on the Sanger dideoxy-mediated chain termination method [207], which requires a DNA template, a DNA primer, DNA polymerase, conventional dNTPs and modified nucleotides that terminate DNA strand elongation (ddNTPs). The double stranded DNA fragment is denatured into single DNA strands and a primer complementary to the known DNA sequence binds to the single stranded DNA template. DNA polymerase then binds to the primer and a new strand of DNA incorporating free nucleotides, complementary to the target DNA sequence, is synthesised. The terminating nucleotides of the ddNTPs are fluorescently labelled and modified to lack the 3'OH group required for the formation of the phosphodiester bond between two nucleotides thus terminating each DNA strand at the point of inclusion. This process is repeated many times thus generating many fragments of different lengths that all terminate in fluorescently labelled bases, corresponding to A, T, G and C. The reaction is then transferred into thin glass capillaries where application of an electrical charge moves negatively charged particles through a gel matrix and DNA fragments are then separated according to size. Finally a laser is used to excite the chain terminating fluorescent base, which is subsequently recorded as a coloured band or peak by the automated sequencer.

2.5.4 Sequencing analysis

Analysis of sequence chromatograms was carried out using BioEdit (see URL). BioEdit is a freeware biological sequence alignment editor and analysis program for Windows 95/98 NT. The program

enables the user to compare the DNA sequence to a reference sequence, enabling identification of differences between 2 or more sequences by eye. This program can therefore be used to detect potential mutations in the chromatograms generated from patient samples.

2.6 Whole exome sequencing

2.6.1 Sample preparation

Genomic DNA was extracted from human blood as described in section 2.4. High quality DNA was required with a concentration of 20 ng/μl to 500 ng/μl and an OD260/280 ratio of greater than 1.8 and OD260/230 ratio of greater than 1.9. Absorbance of the samples was measured using a NanoDrop ND-1000 spectrophotometer at $\lambda = 260 \text{ nm}/280 \text{ nm}$ and $260\text{nm}/230\text{nm}$ respectively.

2.6.2 Sequence capture array and sequencing

Whole exome sequencing (WES) using the Illumina HiSeq 2000 Sequencer was conducted on 3 affected individuals (samples processed by Orogenetics Corporation, USA). WES samples were prepared as an Illumina sequencing library, and in the second step, the sequencing libraries were enriched using the Agilent V4 (51 Mbp) exome enrichment microarray. Briefly, DNA was fragmented and a library was created using standard techniques including end repair, A-tailing and paired adaptor ligation. DNA was hybridised to the array, washed to remove un-tethered strands, and then enriched, eluted and amplified. The enriched DNA was subjected to massively parallel sequencing on the Illumina HiSeq 2000. The captured libraries were sequenced and downstream analysis conducted via DNAnexus Classic (see URLs). Single Nucleotide Polymorphisms, with a threshold coverage of at least 20 reads on the respective nucleotide, were assessed. A filtration strategy was adopted to minimize the number of variants for analysis, discussed in Chapter 4.5.

2.7 Quantitative RT-PCR

2.7.1 Gel extraction

For gel extraction, PCR bands were cut out of the gel and purified using the Qiagen QIAquick Gel extraction kit (Qiagen, Crawley, UK). The procedure involves silica-membrane-based purification of DNA fragments from gels and details of the buffers used in this kit can be found in Appendix 9.

The excised gel bands were incubated in a solubilisation buffer (3x volume of the gel band, Buffer QG) at 50°C until the agarose had melted, before the resolubilised DNA was applied to a silica DNA-binding membrane. The membrane was washed once in 500 µl solubilisation buffer (Buffer QG) to remove any agarose and once in 750 µl ethanol-containing buffer (Buffer PE) to remove salts. DNA was eluted in nuclease-free water before 1 µl of sample was re-run on 1% agarose gel to confirm efficient purification. Alternatively, DNA concentration in ng/ml was determined using a Nanodrop ND-1000 spectrophotometer, with the purity of the DNA determined by calculating the ratio of absorbance at 260 nm and 280 nm. A ratio of ~1.8 was considered to be pure DNA. DNA samples were stored at 20°C.

2.7.2 Standards for quantitative RT-PCR

Samples of known concentration (standards) of the gene of interest were needed to generate a standard curve, from which quantities of 'targets' could be extrapolated. All genes of interest were normalised to *GAPDH*. Gel extracts of the genes of interest and *GAPDH* were used to generate standards. 2 µl of a known concentration of DNA from the gel extract was added to 98 µl of sterile water to generate a '10⁻²' standard. 10 µl of this was added to 90 µl of sterile water to generate the '10⁻³' standard. Further dilutions were established in the same way. The lower the anticipated expression of the gene of interest the more dilutions were required, for instance up to a '10⁻¹⁰' standard.

2.7.3 Quantitative RT-PCR (qPCR)

A quantitation assay is a real-time PCR assay which measures the amount of nucleic acid during each amplification cycle of the PCR. For this purpose fluorescent SYBR Green I dye chemistry was used. This uses the SYBR Green I dye which binds to double stranded DNA formed during PCR. During the PCR, DNA polymerase amplifies the target sequence, which creates the PCR products (amplicons). The SYBR Green I dye then binds to each new copy of double stranded DNA. As the PCR progresses more amplicons are created resulting in an increase in fluorescence intensity proportionate to the amount of PCR produced.

RNA samples were quantified with a spectrophotometer and 1.0 µg of RNA from each sample was reverse transcribed following DNase treatment. Quantitative RT-PCR was set up in triplicate (per sample and standard) on a Stratagene Mx3000P thermocycler using KAPA SYBR Fast qPCR master mix with 200 nM forward and reverse primers targeted to *AAAS*, *TXNRD2* or *GAPDH* (primer sequences, Appendix 1); giving a total volume of 10 µL. KAPA SYBR Fast qPCR master mix is a ready to use cocktail containing all components, except primers and template, for the amplification and detection of DNA in qPCR. This includes a DNA polymerase and SYBR Green I fluorescent dye. ROX reference dye is also utilised to provide an internal fluorescence reference to which the reporter dye signal can be normalised during data analysis. Normalisation is required to correct for fluorescence fluctuations caused by changes in concentration, volume or sample effects. For PCR conditions, after an initial denaturation step of 3 mins at 95°C, PCR cycling was performed for 40 cycles of 95°C for 3 seconds, 55°C for 20 seconds and 72°C for 1 seconds, followed by 1 cycle of 1 min at 95°C, 55°C for 30 seconds and 95°C for 30 seconds.

In the initial cycles of PCR, there is little change in fluorescence signal and an increase in fluorescence above baseline indicates the detection of an accumulated target. Amplification plots are the plots of fluorescence signal versus cycle number (Figure 2.3A). A fixed fluorescence threshold is set in the region associated with exponential growth of the PCR product. The threshold cycle (Ct) is

defined as the fractional cycle number at which fluorescence passes the fixed threshold. The higher the starting copy number of the nucleic target the sooner a significant increase in fluorescence is observed. The no template control (NTC) is a sample that does not contain template and is used to verify amplification quality. The Ct of the NTC should be more than 5 cycles away from that of the target. Dissociation curve analysis is used to determine the melting temperature (T_m) of the PCR product. The T_m is characteristic of the GC content, length and sequence of a DNA product and can be used to establish that the correct DNA product has been amplified.

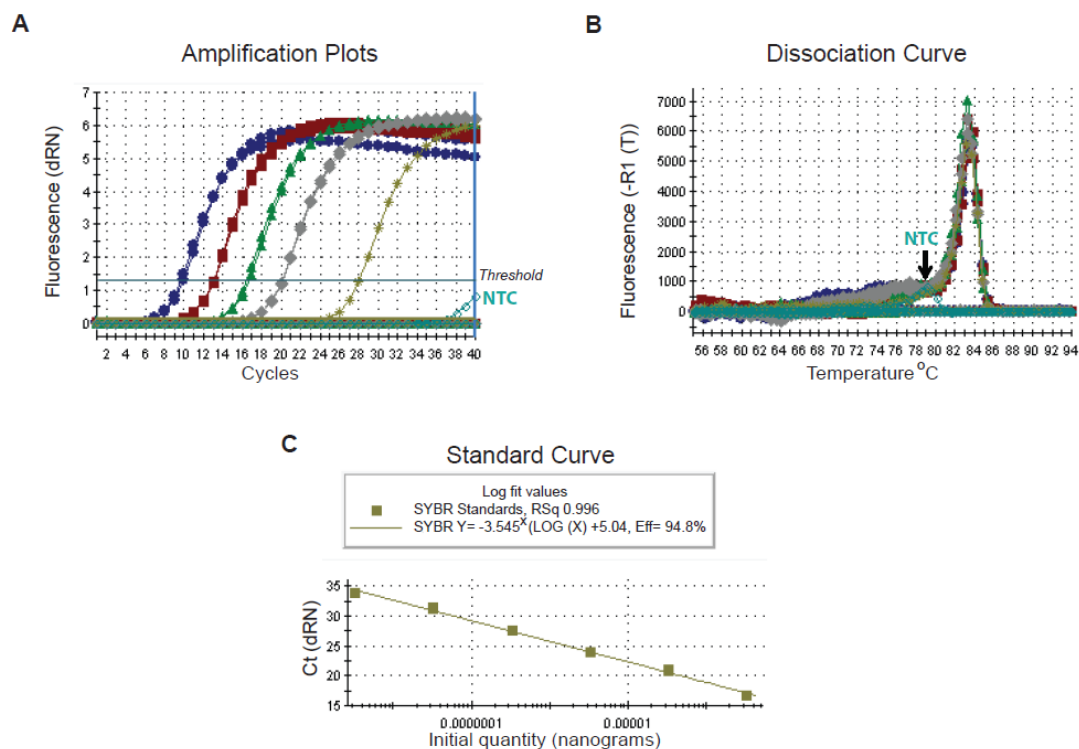


Figure 2.3. Representative images for standards generated during quantitative RT-PCR. (A) Amplification plots of the standards of the gene of interest. The threshold cycle (Ct) is the point at which the amplification plot for each standard crosses the threshold line. (B) Dissociation curve of the standards, with the non-template control (NTC) having a lower melting temperature. (C) Standard curve generated from the Ct of the standards, from which the quantity of a target can then be extrapolated.

In Figure 2.3B the standards of the gene of interest have the same T_m , with the NTC melting at a lower temperature. The standard curve is generated from the Cts of the standards. Adequate PCR efficiency has to be achieved with a minimum of 3 replicates and a minimum of 5 logs of standard template concentration. A slope of $-3.3 \pm 10\%$ reflects an efficiency of $100\% \pm 10\%$ (Figure 2.3C). A PCR reaction of lower efficiency will have lower sensitivity. If the standard curve is of appropriate efficiency it can then be used to extrapolate the quantity of the target.

2.8 Cell viability

2.8.1 Cell counting using haemocytometer

Cells were plated at a seeding density of 2×10^4 cells per well in a 12 well plate. Prior to trypsinising, cells were washed with Dulbecco's Phosphate Buffered Saline allowing removal of any dead cells. Following trypsinisation on day 5, a 50 μ l sample of cells was removed and injected into the Neuberg haemocytometer channel. Cells were counted in all 4 corners (each corresponding to an area of 1.0 mm^2 and a volume of 100 nl) of one of the grids (see Figure 2.4) using the Leica DMIL light microscope with 10x objective. If more than 500 cells were counted, the cell stock was diluted and another sample taken. If there were fewer than 200 cells, all 4 corners of both grids were counted. The total number of cells in the cell suspension corresponded to the number of cells/ml (number of cells/100 nl $\times 10^4$) multiplied by the ml of media in which the cells were diluted. Results for cell numbers are comprised of 5 representative experiments and statistical analysis undertaken was the t test.

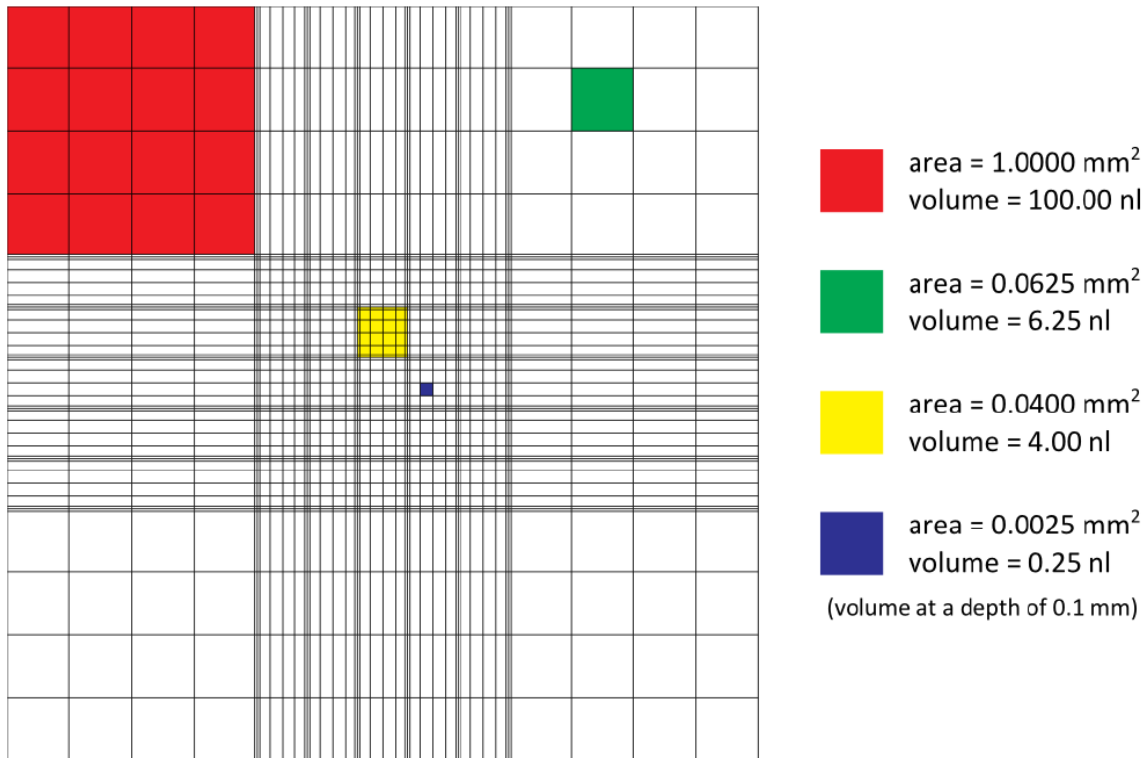


Figure 2.4. Haemocytometer grid

2.8.2 Cell viability assay

The CellTiter96 Aqueous non-radioactive cell proliferation assay (MTS (3-(4,5-dimethylthiazol-2-yl)-5-(3-carboxymethoxyphenyl)-2-(4-sulfophenyl)-2H-tetrazolium) assay) (Promega, Southampton, UK) was used to assess cell viability. The assay consists of a novel tetrazolium compound (MTS) and an electron coupling reagent (phenazine methosulphate; PMS). Details of the reagents can be found in Appendix 9. MTS is bio-reduced by dehydrogenase enzymes found in metabolically active cells into a formazan product that is soluble in tissue culture medium. The absorbance of the formazan at 490 nm can then be directly measured, the amount of 490 nm absorbance being proportional to the number of metabolically active cells in culture.

Cells were plated at a density of 5000 cells per well in a 96 well plate on Day 0. Six wells were plated for each experimental condition required. Cells were incubated for 48 hours in normal media or media treated with 100 μ M H₂O₂ (Sigma Aldrich, Poole, UK). Media was then removed and replaced

with 100 µl fresh normal media. In each 96 well plate standards were established by plating H295R cells at densities between 1000 to 35000 cells per well, in triplicate. Cells were then incubated for 2 hours in a humidified incubator at 37°C. The CellTiter96 kit was used according to the manufacturer's protocol. 100 µl of PMS solution was added to 2 ml of MTS solution. 20 µl of the combined MTS/PMS solution was added to each well and cells were re-incubated in a humidified incubator at 37°C, in darkness. The absorbance of the wells at 490 nm was read at 2.5 hours using an ELISA plate reader (Wallac spectrophotometer). The mean absorbance for each set of cells was representative of the 6 readings. Results are comprised of representatives from 3 to 4 separate experiments with statistical analysis using the Student's t test (GraphPad Prism 5 software).

2.8.3 PARP (Poly-ADP-ribose polymerase) cleavage

Cells (80% confluency in 6 well plates) were incubated in serum-free medium containing 1 mM H₂O₂ for 30 min before the medium was replaced with fresh serum-containing medium in all cells as previously described. After overnight recovery at 37°C, cells were lysed and analysed via Western analysis, using PARP rabbit polyclonal antibody at 1:1000 (Cell Signalling Technology; New England Biolabs, Hertfordshire, UK) and mouse monoclonal GAPDH antibody at 1:5000 (Abcam, Cambridge, UK). Cleaved PARP was quantified using densitometric analysis from 3 representative experiments relative to total PARP. Student's t test was used for statistical analysis (GraphPad Prism 5 software).

2.9 Analysis of cell GSH/GSSG ratio

Glutathione (GSH) is a potent antioxidant which reduces ROS. It functions as an electron donor, which on reducing disulphide bonds between proteins, becomes oxidised itself (GSSG). One can therefore use the ratio of GSH: GSSG as an indicator of cell toxicity; in normal conditions a high GSH: GSSG ratio is maintained.

The GSH/GSSG-Glo assay (Promega, Southampton, UK) is a luciferase based assay with an output measure of luminescence. The assay principle is that the conversion of Luciferin-NT to Luciferin by

glutathione-s-transferase, is dependent on GSH. This reaction is coupled to a firefly luciferase reaction producing light, hence GSH is proportional to luminescence. Details of all reagents can be found in Appendix 9.

AAAS (*or TXNRD2*)-knockdown and control cells were plated at a seeding density of 1×10^5 in duplicate in a luminometer compatible 96 well plate. At 48 hours GSH/GSSG Glo Assay was used according to the manufacturer's guidelines, using a Total Glutathione Lysis Reagent or Oxidised Glutathione Lysis Reagent for each set of cells for the desired endpoint. As a positive control, control cells were treated with 40 μ M menadione for 1 hour prior to the assay. Menadione is a synthetic agent which has been demonstrated to increase levels of GSSG.

Cell medium was removed from wells and 50 μ l of either Total Glutathione Lysis Reagent or Oxidised Glutathione Lysis Reagent was added to each well. The plates were shaken for 5 mins. 50 μ l of Luciferin Generation Reagent was added to each well and the plate incubated for 30 mins. Following application of 100 μ l Luciferin Detection Reagent to each well and equilibration for 15 mins, luminescence was read. The total glutathione measurement and the oxidised glutathione measurement (GSSG) were used to calculate the GSH/GSSG ratio, with a 2-fold adjustment made for GSSG as each mole of oxidised GSSG upon reduction in the assay produces 2 moles of reduced glutathione (GSH):

$$\text{(Net total glutathione RLU- Net GSSG RLU)/ (Net GSSG/2)}$$

Results are comprised of representatives from 3 separate experiments with statistical analysis using the Student's t test (GraphPad Prism software).

2.10 Cortisol analysis

AAAS (*or TXNRD2*)-knockdown and control cells were cultured in serum-free media. Media was extracted when cells were at 90% confluency following 24-hour stimulation with 10 μ M forskolin. Cortisol levels were analysed on a Roche Modular E170 automated immunoassay analyser using

electrochemiluminescent detection; the assay imprecision has been described as less than 6%. Levels were subsequently normalised to 1 mg of protein following Bradford assays of the corresponding cell lysates. For N-acetylcysteine treatment, media was supplemented with 1mM N-acetylcysteine (Sigma Aldrich, Poole, UK) for the 24 hour period.

2.11 Thioredoxin Reductase Assay

A thioredoxin reductase (TXNRD) assay kit (Abcam, Cambridge, UK), a colorimetric assay, was used to assess **total** TXNRD activity in cell lysates from *TXNRD2*-knockdown and control cells. In the assay TXNRDs catalyse the reduction of 5, 5'-dithiobis (2-nitrobenzoic) acid (DTNB) with NADPH to 5-thio-2-nitrobenzoic acid (TNB²⁻), generating a strong yellow colour ($\lambda_{max}=412$ nm). To determine TXNRD-specific activity (as compared to other enzymes such as glutathione reductase and glutathione peroxidase) a thioredoxin reductase specific inhibitor is used. Of note, the kit does not allow for the differentiation of activity of each of the individual TXNRDs. Details of the reagents in the kit can be found in Appendix 9.

Two assays are performed, the first measuring total DTNB reduction by the sample and the second DTNB reduction by the sample in the presence of the inhibitor. The difference between the 2 results is the DTNB reduction by the TXNRDs.

Cells, grown to 90% confluency in T25 flasks, were homogenised in 300 μ l cold Assay Buffer, supplemented with complete, Mini, EDTA-free Protease Inhibitor Cocktail tablets (Roche Diagnostics Ltd, West Sussex, UK), on ice. The samples were centrifuged at 10,000 x g for 15 mins at 4°C. The supernatant was collected for assay and stored on ice. The protein concentration of the supernatant was determined by Bradford assay.

Two sets of samples, in duplicate, were tested with or without the TXNRD inhibitor. 50 μ l of sample was added into each well, in duplicate, in clear 96 well plates. For a positive control 10 μ l of the provided TXNRD control was added to 40 μ l Assay Buffer. To one set of samples 10 μ l of the TXNRD

inhibitor was added for testing background enzyme activity. To the second set, 10 μ l of Assay Buffer was added, for testing total DTNB reduction. TNB standards for the assay were established in duplicate. 0, 2, 4, 6, 8, 10 μ l of the provided TNB standard, were brought to a final volume of 100 μ l with Assay Buffer, generating 0, 10, 20, 30, 40, 50 nmol/well standards.

The reaction mix was comprised of 30 μ l assay buffer, 8 μ l DTNB solution, 2 μ l NADPH. 40 μ l of this reaction mix was added to each sample well and mixed bringing the final volume to 100 μ l. $A_{412\text{nm}}$ was measured using a thermostatic spectrophotometer. $A_{412\text{nm}}$ was measured for 30 minutes at 25°C with readings taken at 30 second intervals. The total change in $A_{412\text{nm}}$ within the linear range was calculated for each sample:

$$\Delta A_{412\text{nm}} = (A_{2t}-A_{1t}) - (A_{2I}-A_{1I})$$

Where the $A_{412\text{nm}}$ was measured at T1 (time of the first reading) to establish the A_{1t} and $A_{412\text{nm}}$ was measured again at T2 to get A_{2t} , in the sample set without the TXNRD inhibitor. The A_{1I} and A_{2I} were derived from the sample set with the TXNRD inhibitor. The $\Delta A_{412\text{nm}}$ was applied to the TNB standard curve to get ΔB nmol of TNB; the TNB amount from the standard curve. TXNRD activity was then calculated as follows:

$$\text{TXNRD activity} = \Delta B / ((T2-T1) \times V) \times \text{Sample dilution factor} = \text{nmol/min/}\mu\text{l} = \text{mU/ml}$$

Where T1 is the time of the first reading (A_{1t} and A_{1I}) (in mins); T2 is the time of the second reading (A_{2t} and A_{2I}) and V is the pretreated sample volume (ml) added to each reaction well. One unit of TXNRD is the amount of enzyme that generates 1 μ mol of TNB per minute at 25°C. The oxidation of 1 mole of NADPH to NADP will generate 2 mole TNB, therefore 1 TNB unit equals 0.5 NADP unit.

2.12 Leukocyte separation

Fresh whole blood was collected in EDTA- containing tubes. Mononuclear cells were extracted using a gradient density centrifugation method with Histopaque-1077 according to the manufacturer's

protocol (Sigma Aldrich, Poole, UK). When blood is layered onto the Histopaque solution 1077, which has a density of 1.077 g/ml, and subjected to centrifugal forces, mononuclear cells are held at the plasma–histopaque interphase while erythrocytes gravitate to the bottom (Figure 2.5). 6 ml histopaque-1077 was added to a 15 ml centrifuge tube and 6 ml blood carefully layered onto it. This was centrifuged at 700g for 30 mins at room temperature (18-26°C). The plasma was carefully aspirated and discarded to within 0.5 cm of the mononuclear layer. The mononuclear layer was then removed into a clean tube. This was washed with 10ml isotonic PBS and centrifuged for 10 mins at 200g. The supernatant was aspirated and discarded and the cells resuspended and washed again as above. Cells were subsequently lysed using 50 µl RIPA buffer, supplemented with complete, Mini, EDTA-free Protease Inhibitor Cocktail tablets (Roche Diagnostics Ltd, West Sussex, UK), placed on ice for 30 mins and centrifuged at 15,000g for 12 minutes at 4°C. The supernatant was subsequently added to an equal volume of Laemmli loading buffer (Sigma Aldrich, Poole, UK) and stored at -80°C for later use.

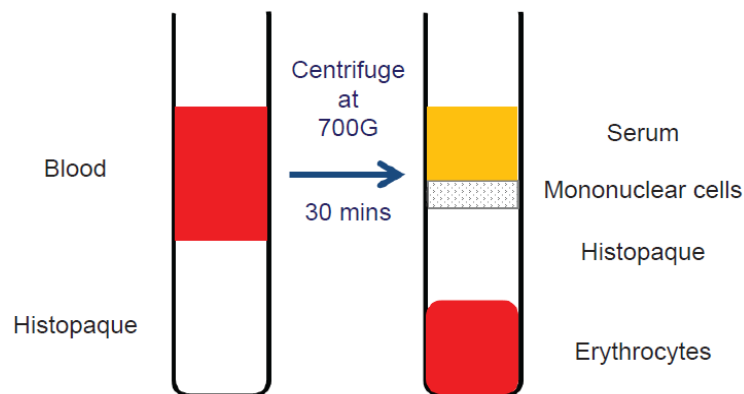


Figure 2.5. Leucocyte separation using Histopaque solution 1077. The mononuclear cells are subsequently used to derive cell lysates.

2.13 Flow cytometry

2.13.1 Cell cycle analysis by flow cytometry

Cell cycle analysis of AAAS-knockdown cells compared with controls was conducted using flow cytometry following propidium iodide treatment of the cells at 50% confluency, on the FACSCalibur cytometer (Becton Dickinson, New Jersey). Briefly, for cell fixation cells were suspended in 0.5 ml of PBS and the cell suspension was added to 5 ml of 1% (w/v) paraformaldehyde in PBS and placed on ice for 15 mins. Cells were centrifuged for 5 mins at 300g and the supernatant discarded. Cells were washed with PBS twice and then resuspended in 0.5 ml of PBS, which was added to 5 ml of ice cold 70% (v/v) ethanol and left to stand for 30 mins on ice. Cells were subsequently spun, the pellet washed with PBS and then resuspended with 0.5 ml of propidium iodide/ RNase A staining buffer (Invitrogen, Paisley, UK). Samples were incubated for 30 mins at room temperature prior to FACS analysis. The CellQuestPro version 6.0 software programme (Becton Dickinson) was used to deconvolute the cellular DNA content frequency histograms to obtain the percentage of cells in the 3 major phases of the cell cycle (G0/1, S, and G2/Mitosis). For representative images of the DNA content frequency histograms for control and AAAS-knockdown H295R cells see Figure 2.6.

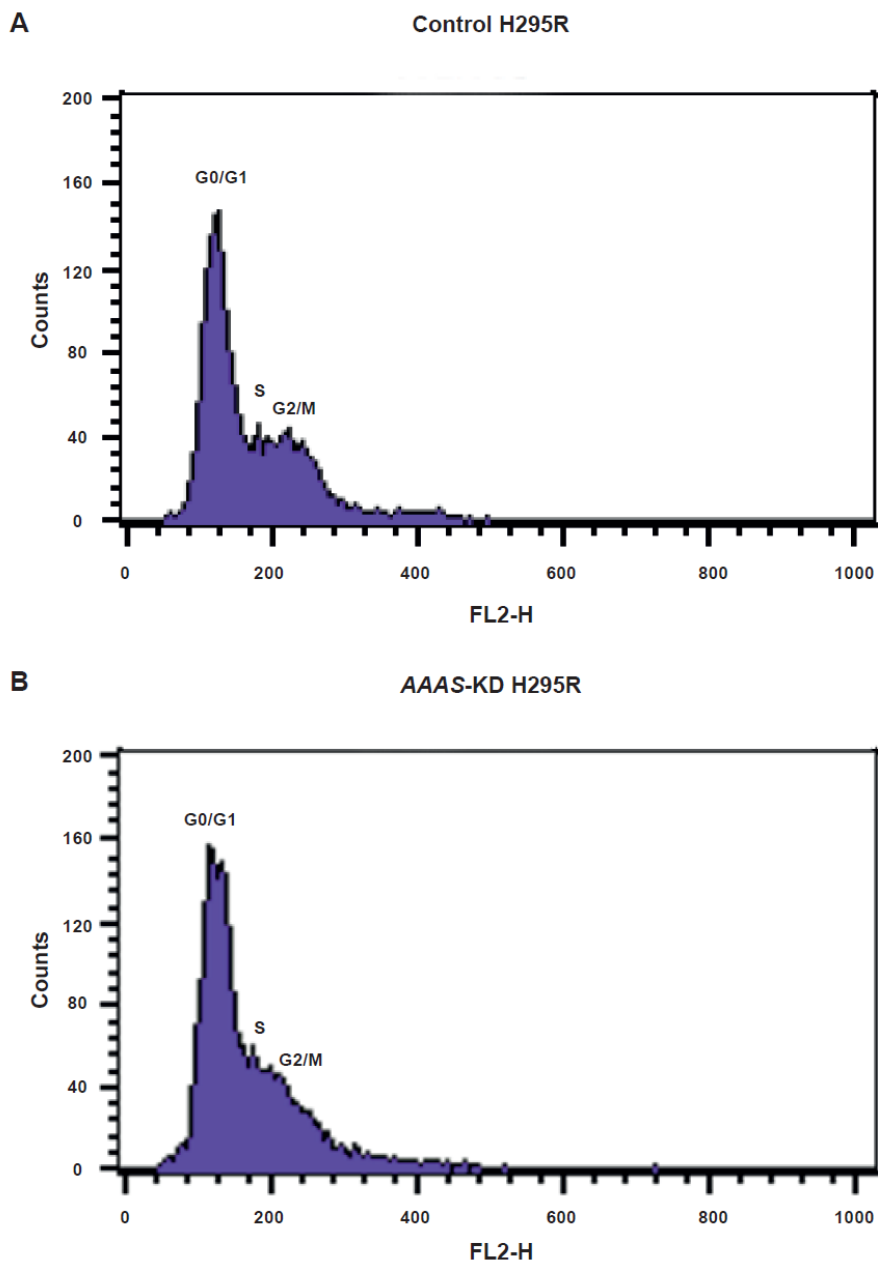


Figure 2.6. Cell cycle arrest in AAAS-knockdown H295R cells. DNA content frequency histograms of (A) control and (B) AAAS-knockdown H295R cells showing blunting of the G2/Mitotic peak in the ALADIN deficient cells.

2.13.2 Mitochondrial superoxide production (MitoSox Red)

MitoSOX Red reagent (Invitrogen, Paisley, UK) is a fluorogenic dye specifically targeted to mitochondria in live cells. Oxidation of MitoSOX Red reagent by mitochondrial superoxide produces

red fluorescence. The reagent is rapidly oxidized by mitochondrial superoxide but not by other ROS and reactive nitrogen species (RNS).

Cells were grown to 50–70% confluence and fresh media added before each experiment. MitoSOX Red was added to a final concentration of 5 μ M according to the manufacturer's recommendation. After 20 mins loading of MitoSOX, *TXNRD2*-knockdown and control cells were trypsinized for 4 mins and neutralized with media. Cells were washed with PBS (with Ca/Mg) (Sigma Aldrich, Poole, UK) and resuspended in fresh media in a sterile FACS tube.

For the determination of mitochondrial superoxide by flow cytometry, measurements were carried out using an LSR Fortessa (BD Bioscience, San Jose, CA), data obtained were recorded and subsequently analysed using DIVA version 6.2 (BD Bioscience, San Jose, CA). 10,000 gated events were recorded. The following steps were carried out for gating: cell debris as represented by distinct low forward and side scatter were gated out for analysis (P1), only singlet events were gated (P2), GFP-positive cells (cells incorporating either scrambled control or *TXNRD2*-knockdown shRNA) were selected (excited by 488 nm blue laser, band pass filter 530/30 nm) (P3), and finally MitoSOX Red was excited by 561 nm yellow/green laser with a band pass filter of 670/30 nm (P4) (Figure 2.7). For quantitative analysis the frequency of events in P4 was multiplied by the median fluorescence intensity (MFI) within P4 to give an integrated MFI (iMFI) [208] reflecting the total functional response of this population of cells to MitoSOX (Figure 5.5B). Student's t test was used for statistical analysis (GraphPad Prism 5 software).

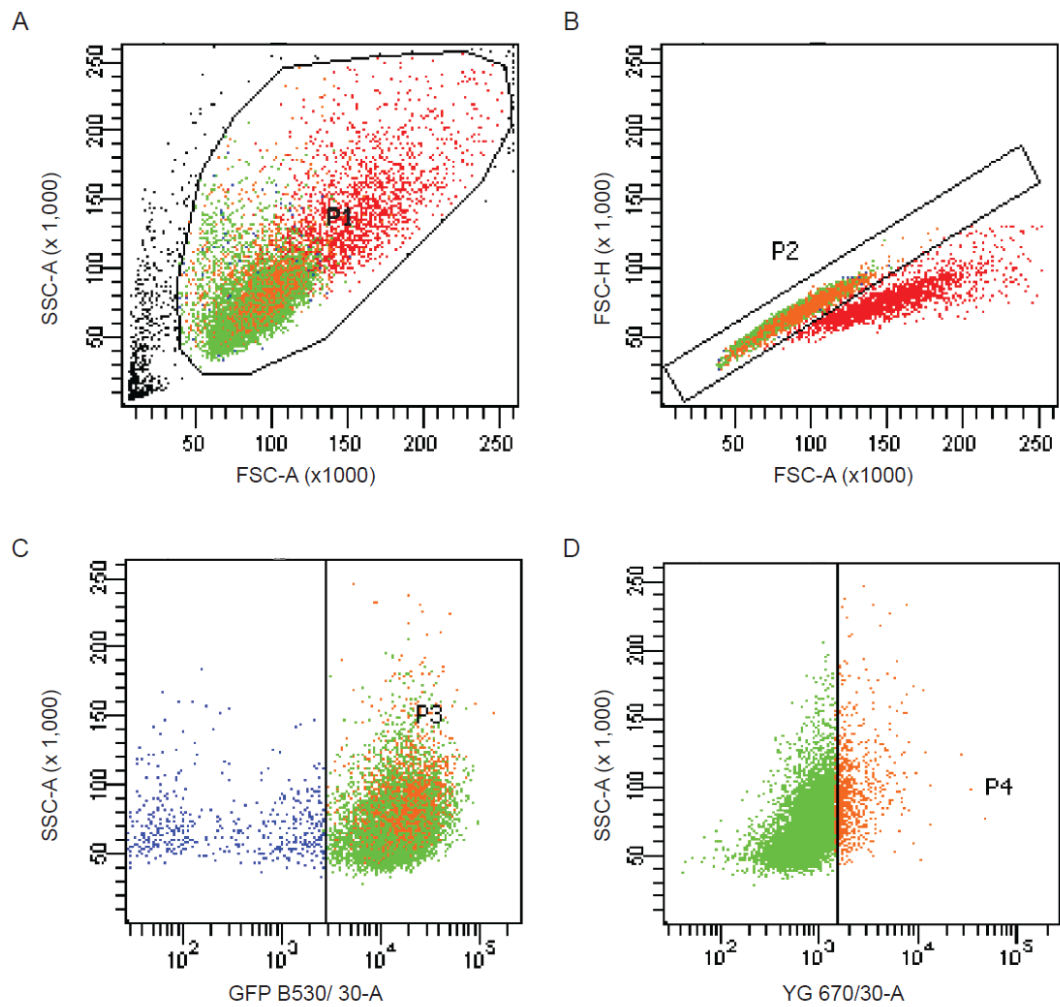


Figure 2.7. Determination of mitochondrial superoxide production, steps used in gating: (A) Low forward and side scatter were gated out for analysis (P1); (B) Singlet events were gated (P2); (C) GFP-positive cells were selected (excited by 488 nm blue laser, band pass filter 530/30 nm) (P3), and (D) finally MitoSOX Red was excited by 561 nm yellow/green laser with a band pass filter of 670/30 nm (P4).

Chapter 3

Deficiency of ALADIN impairs redox homeostasis in human adrenal cells and inhibits steroidogenesis

3.1 Triple A syndrome and oxidative stress

The phenotype in triple A syndrome is complex and all the clinical features are progressive suggesting a degenerative process. The alacrima, achalasia and neurological symptoms are all assumed to be secondary to progressive neurodegeneration. Adrenal insufficiency commonly occurs within the first decade of life though can present later in life. Both neurons and adrenal cells have higher metabolic requirements and are therefore more susceptible to perturbations in redox homeostasis.

Oxidative stress may play a role in the pathogenesis of this disease. Triple A patient dermal fibroblasts have both an overall higher basal intracellular ROS, as measured using the fluorogenic probe dihydrorhodamine (DHR), and higher mitochondrial superoxide species production, as measured by MitoSOX red and FACS analysis [129]. Following induction of oxidative stress with 10 mM of paraquat (1-1'-diethyl-4,4'-bipyridylum dichloride) a further significant increase in ROS production is observed in patient fibroblasts [129]. The authors also investigated the expression of four key ROS-detoxifying enzymes in patient fibroblasts, describing a significant increase in superoxide dismutase 1 (SOD1). Finally, patient cells showed a 1.4 fold increase in doubling time. Taken together, these studies provide supporting evidence that an underlying defect in triple A syndrome is oxidative stress. Long-term stress can induce an irreversible senescent phenotype or stress-induced premature senescence (SIPS) and the authors proposed that the higher basal level of ROS results in SIPS in the patient dermal fibroblasts [129]. ROS play an important role in normal cell cycle regulation but in excess can lead to DNA insult. DNA damage responses during the cell cycle induce an irreversible senescence as a means of maintaining genomic stability [209]. Extrapolating this to what may be seen in adrenal disease, a failure of appropriate proliferation could have impact

on growth and remodelling capabilities of the adrenal gland, certainly histology suggests atrophy of the adrenal cortical zona fasciculata and zona reticularis [11]. ALADIN is ubiquitously expressed yet a tissue-specific phenotype is observed in the condition. The high metabolic demand of the adrenal gland and neurons, may explain the susceptibility of these particular tissues to oxidative stress, and ultimately to disease in triple A syndrome.

3.2 Failure of nuclear import of specific cargo-(es) leads to increased oxidative stress in triple A syndrome patient dermal fibroblasts

In the triple A patient dermal fibroblast model, failure of nuclear import of two DNA repair proteins is described [127, 128]. Patient fibroblasts harbouring the I428Sf mutation, leading to mislocalisation of ALADIN to the cytoplasm, are hypersensitive to the induction of oxidative stress [127]. Treatment with 1 mM of the GSH-depleting agent, BSO leads to reduced cell viability of the patient fibroblasts in comparison to controls, with evidence of DNA fragmentation, characteristic of apoptotic cell death. This effect was partially reversed by the antioxidants decylubiquinone and all-transretinol. Defects in repair of DNA damage have been linked to neurodegenerative disease and the nuclear import of several DNA repair proteins were investigated in this model. Reduced nuclear import of two DNA repair proteins was described; these being aprataxin, mutations of which have been associated with autosomal recessive cerebellar ataxia, and DNA ligase I [127]. Importantly, successful nuclear import of both of these DNA repair proteins, using a modified nuclear localisation signal, did not fully restore the survival of the patient fibroblasts to the level of the controls [128]. This suggested the presence of other proteins that may be imported ALADIN-dependently.

To that effect, full-length human ferritin heavy chain protein (FTH1), which has a DNA-protective role in the nucleus, has been identified as an interacting protein partner for ALADIN *in vitro* [107]. Unlike control cells, no nuclear FTH1 is apparent in triple A patient fibroblasts or lymphocytes implicating ALADIN in the nuclear localisation of FTH1. Apoptosis of SK-N-SH neuroblastoma cells induced by 1 mM H₂O₂ was significantly reduced by transfection of *AAAS* or *FTH1* and maximally by

both genes together. These findings provide compelling evidence that oxidative stress is involved in disease progression and that nuclear import of specific cargo-(es) may be defective [107, 127-129]. How these nuclear import defects lead to an increase in intracellular ROS remains unclear.

3.3 Aims of the study

Current models of the disease, that is, dermal fibroblasts derived from triple A patients and the *Aaas*^{-/-} mouse [67], which does not lead to a triple A syndrome-like phenotype, have significant limitations. Therefore to further understand the functional role of ALADIN in the pathogenesis of triple A syndrome a better model of this complex disease is necessary.

In the present study, I aimed to establish for the first time novel *in vitro* models of the disease by inducing AAAS-knockdown in H295R human adrenocortical tumour cells and SH-SY5Y human neuroblastoma cells, chosen as representative of the predominant cell types affected by the disease. The H295R cell line has been shown to express all key enzymes of steroidogenesis [210-212]. They have the physiological characteristics of zonally undifferentiated human foetal adrenal cells whilst having the ability to produce steroid hormones found in the adult adrenal cortex. They have been used extensively as an *in vitro* model to study the steroidogenic pathway [213-215]. The SH-SY5Y cell line has been widely used in experimental neurological studies including function related to neurodegeneration and neuronal adaptation to toxicity. They are a subline of SK-N-SH cells originally derived from a patient neuroblastoma in the 1970s [216]. This cell line has been used by our group for previous triple A syndrome studies [107].

Using these 2 cell line models, I investigated the potential role of oxidative stress in the pathogenesis of triple A syndrome and anti-oxidant treatment in recovery. These studies provide a better understanding of the pathogenic mechanisms of triple A syndrome looking specifically at affected tissue types.

Results

3.4 AAAS-knockdown in H295R adrenocortical tumour cells and SH-SY5Y neuroblastoma cells

A combination of 2 commercially-available lentiviral shRNA, targeting overlapping regions of exon 5 in the AAAS gene (for specific sequences see Appendix 3), was used to achieve AAAS-knockdown (see Methods Section 2.1). Greater than 70% AAAS-knockdown was established in both cell lines, quantified by real-time qPCR (Figure 3.1A and B). AAAS mRNA expression in AAAS-knockdown (AAAS-KD) H295R cells was significantly reduced to $12.6\% \pm 1.6$ compared with controls ($p < 0.001$, $n=3$) and to $21.1\% \pm 7.4$ in SH-SY5Y AAAS-KD cells ($p < 0.01$, $n=3$). In both cell lines, a reduction in ALADIN protein expression is also observed by immunoblotting (Figure 3.1C and D).

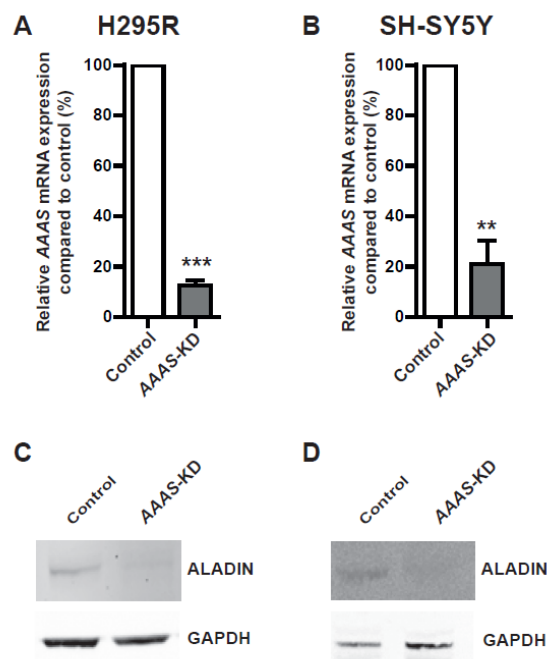


Figure 3.1. Lentiviral shRNA knockdown of the AAAS gene in (A) H295R and (B) SH-SY5Y cells. AAAS mRNA expression was quantified using real-time qPCR and normalised to GAPDH ($n=3$). Control represents transfection with scrambled shRNA. (C) Reduced expression of the protein ALADIN is seen in AAAS-knockdown (AAAS-KD) H295R and (D) SH-SY5Y cells. Data represents mean \pm SD. $p < 0.01$ **, $p < 0.001$ ***.

3.5 AAAS-knockdown results in a reduction in cell viability in H295R cells

Cell number assessed by cell counting, was significantly reduced on day 5 after plating AAAS-KD H295R cells ($10.73 \times 10^4 \pm 1.59 \times 10^4$ (mean \pm SD)), compared with controls ($41.45 \times 10^4 \pm 4.97 \times 10^4$ ($p < 0.0001$, $n=4$)) (Figure 3.2A). MTS assays were used to assess cell viability where absorbance readings are proportional to cellular metabolic activity (Methods 2.8.2). In AAAS-KD H295R cells there was a significant reduction in measured absorbance compared with controls; 0.43 ± 0.01 versus 0.53 ± 0.04 on day 2 after plating ($p < 0.05$, $n=3$) and 0.64 ± 0.05 versus 0.83 ± 0.03 on day 5 ($p < 0.01$, $n=3$) respectively (Figure 3.2B). However, there was no reduction in measured absorbance in AAAS-KD SH-SY5Y cells compared with controls.

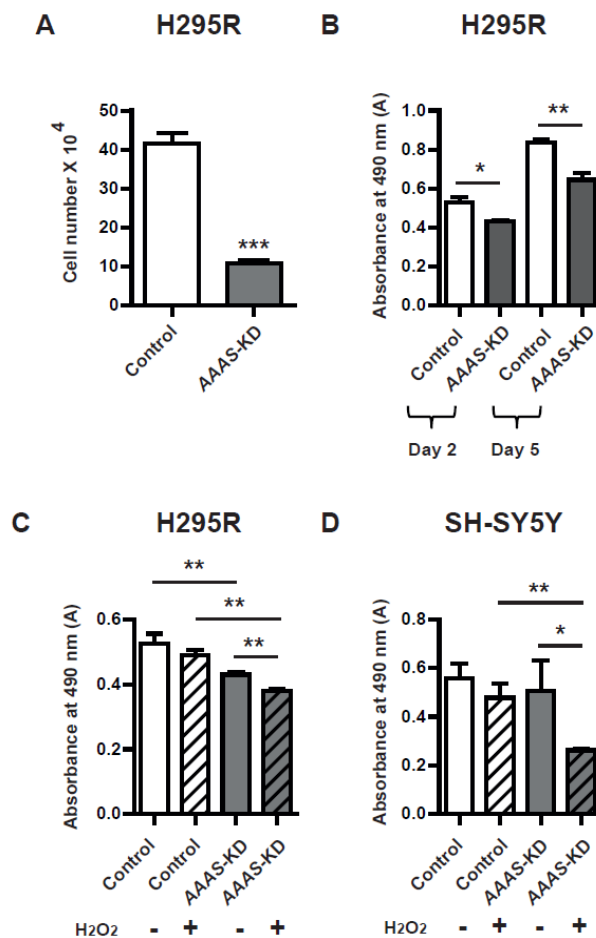


Figure 3.2. A reduction in cell viability of AAAS-KD cells. (A) There was a significant difference in the total number of cells (by cell counting) on day 5 in the AAAS-KD H295R cells ($n=4$) compared with controls following seeding at 2×10^4 cells per well. (B) MTS assays on Day 2 and Day 5 with initial seeding density of 5×10^3 cells per well on day 0. There was a significant reduction in absorbance

readings of AAAS-KD H295R cells in comparison with controls on day 2 (n=3); and day 5 (n=3). (C) Following treatment with 100 μ M H₂O₂, a significant reduction in absorbance readings is seen in AAAS-KD H295R cells (n=3) and (D) AAAS-KD SH-SY5Y cells (n=4) using MTS assays. There was no reduction in absorbance in untreated AAAS-knockdown SH-SY5Y cells compared with controls. Data represents mean \pm SD. p< 0.05*, p< 0.01**, p< 0.001***

3.6 AAAS-knockdown cells are hypersensitive to oxidative stress

Several inducers of oxidative stress have been used in the previous triple A syndrome studies. These include paraquat, BSO (L-buthionine-(S,R)- sulfoximine) and H₂O₂. Paraquat is a herbicide which inhibits the reduction of NADP to NADPH thereby generating superoxide anions, while BSO is a highly selective inhibitor of γ -glutamylcysteine synthetase and its addition to culture medium arrests GSH synthesis. H₂O₂ was chosen to induce oxidative stress in this *in vitro* model, in line with previous work from our group [107]. In addition, H₂O₂ can be found endogenously, produced by reduction of superoxide anions and can contribute to oxidative stress. It readily traverses membranes and is able to access several subcellular compartments. In contrast to the 1 mM concentration used to induce apoptosis in the SK-N-SH neuroblastoma cell model [107], a concentration of 100 μ M H₂O₂ was used for these assays as higher concentrations proved toxic to the cells for this duration of treatment.

In addition to the reduction in cell viability seen at baseline, application of oxidative stress in the form of 100 μ M H₂O₂ for 48 hours resulted in a further significant decrease in cell viability during the MTS assay in AAAS-KD H295R cells (absorbance readings 0.38 ± 0.01 ; mean \pm SD) compared with untreated knockdown cells (0.43 ± 0.01) (p<0.01 n=3) (Figure 3.2C). No significant difference in absorbance was seen between the untreated and treated control H295R cells (Figure 3.2C). There was no reduction in measured absorbance in AAAS-KD SH-SY5Y cells compared with controls, day 2 after plating (Figure 3.2D). However, treatment of AAAS-KD SH-SY5Y cells with 100 μ M hydrogen peroxide resulted in a significant reduction in absorbance readings, 0.26 ± 0.01 , compared with treated controls 0.48 ± 0.05 (p<0.01, n=4) (Figure 3.2D).

3.7 AAAS-knockdown in H295R cells results in cell cycle arrest and an increase in cell death by apoptosis

To further investigate the finding of reduced cell viability of the AAAS-KD H295R cells at baseline, cell cycle analysis of AAAS-KD cells compared with controls was carried out using flow cytometry following propidium iodide treatment (Methods 2.13.1). In flow cytometry, propidium iodide is used as a DNA stain to allow the evaluation of DNA content during cell cycle analysis, thereby delineating the various phases of the cell cycle.

The cell cycle comprises of several phases leading to the division of a single cell into 2 daughter cells; G₀ phase, the resting phase where cells have left the cell cycle; G₁ phase, during which the cell increases in size and checkpoints are in place to ensure the cell is prepared for DNA synthesis; S phase, when DNA replication occurs; G₂ phase, in which checkpoints exist to ensure that the cell is ready to divide and finally; the Mitotic phase, during which orderly division into 2 daughter cells occurs. There was a significant reduction in the proportion of cells in the G₂/Mitotic phase of the cell cycle in the AAAS-KD H295R cell population, $9.2\% \pm 2.7$, compared with controls, $21.0\% \pm 3.0$ ($p < 0.05$, $n=3$). This suggests that ALADIN deficiency causes a reduction in cellular proliferation secondary to cell cycle arrest prior to the G₂/mitotic phase (Figure 3.3A, Methods Figure 2.6).

Apoptosis was assessed by immunoblot analysis of cleaved PARP (Poly ADP ribose polymerase) (Methods 2.8.3). PARP detects single-strand DNA breaks, binds to DNA and signals to DNA-repair enzymes. PARP is inactivated by caspase cleavage in situations where DNA damage is extensive. The cleavage of full length PARP (116kDa) to 85kDa and 27kDa fragments is a well-documented effect of cell death by apoptosis [217, 218]. An increase in the ratio of cleaved PARP relative to total PARP was observed in AAAS-KD H295R cells treated with 1 mM H₂O₂ compared with controls, $20.2 \pm 3.9\%$ versus $12.2 \pm 0.8\%$, respectively ($p < 0.05$, $n=3$) (Figure 3.3B).

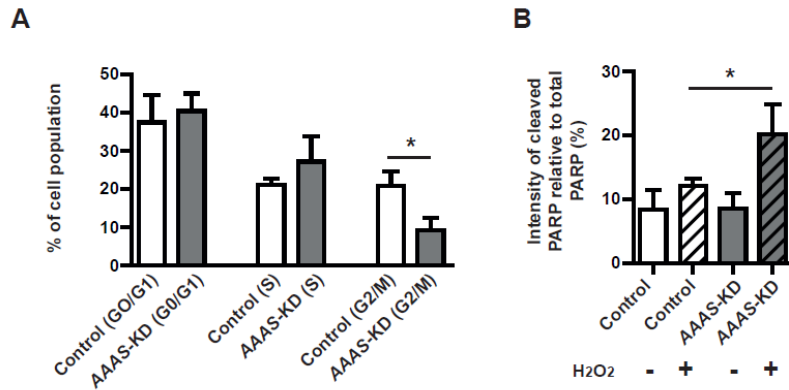


Figure 3.3. Cell cycle arrest and increased apoptosis is observed in AAAS-KD H295R adrenal cells (A) A significant reduction in the % cell population in the G2/ Mitotic phase of the cell cycle is seen in AAAS-KD H295R cells compared to controls suggesting cell cycle arrest (n=3). (B) An increase in cleaved relative to total PARP, measured by densitometric analysis following immunoblotting, is observed in H₂O₂ treated AAAS-KD cells compared with controls (n=3). Data represents mean \pm SD. $p < 0.05^*$

3.8 AAAS-knockdown in H295R cells results in an imbalance of redox homeostasis

Glutathione, a three amino acid peptide (gamma glutamyl-cysteinylglycine), is an abundant antioxidant found in eukaryotic cells, existing in reduced (GSH) and oxidised (GSSG) states. GSH is the predominant form and maintains strong reducing conditions in several subcellular compartments. However with increased ROS formation increased levels of the GSSG are seen (Figure 3.4A). The ratio of oxidised to reduced glutathione is used as a measure of redox thiol status and therefore the intensity of oxidative stress. The luciferase-based GSH/GSSG-Glo assay (Promega, Southampton, UK) was used to assess this ratio in the AAAS-KD H295R cells compared with controls (Methods 2.9).

A significant reduction in the GSH/GSSG ratio is seen in AAAS-KD H295R cells (19.3 ± 2.7 relative light units) compared with controls (26.2 ± 1.9) ($p < 0.05$, n=3) suggesting a baseline increase in oxidative stress in the knockdown cells (Figure 3.4B). As a positive control, a significant reduction in the

GSH/GSSG ratio (0.7 ± 0.2 relative light units) was demonstrated by treatment of the control cells with $40 \mu\text{M}$ menadione, a potent inducer of oxidative stress.

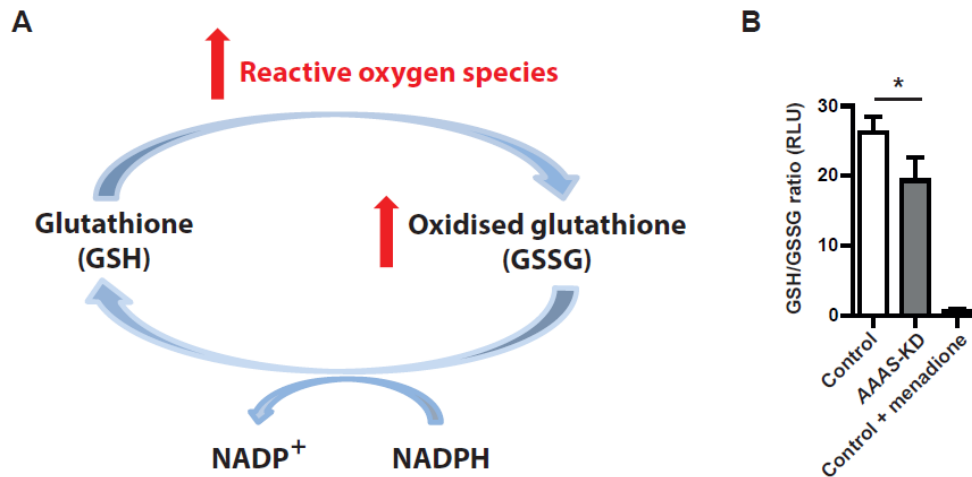


Figure 3.4. An imbalance in redox homeostasis is observed in AAAS-KD H295R adrenal cells. (A) Increased reactive oxygen species leads to an increase in cellular oxidised glutathione (GSSG) and a decrease in the GSH/GSSG ratio. **(B)** The GSH/GSSG ratio was lower in AAAS-KD cells relative to controls (n=3). Oxidative stress induced by treatment with $40 \mu\text{M}$ menadione to control cells further reduces the ratio. RLU, relative light units. Data represents mean \pm SD. $p < 0.05^*$

3.9 Treatment with the anti-oxidant N-acetylcysteine, improves cell viability in AAAS-knockdown cells

N-acetylcysteine (NAC) is a thiol compound, which by providing sulfhydryl groups can act as a precursor to GSH and a direct ROS scavenger. The antioxidant properties of NAC are well documented both *in vivo* and *in vitro*. Application of NAC for 48 hours at a dose of 1 mM , significantly increased absorbance readings in the AAAS-KD H295R cells (0.47 ± 0.06 ; mean \pm SD), compared with untreated knockdown cells (0.28 ± 0.03) ($p < 0.01$, n=4). Higher doses of NAC were found to be toxic to all the cell lines. Absorbance readings were also increased in NAC treated control cells (0.60 ± 0.07) compared with untreated controls (0.47 ± 0.08) ($p < 0.01$, n=4) (Figure

3.5A). However the percentage increase in absorbance readings following NAC application was greater in the AAAS-KD cells ($68.8\% \pm 14.9$) compared with controls ($28.5\% \pm 10.1$) ($p < 0.05$, $n=4$) (Figure 3.5B). A dose of 10 mM NAC for 48 hours significantly increased absorbance readings in AAAS-KD SH-SY5Y cells (0.70 ± 0.08 , mean \pm SD) compared to untreated knockdown cells (0.64 ± 0.07) ($p < 0.05$, $n=4$). However, no significant difference in cell viability was seen in the control SH-SY5Y cells with the same NAC treatment (Figure 3.5C).

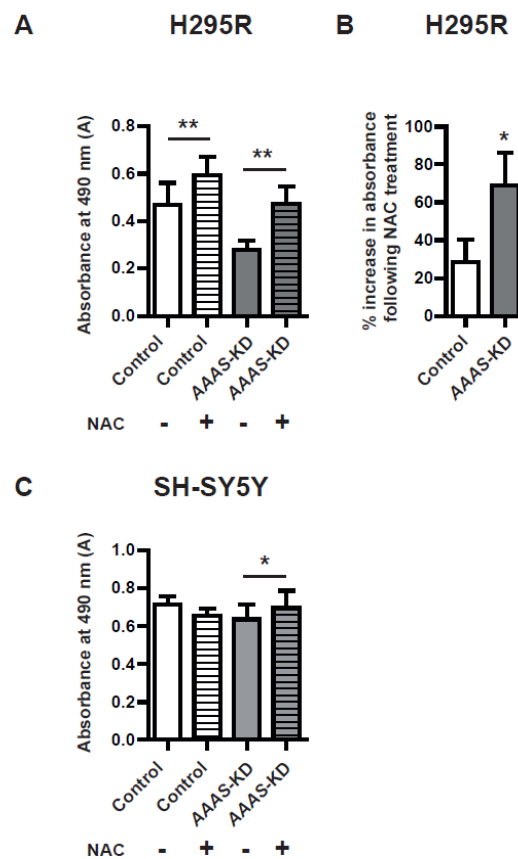


Figure 3.5. Treatment with the anti-oxidant N-acetylcysteine (NAC) improves AAAS-KD cell viability. (A) Treatment with 1mM NAC for 48 hours significantly increases absorbance in both AAAS-KD and control H295R cells ($n=4$). (B) There is a significantly greater % increase in absorbance following treatment in the knockdown cells in comparison with controls ($n=4$). (C) Treatment with 10 mM NAC significantly increases absorbance in AAAS-KD SH-SY5Y cells but not controls ($n=4$). Data represents mean \pm SD. $p < 0.05$ *, $p < 0.01$ **

3.10 AAAS-knockdown affects key components of the steroidogenic pathway including a reduction of steroidogenic acute regulatory protein (STAR) and P450c11 β protein expression

I investigated the expression of three steroidogenic enzymes in the AAAS-knockdown model involved in the production of cortisol: STAR, P450 scc (encoded by *CYP11A1*) and P450c11 β (encoded by *CYP11B1*) (Figure 3.6). Depletion of these key enzymes has been associated with oxidative stress [219, 220] (further described in the discussion 3.12).

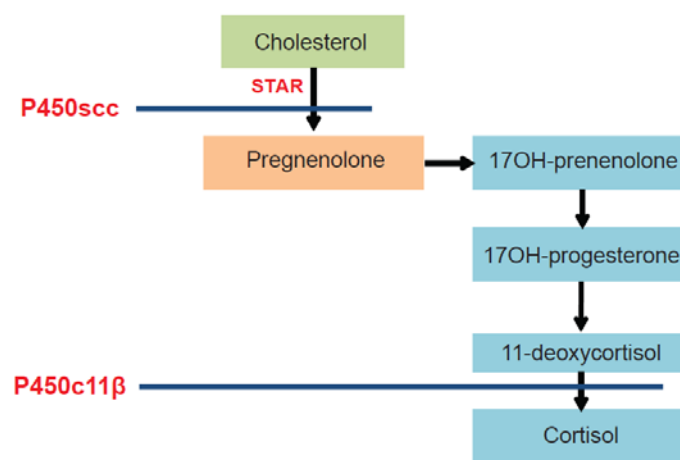


Figure 3.6. The expression of three key enzymes in cortisol production was studied. These are denoted in red and include STAR involved in transport of cholesterol from the OMM to the IMM; P450 scc responsible for conversion of cholesterol to pregnenolone and P450c11 β involved in the final step of cortisol production.

Following immunoblot and densitometric analysis, I observed a significant reduction in the expression of 30kDa STAR relative to GAPDH in AAAS-KD H295R cells compared with controls ($p < 0.01$, $n = 4$) (Figure 3.7A and 3.7B). Furthermore we demonstrate a significant reduction in protein expression of P450c11 β , responsible for the final step in cortisol production ($p < 0.05$, $n = 3$) (Figure 3.7A and 3.7C). There was no significant difference in the expression of the other steroidogenic enzyme investigated, P450 scc (encoded by *CYP11A1*) ($n = 4$) (Figure 3.7A and 3.7D).

The effect on STAR is seen at transcriptional level, with a significant reduction in *STAR* mRNA levels in AAAS-KD cells (0.47 ± 0.01 (mRNA levels relative to GAPDH)) compared with controls (0.62 ± 0.04) ($p < 0.01$, $n=3$). 100 μM H_2O_2 treatment reduces *STAR* mRNA levels (0.38 ± 0.07) in control cells to levels similar to the untreated AAAS-KD cells. In contrast, 100 μM H_2O_2 treatment does not reduce *STAR* mRNA expression further in the AAAS-KD cells (Figure 3.7E).

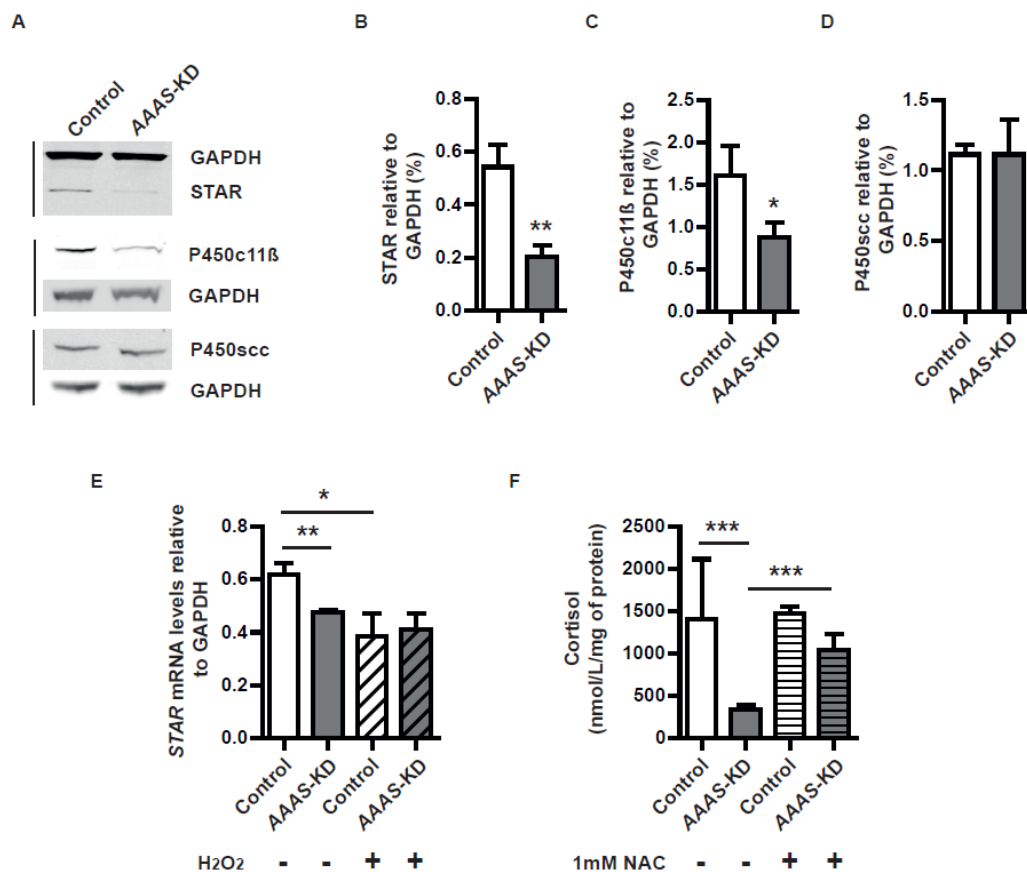


Figure 3.7. STAR and P450c11β (CYP11B1) expression are reduced in AAAS-KD H295R cells with a subsequent reduction in cortisol production. (A) Immunoblot analysis and (B) Densitometric analysis showing a reduction in STAR ($n=4$) and (C) P450c11β protein expression in AAAS-KD H295R cells compared with controls ($n=3$) with (D) no effect on P450scc levels ($n=4$). (E) There is a significant reduction in *STAR* mRNA levels in AAAS-KD cells compared with controls and H_2O_2 treatment of controls reduces levels to that seen with ALADIN deficiency ($n=3$). (F) There is a significant reduction in cortisol production by the untreated AAAS-KD H295R cells compared with controls ($n=9$), with partial improvement following N-acetylcysteine (NAC) treatment ($n=3$). Data represents mean \pm SD. $p < 0.05^*$, $p < 0.01^{**}$, $p < 0.001^{***}$

3.11 AAAS-knockdown in H295R cells results in a significant reduction in cortisol production, which is partially rescued by N-acetylcysteine treatment

Cortisol production was investigated in the AAAS-KD and control H295R cells following 24 hour stimulation with 10 μ M forskolin; cortisol levels were analysed on a Roche Modular E170 automated immunoassay analyser using electrochemiluminescent detection (Methods 2.10). Whilst H295R cells show little response to ACTH stimulation, the organic compound, forskolin, is extensively used to induce steroidogenesis in this cell line, via the activation of the cAMP pathways [221]. This particular concentration of forskolin has been demonstrated to be effective in inducing steroidogenesis.

A significant decrease in cortisol production is observed after stimulation with forskolin in the untreated AAAS-KD H295R cells (344.0 nmol/L/mg of lysate protein \pm 44.4) compared with controls (1404.4 \pm 663.5) ($p < 0.001$, $n = 9$) (Figure 3.7F). Treatment for 24 hours with 1 mM NAC during forskolin stimulation ($n = 3$) significantly increases cortisol production in the AAAS-KD cells (1037.4 nmol/L/mg of lysate protein \pm 154.7) ($p < 0.001$) (Figure 3.7F).

3.12 Discussion

The clinical manifestations of triple A syndrome are progressive and the pathogenic mechanisms involved in the disease process are unclear. Interestingly, despite ubiquitous expression of AAAS mRNA [25], tissue specificity is observed in this condition. In particular, the clinical features of adrenal insufficiency and neurodegeneration affecting the central, peripheral and autonomic nervous systems are not present at birth but develop over time implicating a degenerative process in the pathogenesis of this disorder [12, 13, 15, 22].

Whilst the *Aaas*^{-/-} mouse does not bear a significant phenotype, possibly suggesting some functional redundancy for ALADIN in the mouse model [67], *in vitro* studies on triple A syndrome patient dermal fibroblasts demonstrate an increased susceptibility to oxidative stress [127-129]. Additionally, a reduction in patient fibroblast cell survival and an increase in DNA fragmentation is

reported following exposure to the glutathione-depleting agent, BSO [127]. Triple A syndrome patient dermal fibroblasts are also observed to have higher basal levels of reactive oxygen species and more extensive mitochondrial networks [129]. The precise mechanism(s) for these alterations remain unclear and it is uncertain how reliably observations in dermal fibroblasts can be extrapolated to the tissues affected by triple A syndrome. Disease-causing mutations of the AAAS lead to either ALADIN deficiency or ALADIN mislocalisation suggesting correct targeting of ALADIN to the NPC is required [94]. The failure of nuclear accumulation of DNA repair proteins together with the antioxidant protein FTH1 in triple A syndrome patient dermal fibroblasts may render these cells more susceptible to oxidative stress [107, 127, 128].

This work, revealed a reduction in cell viability following AAAS-knockdown in the adrenocortical H295R cell line, which is further exacerbated by exposure to artificial oxidative stress. Stress induced premature senescence (SIPS) has been described in triple A syndrome patient fibroblasts [129]. The cell cycle analysis of ALADIN deficient adrenal cells suggests that a similar situation exists in adrenal cells probably secondary to cell cycle arrest, with a reduction of the proportion of cells progressing to the G2/Mitotic phase. Control of DNA repair is closely linked to regulation of the cell cycle. Several checkpoints are in place to ensure that DNA is intact before DNA replication and cell division is permitted. The S phase precedes G2/M and replicating DNA is particularly sensitive to DNA-damaging insult during this phase. The DNA-damage response is activated in response to DNA injury, and depending on the extent of damage involved, directs the cell into senescence or apoptosis, or alternatively permits cell survival with activation of DNA repair or damage tolerance mechanisms [222]. Failure of nuclear import of 2 DNA repair proteins, aprataxin and DNA ligase I, reported in triple A syndrome patient dermal fibroblasts [127, 128], may contribute to the cell cycle arrest, forcing the cells into senescence/apoptosis rather than cell survival mechanisms. Additionally, nuclear FTH1 protects against DNA fragmentation and failure of FTH1 nuclear localisation in ALADIN deficient cells may render these cells acutely vulnerable to oxidative stress [107, 119]. Chromosomal

fragility is described in triple A syndrome patients and interestingly, this is also a feature of FGD secondary to a mutation in *MCM4* [173, 223]. *MCM4* is a DNA replicase and a component of the minichromosome maintenance complex, required for the initiation and elongation phases of eukaryotic DNA replication. Thus DNA fragmentation, defective DNA repair and replication appear to be associated with disorders of adrenal insufficiency. *ALADIN* may also play an important role during the cell cycle, as a member of the NPC. Several Nups localise to kinetochores during mitosis, including members of the Nup 107-160 subcomplex and Nup358/RanBP2 [224, 225]. These processes are thought to be integral for the cell to enter into mitosis. Nup358/RanBP2, like *ALADIN*, is located on the cytoplasmic face of the NPC ring. RNA-interference knockdown of this Nup induces G2/M arrest with subsequent mitotic cell death [226]. A missense mutation of human *Nup358/RANBP2* was identified in familial cases of infection triggered acute necrotizing encephalopathy [102]. Depletion of certain Nups also leads to aberrant spindle formation [86]. Therefore it is possible that defective *ALADIN* may impact adversely on cell cycle regulation and cell proliferation at multiple levels.

This impact on cellular proliferation could adversely affect normal adrenal tissue growth and remodelling in response to an insult either as a result of, or independent of *ALADIN* deficiency. Under normal conditions adrenal cell proliferation follows the circadian rhythm of ACTH, with a peak occurring at 0400h, predominantly in the outer zona fasciculata [227]. Chronic ACTH stimulation expands the zona fasciculata with an increase in P450c11 β expression and glucocorticoid secretion [228]. Conversely, suppression of the HPA axis by dexamethasone can cause contraction of the zona fasciculata [228]. The adult adrenal gland is capable of remodelling, as demonstrated by the regeneration of the adrenal cortex following enucleation of the rat adrenal gland and by compensatory adrenal growth in the contralateral adrenal gland following unilateral adrenalectomy [229]. Regeneration can also occur in the human adrenal as evidenced by recovery of adrenal

function following traumatic bilateral haemorrhages [230]. Remodelling may involve differentiation of a stem cell/ progenitor population, de-differentiation of mature cells or cell proliferation.

I also observed an increase in apoptosis in AAAS-knockdown adrenal cells following exposure to artificial oxidative stress. Increased apoptosis combined with impaired cellular proliferation would be in keeping with histopathological findings in post-mortem triple A syndrome adrenal glands. These reveal atrophy of the zona fasciculata, which would be in keeping with a progressive degenerative process [11]. It is also possible that ALADIN deficiency affects cellular proliferation and apoptosis indirectly by impacting on the baseline levels of oxidative stress particularly in the adrenal gland. This may be a result of intracellular ROS interacting with critical cell signalling molecules, thus, regulating several key signalling pathways critical in cellular proliferation and survival [187, 225]. A neurodegenerative process is present in a significant proportion of patients and the other cardinal features of the disease, alacrima and achalasia, are also postulated to manifest secondary to neurological impairment. Autonomic dysfunction at the level of the lacrimal glands has been suggested as the cause of the failure of tear production and a marked reduction of the number of myenteric ganglia and myenteric neurons suggests a lack of intrinsic innervation leads to achalasia [16, 19]. Whilst I do not see a difference in cell viability in untreated AAAS-knockdown neuronal cells, they appear hypersensitive to oxidative stress. The effects of reduction of AAAS expression are less remarkable in the SH-SY5Y cells and this could be a feature of the lower efficacy of the knockdown in this cell line. Alternatively, ALADIN may have adrenal cell specific roles or compensatory mechanisms may exist in other cell types and this warrants further investigation. Nevertheless this preliminary data supports previous suggestions that oxidative stress is also involved in the neurodegenerative process.

Intracellular redox homeostasis is maintained by several mechanisms involving both enzymatic and non-enzymatic anti-oxidant defences. Oxidative stress refers to the imbalance of ROS and oxidants over the capability of the cell to mount an effective anti-oxidant response. A disruption in redox

homeostasis is suggested in the ALADIN deficient adrenal cells with a depletion of GSH. Furthermore, I also demonstrate an improvement in the viability of AAAS-knockdown adrenal and neuronal cell lines following treatment with the anti-oxidant N-acetylcysteine, which replenishes stores of GSH and acts as a direct scavenger of free radicals. There are currently several ongoing clinical trials using N-acetylcysteine, both alone and in combination with other anti-oxidants in the treatment of other neurodegenerative conditions such as Parkinson's disease, Alzheimer's disease and Adrenomyeloneuropathy (AMN) (<http://www.clinicaltrials.gov>). My studies suggest the importance of the glutathione antioxidant pathway in the pathogenesis of triple A syndrome hence anti-oxidant treatments may prove to be a viable therapeutic strategy to slow or even prevent triple A syndrome disease progression.

I demonstrate that AAAS gene deficiency impacts on adrenocortical cell function with a significant reduction in cortisol production in the AAAS-knockdown H295R cells. STAR is fundamental for the transport of cholesterol across the mitochondrial membrane and is the rate-limiting step for steroidogenesis. There is evidence that STAR is particularly sensitive to ROS. In Leydig cells, oxidative stress inhibits the mitochondrial import and processing of STAR with a reduction in the 30-kDa intramitochondrial form of STAR, resulting in a reduction in steroidogenesis. Whilst several studies in Leydig cells demonstrate a clear reduction in 30 kDa STAR expression in response to reactive oxygen species, it is unclear whether there is also an effect of ROS at the transcriptional level as current data are inconsistent [219, 220] Consistent with the findings of Shi and colleagues who demonstrate an effect on STAR promoter activity in Leydig cells, for the first time I demonstrate that an imbalance of redox homeostasis in AAAS-knockdown cells reduces both STAR mRNA and the expression of 30 kDa STAR protein in adrenocortical cells with no effect on P450_{scc} expression [220]. Interestingly, I also see a significant reduction of P450_{c11β} protein expression in the AAAS-knockdown cells. P450_{c11β} catalyses the final step in cortisol production and is cited as one of the most ROS-producing steps of steroidogenesis [178]. This is in contrast to the P450_{scc} system where much smaller amounts of ROS

are produced. More recently a new model for H₂O₂-mediated physiological control of steroidogenesis in the adrenal has been described. H₂O₂ is produced as a by-product of steroidogenesis [206]. Specific mitochondrial antioxidant mechanisms exist in the adrenal cortex and when the antioxidant capacity is exceeded, there is an accumulation of H₂O₂ in the mitochondria with overflow into the cytosol that triggers a reduction in STAR protein expression [206]. It is possible that a similar mechanism causes a reduction in P450c11 β expression, protecting the adrenal from further oxidative damage. This may explain the particular susceptibility of the zona fasciculata to disease, with predominance of glucocorticoid deficiency. Recently, Korytowski *et al* also described an additional mechanism by which steroidogenesis may be compromised by oxidative stress in Leydig cells. In this model, STAR-mediated trafficking of redox active cholesterol hydroperoxides results in mitochondrial toxicity rendering these steroidogenic cells susceptible to further oxidative insult [231].

Whilst it is accepted that STAR plays a critical role in adrenal and gonadal steroidogenesis, *STAR* mutations can present with a spectrum of phenotypes ranging from LCAH to milder atypical or nonclassic forms of LCAH [168, 171]. Nonclassic LCAH is caused by *STAR* mutations that retain partial activity and may present with a phenotype analogous to FGD. I hypothesise that ALADIN deficiency leads to an imbalance in cellular redox homeostasis resulting in a reduction in STAR and consequent impairment of cortisol and less frequently, mineralocorticoid production. Preservation of mineralocorticoid synthesis may reflect not only the relative preservation of zona glomerulosa but also the lower production rate of aldosterone compared to cortisol. Interestingly, gonadal dysfunction is not reported in triple A syndrome. This suggests that the impairment of STAR is mild similar to patients with the p.R188C/R192C *STAR* mutations in which the protein retains 25-30% functionality or that other mechanisms also contribute to the adrenal phenotype [168].

Oxidative stress has been implicated in the pathogenesis of numerous other neurodegenerative diseases and in several adrenal conditions. One such disorder is X-linked ALD where mutations in

ABCD1 (encoding the peroxisomal ABCD transporter) result in tissue and plasma accumulation of VLCFAs. Similar to triple A syndrome, this disorder is also characterised by graded damage to the nervous system together with adrenal insufficiency. The toxic effects of the excessive VLCFAs are thought to result from an increase in steady-state ROS production, depletion of GSH and, therefore, dysregulation of the cell redox homeostasis [232, 233]. More recently, mutations in the anti-oxidant gene *NNT*, encoding nicotinamide nucleotide transhydrogenase, which supplies high concentrations of NADPH necessary for the regeneration of GSH from GSSG, have been reported to cause FGD with ACTH-resistant adrenal failure [173]. Thus, there is an emerging picture of defects in antioxidant defence impacting specifically on the adrenal gland. It is possible that functional compensation by overlapping antioxidant defence mechanisms protects other cell types or tissues unaffected in these disorders. In FGD secondary to *NNT* mutations, an isolated adrenal defect has so far been described, in comparison to ALD and triple A syndrome where a more severe phenotype is seen with additional neurological disease. It is likely that there is more robust compensation for defective *NNT*, and certainly mitochondrial NADPH can also be generated by NADP-linked malic enzyme and NADP-linked isocitrate dehydrogenase [234].

The precise mechanisms by which antioxidant defences are impaired in triple A syndrome need to be further characterised. However, using *AAAS*-knockdown adrenal and neuronal cells I provide further compelling evidence that oxidative stress is involved in the progression of triple A syndrome. As the adrenal cortex and neural tissue are highly oxidative environments this may explain the susceptibility of these tissues in the absence of functional ALADIN.

Chapter 4

A stop gain mutation in the mitochondrial antioxidant, Thioredoxin reductase 2 (*TXNRD2*) is associated with familial glucocorticoid deficiency (FGD).

4.1 Aetiology and molecular genetics of FGD

Familial glucocorticoid deficiency (FGD; OMIM #202200) is characterised by ACTH resistance and glucocorticoid deficiency, with typical biochemical findings of low serum cortisol levels and high plasma ACTH. Classical ACTH resistance is primarily caused by mutations in the ACTH receptor (melanocortin 2 receptor; *MC2R*) and the melanocortin 2 receptor accessory protein (*MRAP*), required for trafficking *MC2R* to the cell surface and subsequent signalling [138, 159]. Mutations in *MC2R* and *MRAP* thus disrupt ACTH signalling in the zona fasciculata and reticularis resulting in glucocorticoid and adrenal androgen deficiencies respectively.

Direct sequencing of *MC2R* in 1993 led to the first description of a disease-causing mutation in FGD; the identification of the p.S74I mutation in *MC2R* in 2 siblings with FGD [138]. The next gene discovery in the FGD cohort was the identification of the adrenal specific gene, *MRAP* (melanocortin receptor 2 accessory protein) in 2005 [159]. For this a whole genome scan was undertaken by single nucleotide polymorphism (SNP) array in one family followed by homozygosity mapping, RT-PCR of candidate genes within the region together with screening for adrenal expression. This discovery has provided invaluable information about the mechanism of ACTH signalling in the adrenal cortex. Mutations in *MC2R* and *MRAP* have since accounted for 25% and 20% of disease pathogenesis within the patient cohort, respectively [131] (Figure 4.1).

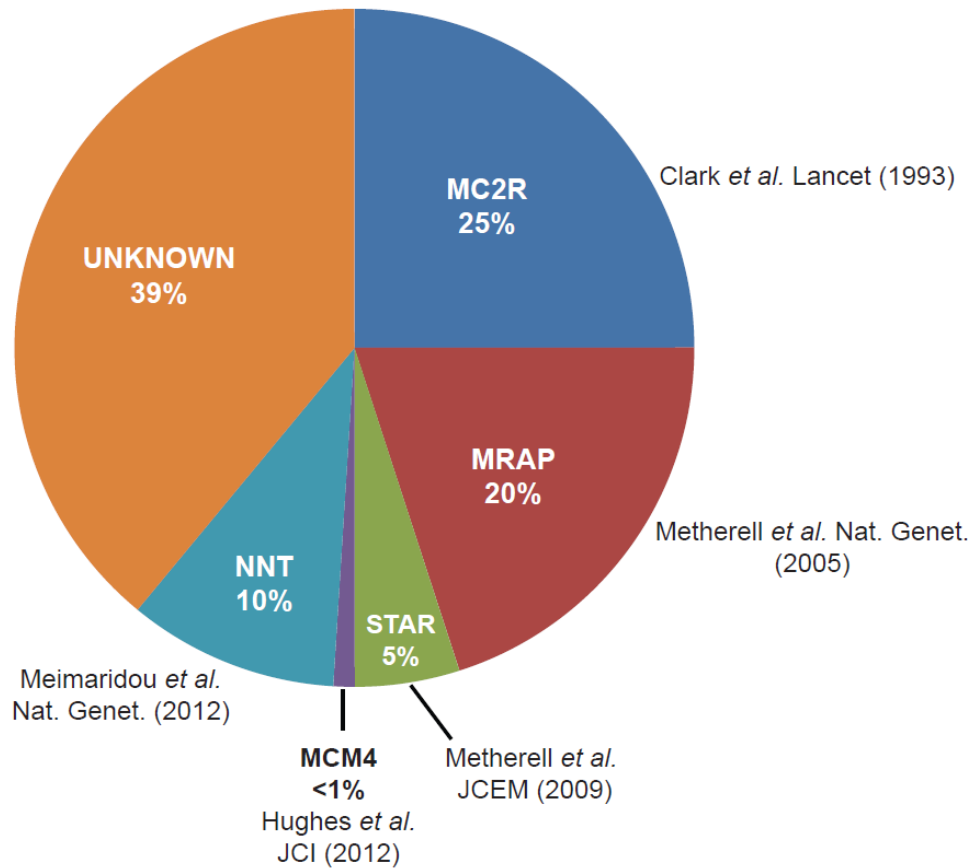


Figure 4.1. Aetiology of disease within the FGD cohort, comprising more than 250 patients. The majority of cases are caused by defective ACTH signaling and mutations in *MC2R* and *MRAP*. 39% of cases remain of unknown aetiology.

It is however with the use of targeted sequencing that we have seen rapid identification of disease-causing genes within our FGD cohort. Autozygosity mapping in 8 affected children from 3 kindreds from the Irish traveller community localised the disease locus to the pericentric region on chromosome 8 and targeted exome capture and high throughput sequencing identified the causal variant, c.71-1insG, in minichromosome maintenance 4 protein (*MCM4*; OMIM #609981) in 2012. This mutation is responsible for FGD in the Irish traveller population, incorporating a phenotype of short stature, natural killer cell deficiency and chromosomal fragility. Closely following this discovery, linkage to a further locus on chromosome 5 was identified in 3 consanguineous families

by SNP genotyping with identification of a mutation in nicotinamide nucleotide transhydrogenase (*NNT*, OMIM #614736) in 2012 [177]. Mutations in *NNT*, spread throughout the gene, have accounted for disease within 10% of the cohort (Figure 4.1). *NNT*, located in the inner mitochondrial membrane, plays an important role in NADPH generation in the mitochondria. The transhydrogenase activity of *NNT* catalyses the interconversion of NADH and NADPH with the generation of NADPH as the predominant direction. High concentrations of reduced nicotinamide adenine dinucleotide phosphate (NADPH) are required by the thioredoxin and glutathione systems to detoxify mitochondrial H₂O₂. Without *NNT*, the production of NADPH is compromised, causing the mitochondria to become more sensitive to oxidative stress.

Thus, within a short space of time, targeted sequencing has allowed for the identification of causative genes in differing biological pathways. These discoveries have provided invaluable information about pathways, other than defective ACTH signalling, leading to primary adrenal insufficiency.

4.2 Aims of the study

Thirty-nine percent of cases within the FGD cohort have unknown aetiology and the novel pathogenic mechanisms described above have highlighted alternative biological pathways for further investigation (Figure 4.1). In this study, I describe the investigation of several affected individuals within an extended consanguineous Kashmiri family (for pedigree see Figure 4.2), in whom sequencing of coding exon/intron boundaries of *MC2R*, *MRAP*, *STAR*, *MCM4* and *NNT* genes had been undertaken and no mutations found. I aimed to identify the disease-associated mutation in this kindred and carry out functional validation of any putative candidate(s).

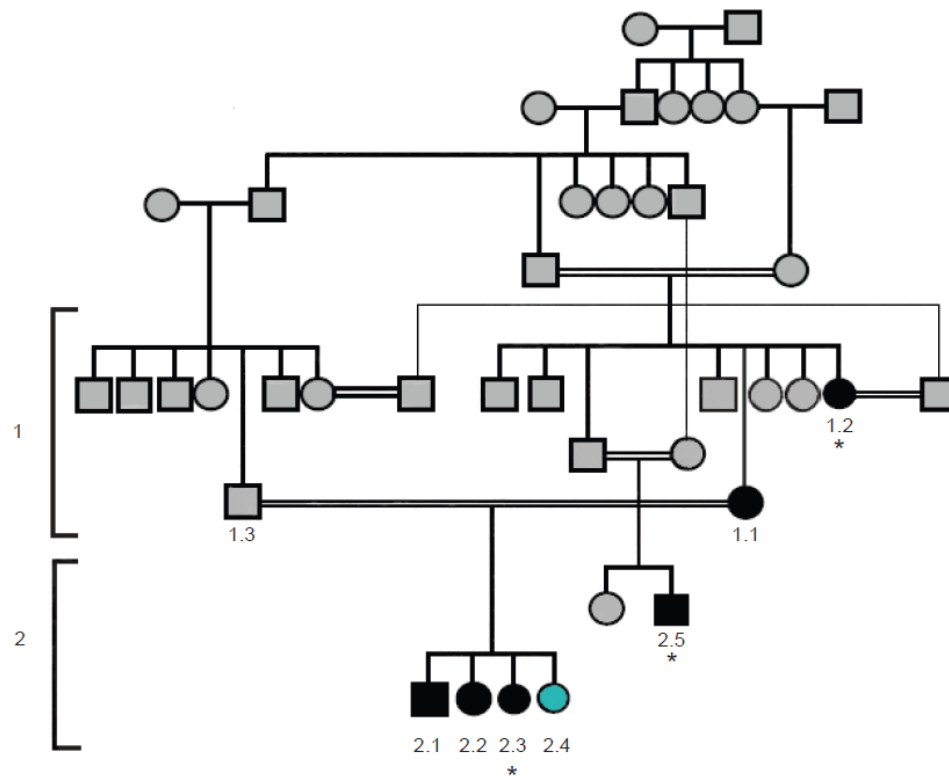


Figure 4.2. Pedigree of the affected kindred. Black-filled symbols indicate affected individuals. Grey-filled symbols indicate unaffected individuals. The individual shaded in blue, patient 2.4, is undergoing annual screening for FGD. The asterisks denote the three affected individuals who were subjected to whole exome sequencing.

4.3 Study approval

This study was approved by the Outer North East London Research Ethics Committee, reference number 09/H0701/12.

4.4 Clinical Case Reports

Affected individuals within the kindred exhibited a wide spectrum of severity in symptoms at diagnosis with late onset in several family members (Table 4.1). The index case (patient 1.1), whose parents were first cousins, was diagnosed with isolated glucocorticoid deficiency at the age of 10.8 years following hyperpigmentation during febrile illnesses. Biochemical results revealed ACTH resistance: raised 0900h plasma ACTH (160 ng/L, normal <50) and low 0900h serum cortisol levels

(<10 nmol/L, normal range 200-600). Her sister (patient 1.2) was subsequently diagnosed, aged 4.5 years, with a two-year preceding history of hyperpigmentation.

The children of the index case (patients 2.1 to 2.3) were screened from birth and diagnosed with glucocorticoid deficiency between the ages of 0.1 and 6.9 years. Patient 2.5 presented at 0.1 years with cardiac failure secondary to congenital truncus arteriosus and a ventricular septal defect. During his admission he was diagnosed with isolated glucocorticoid deficiency. He is the only affected member of the kindred known to have comorbidity. Echocardiograms and ECGs were normal in all individuals homozygous for the mutation except patient 1.2, who has trivial tricuspid and mitral valve regurgitation. All clinically affected individuals demonstrated a poor cortisol response to ACTH stimulation (125 µg tetracosactide (synacthen) intramuscularly) requiring standard glucocorticoid replacement therapy. All have normal mineralocorticoid production. The post-pubertal patients, patients 1.2 and 1.2, both have reduced androstenedione and DHEAS levels. Patient 2.4 is currently clinically well aged 7.4 years with normal biochemistry and is under close clinical surveillance. Interestingly, she had raised ACTH levels in early infancy (0900h ACTH of 124 ng/L at 0.02 years of age; corresponding cortisol of 305 nmol/L), which subsequently normalised. Her older sister, individual 2.2, similarly had raised ACTH levels in infancy (0900h ACTH 171 ng/L at 0.98 years of age; corresponding cortisol of 448 nmol/L) which normalised, but she was later diagnosed with isolated glucocorticoid deficiency at 6.9 years of age.

Pt	Sex	Age (yr)	Age at diagnosis (yr)	Mode of presentation	Relevant clinical history	Degree of pigmentation at presentation	0900h Cortisol (nmol/L)	0900h ACTH (ng/L)	Max. cortisol with ACTH stimulation (nmol/L)	ECHO
1.1	F	33.8	10.8	Hyper-Pigmentation	Asymptomatic until diagnosis	Moderate	<10	160	Not done	Normal
1.2	F	27.1	4.5	Hyper-Pigmentation	Asymptomatic until diagnosis	Severe	<25	500	<25	Trivial TR and MR
2.1	M	13.9	2.9	Screening	Mild neonatal jaundice	None	65	8130	61	Normal
2.2	F	9.5	6.9	Screening	Asymptomatic	Mild	158	514	33	Normal
2.3	F	8.6	0.1	Screening	Asymptomatic	Severe	28	3249	147	Normal
2.4	F	7.4	-	Currently well	Asymptomatic	None	262*	23.2*	1052*	Normal
2.5	M	2.1	0.1	Poor feeding	Heart failure secondary to cardiac defect	Mild	46	>1240	190	Truncus arteriosus and VSD

Table 4.1. Clinical details of the members of the kindred. 0900h cortisol normal range 200-600 nmol/L, 0900h adrenocorticotrophic hormone (ACTH) normal range <50 ng/L. Maximum cortisol with ACTH stimulation normal >550 nmol/L. VSD, ventricular septal defect; TR, tricuspid regurgitation; MR, mitral regurgitation. Biochemical data at time of diagnosis. *Most recent levels

4.5 A stop gain mutation in *TXNRD2* is associated with disease in the kindred

Whole exome sequencing (WES) has been used as a powerful tool in gene discovery since the description of the first application of the technique to identify the gene for a rare monogenic condition of unknown cause; the discovery of *DHODH* mutations causing Miller syndrome (OMIM #263750) [220]. It has been a particularly useful tool in the study of diseases of autosomal recessive inheritance, where more extensive filtering of candidates is possible. In the case of the family I have been studying, an autosomal recessive pattern of inheritance was suggested by the pedigree (Figure 4.2). Affected individuals were mutation negative for the known genetic causes of FGD. In keeping with the other known causes of FGD, I hypothesised that a rare non-synonymous homozygous mutation would be associated with disease in this extensive kindred. To identify the causative genetic variant in this family I adopted a WES approach followed by Sanger sequencing to assess segregation within the kindred.

WES of 3 affected individuals (denoted by the asterisks in the pedigree, Figure 4.2) was conducted using the Illumina HiSeq 2000 Sequencer (samples processed by Otogenetics Corporation, USA) (Methods 2.6). The number of variants was reduced by the following strategy; (i) identifying variants that were common to all 3 individuals (ii) excluding variants that were heterozygous (iii) removing variants, annotated in SNP databases (Ensembl SNP database, release 54, see URL), with a minor allele frequency of >0.01 and (iv) evaluating non-synonymous coding variants, splice variants and indels only (Figure 4.3). Variant calling in the 3 individuals identified over 300,000 variants, approximately 20,000 of which were homozygous variants common to all 3 individuals. Rarity filtering identified 35 possible candidates with a MAF of <0.01 in dbSNP (Appendix 6). The final step of the filtering process reduced this further to 4 candidates (Appendix 7). Sanger sequencing of candidate variants was then carried out in the whole family to analyse segregation of the disease.

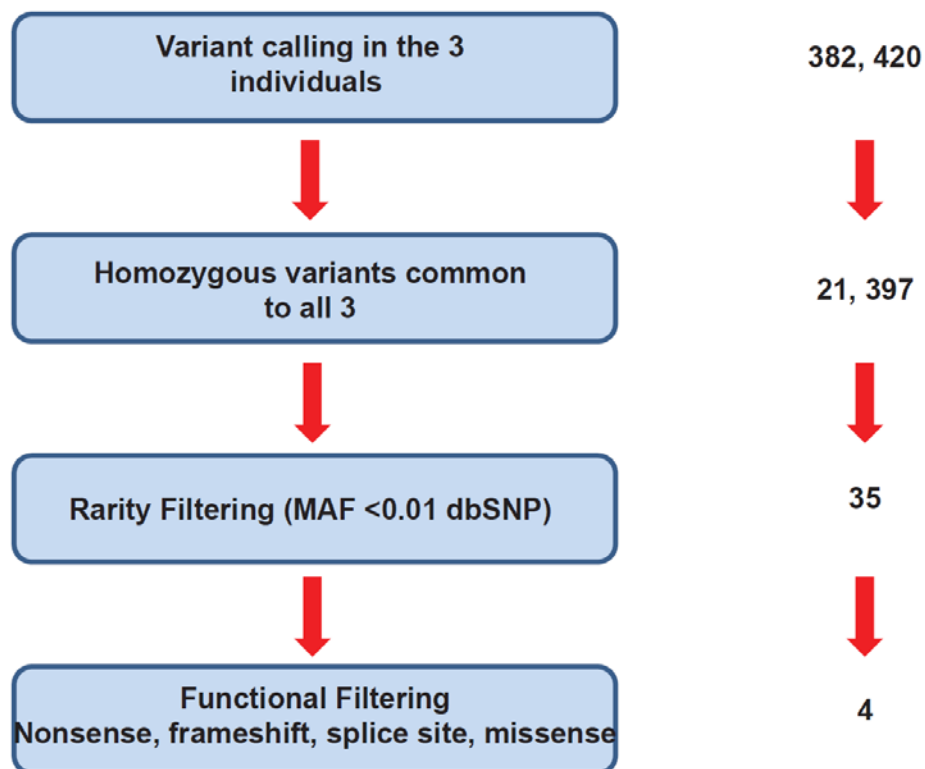


Figure 4.3. Whole exome sequencing filtering strategy. The number of variants was reduced at each stage after initial variant calling.

Four rare homozygous variants within coding sequences, common to all 3 individuals, were identified following application of our filtration strategy (Figure 4.3; Appendix 7). Three variants in two candidate genes did not segregate with the disease. All three variants are in dbSNP; the *OR2T35* variant (rs370874670) and the two *MUC4* variants (rs374495657 and rs202060675), but there is no frequency or population data. The variants were discounted on the basis that disease affected patient 2.2 was wildtype for rs370874670 in *OR2T35* and the unaffected husband of patient 1.1 (individual 1.3) was homozygous for both changes in *MUC4*.

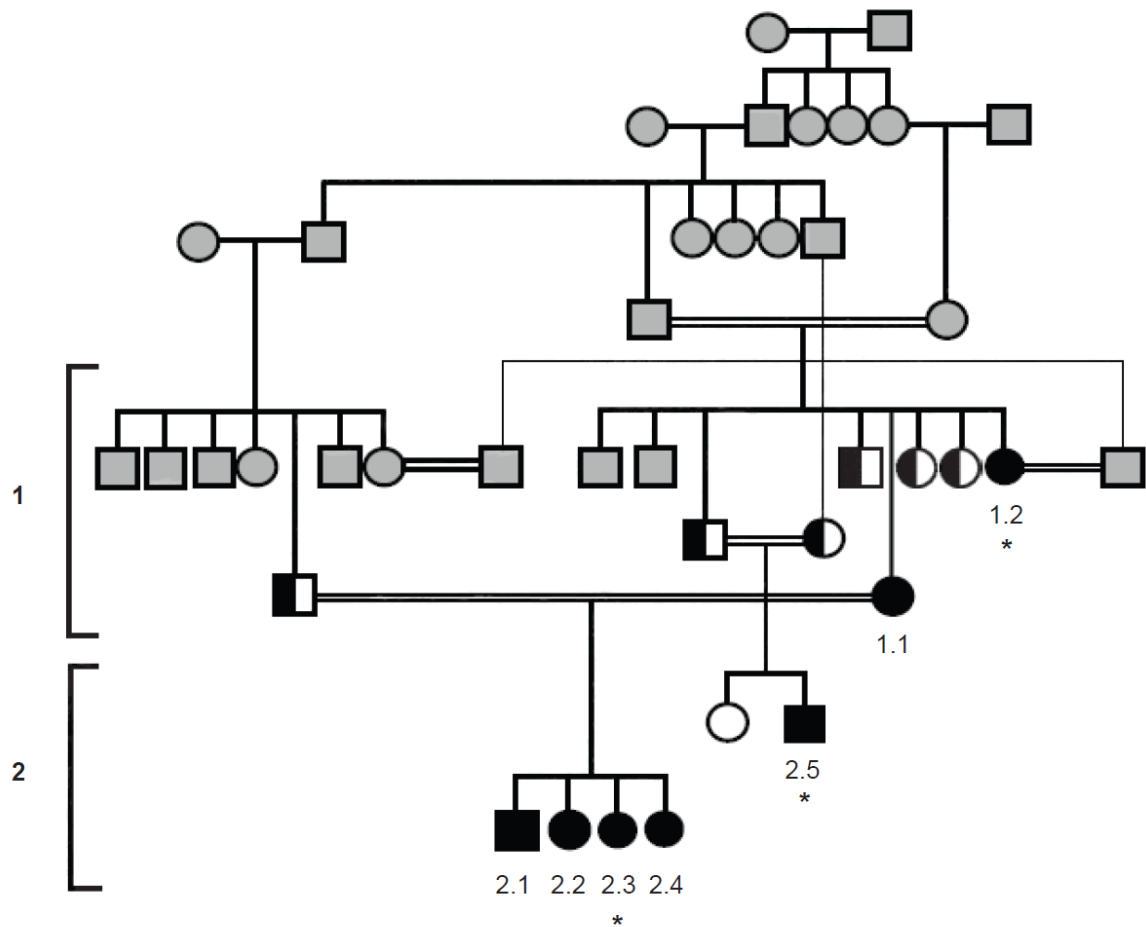


Figure 4.4. Segregation of the p.Y447* *TXNRD2* mutation in the pedigree. Black-filled symbols indicate individuals homozygous and half-filled indicate individuals heterozygous for the p.Y447* *TXNRD2* mutation. White-filled symbols indicate wild-type individuals. Grey-filled symbols indicate individuals not tested. The asterisks denote the three affected individuals who were subjected to WES.

Only one variant, a stop gain mutation (c.1341T>G; p.Y447*) within exon 15 of *TXNRD2* (RefSeq accession number NM_006440.3), encoding mitochondrial thioredoxin reductase 2 (*TXNRD2*), segregated with the disease in this kindred (Figure 4.4 and 4.5). Individuals heterozygous for the change were clinically unaffected. Two SNPs at this position are annotated in dbSNP (ID rs202059967) an A>G change and the A>C change reported here. The A>G change is silent and seen in only 1/12686 alleles in NHLBI *GO Exome Sequencing Project*, ESP6500 (See URLs), the A>C change is not recorded in this database but is listed in dbSNP EXOME_CHIP data (submitter SNP ID

ss491568437), with no frequency data. Sequencing of >1000 healthy adult British Pakistanis revealed a minor allele frequency of 1.04% for this variant, genotypes were A/A=1080; A/C=23; C/C=0. Importantly, in this control population, the variant was never seen in homozygosity. One other stop gain mutation (p.R441*; rs200162480) is listed for *TXNRD2* but is only present in heterozygosity in one individual (1/12730 alleles). The coding exons of *TXNRD2* were sequenced in 50 patients with a clinical diagnosis of FGD by a combination of whole exome and Sanger sequencing. WES data was analysed in each individual and for any exonic region with a coverage of <20 reads PCR amplification and Sanger sequencing was carried out. Sequencing within this cohort revealed variants at rs5748469 (p.A66S), rs5992495 (p.S299R) and rs1139793 (p.I370T) with MAF of 30%, 17.5% and 25% respectively, in keeping with their frequencies in the European American cohort from *GO-ESP* (see URL). This would fit with the fact that most of our FGD patients are of European extraction. No other variants were discovered in 100 FGD alleles making this *TXNRD2* mutation a rare cause of FGD.

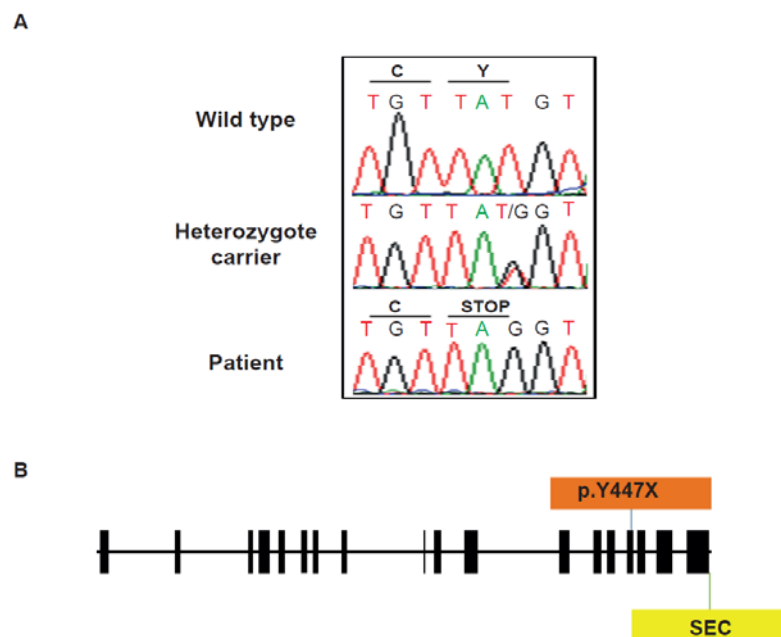


Figure 4.5. Identification of p.Y447* *TXNRD2* mutation. (A) Partial sequence chromatograms of genomic DNA from wild-type, heterozygote carrier and a patient, showing the base change from T to G in exon 15, resulting in a premature stop codon. (B) Gene structure of *TXNRD2*; p.Y447* mutation prior to the selenocysteine active site (SEC).

4.6 Expression of TXNRD2 in affected individuals

The mutation was predicted to cause a protein truncation prior to the selenocysteine active site (SEC), with a predicted truncated protein size of approximately 52 kDa (Figure 4.5), the full length protein being 56kDa. To investigate the effect of the mutation, RT-PCR of patient cDNA was carried out (primer sequences, Appendix 2) and protein expression in patient leukocytes was determined by western blot analysis of TXNRD2 (rabbit polyclonal anti-TXNRD2 antibody; immunogen incorporating amino acid sequence 203 to 353 of TXNRD2). Leukocytes were extracted using a gradient density centrifugation method with Histopaque-1077 (Sigma Aldrich, Poole, UK) (Methods 2.12). Western blotting of patient lysates revealed absence of the protein in homozygous patients in comparison to a heterozygote carrier and an age and sex-matched control (Figure 4.6). In contrast, western blotting for the cytoplasmic thioredoxin reductase 1 revealed patients express TXNRD1 at similar levels to controls (Figure 4.6) GAPDH was used as a loading control.

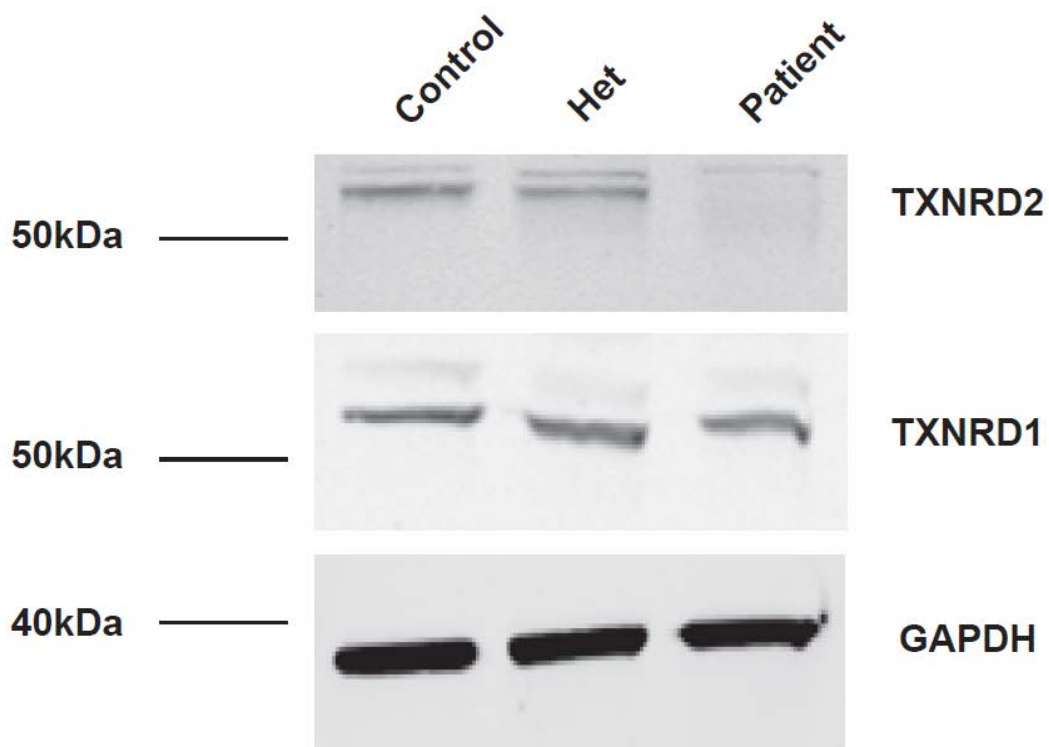


Figure 4.6. p.Y447* TXNRD2 mutation leads to loss of TXNRD2 protein. Lysates from a homozygous patient, heterozygote carrier (Het) and control human lymphocytes were immunoblotted with an

anti-TXNRD2 antibody. While control and the heterozygote carriers expressed the 56 kDa protein, this is absent in the homozygote patient with no evidence of a truncated protein. All individuals express cytoplasmic TXNRD1 at similar levels.

To determine whether mRNA of the mutant allele was present, RNA was extracted from patient blood using the PAXgene Blood RNA kit (Qiagen, Crawley, UK) (Methods 2.3.3). Reverse transcription of the samples and RT-PCR were then carried out. The absence of a *TXNRD2* fragment on amplification from cDNA of the homozygote patient coupled with the finding that direct sequencing of amplicons from the heterozygote carrier revealed amplification of the wild-type sequence alone was consistent with nonsense-mediated decay (Figure 4.7) of mRNA.

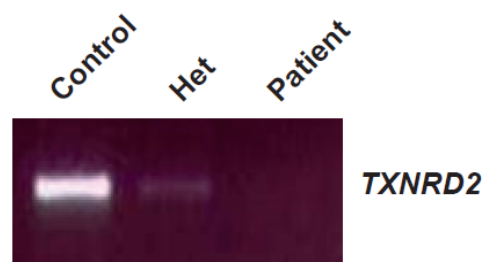


Figure 4.7. RT-PCR of *TXNRD2*. Amplification of a fragment of *TXNRD2* from cDNA of patient, heterozygote carrier and control suggested nonsense mediated decay of mRNA.

4.7 Discussion

In 2009 in a proof of concept study, Ng and colleagues demonstrated that candidate genes for monogenic disorders, in this case a rare dominantly inherited disorder, Freeman-Sheldon syndrome (OMIM #193700), could be identified by WES a small number of unrelated individuals [235]. Subsequently the same group demonstrated mutations in *DHODH* caused Miller syndrome (OMIM #263750) in 4 affected individuals in 3 independent kindreds, in the first successful application of exome sequencing to identify the gene for a rare monogenic condition of unknown cause [220]. Since these first studies there has been a rapid expansion in the use of WES in gene discovery.

In this study, I describe the use of WES to identify the first homozygous mutation in the mitochondrial selenoprotein, thioredoxin reductase 2 (*TXNRD2*) associated with FGD in a consanguineous Kashmiri kindred. Absence of the 56 kDa TXNRD2 is associated with adrenal insufficiency in this kindred, with all affected members being homozygous for the identified genetic defect. TXNRD2 is one of 25 human selenoproteins, which require insertion of a highly reactive selenocysteine residue for enzymatic activity. Selenium (Se) is an essential trace element which can be incorporated into proteins and some modified tRNAs, as selenomethionine, competing with sulphur in the biosynthesis of methionine, a process which involves little regulation. On the other hand the biosynthesis of selenocysteine (Sec), the 21st amino acid, and its cotranslational incorporation into specific proteins (selenoproteins) is highly regulated. The UGA codon acts as an opal stop codon during translation. However it can also encode the translational incorporation of Sec into target proteins when their mRNA contains a distinct hairpin mRNA sequence downstream of the UGA codon in the 3'-untranslated region (UTR) [236]. This sequence termed the Sec insertion sequence (SECIS) competes for release factors that would otherwise cause disassembly of the mRNA-ribosomal complex and termination of translation. The SECIS structure recruits SBP2 (selenocysteine binding protein 2) and binds Sec-specific elongation factor (EFSec) loaded with its tRNA^{Sec}, allowing for cotranslational incorporation of Sec at the UGA [237-239] (Figure 4.8). SBP2 stably associates with the ribosome and mutagenic analysis has demonstrated that this association is necessary for Sec insertion and a conformational change occurs in the ribosomes [240]. Further components of the complex network of proteins required for this process continue to be identified. Failure of the above process can result in recoding the UGA codon as a stop codon with subsequent nonsense-mediated decay of the resulting protein.

Selenoproteins have diverse functions including metabolism of thyroid hormones (deiodinases), transporting selenium to peripheral tissues (selenoprotein P), and protein folding and ER stress (Sep-15, SELM, and SELS). Several selenoproteins, including the thioredoxin reductases (TXNRD 1-3) and

glutathione peroxidases (GPX 1-4, 6) contribute significantly to redox regulation. The selenocysteine residue confers high redox activity [241]. TXNRD2 is predominantly mitochondrial and one of three thioredoxin reductases. It is responsible for reducing thioredoxin 2 (TXN2) and other substrates. Within the mitochondria the thioredoxin and glutathione systems, reliant on the provision of NADPH/H⁺ by NNT, contribute to the maintenance of redox homeostasis, discussed further in Chapter 5.

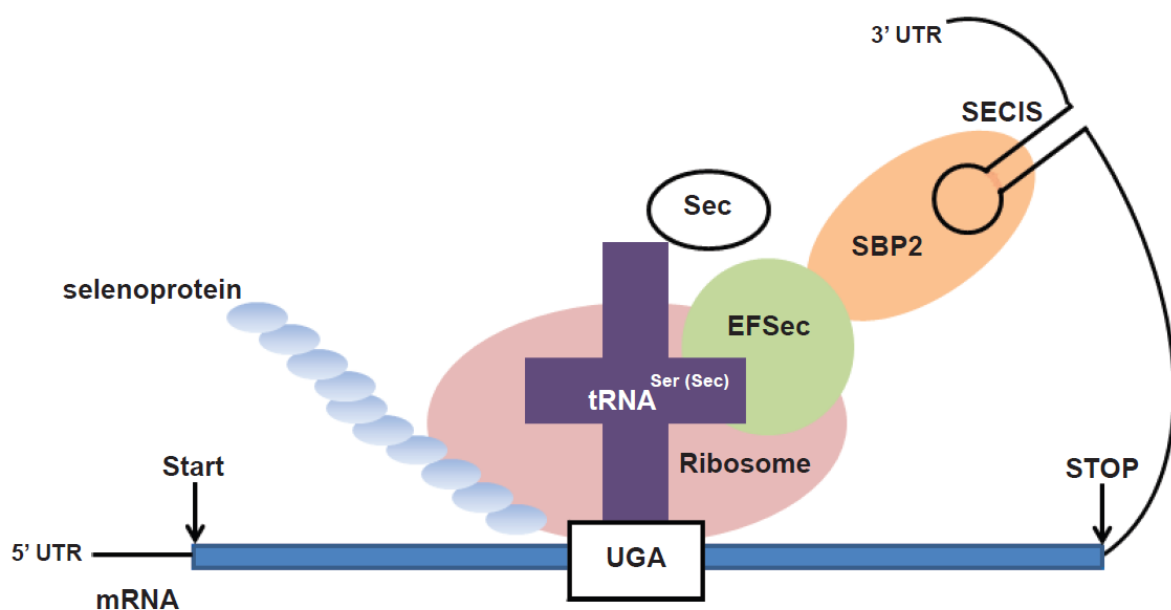


Figure 4.8. Selenoprotein biosynthesis with incorporation of Sec at UGA codons. Co-translational incorporation of Sec into proteins occurs at the UGA codon, which recruits Sec-loaded tRNA^{Ser (Sec)} to the ribosome. This occurs via an interaction of Sec-specific translation factor EFSec with the SECIS binding protein 2 (SBP2). SBP2 recognises the 3'-UTR hairpin loop SECIS mRNA structure in all mRNAs encoding Sec-containing proteins.

Two inherited human diseases have been associated, thus far, with mutations in selenoproteins and associated proteins; these include mutations in *SECISBP2* and *SEPN1*. *SEPN1* mutations encoding selenoprotein N1 lead to rigid spine syndrome (OMIM #602771), a rare form of congenital muscle dystrophy [242]. Selenoprotein N is an integral membrane glycoprotein in the endoplasmic reticulum with a postulated role in myogenesis. Mutations in *SECISBP2*, encoding SBP2, lead to reduced Sec insertion in several selenoproteins including the deiodinases, GPX, TXNRD, SEPN1, and a

reduction in these have been linked to clinical features of thyroid dysfunction, gastrointestinal disturbance, infertility and myopathy [243]. Se supplementation appears to have no effect on clinical phenotype. Interestingly no SBP2 patient has thus far been identified to have adrenal insufficiency (personal communication, Chatterjee 2013). In SBP2 deficiency there is still some low level of expression of all selenoproteins affected. In this instance, whilst there is a reduction in the thioredoxin reductases, there is still scope for some functional activity of TXNRD2 in comparison to our adrenal insufficient patients with absence of TXNRD2. This low level of functional activity may be sufficient to protect the SBP2 patients from adrenal insufficiency. It is also possible that a hierarchy of selenoproteins exists with preferential preservation of Sec insertion in those selenoproteins that are biologically most important in SBP2 deficiency. Certainly mouse knockout models suggest TXNRD2 may feature highly within such a hierarchy. Whilst individual disruption of certain selenoproteins including several Gpxs (Gpx1 to 3), selenoprotein P and type 2 iodothyronine deiodinase induce mild phenotypes in mice [244-249], mice lacking Txnrd2, Txnrd1 (thioredoxin reductase 1), Txn1 (thioredoxin 1) and Txn2 (thioredoxin 2) die in early embryogenesis [250-253]. Furthermore, interestingly, in transgenic mice that expressed a variant of the tRNA species mediating Sec insertion, that lacked a modified base corresponding to the wild type tRNA species, synthesis of selenoproteins was differentially affected, with Txnrd1, Txnrd2 and Gpx4 least affected [254, 255]. Amongst the thioredoxin reductases themselves, there is a prioritisation of Txnrd2 over Txnrd1 during Se deficiency such that Txnrd1 expression is more sensitive to Se supply than Txnrd2 [256].

The wide variability in age at presentation within this family and the comorbidity in patient 2.5 is interesting and suggests the presence of modifiers of disease, either genetic or environmental. Phenotypic heterogeneity amongst affected members of the same kindred has been demonstrated in several disorders including other disorders of primary adrenal insufficiency such as triple A syndrome [13]. Given the complex network of proteins involved in antioxidant defence it is possible

that other variants within this network contribute to phenotypic differences. As *TXNRD2* is ubiquitously expressed in humans, individuals with this genetic defect are potentially at risk of developing extra-adrenal manifestations. *Txnrd2* deletion in mice is embryonically lethal at day 13 as a consequence of a combination of cardiac and haematopoietic defects [250]. Knockout mice are severely anaemic with reduced colonies of all types of haematopoietic cell types, though differentiation is not affected. The full blood counts in all affected individuals within this family were normal with no evidence of haematopoietic problems. The knockout mice are described to have thinner ventricular walls and trabeculae. Cardiac specific ablation of *Txnrd2* results in a fatal dilated cardiomyopathy (DCM) with mitochondrial dysfunction of cardiomyocytes [250]. Thus in mice the *TXNRD2* system is clearly indispensable for normal cardiac development and function. Hemizygous mouse models for *Txnrd2* (*Txnrd2*^{+/-}) show no apparent phenotype even in combination with selenium deficiency [257]. In humans, two novel heterozygous mutations affecting the FAD (flavin adenine dinucleotide) region of *TXNRD2* were identified in 3 of 227 patients with a diagnosis of DCM screened [258]. The role of selenium in cardiomyopathy has also been described in Keshan's disease, originally described in North East China where selenium deficiency induced heart failure is well documented [259]. Interestingly, in our affected homozygote individuals, with complete absence of *TXNRD2*, we observed no evidence of cardiomyopathy or conduction disease. One affected family member presented with truncus arteriosus and ventricular septal defect, an extremely rare congenital cardiac anomaly. In light of the high consanguinity within this kindred the cardiac defect in this patient is likely to be caused by another gene defect. Approximately 40% of truncus arteriosus cases are associated with Di George syndrome, secondary to haploinsufficiency of a region of varying length on chromosome 22q11.2 [260]. Several genes within this commonly deleted region have been linked to defects in cardiac development including *TBX1* and *Crkl*, essential for survival, proliferation and migration of neural crest cells [261, 262]. Interestingly, *TXNRD2* falls within this region on chromosome 22, raising the possibility that *TXNRD2* contributes to the cardiac phenotype

of Di George syndrome. As heterozygote carriers of the p.Y447* *TXNRD2* mutation have normal adrenal function, we would predict that haploinsufficiency of *TXNRD2* would not lead to an abnormal adrenal phenotype, and consistent with this, I have been unable to identify any published reports of adrenal insufficiency in Di George syndrome.

A role for the thioredoxin system has been postulated in several human conditions. It is proposed that thioredoxin-related antioxidant defence may be important in protecting against age-related oxidative stress. To that effect transgenic mice overexpressing *Txn1* are reported to have a longer life span and are more resistant to oxidative-induced stress [263]. In age-related cataract development, the thioredoxin system has been shown to revive the inactivated enzyme glutathione reductase, protecting against oxidative stress [264]. *TXNRD* upregulation is seen in conditions such as Alzheimer's disease where oxidative stress is implied and the system is suggested as a potential therapeutic target [265]. Intronic SNPs in *TXNRD1*, rs6539137 and rs4630362, were significantly associated with another neurodegenerative disease, familial amyotrophic lateral sclerosis, and the authors suggest that *TXNRD1* may act as an important genetic modifier of disease [263]. The upregulation of *TXNRD*, mainly cytosolic *TXNRD1*, has been reported in several cancer cell lines and human cancers. The role of selenoproteins has been investigated in the carcinogenic process. Indeed, the thioredoxin system has been proposed as a therapeutic target for cancer related disease. Several groups have proposed associations of selenoprotein genotypes, including SNPs in *TXNRD1* and *TXNRD2* affecting cancer risk in conjunction with lifestyle factors. Intronic SNPs in *TXNRD1* and *TXNRD2* are postulated to significantly alter risk of high-grade or advanced stage prostate cancer in a population with suboptimal Se intake [266]. SNPs in *TXNRD2* have also been discussed in association with rectal and colon cancer risk [267]. The functional significance of the SNPs in the conditions described above has not been fully explored and characterisation will be challenging given their intronic nature. There is no history of early onset cancer reported in our family.

This is the first report of a homozygous mutation in any component of the thioredoxin system associated with inherited disease and the first mutation in *TXNRD2* associated with an adrenal phenotype in humans, signifying the importance of the thioredoxin system in maintaining redox homeostasis in the adrenocortical environment. Clinical surveillance, including regular cardiac review, and careful phenotyping of the affected individuals in this family will be necessary, together with functional interrogation of the candidate identified to better understand the role of TXNRD2 in primary adrenal insufficiency. It will be important to assess whether other organ systems will be affected over time and furthermore whether this mutation poses a cancer risk. Characterisation of the effect of TXNRD2 deficiency specifically in the adrenocortical environment is discussed further in Chapter 5.

Chapter 5

***TXNRD2*-knockdown in human adrenocortical cells causes an imbalance in redox homeostasis**

5.1 Mitochondrial *TXNRD2*

The thioredoxin family of proteins, to which *TXNRD2* belongs, plays a crucial role in regulating cellular redox homeostasis. This protein family comprises the thioredoxins, glutaredoxins and peroxiredoxins, all of which share a thioredoxin fold and an active site motif containing one or more cysteine (Cys) residues [268]. Cys residues may be involved in inter or intra-molecular disulphide bond(s), or they may exist as unbound thiols and it is the free Cys that forms an integral part of enzyme catalytic activity [269]. Surface-exposed Cys residues in a variety of proteins are potential targets for redox based modifications, and thiols can be reversibly oxidized to disulphides. The presence of disulphide bonds in peptides or proteins confers a relatively rigid structure and can affect protein function or activity [269]. Other reversible modifications include thiols being modified to sulfenic acid and glutathionylation, the process by which Cys side chains form disulphide bonds with GSH. These redox-based modifications can regulate protein activity and hence redox signalling can regulate several cellular processes in a fast and specific manner. The thioredoxin system itself comprises thioredoxin (TXN), the selenoprotein thioredoxin reductase (*TXNRD*) and the electron donor NADPH (Figure 5.1). The protein disulphide in the active site of TXN is reduced by *TXNRD*, receiving electrons from NADPH [270]. Reduced TXN in turn binds to the target protein disulphide, thereby reducing the target protein.

Mammalian genomes encode two main thioredoxin systems; the cytosolic and mitochondrial systems. *TXNRD2*, one of three thioredoxin reductases, is predominantly mitochondrial, whilst *TXNRD1* is cytosolic and the recently discovered *TXNRD3* is localised to the microsome [271-273]. The mitochondrial localisation signal of *TXNRD2* is present in the N-terminus, though some transcripts have been described without this localisation signal [274]. The functional significance of these latter transcripts has yet to be determined. *TXNRD2* exists as an anti-parallel homodimer

[275]. The N and C-terminal redox active centres of the two subunits functionally interact and transfer electrons from NADPH/H^+ to TXN2 and other substrates [275]. NNT provides the high concentrations of NADPH/H^+ required by the thioredoxin and glutathione systems to maintain redox homeostasis (Figure 5.1). The glutathione and thioredoxin systems act in parallel in mitochondria to maintain Peroxiredoxin 3 (PRDX3), an important mitochondrial antioxidant, in reduced form.

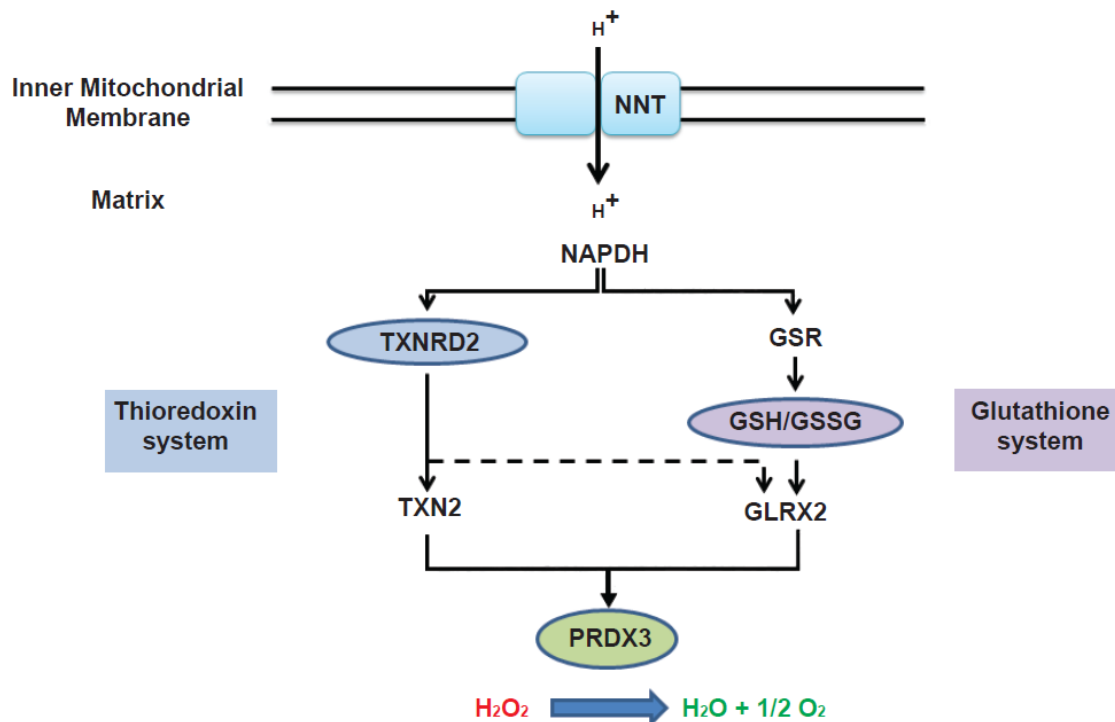


Figure 5.1. The thioredoxin and glutathione systems maintain mitochondrial redox homeostasis. TXNRD2 reduces thioredoxin 2 (TXN2) and glutaredoxin 2 (GLRX2), both of which can reduce PRDX3, which in turn detoxifies H_2O_2 in mitochondria. Glutathione reductase (GSR) and glutathione (GSH) contribute to the process through reduction of GLRX2. Nicotinamide nucleotide transhydrogenase (NNT) provides the high concentrations of NADPH required by both the thioredoxin and glutathione systems.

5.2 Aims of the study

Absence of *TXNRD2* is associated with adrenal insufficiency in the consanguineous kindred described in detail in chapter 4, with all affected members being homozygous for the identified genetic defect. To further investigate the effect of *TXNRD2* deficiency in the adrenocortical environment, *TXNRD2*-knockdown was established in the H295R human adrenocortical cell line. I investigated the effect of *TXNRD2* deficiency on redox homeostasis in the adrenocortical environment and the potential impact on steroidogenesis.

5.3 *TXNRD2* is highly expressed in the human adrenal cortex

The expression of *TXNRD2* and *GAPDH* mRNA was investigated using a panel of cDNAs derived from 11 adult tissues (adrenal cortex, heart, liver, testes, thyroid, lung, kidney, spleen, ovary, brain, skeletal muscle). Quantitative real-time PCR was performed for each tissue. Whilst *TXNRD2* mRNA is ubiquitously expressed in all the human tissues tested, highest levels were observed in the adrenal cortex (Figure 5.2), consistent with mouse expression profiles [276].

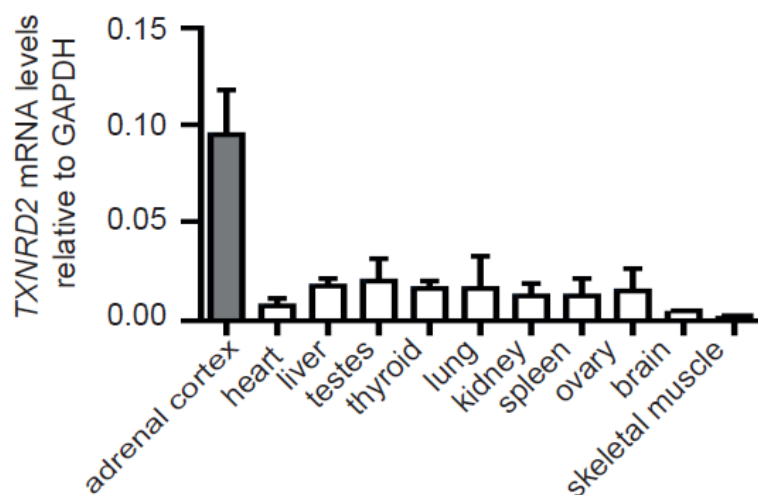


Figure 5.2. *TXNRD2* is expressed in all human tissues investigated, with highest *TXNRD2* mRNA levels in the adrenal cortex.

5.4 *TXNRD2*-knockdown in H295R adrenocortical cells

Stable knockdown of *TXNRD2* was established in H295R human adrenocortical cells by lentiviral shRNA transduction (Methods Section 2.1.2). Lentiviral plasmids (V3LHS_354173) were obtained from OpenBiosystems in a p.GIPZ backbone and contained shRNA specific for human *TXNRD2* (NM 10587) under the control of a CMV promoter, plus genes for puromycin resistance and green fluorescence protein (GFP) (for sequences and vector maps see Appendices 3 and 4). A control cell line was generated using a lentiviral plasmid vector containing a shRNA insert that does not target human and mouse genes (Open Biosystems). A significant reduction in *TXNRD2* mRNA is observed following knockdown in comparison to controls (n=4) (Figure 5.3A). This is confirmed by western blot analysis demonstrating approximately 95% knockdown in protein levels (n=4) (Figure 5.3B).

Cell viability was assessed using the MTS assay (CellTiter96 Aqueous non-radioactive cell proliferation assay, Promega, Southampton, UK) where absorbance readings are proportional to cellular metabolic activity (Methods 2.8.2). *TXNRD2*-knockdown in the H295R human adrenocortical cell line by shRNA had no effect on cell viability (Figure 5.3C). A colorimetric, thioredoxin reductase (TXNRD) assay kit (Abcam, Cambridge, UK) was used to assess **total** TXNRD activity in cell lysates from *TXNRD2*-knockdown and control cells (Methods 2.11). In the assay TXNRDs catalyse the reduction of 5, 5'-dithiobis (2-nitrobenzoic) acid (DTNB) with NADPH to 5-thio-2-nitrobenzoic acid (TNB²⁻), generating a strong yellow colour ($\lambda_{max}=412$ nm). Of note, the kit does not allow for the differentiation of activity of the mitochondrial and cytosolic forms of TXNRD. Interestingly, *TXNRD2*-knockdown did not have any significant impact on **total** TXNRD activity (p=0.7, n=4), suggesting possible compensatory upregulation of the activity of the other TXNRDs (Figure 5D). Cytosolic TXNRD1 protein expression itself is not significantly different in the *TXNRD2*-KD cells in comparison to controls (p=0.5, n=4) (Figure 5E).

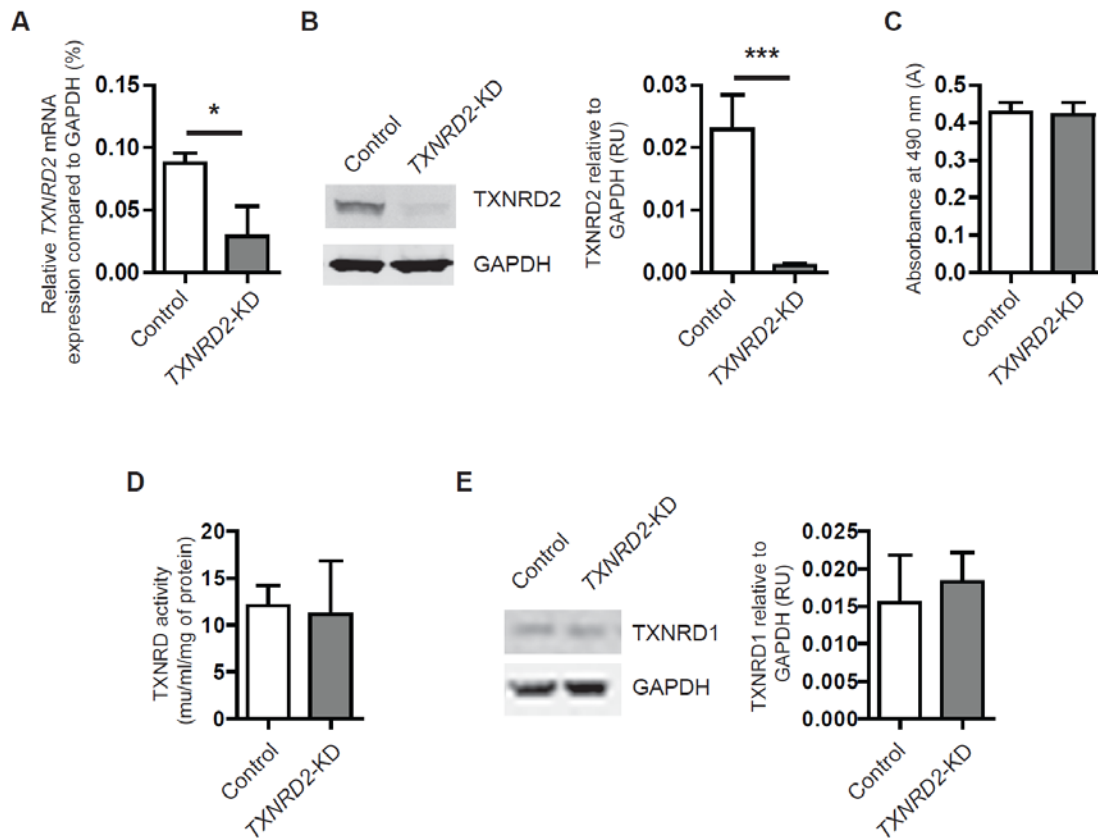


Figure 5.3. Lentiviral shRNA knockdown of the *TXNRD2* gene in H295R cells. (A) *TXNRD2* mRNA expression was quantified using real-time qPCR and normalised to GAPDH (n=4). Control represents transfection with scrambled shRNA. (B) Reduced expression of the protein TXNRD2 is seen in *TXNRD2*-knockdown (*TXNRD2*-KD) H295R cells; western blot with densitometric analysis. (C) No difference in cell viability is seen at baseline between *TXNRD2*-KD and control cells using the MTS assays. (D) There is no difference between total TXNRD activity in *TXNRD2*-KD H295R cell lysates in comparison to controls using the TXNRD assay (n=4). (E) No difference in TXNRD1 protein expression is seen in *TXNRD2*-KD H295R cells; western blot with densitometric analysis. RU, relative units. Data represents mean \pm SD. $p < 0.05^*$, $p < 0.001^{***}$.

5.5 *TXNRD2*-knockdown in H295R adrenocortical cells results in an imbalance of redox homeostasis

The glutathione and thioredoxin systems maintain reduced peroxiredoxin 3 (PRDX3) (Figure 5.1), which is integral for redox regulation within the adrenal [206]. In the absence of TXNRD2, increased pressure on the glutathione system was hypothesised. The luciferase-based GSH/GSSG-Glo assay

(Promega, Southampton, UK) was used to assess the GSH/GSSG (Reduced: oxidised glutathione) ratio in the *TXNRD2*-KD H295R cells compared to controls (Methods 2.9).

A clear impact on redox homeostasis was demonstrated, with increased pressure on the glutathione system observed as a decrease in the GSH/GSSG ratio (10.3 ± 1.3 vs 7.7 ± 0.4 in control vs knockdown cells respectively; $p=0.02$, $n=4$) (Figure 5.4A-B). As a positive control, a significant reduction in the GSH/GSSG ratio (0.4 ± 0.1 RLU) was demonstrated by treatment of the control cells with 25 μ M menadione, a potent inducer of oxidative stress.

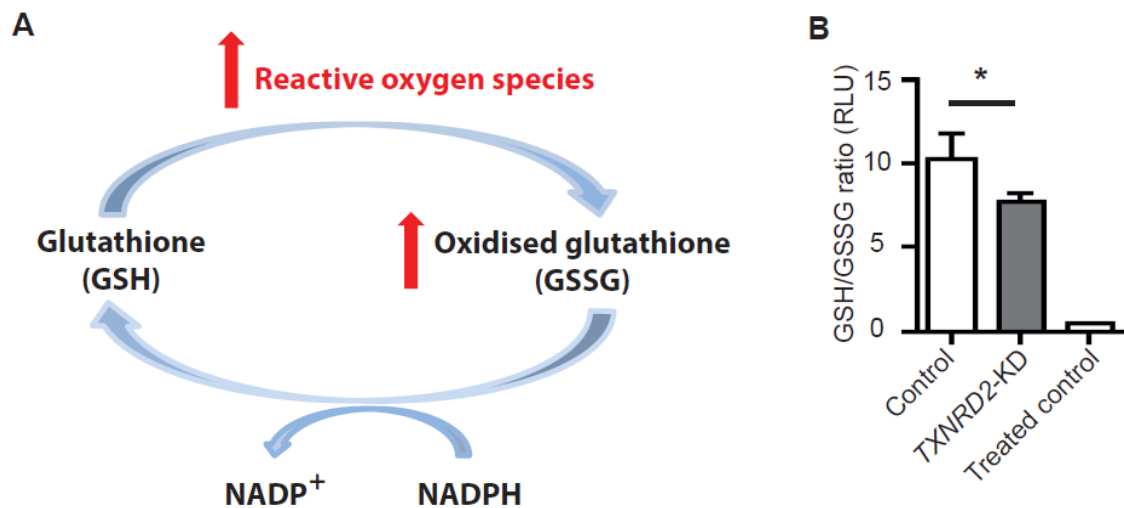


Figure 5.4. TXNRD2 deficiency in H295R cells leads to increased pressure on the glutathione system. (A) Increased reactive oxygen species leads to an increase in cellular oxidised glutathione (GSSG) and a decrease in the GSH/GSSG ratio. (B) Increased pressure on the glutathione system is observed in TXNRD2 deficiency with a significant decrease in the reduced: oxidised glutathione (GSH: GSSG) ratio. Oxidative stress induced by 25 μ M menadione in the control cells reduced this ratio to 0.4 ± 0.1 ($n=4$). RLU, relative light units. Error bars represent standard deviation. * $p < 0.05$.

During H_2O_2 elimination, two reduced PRDX3 subunits are converted to an oxidised disulphide-linked dimer that is reduced again by the TXNRD2/TXN2 system [203]. Cell lysates from *TXNRD2*-KD and control cells were western blotted in non-reducing conditions to compare the ratio of the

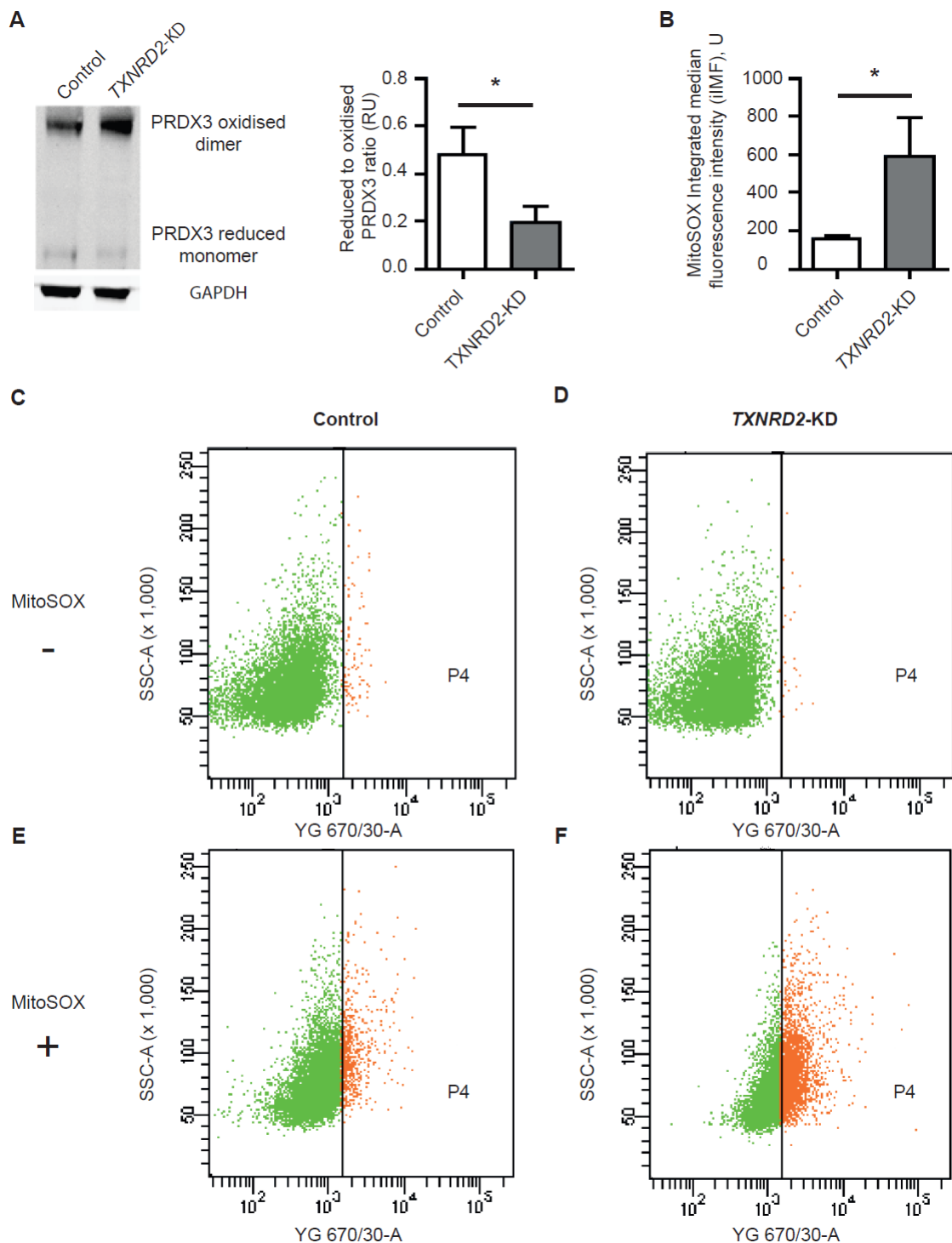


Figure 5.5. TXNRD2-KD in H295R cells leads to impaired mitochondrial redox homeostasis. (A) TXNRD2-KD leads to a decrease in the reduced to oxidised PRDX3 ratio, western blot with densitometric analysis (n=3). (B) Quantitative analysis of superoxide production by MitoSOX, shows a significant increase in superoxide production in KD cells relative to controls; (n=3) following fluorescence-activated cell sorting (FACS): (C) Control and (D) TXNRD2-KD H295R cells before

application of MitoSOX reagent. Following application of MitoSOX reagent for assessment of mitochondrial superoxide production a greater frequency of events is observed in area P4 (See Methods 2.13.2) for both (E) control H295R cells and (F) *TXNRD2*-KD cells with an approximately 3-fold increase observed in the *TXNRD2*-KD cells in comparison to control cells, reflective of increased mitochondrial superoxide production. RU, relative units. Error bars represent standard deviation. * $p < 0.05$.

monomeric (reduced) to dimeric (oxidised) form of PRDX3 (Methods 2.2.1). The ability to maintain mitochondrial PRDX3 in its reduced form is impaired, with a significant decrease in the ratio of the reduced to oxidised form in the *TXNRD2*-deficient cells compared to controls 0.19 ± 0.06 vs 0.48 ± 0.09 respectively; $p = 0.02$, $n = 3$ (Figure 5.5A).

Finally, the MitoSox Red fluorogenic probe was used to investigate mitochondrial superoxide production by flow cytometry (Methods 2.13.2). As a consequence of *TXNRD2*-knockdown in the adrenocortical cells, an approximately 3-fold increase in levels of mitochondrial reactive oxygen species (ROS) are seen, further demonstrating an impairment of redox regulation (Figure 5.5B-F, Methods Figure 2.7).

5.6 Steroidogenesis in *TXNRD2*-deficient H295R cells

In the *AAAS*-KD H295R model, a clear impact on protein expression is seen in STAR and mitochondrial P450c11 β (CYP11B1) with a subsequent reduction in cortisol expression. To ascertain if the same were true in the *TXNRD2*-deficient H295R model investigated the protein expression of STAR, P450scc and P450c11 β followed by measurement of cortisol production.

Western blotting of lysates from *TXNRD2*-KD and control H295R cells revealed no significant difference in STAR ($p = 0.8$, $n = 4$), P450c11 β ($p = 0.9$, $n = 3$), or P450scc protein expression ($p = 0.3$, $n = 3$) (Figure 5.6A-D). Cortisol production was analysed on a Roche Modular E170 automated immunoassay analyser, following 24 hour stimulation of the cells with 10 μ M forskolin (Methods 2.10). There was no significant difference in cortisol production in *TXNRD2*-deficient H295R cells (1520.4 nmol/L/mg of lysate protein \pm 284.3) in comparison with controls (1729.7 nmol/L/mg of

lysate protein \pm 276.4), ($p=0.3$, $n=5$) (Figure 5.6E). These findings are somewhat surprising given the proposed role that TXNRD2 has in mitochondrial antioxidant defence. Potential reasons for this discrepancy in findings between the AAAS-KD and TXNRD2-KD are discussed further in Section 5.7.

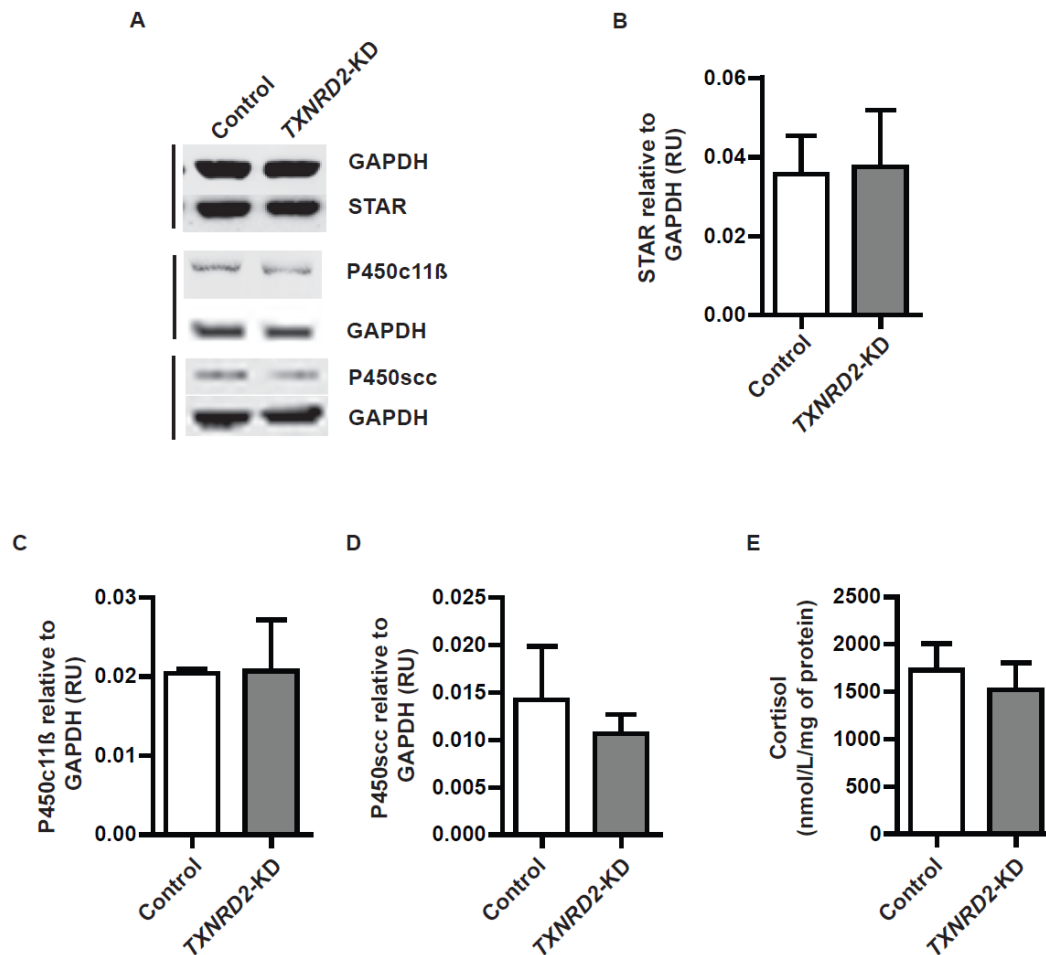


Figure 5.6. There is no significant impact on steroidogenesis in TXNRD2-deficient H295R cells compared with controls. (A) Immunoblot analysis and (B) Densitometric analysis reveals no effect on STAR ($n=4$), (C) P450c11 β ($n=3$) or (D) P450scc ($n=3$) protein expression in TXNRD2-KD H295R cells. (E) Furthermore, there is no significant difference in cortisol production in forskolin-treated TXNRD2-KD H295R cells compared with controls ($n=5$). Data represents mean \pm SD.

5.7 Discussion

Under conditions of selenium deficiency, some selenoproteins and some tissues are protected at the expense of others. Selenium is preferentially distributed to organs such as the brain, endocrine and

reproductive organs [277]. The testes and adrenals in particular have greatest retention of selenium in conditions of selenium deficiency [199]. Indeed selenium deficiency results in a marked decrease in selenoprotein glutathione peroxidase activity and subsequent cortisol production in an adrenal cell line [200]. In this section of work I investigated the role of the selenoprotein, TXNRD2 in the human adrenocortical environment. Particularly high *TXNRD2* mRNA levels were noted in the adrenal cortex compared to the other human tissues investigated, suggesting a critical role in this tissue. This reflects expression data in the mouse and high TXNRD2 levels are also reported in the bovine adrenal cortex [197, 276].

There are 3 distinct thioredoxin reductases: cytosolic thioredoxin reductase 1 (TXNRD1) [272], mitochondrial thioredoxin reductase 2 (TXNRD2) [278], and the most recently identified thioredoxin reductase 3 (TXNRD3), isolated from the microsomal fraction of mouse testes [273]. This final TXNRD, which has combined thioredoxin and glutathione reductase activities and can thus reduce several components of the glutathione system, is mainly expressed in the testes and has been implicated in sperm maturation [258, 273]. Each TXNRD is expressed from a different gene and each reduces substrates in different subcellular compartments. TXNRD1 and 2 are flavoproteins containing a FAD-binding domain within the N-terminus, an NADPH binding domain and an interface domain for dimerization. It is the redox active site of the C-terminal domain that contains the selenocysteine (Sec) moiety critical for thioredoxin reductase activity as both an acceptor and donor of electrons [279, 280]. The thioredoxin reductases function within an anti-parallel homodimer allowing interaction between the two N- and C-terminal-located redox active centres (Figure 5.7). Electrons provided by NADPH/H⁺ are delivered to the redox centre of the N-terminal FAD-binding domain and are transferred to the C-terminal redox active site of the adjacent monomer with final delivery to the substrate [275].

The major substrate for TXNRD2 is mitochondrial thioredoxin 2 (TXN2) (Figure 5.1). However, the readily accessible and reactive C-terminal catalytic centre and Sec element allows for high versatility

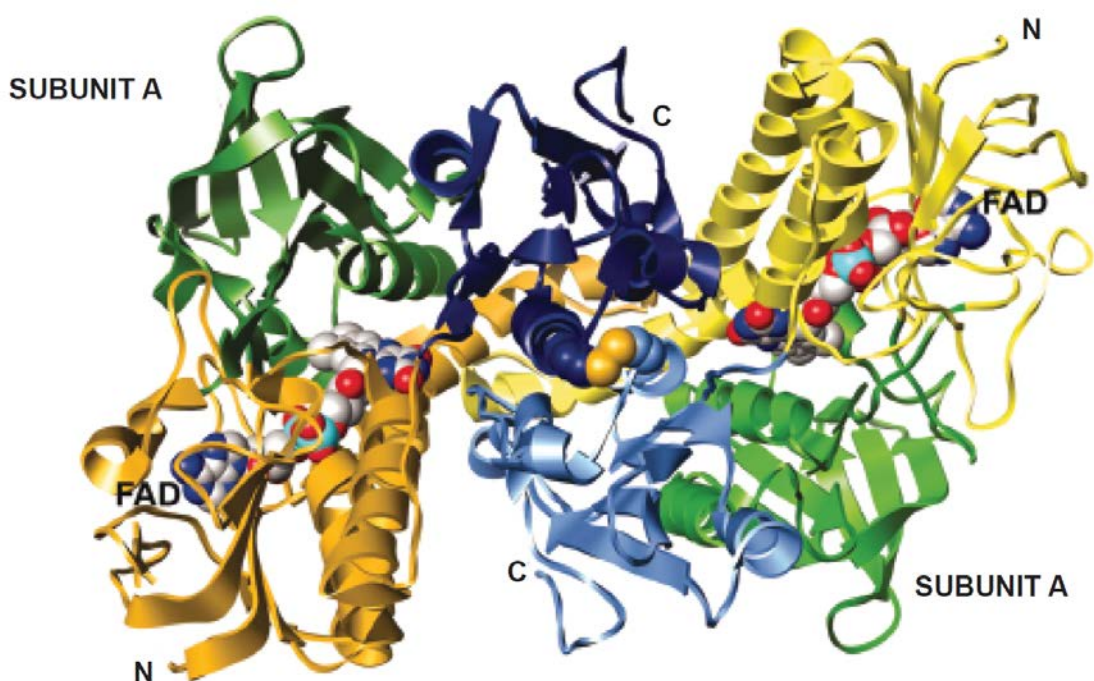


Figure 5.7. Ribbon representation of the overall structure of the mouse Txnrd2 homodimer. Subunit A is shown in dark colours, and subunit B is shown in light colours. The protein is comprised of three domains: a FAD-binding domain (yellow), an NADP(H)-binding domain (green), and an interface domain (blue). Bound FAD molecules are represented as space-filling models with carbon atoms coloured in grey, nitrogen atoms in blue, oxygen atoms in red, and phosphorous atoms in cyan. *Images reproduced with author's permission [275].*

and the thioredoxin reductases are also involved in reduction of various other substrates including H_2O_2 , lipid peroxides, vitamin A, C and K amongst others [281-283]. Mammalian cells have 2 main TXN systems; the cytosolic thioredoxin 1 (TXN1) and mitochondrial TXN2, reduced by TXNRD1 and TXNRD2 respectively. Mitochondrial TXN2 is a small redox active protein with two redox active cysteinyl residues, whilst cytosolic TXN1 has 3 additional cysteine residues at its active site. TXN1 and TXN2 share 35% sequence homology and similar catalytic properties *in vitro* [284]. The TXNs have roles in cell to cell communication, signal transduction, DNA metabolism and repair, transcription regulation and protein folding and degradation [282, 285]. TXN1 is involved in redox

signalling and can regulate the activities of many oxidative-sensitive transcription factors including Nrf-2, NF- κ B and P53 [286, 287]. TXN1 and TXN2 can both reduce methionine sulfoxide reductases and are thus involved in the repair of oxidized free methionine and protein methionine [288]. Both forms also importantly provide defence against oxidative stress by acting as electron donors for peroxiredoxins, which are rapid scavengers of H₂O₂ [289].

Peroxiredoxin 3 (PRDX3) is one of six PRDX isoforms and is restricted to the matrix of the mitochondria. It is reported to be the most important H₂O₂ eliminating enzyme in the mitochondria of the adrenal cortex with hyperoxidation of PRDX3 resulting in diminished steroidogenesis [206]. During H₂O₂ elimination, two reduced PRDX3 subunits are converted to an oxidised disulphide-linked dimer that is reduced again by TXN2 [203]. Thus PRDX3, together with mitochondrial-specific TXN2 and TXNRD2, provide a primary line of defence against H₂O₂ produced by the mitochondrial respiratory chain in the adrenal gland. Additionally, Glutaredoxin 2 (GLRX2) has recently been identified as another electron donor for PRDX3 [204]. GLRX2 also has high affinity for the GSH moiety and catalyses the reduction of mixed disulphides, including glutathionylated proteins [290]. GLRX2 itself is reduced by TXNRD2 as well as GSH and the mitochondrial thioredoxin and GSH systems function in parallel to protect against oxidative stress [204] (Figure 5.1). Overlap between the thioredoxin and GSH systems is further indicated by findings in *ex vivo* cultures of *Txnrd2*^{-/-} mouse embryonic fibroblasts, where proliferation and survival is compromised by addition of the GSH-depleting agent, BSO [250]. In my *in vitro* knockdown adrenocortical model I demonstrated that the glutathione system is unable to fully compensate for the TXNRD2 deficiency leading to an increase in the oxidised PRDX3 dimer and increased mitochondrial superoxide production.

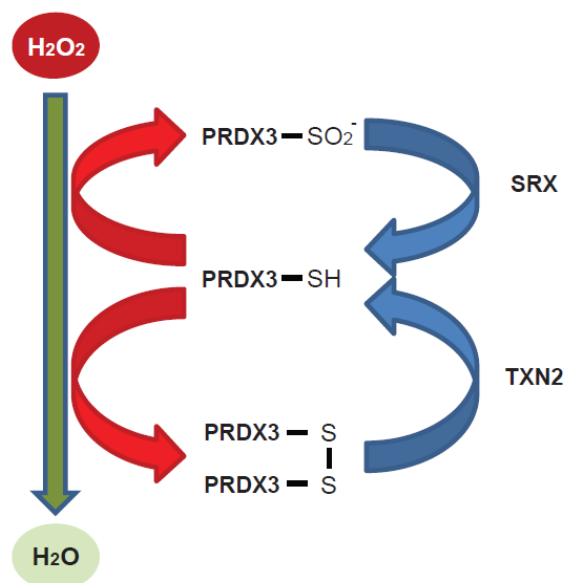


Figure 5.8. Maintenance of reduced peroxiredoxin 3 (PRDX3-SH) by thioredoxin 2 (TXN2) and sulfiredoxin (SRX). PRDX3, in its reduced form, detoxifies H_2O_2 in the mitochondria. This process induces the formation of disulphide PRDX3 which in turn is reduced back to PRDX3-SH by TXN2. With excessive H_2O_2 PRDX3 is hyper oxidised to an inactive sulfinic form ($PRDX3-SO_2^-$) and this hyper oxidation is reversed by SRX.

During catalysis PRDX can also be hyperoxidised to an inactive sulfinic form [205] (Figure 5.8). Only Prdx3 is found in sulfinic form in the adrenal cortex, accounting for approximately 10 to 20% of all Prdx3 in the mouse adrenal cortex [206]. The enzyme sulfiredoxin (SRX) reverses this hyperoxidation in a slow process which requires ATP hydrolysis and reducing elements including TXN2 and GSH [291]. SRX is a cytosolic protein that translocates into mitochondria when cells are under oxidative stress [292]. Treatment of adrenocortical cells with ACTH leads to further translocation of Srx into the mitochondria [206]. Thus SRX together with the TXN2 system, plays a crucial role in maintaining active PRDX3. With increasing H_2O_2 production the capacity for Srx to carry out this reversal is exceeded and levels of inactive sulfinic Prdx3 increase with subsequent H_2O_2 build up [206]. This in turn leaks into the cytosol leading to the phosphorylation (activation) of p38 mitogen-activated protein (MAP) kinase with consequent inhibition of STAR synthesis, the precise mechanism of which is currently unclear. Interestingly, levels of inactivated Prdx3, Srx, and activated p38 demonstrate

diurnal variation and conditional ablation of *Srx* in steroidogenic tissues in mice leads to build up of sulfenic Prdx3 and suppression of the diurnal production of corticosterone [206]. The authors propose that this build-up of inactive sulfenic Prdx3 plays a physiological role in signifying that sufficient cortisol has been synthesized, thus exerting a level of negative feedback independent of the HPA axis. It is also therefore possible that this mechanism comes into play in pathophysiology, in conditions where mitochondrial redox homeostasis is impaired. One could postulate that defects in the TXNRD2/TXN2 and SRX system may have the most impact in this regard.

Oxidative stress impedes steroidogenesis and steroidogenesis itself induces oxidative stress as a result of electron leak throughout the steroidogenic pathway. Within the mitochondria this leak can occur at various points in the pathway, through components such as ferredoxin, ferredoxin reductase and the cytochrome P450 enzymes [178]. The final step of cortisol production, catalysed by P450c11 β 1 within the mitochondria, accounts for a significant proportion of electron leak during steroidogenesis [178]. This, together with the higher production of cortisol in comparison to aldosterone, may explain the particular susceptibility of the zona fasciculata to oxidative stress and hence individuals with *TXNRD2* and *NNT* mutations develop primarily glucocorticoid deficiency.

Oxidative stress is also demonstrated to have an effect on the expression of key players in steroidogenesis including STAR and P450c11 β [219, 220]. Indeed this is seen in the triple A syndrome *in vitro* model, described in Chapter 3. One would therefore expect in conditions where mitochondrial redox homeostasis is specifically impaired, as in *TXNRD2* deficiency, expression of these enzymes with mitochondrial localisation, would be similarly reduced. Instead in our *TXNRD2*-KD H295R model there are no observable differences. Indeed we do not see a difference in cortisol production in this *in vitro* model. There are several possible explanations for this. One needs to consider the role of potential compensatory systems in the maintenance of redox homeostasis for steroidogenesis. Certainly the glutathione and glutathione reductase system have a part to play and we see increased pressure on this system within our model. A potential role for the other forms of

TXNRD also needs to be considered, in particular TXNRD1. The embryonic phenotypes of *Txnrd1* and *Txnrd2* knockout mice are less severe than the knockouts for *Txn1* and *Txn2*, implying that there may be some functional overlap between *Txnrd1* and *Txnrd2* during embryogenesis [250-253]. Interestingly, *TXNRD1*-silencing in HeLa cells, resulting in approximately 90% knockdown, demonstrates no increase in the TXN1 redox state, suggesting that even 10% residual TXNRD1 activity is sufficient for activity and/or there are other enzymes aside from TXNRD1 that can reduce TXN1 [293]. This may also therefore be the case for mitochondrial thioredoxin system. Furthermore *in vitro* studies suggest that *Txnrd1* and *Txnrd2* appear to lack preferences towards *Txn1* and *Txn2* and both thioredoxins appear to be equally good substrates for both *Txnrd1* and *Txnrd2* [274]. TXNRD1 is demonstrated to have cytoplasmic location [272]. However, the transcription of human *TXNRD1* is a complex process and alternative splicing in the 5' region lends to different isoforms, one of which is noted to encode a mitochondrial localisation system [294]. Certainly in my knockdown model the total thioredoxin reductase activity was not significantly diminished indicating potential TXNRD1 activity upregulation. Thus more compensation than originally anticipated may exist. It is possible that genetic variability in these complex compensatory mechanisms could influence the age of presentation of adrenal insufficiency in the kindred studied and indeed in some of the patients, the rather late presentation in comparison to other inherited forms of FGD.

In considering the lack of impact on steroidogenesis seen in my *in vitro* model, one needs to also consider the model system itself. The H295R cell line is a human adrenocortical tumour cell line. This clonal cell line has been used extensively as an *in vitro* model for steroidogenesis. Since conducting my experiments further data has been published relating to the use of this model system for investigating steroidogenesis, specifically in the context of the peroxiredoxin and sulfiredoxin systems [295]. Cultured H295R cells, which produce cortisol upon stimulation with forskolin, express SRX at a high level in order to survive in ambient conditions. Furthermore the total levels of PRDX3 are greatly reduced in the cell line in comparison to the adrenal gland [295]. Taken together this is

likely to lead to very little in the way of PRDX3 hyperoxidation, and indeed the authors demonstrate that forskolin stimulation does not lead to PRDX3 hyperoxidation in this cell line [295]. Thus in my model, whilst the levels of the PRDX3 oxidised dimer are increased in the *TXNRD2*-knockdown cells, with some impact on mitochondrial superoxide production, it is possible that high levels of SRX present in this *in vitro* model prevent PRDX3 hyperoxidation and therefore ameliorate any impact on steroidogenesis.

There is compelling evidence that the *TXNRD2* mutation identified is associated with disease in this family. *TXNRD2* is abundantly expressed in the adrenal cortex and is downstream of NNT (mutations of which are associated with FGD in a significant proportion of our cohort). Absence of the 56 kDa *TXNRD2* protein is seen in patient lysates and there is a clear impact on redox homeostasis in the *TXNRD2*-deficient H295R cells. However whilst I see an increase in mitochondrial ROS production in *TXNRD2*-deficient H295R cells I do not observe a difference in steroidogenesis in this *in vitro* model. This potentially relates to challenges in disease modelling; therefore to further interrogate the potential impact of *TXNRD2* deficiency on steroidogenesis other models of disease need to be considered in any future investigations, discussed further in Chapter 6.

Chapter 6

General discussion and future work

6.1 Oxidative stress and adrenocortical insufficiency

Reactive Oxygen Species (ROS) play an important physiological role in steroidogenesis however in excess they can have deleterious effects on adrenal function. Steroidogenesis itself increases the generation of ROS rendering the adrenal gland susceptible to oxidative damage.

In redox terms, mitochondria are the most reducing compartment in mammalian cells and have the highest rates of electron transfer (accounting for greater than 90% of electrons to O₂ as the terminal electron acceptor); they are therefore highly sensitive to oxidation. Mitochondria are also responsible for the majority of cellular ROS production secondary to electron leak as a consequence of respiration. Further electron leak by the cytochrome P450 enzymes during steroidogenesis renders adrenal mitochondria acutely vulnerable to redox imbalance [178]. Inherited mutations in *NNT* disrupt mitochondrial redox homeostasis leading to FGD [177]. *NNT* uses energy from the mitochondrial proton gradient to regenerate NADPH from NADP⁺, using NADH produced in the tricarboxylic acid (TCA) cycle. NADPH in turn is required as a reducing agent for the two major mitochondrial thiol antioxidant systems, dependent upon GSH and thioredoxin. I have described a mutation in *TXNRD2*, which acts downstream of *NNT*, associated with FGD. *TXNRD2* encodes a selenoprotein with important functions in preventing oxidative damage in the mitochondria. As mitochondria function as the 'power house' of the cells and there is high lipid turnover here during steroidogenesis, it is unsurprising that that the adrenal is particularly sensitive to defects in mitochondrial antioxidant defence. It remains to be seen whether other manifestations of *TXNRD2* dysfunction will develop and patients in both cohorts remain under close follow-up. Careful phenotyping during follow-up will help further elucidate the role of *NNT* and *TXNRD2* in human biology.

Peroxisomes also play an important role in lipid metabolism and are in close communication with mitochondria. Peroxisomal dysfunction too has been associated with adrenal insufficiency. X-linked adrenoleukodystrophy (ALD) is an inherited neurometabolic disorder incorporating neurodegenerative disease and adrenal insufficiency [9]. The disease is caused by mutations in the *ABCD1* gene on Xq28, encoding the adrenoleukodystrophy protein (ALDP), a member of the peroxisomal ATP-binding cassette (ABC) transporters. ALDP imports VLCFA-CoA esters into the peroxisome for degradation by β -oxidation [296], with particularly high expression in cells characterised by steroid hormone production (the adrenal gland and testis) [297].

Histology from both ALD mouse models and human specimens suggests involvement of oxidative stress in the pathogenesis of the disease, with evidence of increased MnSOD and lipid peroxidation [298]. Increased ROS production, depletion of GSH and decreased mitochondrial membrane potential are described in patient dermal fibroblasts [299]. VLCFAs are substrates of β -oxidation within the peroxisomes, a process that aids acyl-CoA availability and subsequent synthesis of plasmalogens, phospholipids with reported antioxidant properties [300-302]. As both organelles are in communication, generation of ROS within peroxisomes can disturb the mitochondrial redox balance [303]. VLCFAs may also have direct effects on mitochondrial function and structural abnormalities including lipid accumulation are seen within the mitochondria in *Abcd1*^{-/-} mice [304]. It is also proposed that VLCFAs may be involved in signalling within the immune system exacerbating inflammation which in turn can have further effects on ROS and RNS generation [305]. Whilst mouse models for X-linked ALD are able to recapitulate some of the neurodegenerative aspects of the human disease; with regards to adrenal function, similar to the *Aaas*^{-/-} model, no effect is seen on corticosterone production at either basally or upon stress [304, 307, 308].

Nuclei, like mitochondria, also have reduced redox potentials, however they are relatively resistant to oxidation [309]. This is of significance as sequestration of DNA within the nuclei protects the genome from reactive chemicals that can build up in other subcellular compartments. Despite this,

H₂O₂, nitric oxide and organic hydroperoxides can diffuse into nuclei. The GSH and thioredoxin systems (through TXN1) also play a role in the nucleus. The GSH system has been demonstrated to play a role in protecting DNA and DNA binding proteins from oxidative stress [310, 311]. Furthermore it regulates nuclear matrix organisation, chromosome consolidation, DNA synthesis and DNA repair [312-314]. GSH is postulated to act as a 'redox sensor' at the onset of DNA synthesis by providing the appropriate redox environment for DNA replication thereby safeguarding DNA integrity [315]. Both the GSH and TXN1 systems may also play a role in providing a more reducing environment for binding of transcription factors to DNA [316, 317]. The antioxidant TXN1 also translocates from the cytoplasm into the nucleus during conditions of oxidative stress [318]. Nuclear GSH and TXN1 function distinctly from the respective cytoplasmic systems. Whilst TXN1 appears to shuttle freely into the nucleus the mechanism of GSH transport into the nucleus is unknown [315]. The NPC is the sole site of transport between the nucleus and cytoplasm. The NPC has been implicated in adrenocortical insufficiency, with mutations in *AAAS*, encoding ALADIN an NPC protein, causing triple A syndrome [24, 25]. Failure of nuclear import of DNA repair proteins and FTH1, with antioxidant properties, is reported in triple A syndrome patient dermal fibroblasts [107, 127, 128]. How these nuclear import defects lead to an increase in intracellular ROS remains unclear. DNA fragmentation and increased apoptosis are reported as a consequence of these defects. Furthermore, increased chromosomal fragility is also reported [223], a finding that has also recently been described in cases of FGD within the Irish traveller community, caused by mutations in the DNA replicase mini chromosome maintenance protein 4 (*MCM4*) [173]. In this study I have demonstrated that ALADIN-deficient adrenal cells are more susceptible to oxidative stress, with a decrease in the reduced to oxidised glutathione (GSH/GSSG) ratio. These cells are more prone to cell cycle arrest and apoptosis. I have demonstrated that *AAAS*-knockdown in H295R cells also affects key components of the steroidogenic pathway, STAR and P450c11 β expression, with an impact on cortisol production,

an effect that is partially reversed with antioxidant N-acetylcysteine treatment, which replenishes GSH.

In triple A syndrome and ALD, the zona fasciculata and zona reticularis are most impacted, affecting glucocorticoid and adrenal androgen production [10, 150]. Deficiency of adrenal androgens which is reported in both conditions, can be a sensitive marker of adrenal insufficiency and occurs prior to glucocorticoid deficiency [10]. In our kindred with the *TXNRD2* mutation, the post-pubertal patients are also noted to have low adrenal androgens. This has not been previously reported in the cohort of patients with FGD and *NNT* mutations. Steroid production is itself associated with ROS production. Therefore, in these disorders involving defects in antioxidant defence, it stands to reason that the layers of the adrenal cortex are affected in order of relative steroid production, with the zona glomerulosa and mineralocorticoid production least affected and in some cases, not affected at all.

Further interrogation of the pathogenic mechanisms in triple A syndrome and FGD secondary to *TXNRD2* mutations is required. It is very likely that excessive oxidative stress impacts negatively on steroidogenic cells at a number of different levels. Grossly, oxidative stress may adversely affect cell proliferation leading to increased apoptosis. Further interrogation of DNA damage including DNA fragmentation would be useful in both the *AAAS*- and *TXNRD2*-knockdown H295R models. More subtle effects on cell signalling are also likely; including the steroidogenic machinery itself such as the *PRDX3*-*SRX* systems as described by Kil and colleagues [206]. It would be interesting to investigate the impact that increased oxidative stress may have on ACTH signalling including the interaction of MRAP with MC2R at the ER and the correct folding or trafficking of the receptor to the plasma membrane.

In each of the adrenal insufficiency conditions, exploring compensatory mechanisms would be of particular interest since these could potentially be manipulated as future therapeutic targets. In the *TXNRD2*-deficient model further exploring the compensatory role of the glutathione system and

other TXNRDs is warranted. Specific interrogation of the mitochondrial subcellular compartment is indicated. In the first instance, repeating the thioredoxin reductase assay with mitochondrial fractions of lysates from the *TXNRD2*-knockdown and control cells would be useful to ascertain the effect of knockdown within this subcellular compartment. An ability to sustain thioredoxin reductase activity in this compartment would suggest either that the low level of TXNRD2 remaining in the knockdown is sufficient for activity or alternatively that other TXNRDs are present in the compartment and able to compensate. In depth investigation of mitochondrial function in these TXNRD2 deficient cells could be achieved by isolation of mitochondria allowing measurement of several parameters including mitochondrial respiration, ROS production and scavenging and susceptibility to apoptotic events. However disadvantages of this approach include the substantial cell number required to provide enough mitochondrial isolate for the experiments needed and the transient rupture of mitochondrial membranes can occur during the procedure. Furthermore, it is becoming evident that mitochondrial morphology is integral to its activity and disruption of mitochondrial architecture can occur during the isolation procedure resulting in impairment of function [319, 320]. Newer techniques involving extracellular flux analysis in intact and permeabilised cells allow investigation of mitochondrial activity without significantly disrupting mitochondrial architecture [321]. Techniques such as this could provide detailed information regarding mitochondrial activity, allowing for further interrogation of the mitochondrial antioxidants implicated in FGD, including TXNRD2.

Whilst the NNT and TXNRD2 pathways are relatively well studied, delineating the function of ALADIN is more challenging. Very little is known about this NPC protein and various strategies may be considered to identify the cellular systems in which ALADIN may play a role. Strategies to consider include identifying further interacting protein partners for ALADIN. FTH1 was identified as an interacting protein partner of ALADIN using a bacterial two-hybrid screen [107]. Yeast two-hybrid screens are advantageous in that interactions at low affinity can be detected though this can also

generate false positives. Protein-protein interactions can be investigated in a species-specific manner using high throughput mammalian 2 hybrid techniques [322, 323]. All of these techniques allow for mass screening and further focused studies on individual candidates would then be required to understand the interaction in context.

Techniques such as RNA-seq could also prove to be useful in delineating differences in the transcriptome between control and AAAS-knockdown cells, thereby identifying biological pathways which are disrupted in triple A syndrome. This technique could also be applied comparing adrenal tissue from AAAS^{-/-} and wild-type mouse models. Defective nuclear import is described in triple A syndrome and given ALADIN's position at the NPC, it is highly likely that transport of other proteins across the NPC is also impaired. Identifying the subcellular distribution of proteins and more importantly the changes in their localisation depending on experimental conditions is challenging. Techniques of 'spatial proteomics' may be useful in this regard, involving high throughput mass-spectrometry based proteomics [324]. This would, for instance, allow for comparison of the nuclear and cytoplasmic fractions of ALADIN-deficient and control cells, at baseline and in conditions of oxidative stress, thereby identifying subtle changes in transport across the NPC.

There remain a population of triple A syndrome patients with adrenal insufficiency who are AAAS-mutation negative. Adopting a genomic approach by exploring genetic variants in this cohort of patients could provide further useful information of the role that ALADIN may play in human biology. WES in the cohort of triple A syndrome patients without AAAS mutations and those patients who are mutation negative for known causes of FGD may provide further candidates within antioxidant defence associated with adrenal disease. In both triple A syndrome and FGD related to the TXNRD2 variant, variability in disease presentation is described. This indicates potential genetic or environmental modifiers of these autosomal recessive diseases. It would be of interest to look for variants in genes encoding other antioxidant proteins, in addition to AAAS or TXNRD2 mutations, which may contribute to the phenotype seen in each of the conditions. This could involve targeted

sequencing of a designated panel of antioxidant genes or alternatively WES with filtering for the 'targeted' genes. Validation of genetic modifiers is likely to be difficult, particularly when considering that on average each person carries approximately 300 loss of function variants and 50 to 100 variants implicated in inherited disease as demonstrated by data generated from the 1000 genomes project [325]. Furthermore, particularly in the case of TXNRD2, with limited numbers of patients, this type of experiment would be difficult to power. Despite the challenges involved, this could provide further information about critical antioxidant pathways in steroidogenesis.

6.2 Models of disease

6.2.1 *In vitro* models of disease

In this thesis I have used lentiviral shRNA knockdown techniques to study the silencing of particular target genes in the *in vitro* environment. However as demonstrated, particularly in the TXNRD2-knockdown H295R model, there are several limitations to using a tumour cell line for the purposes of this work, particularly with regards to interrogating anti-oxidant systems, as discussed in Chapter 5. Kil and colleagues describe hyperoxidised PRDX3 impacting steroidogenesis [206]. Despite observing increased levels of the PRDX3 oxidised dimer in my TXNRD2-knockdown cells, there was no effect of knockdown on cortisol production. The high levels of SRX present in this *in vitro* model potentially prevent PRDX3 hyperoxidation and therefore may ameliorate any impact on steroidogenesis in this particular model [295].

A novel and potentially exciting and productive alternative would be to use iPS cells. Human embryonic stem cells and human induced pluripotent stems (iPS) cells are being used increasingly in the fields of developmental biology and regenerative medicine. Mouse and human mesenchymal stem cells can be induced to differentiate into steroid-producing cells, though these have not been well characterised. Sonoyama and colleagues have recently demonstrated that human iPS cells (generated from human dermal fibroblasts) can be differentiated into adrenocortical lineage cells [326]. This was achieved in a multistep process, involving differentiation into the mesodermal

lineage in the first instance with subsequent introduction of the orphan nuclear receptor steroidogenic factor-1 (SF-1). SF1 performs an essential role in the formation of steroidogenic tissues [327]. These iPS cells demonstrated mRNA expression of genes encoding adrenocortical or gonad-specific steroidogenic enzymes such as CYP17A1, CYP21A2 and CYP11B1 [326]. Additionally, these cells produced steroid hormones including progesterone, corticosterone and cortisol. The iPS cell model has the advantage of using patient cells, dermal fibroblasts; allowing for investigation of disease in patient-derived differentiated steroidogenic cells. This would provide a more faithful model of the disease and would also allow comparison of the effects of different types of disease-causing mutations. Of course, models like these need to be carefully characterised prior to use. Difficulties with this type of model include the relatively poor proliferation of differentiated cells in comparison to undifferentiated cells, limiting mass expansion of cells for experimental use. Furthermore, as with the clonal tumour cell lines, antioxidant mechanisms are likely to be altered in order for cells to survive in culture in ambient conditions. As the PRDX3-SRX system potentially plays an important role in signalling during steroidogenesis, establishing a model system that does not distort antioxidant defence at baseline is ideal. Kil and colleagues have recently demonstrated the use of organ culture systems, in this case isolated whole adrenal organs from mice, as suitable for the study of this mechanism *ex vivo* [295].

6.2.2 *In vivo* models of disease

In all the adrenal insufficiency conditions discussed above, mouse models of the disease do not faithfully recapitulate the human phenotype. With regards to ALD, FGD related to NNT, and triple A syndrome it is possible that additional mechanisms of antioxidant defence exist within the adrenocortical environment of the mouse, conferring relative protection. The *Txnrd2*-knockout mouse model is interesting in that it leads to embryonic lethality [250]. In mouse models certainly, the thioredoxin system appears to be of greater significance than the glutathione system, with knockout of various components of the thioredoxin system having far greater phenotypic impact

[250-253]. It is possible that in humans the glutathione system has greater weight in the adrenal. Establishing a mouse model with adrenal-specific knockout of *Txnrd2* may provide further insight into the role of TXNRD2 in steroidogenesis. The adrenal cortex is dynamic and is able to remodel to maintain homeostasis. It is proposed that during this process of remodelling, stem cells/progenitor cells are recruited into the zona glomerulosa and fasciculata. The thioredoxins are required for proliferation and protection from apoptosis and are clearly important during embryogenesis as demonstrated by the embryonic lethality of the various thioredoxin knockout models [250-253]. An adrenal-specific *Txnrd2*-knockout model would allow for the investigation of a possible role for TXNRD2 in adrenal development during embryogenesis and remodelling thereafter.

Given the potential limitations of mouse models to study the adrenal aspects of these diseases consideration should be given to other available *in vivo* models for further investigation of precise pathogenic mechanisms. Non-human primate models such as *Papio hamadryas* (baboons) and *Macaca mulatta* (rhesus monkeys) have been used to study age-related changes in endocrine function [328]. These have an advantage over rodents in that they produce DHEA/ DHEAS, with a steroidogenic profile therefore more reflective of that in man. Similar to man, DHEA/ DHEAS production decreases significantly whilst glucocorticoid production varies little with age [328, 329]. However older monkeys demonstrate reduced HPA axis sensitivity to glucocorticoid regulation, with a delay in normalisation of the axis after stimulation. This suggests impairment of negative feedback mechanisms, a phenomenon also observed in man. These non-human primate models have been used to study the effect of corticosteroids on antioxidant defence, in the context of aging [330-332]. Circadian rhythmicity of SOD in erythrocytes correlates well with the characterised rhythmicity of DHEAS and cortisol [332]. Additionally a similar age-related flattening of these SOD circadian rhythms is observed, suggesting a possible regulatory effect of corticosteroids on antioxidant defence. Age-related changes in stress responsiveness of SOD (increasing with age) and glutathione reductase (decreasing with age) are also described in non-human primate models [330]. This in turn

can lead to peroxide oxidation of lipids, haemolysis of erythrocytes and a diminished reliability of oxygen transport. The primate model is not however a practical model for further adrenal studies, particularly given efforts being made to refine, reduce, and indeed replace animal models.

Zebrafish, however, are increasingly being used in steroid hormone research, particularly in relation to the effects of endocrine disruptors, such as oestrogenic compounds, gestagens and selenomethionine, which have negative impacts on steroidogenesis [333]. Zebrafish are amenable to genetic manipulation and furthermore the zebrafish genome has been completely sequenced (http://www.sanger.ac.uk/Projects/D_rerio/), providing a useful model for the study of candidate genes. Zebrafish express both *aaas* and *tnxrd2*, as yet there is no published data in relation to these genes in the zebrafish model. Importantly, in comparison to many other fish species the majority of endocrine-related genes are present in single copies simplifying knockdown approaches [334]. Additionally with multiple progeny following single mating and rapid embryonic development, zebrafish pose an attractive *in vivo* model system. Steroid synthesis in zebrafish occurs in several peripheral tissues including the gonads, brain and the interrenal. The interrenal comprises specialised cells within the head kidney that are homologous to the mammalian adrenal gland [335]. Steroidogenesis here is under the control of the hypothalamus-pituitary-interrenal axis, and similar to the mammalian system the first and rate limiting step involves mitochondrial transport of cholesterol by STAR [336]. Most of the steroidogenic enzymes apart from *Cyp11B* and *CYP21a1* have been identified within zebrafish (Busby et al. 2010). The biosynthetic pathways, given the homology of the identified enzymes with mammalian counterparts, are postulated to be similar though the precise pathways need to be further functionally characterised [333, 337]. The receptors of these steroid hormones and subsequent signalling cascades are highly similar to those in mammals and relatively well characterised in adult zebrafish. Cortisol is the main stress hormone in zebrafish with demonstrated impact on metabolic processes, immune regulation and influence on circadian cell

cycle rhythmicity [338-340]. Additionally, cortisol from whole zebrafish and in zebrafish-holding water can be measured in high throughput assays enabling large scale sampling [341-343].

Oxidation-sensitive transcription factors and key components of antioxidant defence are also well conserved in zebrafish. Enzymes involved in *de novo* glutathione biosynthesis, glutathione peroxidase 1 (gpx1), Mn- and CuZn dependent superoxide dismutases and catalase are well documented in zebrafish [344-348]. The expression levels of these antioxidant enzymes are significantly increased in response to pollutants and drugs [349, 350]. Zebrafish larvae are optically transparent enabling the use of fluorescent probes, such as the fluorogenic dye 2',7'-dihydrodichlorofluoresceindiacetate (H₂DCFDA), to study cellular shifts in oxidation *in vivo* [351, 352]. Furthermore, genetically encoded (GFP) - derivatives (Hyper or RoGFP) with highly selective probes for peroxides, have also been developed to investigate spatiotemporal gradients of ROS, which could be of particular use to study the compartment specific effects of various defects in antioxidant defence [353, 354]. The use of these genetically encoded sensors have been demonstrated in zebrafish [355]. Given the similarities in key components of the steroidogenic and antioxidant pathways, the zebrafish model may prove to be highly useful to elucidate the roles of antioxidant candidates in steroidogenesis, allowing for high throughput studies.

6.3 Conclusion

Disruption of normal function within several sub-cellular organelles has been associated with inherited primary adrenal disease, with evidence of oxidative damage. Interestingly, in all cases, the proteins involved are ubiquitously expressed, albeit enriched in the adrenal cortex. Antioxidant defence within eukaryotic cells is complex and several overlapping systems exist which may confer relative protection in other organ systems. Defining the precise pathological mechanisms involved in these conditions will be invaluable in providing information on prognosis and directing patient surveillance. Furthermore, it may be possible to identify and manipulate compensatory mechanisms to delay onset or prevent progression of disease.

Uniform Resource Locator (URL)

BioEdit, <http://www.mbio.ncsu.edu/BioEdit/>

dbSNP, www.ncbi.nlm.nih.gov/SNP/

DNAexus Classic, <https://dnanexus.com/>

Ensembl, <http://www.ensembl.org/index.html>

Exome Variant Server, NHLBI Exome Sequencing Project, Seattle, Washington, <http://evs.gs.washington.edu/EVS/> [accessed October 2012].

REFERENCES

1. Papadopoulos, V. and W.L. Miller, *Role of mitochondria in steroidogenesis*. Best Pract Res Clin Endocrinol Metab, 2012. **26**(6): p. 771-90.
2. Takemori, H. and M. Okamoto, *Regulation of CREB-mediated gene expression by salt inducible kinase*. J Steroid Biochem Mol Biol, 2008. **108**(3-5): p. 287-91.
3. Ariyoshi, N., et al., *Characterization of the rat Star gene that encodes the predominant 3.5-kilobase pair mRNA. ACTH stimulation of adrenal steroids in vivo precedes elevation of Star mRNA and protein*. J Biol Chem, 1998. **273**(13): p. 7610-9.
4. Manna, P.R., M.T. Dyson, and D.M. Stocco, *Regulation of the steroidogenic acute regulatory protein gene expression: present and future perspectives*. Mol Hum Reprod, 2009. **15**(6): p. 321-33.
5. Miller, W.L., *Minireview: regulation of steroidogenesis by electron transfer*. Endocrinology, 2005. **146**(6): p. 2544-50.
6. Charmandari, E., N.C. Nicolaidis, and G.P. Chrousos, *Adrenal insufficiency*. Lancet, 2014.

7. Erichsen, M.M., et al., *Clinical, immunological, and genetic features of autoimmune primary adrenal insufficiency: observations from a Norwegian registry*. J Clin Endocrinol Metab, 2009. **94**(12): p. 4882-90.
8. Cutolo, M., *Autoimmune polyendocrine syndromes*. Autoimmun Rev, 2014. **13**(2): p. 85-9.
9. Kemp, S., J. Berger, and P. Aubourg, *X-linked adrenoleukodystrophy: clinical, metabolic, genetic and pathophysiological aspects*. Biochim Biophys Acta, 2012. **1822**(9): p. 1465-74.
10. Wichers-Rother, M., et al., *Adrenal steroids in adrenomyeloneuropathy. Dehydroepiandrosterone sulfate, androstenedione and 17alpha-hydroxyprogesterone*. J Neurol, 2005. **252**(12): p. 1525-9.
11. Allgrove, J., et al., *Familial glucocorticoid deficiency with achalasia of the cardia and deficient tear production*. Lancet, 1978. **1**(8077): p. 1284-6.
12. Houlden, H., et al., *Clinical and genetic characterization of families with triple A (Allgrove) syndrome*. Brain, 2002. **125**(Pt 12): p. 2681-90.
13. Milenkovic, T., et al., *Triple A syndrome: 32 years experience of a single centre (1977-2008)*. Eur J Pediatr, 2010. **169**(11): p. 1323-8.
14. Huebner, A., et al., *New insights into the molecular basis of the triple A syndrome*. Endocr Res, 2002. **28**(4): p. 733-9.
15. Vallet, A.E., et al., *Neurological features in adult Triple-A (Allgrove) syndrome*. J Neurol, 2012. **259**(1): p. 39-46.
16. Brooks, B.P., et al., *Triple-A syndrome with prominent ophthalmic features and a novel mutation in the AAAS gene: a case report*. BMC Ophthalmol, 2004. **4**: p. 7.
17. Moschos, M.M., et al., *New ophthalmic features in a family with triple A syndrome*. Int Ophthalmol, 2011. **31**(3): p. 239-43.
18. Alhussaini, B., et al., *Clinical and manometric characteristics of Allgrove syndrome*. J Pediatr Gastroenterol Nutr, 2011. **53**(3): p. 271-4.

19. Khelif, K., et al., *Achalasia of the cardia in Allgrove's (triple A) syndrome: histopathologic study of 10 cases*. Am J Surg Pathol, 2003. **27**(5): p. 667-72.
20. Huebner, A., L.L. Elias, and A.J. Clark, *ACTH resistance syndromes*. J Pediatr Endocrinol Metab, 1999. **12 Suppl 1**: p. 277-93.
21. Kimber, J., et al., *Allgrove or 4 "A" syndrome: an autosomal recessive syndrome causing multisystem neurological disease*. J Neurol Neurosurg Psychiatry, 2003. **74**(5): p. 654-7.
22. Huebner, A., et al., *Triple A syndrome--clinical aspects and molecular genetics*. Endocr Res, 2000. **26**(4): p. 751-9.
23. Weber, A., et al., *Linkage of the gene for the triple A syndrome to chromosome 12q13 near the type II keratin gene cluster*. Hum Mol Genet, 1996. **5**(12): p. 2061-6.
24. Tullio-Pelet, A., et al., *Mutant WD-repeat protein in triple-A syndrome*. Nat Genet, 2000. **26**(3): p. 332-5.
25. Handschug, K., et al., *Triple A syndrome is caused by mutations in AAAS, a new WD-repeat protein gene*. Hum Mol Genet, 2001. **10**(3): p. 283-90.
26. Brooks, B.P., et al., *Genotypic heterogeneity and clinical phenotype in triple A syndrome: a review of the NIH experience 2000-2005*. Clin Genet, 2005. **68**(3): p. 215-21.
27. Huebner, A., et al., *The triple A syndrome is due to mutations in ALADIN, a novel member of the nuclear pore complex*. Endocr Res, 2004. **30**(4): p. 891-9.
28. Sandrini, F., et al., *Spectrum of mutations of the AAAS gene in Allgrove syndrome: lack of mutations in six kindreds with isolated resistance to corticotropin*. J Clin Endocrinol Metab, 2001. **86**(11): p. 5433-7.
29. Koehler, K., et al., *Mutations in GMPPA cause a glycosylation disorder characterized by intellectual disability and autonomic dysfunction*. Am J Hum Genet, 2013. **93**(4): p. 727-34.
30. Storr, H.L., et al., *Identification of the sites of expression of triple A syndrome mRNA in the rat using in situ hybridisation*. Neuroscience, 2005. **131**(1): p. 113-23.

31. Smith, T.F., et al., *The WD repeat: a common architecture for diverse functions*. Trends Biochem Sci, 1999. **24**(5): p. 181-5.
32. Li, D. and R. Roberts, *WD-repeat proteins: structure characteristics, biological function, and their involvement in human diseases*. Cell Mol Life Sci, 2001. **58**(14): p. 2085-97.
33. Wall, M.A., et al., *The structure of the G protein heterotrimer Gi alpha 1 beta 1 gamma 2*. Cell, 1995. **83**(6): p. 1047-58.
34. Neer, E.J., et al., *The ancient regulatory-protein family of WD-repeat proteins*. Nature, 1994. **371**(6495): p. 297-300.
35. Waters, M.G., T. Serafini, and J.E. Rothman, *'Coatomer': a cytosolic protein complex containing subunits of non-clathrin-coated Golgi transport vesicles*. Nature, 1991. **349**(6306): p. 248-51.
36. King, S.M., et al., *The 78,000-M(r) intermediate chain of Chlamydomonas outer arm dynein is a microtubule-binding protein*. J Cell Biol, 1995. **131**(2): p. 399-409.
37. Wilkerson, C.G., et al., *The 78,000 M(r) intermediate chain of Chlamydomonas outer arm dynein is a WD-repeat protein required for arm assembly*. J Cell Biol, 1995. **129**(1): p. 169-78.
38. Verreault, A., et al., *Nucleosome assembly by a complex of CAF-1 and acetylated histones H3/H4*. Cell, 1996. **87**(1): p. 95-104.
39. Zou, H., et al., *An APAF-1.cytochrome c multimeric complex is a functional apoptosome that activates procaspase-9*. J Biol Chem, 1999. **274**(17): p. 11549-56.
40. Cecconi, F., *Apaf1 and the apoptotic machinery*. Cell Death Differ, 1999. **6**(11): p. 1087-98.
41. Reubold, T.F. and S. Eschenburg, *A molecular view on signal transduction by the apoptosome*. Cell Signal, 2012. **24**(7): p. 1420-5.
42. Blanco, M.A., et al., *APC(ste9/srw1) promotes degradation of mitotic cyclins in G(1) and is inhibited by cdc2 phosphorylation*. EMBO J, 2000. **19**(15): p. 3945-55.

43. Tan, G.S., J. Magurno, and K.F. Cooper, *Ama1p-activated anaphase-promoting complex regulates the destruction of Cdc20p during meiosis II*. Mol Biol Cell, 2011. **22**(3): p. 315-26.
44. Chan, K.T., S.J. Creed, and J.E. Bear, *Unraveling the enigma: progress towards understanding the coronin family of actin regulators*. Trends Cell Biol, 2011. **21**(8): p. 481-8.
45. Reiner, O., et al., *Isolation of a Miller-Dieker lissencephaly gene containing G protein beta-subunit-like repeats*. Nature, 1993. **364**(6439): p. 717-21.
46. Lo Nigro, C., et al., *Point mutations and an intragenic deletion in LIS1, the lissencephaly causative gene in isolated lissencephaly sequence and Miller-Dieker syndrome*. Hum Mol Genet, 1997. **6**(2): p. 157-64.
47. Kousar, R., et al., *Mutations in WDR62 gene in Pakistani families with autosomal recessive primary microcephaly*. BMC Neurol, 2011. **11**: p. 119.
48. Bilguvar, K., et al., *Whole-exome sequencing identifies recessive WDR62 mutations in severe brain malformations*. Nature, 2010. **467**(7312): p. 207-10.
49. Mookherjee, S., et al., *WDR36 variants in East Indian primary open-angle glaucoma patients*. Mol Vis, 2011. **17**: p. 2618-27.
50. Fan, B.J., et al., *Different WDR36 mutation pattern in Chinese patients with primary open-angle glaucoma*. Mol Vis, 2009. **15**: p. 646-53.
51. Chi, Z.L., et al., *Mutant WDR36 directly affects axon growth of retinal ganglion cells leading to progressive retinal degeneration in mice*. Hum Mol Genet, 2010. **19**(19): p. 3806-15.
52. Yuan, X., et al., *Activation of RNA polymerase I transcription by cockayne syndrome group B protein and histone methyltransferase G9a*. Mol Cell, 2007. **27**(4): p. 585-95.
53. Cronshaw, J.M., et al., *Proteomic analysis of the mammalian nuclear pore complex*. J Cell Biol, 2002. **158**(5): p. 915-27.

54. DeGrasse, J.A., et al., *Evidence for a shared nuclear pore complex architecture that is conserved from the last common eukaryotic ancestor*. Mol Cell Proteomics, 2009. **8**(9): p. 2119-30.
55. Rout, M.P., et al., *The yeast nuclear pore complex: composition, architecture, and transport mechanism*. J Cell Biol, 2000. **148**(4): p. 635-51.
56. Bagley, S., et al., *The nuclear pore complex*. J Cell Sci, 2000. **113 (Pt 22)**: p. 3885-6.
57. Tran, E.J. and S.R. Wentz, *Dynamic nuclear pore complexes: life on the edge*. Cell, 2006. **125**(6): p. 1041-53.
58. Brohawn, S.G., et al., *The nuclear pore complex has entered the atomic age*. Structure, 2009. **17**(9): p. 1156-68.
59. Mitchell, J.M., et al., *Pom121 links two essential subcomplexes of the nuclear pore complex core to the membrane*. J Cell Biol, 2010. **191**(3): p. 505-21.
60. Funakoshi, T., et al., *Localization of Pom121 to the inner nuclear membrane is required for an early step of interphase nuclear pore complex assembly*. Mol Biol Cell, 2011. **22**(7): p. 1058-69.
61. Onischenko, E., et al., *Role of the Ndc1 interaction network in yeast nuclear pore complex assembly and maintenance*. J Cell Biol, 2009. **185**(3): p. 475-91.
62. Rasala, B.A., et al., *Capture of AT-rich chromatin by ELYS recruits POM121 and NDC1 to initiate nuclear pore assembly*. Mol Biol Cell, 2008. **19**(9): p. 3982-96.
63. Stavru, F., et al., *NDC1: a crucial membrane-integral nucleoporin of metazoan nuclear pore complexes*. J Cell Biol, 2006. **173**(4): p. 509-19.
64. Stavru, F., et al., *Nuclear pore complex assembly and maintenance in POM121- and gp210-deficient cells*. J Cell Biol, 2006. **173**(4): p. 477-83.
65. Alber, F., et al., *The molecular architecture of the nuclear pore complex*. Nature, 2007. **450**(7170): p. 695-701.

66. Rabut, G., V. Doye, and J. Ellenberg, *Mapping the dynamic organization of the nuclear pore complex inside single living cells*. Nat Cell Biol, 2004. **6**(11): p. 1114-21.
67. Huebner, A., et al., *Mice lacking the nuclear pore complex protein ALADIN show female infertility but fail to develop a phenotype resembling human triple A syndrome*. Mol Cell Biol, 2006. **26**(5): p. 1879-87.
68. Cronshaw, J.M. and M.J. Matunis, *The nuclear pore complex protein ALADIN is mislocalized in triple A syndrome*. Proc Natl Acad Sci U S A, 2003. **100**(10): p. 5823-7.
69. Rout, M.P. and S.R. Wente, *Pores for thought: nuclear pore complex proteins*. Trends Cell Biol, 1994. **4**(10): p. 357-65.
70. Weirich, C.S., et al., *The N-terminal domain of Nup159 forms a beta-propeller that functions in mRNA export by tethering the helicase Dbp5 to the nuclear pore*. Mol Cell, 2004. **16**(5): p. 749-60.
71. Hodel, A.E., et al., *The three-dimensional structure of the autoproteolytic, nuclear pore-targeting domain of the human nucleoporin Nup98*. Mol Cell, 2002. **10**(2): p. 347-58.
72. Bayliss, R., T. Littlewood, and M. Stewart, *Structural basis for the interaction between FxFG nucleoporin repeats and importin-beta in nuclear trafficking*. Cell, 2000. **102**(1): p. 99-108.
73. Bednenko, J., G. Cingolani, and L. Gerace, *Importin beta contains a COOH-terminal nucleoporin binding region important for nuclear transport*. J Cell Biol, 2003. **162**(3): p. 391-401.
74. Pemberton, L.F. and B.M. Paschal, *Mechanisms of receptor-mediated nuclear import and nuclear export*. Traffic, 2005. **6**(3): p. 187-98.
75. Fontoura, B.M., G. Blobel, and N.R. Yaseen, *The nucleoporin Nup98 is a site for GDP/GTP exchange on ran and termination of karyopherin beta 2-mediated nuclear import*. J Biol Chem, 2000. **275**(40): p. 31289-96.

76. Matsuura, Y. and M. Stewart, *Nup50/Npap60 function in nuclear protein import complex disassembly and importin recycling*. EMBO J, 2005. **24**(21): p. 3681-9.
77. Oeffinger, M. and D. Zenklusen, *To the pore and through the pore: A story of mRNA export kinetics*. Biochim Biophys Acta, 2012. **1819**(6): p. 494-506.
78. Capelson, M. and M.W. Hetzer, *The role of nuclear pores in gene regulation, development and disease*. EMBO Rep, 2009. **10**(7): p. 697-705.
79. Strawn, L.A., et al., *Minimal nuclear pore complexes define FG repeat domains essential for transport*. Nat Cell Biol, 2004. **6**(3): p. 197-206.
80. Pyhtila, B. and M. Rexach, *A gradient of affinity for the karyopherin Kap95p along the yeast nuclear pore complex*. J Biol Chem, 2003. **278**(43): p. 42699-709.
81. Seedorf, M., et al., *Interactions between a nuclear transporter and a subset of nuclear pore complex proteins depend on Ran GTPase*. Mol Cell Biol, 1999. **19**(2): p. 1547-57.
82. Cronshaw, J.M. and M.J. Matunis, *The nuclear pore complex: disease associations and functional correlations*. Trends Endocrinol Metab, 2004. **15**(1): p. 34-9.
83. Galy, V., et al., *Nuclear retention of unspliced mRNAs in yeast is mediated by perinuclear Mlp1*. Cell, 2004. **116**(1): p. 63-73.
84. Imamoto, N. and T. Funakoshi, *Nuclear pore dynamics during the cell cycle*. Curr Opin Cell Biol, 2012.
85. Chan, G.K., S.T. Liu, and T.J. Yen, *Kinetochore structure and function*. Trends Cell Biol, 2005. **15**(11): p. 589-98.
86. Blower, M.D., et al., *A Rae1-containing ribonucleoprotein complex is required for mitotic spindle assembly*. Cell, 2005. **121**(2): p. 223-34.
87. Casolari, J.M., et al., *Genome-wide localization of the nuclear transport machinery couples transcriptional status and nuclear organization*. Cell, 2004. **117**(4): p. 427-39.

88. Schmid, M., et al., *Nup-PI: the nucleopore-promoter interaction of genes in yeast*. Mol Cell, 2006. **21**(3): p. 379-91.
89. Akhtar, A. and S.M. Gasser, *The nuclear envelope and transcriptional control*. Nat Rev Genet, 2007. **8**(7): p. 507-17.
90. Ishii, K., et al., *Chromatin boundaries in budding yeast: the nuclear pore connection*. Cell, 2002. **109**(5): p. 551-62.
91. Griffis, E.R., et al., *Distinct functional domains within nucleoporins Nup153 and Nup98 mediate transcription-dependent mobility*. Mol Biol Cell, 2004. **15**(4): p. 1991-2002.
92. Kind, B., et al., *The nuclear pore complex protein ALADIN is anchored via NDC1 but not via POM121 and GP210 in the nuclear envelope*. Biochem Biophys Res Commun, 2009. **390**(2): p. 205-10.
93. Yamazumi, Y., et al., *The transmembrane nucleoporin NDC1 is required for targeting of ALADIN to nuclear pore complexes*. Biochem Biophys Res Commun, 2009. **389**(1): p. 100-4.
94. Krumbholz, M., K. Koehler, and A. Huebner, *Cellular localization of 17 natural mutant variants of ALADIN protein in triple A syndrome - shedding light on an unexpected splice mutation*. Biochem Cell Biol, 2006. **84**(2): p. 243-9.
95. Zhang, X., et al., *Mutation in nuclear pore component NUP155 leads to atrial fibrillation and early sudden cardiac death*. Cell, 2008. **135**(6): p. 1017-27.
96. Grimaldi, M.R., et al., *nup154 genetically interacts with cup and plays a cell-type-specific function during Drosophila melanogaster egg-chamber development*. Genetics, 2007. **175**(4): p. 1751-9.
97. Gigliotti, S., et al., *Nup154, a new Drosophila gene essential for male and female gametogenesis is related to the nup155 vertebrate nucleoporin gene*. J Cell Biol, 1998. **142**(5): p. 1195-207.

98. Ghannam, G., et al., *The oncogene Nup98-HOXA9 induces gene transcription in myeloid cells.* J Biol Chem, 2004. **279**(2): p. 866-75.
99. Wang, G.G., et al., *Haematopoietic malignancies caused by dysregulation of a chromatin-binding PHD finger.* Nature, 2009. **459**(7248): p. 847-51.
100. De Keersmaecker, K., et al., *Intrinsic differences between the catalytic properties of the oncogenic NUP214-ABL1 and BCR-ABL1 fusion protein kinases.* Leukemia, 2008. **22**(12): p. 2208-16.
101. Graux, C., et al., *Heterogeneous patterns of amplification of the NUP214-ABL1 fusion gene in T-cell acute lymphoblastic leukemia.* Leukemia, 2009. **23**(1): p. 125-33.
102. Neilson, D.E., et al., *Infection-triggered familial or recurrent cases of acute necrotizing encephalopathy caused by mutations in a component of the nuclear pore, RANBP2.* Am J Hum Genet, 2009. **84**(1): p. 44-51.
103. Werner, A., A. Flotho, and F. Melchior, *The RanBP2/RanGAP1*SUMO1/Ubc9 complex is a multisubunit SUMO E3 ligase.* Mol Cell, 2012. **46**(3): p. 287-98.
104. Cho, K.I., et al., *Association of the kinesin-binding domain of RanBP2 to KIF5B and KIF5C determines mitochondria localization and function.* Traffic, 2007. **8**(12): p. 1722-35.
105. Basel-Vanagaite, L., et al., *Mutated nup62 causes autosomal recessive infantile bilateral striatal necrosis.* Ann Neurol, 2006. **60**(2): p. 214-22.
106. Wesierska-Gadek, J., et al., *Characterization of autoantibodies against components of the nuclear pore complexes: high frequency of anti-p62 nucleoporin antibodies.* Ann N Y Acad Sci, 2007. **1109**: p. 519-30.
107. Storr, H.L., et al., *Deficiency of ferritin heavy-chain nuclear import in triple a syndrome implies nuclear oxidative damage as the primary disease mechanism.* Mol Endocrinol, 2009. **23**(12): p. 2086-94.

108. Alkhateeb, A.A. and J.R. Connor, *Nuclear ferritin: A new role for ferritin in cell biology*. Biochim Biophys Acta, 2010. **1800**(8): p. 793-7.
109. Boyd, D., et al., *Structural and functional relationships of human ferritin H and L chains deduced from cDNA clones*. J Biol Chem, 1985. **260**(21): p. 11755-61.
110. Levi, S., et al., *Evidence of H- and L-chains have co-operative roles in the iron-uptake mechanism of human ferritin*. Biochem J, 1992. **288 (Pt 2)**: p. 591-6.
111. Harrison, P.M. and P. Arosio, *The ferritins: molecular properties, iron storage function and cellular regulation*. Biochim Biophys Acta, 1996. **1275**(3): p. 161-203.
112. Hentze, M.W., et al., *Oxidation-reduction and the molecular mechanism of a regulatory RNA-protein interaction*. Science, 1989. **244**(4902): p. 357-9.
113. Sammarco, M.C., et al., *Ferritin L and H subunits are differentially regulated on a post-transcriptional level*. J Biol Chem, 2008. **283**(8): p. 4578-87.
114. Torti, F.M. and S.V. Torti, *Regulation of ferritin genes and protein*. Blood, 2002. **99**(10): p. 3505-16.
115. Levi, S., et al., *A human mitochondrial ferritin encoded by an intronless gene*. J Biol Chem, 2001. **276**(27): p. 24437-40.
116. Arosio, P., R. Ingrassia, and P. Cavadini, *Ferritins: a family of molecules for iron storage, antioxidation and more*. Biochim Biophys Acta, 2009. **1790**(7): p. 589-99.
117. Linsenmayer, T.F., et al., *Nuclear ferritin in corneal epithelial cells: tissue-specific nuclear transport and protection from UV-damage*. Prog Retin Eye Res, 2005. **24**(2): p. 139-59.
118. Cai, C.X., D.E. Birk, and T.F. Linsenmayer, *Ferritin is a developmentally regulated nuclear protein of avian corneal epithelial cells*. J Biol Chem, 1997. **272**(19): p. 12831-9.
119. Thompson, K.J., et al., *Regulation, mechanisms and proposed function of ferritin translocation to cell nuclei*. J Cell Sci, 2002. **115**(Pt 10): p. 2165-77.

120. Surguladze, N., et al., *Characterization of nuclear ferritin and mechanism of translocation*. Biochem J, 2005. **388**(Pt 3): p. 731-40.
121. Pante, N. and M. Kann, *Nuclear pore complex is able to transport macromolecules with diameters of about 39 nm*. Mol Biol Cell, 2002. **13**(2): p. 425-34.
122. Cai, C.X. and T.F. Linsenmayer, *Nuclear translocation of ferritin in corneal epithelial cells*. J Cell Sci, 2001. **114**(Pt 12): p. 2327-34.
123. Millholland, J.M., et al., *Ferritoid, a tissue-specific nuclear transport protein for ferritin in corneal epithelial cells*. J Biol Chem, 2003. **278**(26): p. 23963-70.
124. Ferreira, C., et al., *Early embryonic lethality of H ferritin gene deletion in mice*. J Biol Chem, 2000. **275**(5): p. 3021-4.
125. Darshan, D., et al., *Conditional deletion of ferritin H in mice induces loss of iron storage and liver damage*. Hepatology, 2009. **50**(3): p. 852-60.
126. Arosio, P. and S. Levi, *Cytosolic and mitochondrial ferritins in the regulation of cellular iron homeostasis and oxidative damage*. Biochim Biophys Acta, 2010. **1800**(8): p. 783-92.
127. Hirano, M., et al., *ALADINI482S causes selective failure of nuclear protein import and hypersensitivity to oxidative stress in triple A syndrome*. Proc Natl Acad Sci U S A, 2006. **103**(7): p. 2298-303.
128. Kiriyaama, T., et al., *Restoration of nuclear-import failure caused by triple A syndrome and oxidative stress*. Biochem Biophys Res Commun, 2008. **374**(4): p. 631-4.
129. Kind, B., et al., *Intracellular ROS level is increased in fibroblasts of triple A syndrome patients*. J Mol Med (Berl), 2010. **88**(12): p. 1233-42.
130. Shepard, T.H., B.H. Landing, and D.G. Mason, *Familial Addison's disease; case reports of two sisters with corticoid deficiency unassociated with hypoadosteronism*. AMA J Dis Child, 1959. **97**(2): p. 154-62.

131. Meimaridou, E., et al., *ACTH resistance: genes and mechanisms*. *Endocr Dev*, 2013. **24**: p. 57-66.
132. Chan, L.F., et al., *Functional consequence of a novel Y129C mutation in a patient with two contradictory melanocortin-2-receptor mutations*. *Eur J Endocrinol*, 2009. **160**(4): p. 705-10.
133. Modan-Moses, D., et al., *Unusual presentation of familial glucocorticoid deficiency with a novel MRAP mutation*. *J Clin Endocrinol Metab*, 2006. **91**(10): p. 3713-7.
134. Turan, S., et al., *An atypical case of familial glucocorticoid deficiency without pigmentation caused by coexistent homozygous mutations in MC2R (T152K) and MC1R (R160W)*. *J Clin Endocrinol Metab*, 2012. **97**(5): p. E771-4.
135. Valverde, P., et al., *Variants of the melanocyte-stimulating hormone receptor gene are associated with red hair and fair skin in humans*. *Nat Genet*, 1995. **11**(3): p. 328-30.
136. Weber, A., et al., *Diminished adrenal androgen secretion in familial glucocorticoid deficiency implicates a significant role for ACTH in the induction of adrenarche*. *Clin Endocrinol (Oxf)*, 1997. **46**(4): p. 431-7.
137. Mountjoy, K.G., et al., *The cloning of a family of genes that encode the melanocortin receptors*. *Science*, 1992. **257**(5074): p. 1248-51.
138. Clark, A.J., L. McLoughlin, and A. Grossman, *Familial glucocorticoid deficiency associated with point mutation in the adrenocorticotropin receptor*. *Lancet*, 1993. **341**(8843): p. 461-2.
139. Clark, A.J., et al., *The genetics of familial glucocorticoid deficiency*. *Best Pract Res Clin Endocrinol Metab*, 2009. **23**(2): p. 159-65.
140. Swords, F.M., et al., *Impaired desensitization of a mutant adrenocorticotropin receptor associated with apparent constitutive activity*. *Mol Endocrinol*, 2002. **16**(12): p. 2746-53.
141. Clark, A.J., et al., *Inherited ACTH insensitivity illuminates the mechanisms of ACTH action*. *Trends Endocrinol Metab*, 2005. **16**(10): p. 451-7.

142. Butler, A.A., et al., *A unique metabolic syndrome causes obesity in the melanocortin-3 receptor-deficient mouse*. *Endocrinology*, 2000. **141**(9): p. 3518-21.
143. Chen, A.S., et al., *Inactivation of the mouse melanocortin-3 receptor results in increased fat mass and reduced lean body mass*. *Nat Genet*, 2000. **26**(1): p. 97-102.
144. Marsh, D.J., et al., *Response of melanocortin-4 receptor-deficient mice to anorectic and orexigenic peptides*. *Nat Genet*, 1999. **21**(1): p. 119-22.
145. Chagnon, Y.C., et al., *Linkage and association studies between the melanocortin receptors 4 and 5 genes and obesity-related phenotypes in the Quebec Family Study*. *Mol Med*, 1997. **3**(10): p. 663-73.
146. Ogawa, K., et al., *A novel mechanism for regulating clonal propagation of mouse ES cells*. *Genes Cells*, 2004. **9**(5): p. 471-7.
147. Cone, R.D., et al., *Cloning and functional characterization of a family of receptors for the melanotropic peptides*. *Ann N Y Acad Sci*, 1993. **680**: p. 342-63.
148. Arnaldi, G., et al., *ACTH receptor mRNA in human adrenocortical tumors: overexpression in aldosteronomas*. *Endocr Res*, 1998. **24**(3-4): p. 845-9.
149. Kelch, R.P., et al., *Hereditary adrenocortical unresponsiveness to adrenocorticotrophic hormone*. *J Pediatr*, 1972. **81**(4): p. 726-36.
150. Clark, A.J. and A. Weber, *Adrenocorticotropin insensitivity syndromes*. *Endocr Rev*, 1998. **19**(6): p. 828-43.
151. Chida, D., et al., *Melanocortin 2 receptor is required for adrenal gland development, steroidogenesis, and neonatal gluconeogenesis*. *Proc Natl Acad Sci U S A*, 2007. **104**(46): p. 18205-10.
152. Chan, L.F., et al., *Homozygous nonsense and frameshift mutations of the ACTH receptor in children with familial glucocorticoid deficiency (FGD) are not associated with long-term mineralocorticoid deficiency*. *Clin Endocrinol (Oxf)*, 2009. **71**(2): p. 171-5.

153. Lin, L., et al., *Severe loss-of-function mutations in the adrenocorticotropin receptor (ACTHR, MC2R) can be found in patients diagnosed with salt-losing adrenal hypoplasia*. Clin Endocrinol (Oxf), 2007. **66**(2): p. 205-10.
154. Elias, L.L., et al., *Tall stature in familial glucocorticoid deficiency*. Clin Endocrinol (Oxf), 2000. **53**(4): p. 423-30.
155. Evans, J.F., et al., *Adrenocorticotropin evokes transient elevations in intracellular free calcium ([Ca²⁺]_i) and increases basal [Ca²⁺]_i in resting chondrocytes through a phospholipase C-dependent mechanism*. Endocrinology, 2005. **146**(7): p. 3123-32.
156. Gabbitas, B. and E. Canalis, *Cortisol enhances the transcription of insulin-like growth factor-binding protein-6 in cultured osteoblasts*. Endocrinology, 1996. **137**(5): p. 1687-92.
157. Chung, T.T., et al., *The majority of adrenocorticotropin receptor (melanocortin 2 receptor) mutations found in familial glucocorticoid deficiency type 1 lead to defective trafficking of the receptor to the cell surface*. J Clin Endocrinol Metab, 2008. **93**(12): p. 4948-54.
158. Schimmer, B.P., et al., *Adrenocorticotropin-resistant mutants of the Y1 adrenal cell line fail to express the adrenocorticotropin receptor*. J Cell Physiol, 1995. **163**(1): p. 164-71.
159. Metherell, L.A., et al., *Mutations in MRAP, encoding a new interacting partner of the ACTH receptor, cause familial glucocorticoid deficiency type 2*. Nat Genet, 2005. **37**(2): p. 166-70.
160. Xu, A., et al., *Identification of novel putative membrane proteins selectively expressed during adipose conversion of 3T3-L1 cells*. Biochem Biophys Res Commun, 2002. **293**(4): p. 1161-7.
161. Sebag, J.A. and P.M. Hinkle, *Melanocortin-2 receptor accessory protein MRAP forms antiparallel homodimers*. Proc Natl Acad Sci U S A, 2007. **104**(51): p. 20244-9.
162. Sebag, J.A. and P.M. Hinkle, *Regions of melanocortin 2 (MC2) receptor accessory protein necessary for dual topology and MC2 receptor trafficking and signaling*. J Biol Chem, 2009. **284**(1): p. 610-8.

163. Xing, Y., et al., *ACTH is a potent regulator of gene expression in human adrenal cells*. J Mol Endocrinol, 2010. **45**(1): p. 59-68.
164. Hofland, J., et al., *Melanocortin 2 receptor-associated protein (MRAP) and MRAP2 in human adrenocortical tissues: regulation of expression and association with ACTH responsiveness*. J Clin Endocrinol Metab, 2012. **97**(5): p. E747-54.
165. Roy, S., M. Rached, and N. Gallo-Payet, *Differential regulation of the human adrenocorticotropin receptor [melanocortin-2 receptor (MC2R)] by human MC2R accessory protein isoforms alpha and beta in isogenic human embryonic kidney 293 cells*. Mol Endocrinol, 2007. **21**(7): p. 1656-69.
166. Chan, L.F., et al., *MRAP and MRAP2 are bidirectional regulators of the melanocortin receptor family*. Proc Natl Acad Sci U S A, 2009. **106**(15): p. 6146-51.
167. Gorrigan, R.J., et al., *Localisation of the melanocortin-2-receptor and its accessory proteins in the developing and adult adrenal gland*. J Mol Endocrinol, 2011. **46**(3): p. 227-32.
168. Metherell, L.A., et al., *Nonclassic lipid congenital adrenal hyperplasia masquerading as familial glucocorticoid deficiency*. J Clin Endocrinol Metab, 2009. **94**(10): p. 3865-71.
169. Bose, H.S., et al., *The pathophysiology and genetics of congenital lipid adrenal hyperplasia*. N Engl J Med, 1996. **335**(25): p. 1870-8.
170. Hasegawa, T., et al., *Developmental roles of the steroidogenic acute regulatory protein (StAR) as revealed by StAR knockout mice*. Mol Endocrinol, 2000. **14**(9): p. 1462-71.
171. Fluck, C.E., et al., *Characterization of novel StAR (steroidogenic acute regulatory protein) mutations causing non-classic lipid adrenal hyperplasia*. PLoS One, 2011. **6**(5): p. e20178.
172. Baker, B.Y., et al., *Nonclassic congenital lipid adrenal hyperplasia: a new disorder of the steroidogenic acute regulatory protein with very late presentation and normal male genitalia*. J Clin Endocrinol Metab, 2006. **91**(12): p. 4781-5.

173. Hughes, C.R., et al., *MCM4 mutation causes adrenal failure, short stature, and natural killer cell deficiency in humans*. J Clin Invest, 2012. **122**(3): p. 814-20.
174. Gineau, L., et al., *Partial MCM4 deficiency in patients with growth retardation, adrenal insufficiency, and natural killer cell deficiency*. J Clin Invest, 2012. **122**(3): p. 821-32.
175. Shima, N., T.R. Buske, and J.C. Schimenti, *Genetic screen for chromosome instability in mice: Mcm4 and breast cancer*. Cell Cycle, 2007. **6**(10): p. 1135-40.
176. Chuang, C.H., et al., *Incremental genetic perturbations to MCM2-7 expression and subcellular distribution reveal exquisite sensitivity of mice to DNA replication stress*. PLoS Genet, 2010. **6**(9): p. e1001110.
177. Meimaridou, E., et al., *Mutations in NNT encoding nicotinamide nucleotide transhydrogenase cause familial glucocorticoid deficiency*. Nat Genet, 2012. **44**(7): p. 740-2.
178. Hanukoglu, I., *Antioxidant protective mechanisms against reactive oxygen species (ROS) generated by mitochondrial P450 systems in steroidogenic cells*. Drug Metab Rev, 2006. **38**(1-2): p. 171-96.
179. Toye, A.A., et al., *A genetic and physiological study of impaired glucose homeostasis control in C57BL/6J mice*. Diabetologia, 2005. **48**(4): p. 675-86.
180. Huang, T.T., et al., *Genetic modifiers of the phenotype of mice deficient in mitochondrial superoxide dismutase*. Hum Mol Genet, 2006. **15**(7): p. 1187-94.
181. Kim, A., et al., *Genetic modifier of mitochondrial superoxide dismutase-deficient mice delays heart failure and prolongs survival*. Mamm Genome, 2010. **21**(11-12): p. 534-42.
182. Kulkarni, R.N., et al., *Impact of genetic background on development of hyperinsulinemia and diabetes in insulin receptor/insulin receptor substrate-1 double heterozygous mice*. Diabetes, 2003. **52**(6): p. 1528-34.
183. Rossmeis, M., et al., *Variation in type 2 diabetes--related traits in mouse strains susceptible to diet-induced obesity*. Diabetes, 2003. **52**(8): p. 1958-66.

184. Wong, N., et al., *The deletion variant of nicotinamide nucleotide transhydrogenase (Nnt) does not affect insulin secretion or glucose tolerance*. *Endocrinology*, 2010. **151**(1): p. 96-102.
185. Hamre, K., et al., *Differential strain susceptibility following 1-methyl-4-phenyl-1,2,3,6-tetrahydropyridine (MPTP) administration acts in an autosomal dominant fashion: quantitative analysis in seven strains of *Mus musculus**. *Brain Res*, 1999. **828**(1-2): p. 91-103.
186. Sena, L.A. and N.S. Chandel, *Physiological roles of mitochondrial reactive oxygen species*. *Mol Cell*, 2012. **48**(2): p. 158-67.
187. Ray, P.D., B.W. Huang, and Y. Tsuji, *Reactive oxygen species (ROS) homeostasis and redox regulation in cellular signaling*. *Cell Signal*, 2012. **24**(5): p. 981-90.
188. Hornig, D., *Distribution of ascorbic acid, metabolites and analogues in man and animals*. *Ann N Y Acad Sci*, 1975. **258**: p. 103-18.
189. Hanukoglu, I. and Z. Hanukoglu, *Stoichiometry of mitochondrial cytochromes P-450, adrenodoxin and adrenodoxin reductase in adrenal cortex and corpus luteum. Implications for membrane organization and gene regulation*. *Eur J Biochem*, 1986. **157**(1): p. 27-31.
190. Grinberg, A.V., et al., *Adrenodoxin: structure, stability, and electron transfer properties*. *Proteins*, 2000. **40**(4): p. 590-612.
191. Ziegler, G.A., et al., *The structure of adrenodoxin reductase of mitochondrial P450 systems: electron transfer for steroid biosynthesis*. *J Mol Biol*, 1999. **289**(4): p. 981-90.
192. Rapoport, R., D. Sklan, and I. Hanukoglu, *Electron leakage from the adrenal cortex mitochondrial P450_{scc} and P450_{c11} systems: NADPH and steroid dependence*. *Arch Biochem Biophys*, 1995. **317**(2): p. 412-6.
193. Carpenter, K.J., *The discovery of vitamin C*. *Ann Nutr Metab*, 2012. **61**(3): p. 259-64.
194. Svirbely, J.L. and A. Szent-Gyorgyi, *The chemical nature of vitamin C*. *Biochem J*, 1932. **26**(3): p. 865-70.

195. Gruber, K.A., L.V. O'Brien, and R. Gerstner, *Vitamin A: not required for adrenal steroidogenesis in rats*. Science, 1976. **191**(4226): p. 472-5.
196. Azhar, S., L. Cao, and E. Reaven, *Alteration of the adrenal antioxidant defense system during aging in rats*. J Clin Invest, 1995. **96**(3): p. 1414-24.
197. Watabe, S., et al., *Mitochondrial thioredoxin reductase in bovine adrenal cortex its purification, properties, nucleotide/amino acid sequences, and identification of selenocysteine*. Eur J Biochem, 1999. **264**(1): p. 74-84.
198. Palmieri, F., *Mitochondrial carrier proteins*. FEBS Lett, 1994. **346**(1): p. 48-54.
199. Behne, D. and T. Hofer-Bosse, *Effects of a low selenium status on the distribution and retention of selenium in the rat*. J Nutr, 1984. **114**(7): p. 1289-96.
200. Chanoine, J.P., et al., *Modulation of steroidogenesis by selenium in a novel adrenal cell line developed using targeted tumorigenesis*. Biofactors, 2001. **14**(1-4): p. 229-38.
201. Imai, H., et al., *Depletion of selenoprotein GPx4 in spermatocytes causes male infertility in mice*. J Biol Chem, 2009. **284**(47): p. 32522-32.
202. Cox, A.G., C.C. Winterbourn, and M.B. Hampton, *Mitochondrial peroxiredoxin involvement in antioxidant defence and redox signalling*. Biochem J, 2010. **425**(2): p. 313-25.
203. Zhang, H., Y.M. Go, and D.P. Jones, *Mitochondrial thioredoxin-2/peroxiredoxin-3 system functions in parallel with mitochondrial GSH system in protection against oxidative stress*. Arch Biochem Biophys, 2007. **465**(1): p. 119-26.
204. Hanschmann, E.M., et al., *Both thioredoxin 2 and glutaredoxin 2 contribute to the reduction of the mitochondrial 2-Cys peroxiredoxin Prx3*. J Biol Chem, 2010. **285**(52): p. 40699-705.
205. Woo, H.A., et al., *Reversing the inactivation of peroxiredoxins caused by cysteine sulfinic acid formation*. Science, 2003. **300**(5619): p. 653-6.
206. Kil, I.S., et al., *Feedback control of adrenal steroidogenesis via H₂O₂-dependent, reversible inactivation of peroxiredoxin III in mitochondria*. Mol Cell, 2012. **46**(5): p. 584-94.

207. Sanger, F., S. Nicklen, and A.R. Coulson, *DNA sequencing with chain-terminating inhibitors*. 1977. *Biotechnology*, 1992. **24**: p. 104-8.
208. Darrah, P.A., et al., *Multifunctional TH1 cells define a correlate of vaccine-mediated protection against Leishmania major*. *Nat Med*, 2007. **13**(7): p. 843-50.
209. Burhans, W.C. and N.H. Heintz, *The cell cycle is a redox cycle: linking phase-specific targets to cell fate*. *Free Radic Biol Med*, 2009. **47**(9): p. 1282-93.
210. Gazdar, A.F., et al., *Establishment and characterization of a human adrenocortical carcinoma cell line that expresses multiple pathways of steroid biosynthesis*. *Cancer Res*, 1990. **50**(17): p. 5488-96.
211. Harvey, P.W. and D.J. Everett, *The adrenal cortex and steroidogenesis as cellular and molecular targets for toxicity: critical omissions from regulatory endocrine disrupter screening strategies for human health?* *J Appl Toxicol*, 2003. **23**(2): p. 81-7.
212. Staels, B., D.W. Hum, and W.L. Miller, *Regulation of steroidogenesis in NCI-H295 cells: a cellular model of the human fetal adrenal*. *Mol Endocrinol*, 1993. **7**(3): p. 423-33.
213. Hecker, M., et al., *Human adrenocarcinoma (H295R) cells for rapid in vitro determination of effects on steroidogenesis: hormone production*. *Toxicol Appl Pharmacol*, 2006. **217**(1): p. 114-24.
214. Hilscherova, K., et al., *Assessment of the effects of chemicals on the expression of ten steroidogenic genes in the H295R cell line using real-time PCR*. *Toxicol Sci*, 2004. **81**(1): p. 78-89.
215. Zhang, X., et al., *Quantitative RT-PCR methods for evaluating toxicant-induced effects on steroidogenesis using the H295R cell line*. *Environ Sci Technol*, 2005. **39**(8): p. 2777-85.
216. Biedler, J.L., L. Helson, and B.A. Spengler, *Morphology and growth, tumorigenicity, and cytogenetics of human neuroblastoma cells in continuous culture*. *Cancer Res*, 1973. **33**(11): p. 2643-52.

217. Nicholson, D.W., et al., *Identification and inhibition of the ICE/CED-3 protease necessary for mammalian apoptosis*. Nature, 1995. **376**(6535): p. 37-43.
218. Oliver, F.J., et al., *Importance of poly(ADP-ribose) polymerase and its cleavage in apoptosis. Lesson from an uncleavable mutant*. J Biol Chem, 1998. **273**(50): p. 33533-9.
219. Diemer, T., et al., *Reactive oxygen disrupts mitochondria in MA-10 tumor Leydig cells and inhibits steroidogenic acute regulatory (StAR) protein and steroidogenesis*. Endocrinology, 2003. **144**(7): p. 2882-91.
220. Shi, Z., et al., *Perfluorododecanoic acid-induced steroidogenic inhibition is associated with steroidogenic acute regulatory protein and reactive oxygen species in cAMP-stimulated Leydig cells*. Toxicol Sci, 2010. **114**(2): p. 285-94.
221. Parmar, J., R.E. Key, and W.E. Rainey, *Development of an adrenocorticotropin-responsive human adrenocortical carcinoma cell line*. J Clin Endocrinol Metab, 2008. **93**(11): p. 4542-6.
222. Recolin, B., et al., *Molecular mechanisms of DNA replication checkpoint activation*. Genes (Basel), 2014. **5**(1): p. 147-75.
223. Reshmi-Skarja, S., et al., *Chromosomal fragility in patients with triple A syndrome*. Am J Med Genet A, 2003. **117A**(1): p. 30-6.
224. Liodice, I., et al., *The entire Nup107-160 complex, including three new members, is targeted as one entity to kinetochores in mitosis*. Mol Biol Cell, 2004. **15**(7): p. 3333-44.
225. Klein, J.A. and S.L. Ackerman, *Oxidative stress, cell cycle, and neurodegeneration*. J Clin Invest, 2003. **111**(6): p. 785-93.
226. Hashizume, C., A. Kobayashi, and R.W. Wong, *Down-modulation of nucleoporin RanBP2/Nup358 impaired chromosomal alignment and induced mitotic catastrophe*. Cell Death Dis, 2013. **4**: p. e854.

227. Miyamoto, H., et al., *Studies on cytogenesis in adult rat adrenal cortex: circadian and zonal variations and their modulation by adrenocorticotrophic hormone*. J Biochem, 1999. **126**(6): p. 1175-83.
228. Dallman, M.F., *Control of adrenocortical growth in vivo*. Endocr Res, 1984. **10**(3-4): p. 213-42.
229. Bland, M.L., M. Desclozeaux, and H.A. Ingraham, *Tissue growth and remodeling of the embryonic and adult adrenal gland*. Ann N Y Acad Sci, 2003. **995**: p. 59-72.
230. Feuerstein, B. and D.H. Streeten, *Recovery of adrenal function after failure resulting from traumatic bilateral adrenal hemorrhages*. Ann Intern Med, 1991. **115**(10): p. 785-6.
231. Korytowski, W., et al., *Deleterious cholesterol hydroperoxide trafficking in steroidogenic acute regulatory (StAR) protein-expressing MA-10 Leydig cells: implications for oxidative stress-impaired steroidogenesis*. J Biol Chem, 2013. **288**(16): p. 11509-19.
232. Galea, E., et al., *Oxidative stress underlying axonal degeneration in adrenoleukodystrophy: A paradigm for multifactorial neurodegenerative diseases?* Biochim Biophys Acta, 2012.
233. Kemp, S., J. Berger, and P. Aubourg, *X-linked adrenoleukodystrophy: Clinical, metabolic, genetic and pathophysiological aspects*. Biochim Biophys Acta, 2012.
234. Hanukoglu, I. and R. Rapoport, *Routes and regulation of NADPH production in steroidogenic mitochondria*. Endocr Res, 1995. **21**(1-2): p. 231-41.
235. Ng, S.B., et al., *Targeted capture and massively parallel sequencing of 12 human exomes*. Nature, 2009. **461**(7261): p. 272-6.
236. Berry, M.J., et al., *Recognition of UGA as a selenocysteine codon in type I deiodinase requires sequences in the 3' untranslated region*. Nature, 1991. **353**(6341): p. 273-6.
237. Copeland, P.R. and D.M. Driscoll, *Purification, redox sensitivity, and RNA binding properties of SECIS-binding protein 2, a protein involved in selenoprotein biosynthesis*. J Biol Chem, 1999. **274**(36): p. 25447-54.

238. Fagegaltier, D., et al., *Characterization of mSelB, a novel mammalian elongation factor for selenoprotein translation*. EMBO J, 2000. **19**(17): p. 4796-805.
239. Tujebajeva, R.M., et al., *Decoding apparatus for eukaryotic selenocysteine insertion*. EMBO Rep, 2000. **1**(2): p. 158-63.
240. Caban, K. and P.R. Copeland, *Selenocysteine insertion sequence (SECIS)-binding protein 2 alters conformational dynamics of residues involved in tRNA accommodation in 80 S ribosomes*. J Biol Chem, 2012. **287**(13): p. 10664-73.
241. Holmgren, A., *Antioxidant function of thioredoxin and glutaredoxin systems*. Antioxid Redox Signal, 2000. **2**(4): p. 811-20.
242. Ferreiro, A., et al., *Mutations of the selenoprotein N gene, which is implicated in rigid spine muscular dystrophy, cause the classical phenotype of multiminicore disease: reassessing the nosology of early-onset myopathies*. Am J Hum Genet, 2002. **71**(4): p. 739-49.
243. Schoenmakers, E., et al., *Mutations in the selenocysteine insertion sequence-binding protein 2 gene lead to a multisystem selenoprotein deficiency disorder in humans*. J Clin Invest, 2010. **120**(12): p. 4220-35.
244. Cheng, W.H., et al., *Cellular glutathione peroxidase knockout mice express normal levels of selenium-dependent plasma and phospholipid hydroperoxide glutathione peroxidases in various tissues*. J Nutr, 1997. **127**(8): p. 1445-50.
245. de Jesus, L.A., et al., *The type 2 iodothyronine deiodinase is essential for adaptive thermogenesis in brown adipose tissue*. J Clin Invest, 2001. **108**(9): p. 1379-85.
246. Esworthy, R.S., et al., *Mice with combined disruption of Gpx1 and Gpx2 genes have colitis*. Am J Physiol Gastrointest Liver Physiol, 2001. **281**(3): p. G848-55.
247. Hill, K.E., et al., *Deletion of selenoprotein P alters distribution of selenium in the mouse*. J Biol Chem, 2003. **278**(16): p. 13640-6.

248. Jin, R.C., et al., *Glutathione peroxidase-3 deficiency promotes platelet-dependent thrombosis in vivo*. *Circulation*, 2011. **123**(18): p. 1963-73.
249. Yant, L.J., et al., *The selenoprotein GPX4 is essential for mouse development and protects from radiation and oxidative damage insults*. *Free Radic Biol Med*, 2003. **34**(4): p. 496-502.
250. Conrad, M., et al., *Essential role for mitochondrial thioredoxin reductase in hematopoiesis, heart development, and heart function*. *Mol Cell Biol*, 2004. **24**(21): p. 9414-23.
251. Jakupoglu, C., et al., *Cytoplasmic thioredoxin reductase is essential for embryogenesis but dispensable for cardiac development*. *Mol Cell Biol*, 2005. **25**(5): p. 1980-8.
252. Matsui, M., et al., *Early embryonic lethality caused by targeted disruption of the mouse thioredoxin gene*. *Dev Biol*, 1996. **178**(1): p. 179-85.
253. Nonn, L., et al., *The absence of mitochondrial thioredoxin 2 causes massive apoptosis, exencephaly, and early embryonic lethality in homozygous mice*. *Mol Cell Biol*, 2003. **23**(3): p. 916-22.
254. Carlson, B.A., et al., *Selective rescue of selenoprotein expression in mice lacking a highly specialized methyl group in selenocysteine tRNA*. *J Biol Chem*, 2005. **280**(7): p. 5542-8.
255. Moustafa, M.E., et al., *Selective inhibition of selenocysteine tRNA maturation and selenoprotein synthesis in transgenic mice expressing isopentenyladenosine-deficient selenocysteine tRNA*. *Mol Cell Biol*, 2001. **21**(11): p. 3840-52.
256. Crosley, L.K., et al., *Differential regulation of expression of cytosolic and mitochondrial thioredoxin reductase in rat liver and kidney*. *Arch Biochem Biophys*, 2007. **459**(2): p. 178-88.
257. Kiermayer, C., et al., *Effect of selenium on thioredoxin reductase activity in Txnrd1 or Txnrd2 hemizygous mice*. *Biol Chem*, 2007. **388**(10): p. 1091-7.
258. Sibbing, D., et al., *Mutations in the mitochondrial thioredoxin reductase gene TXNRD2 cause dilated cardiomyopathy*. *Eur Heart J*, 2011. **32**(9): p. 1121-33.

259. Chen, J., *An original discovery: selenium deficiency and Keshan disease (an endemic heart disease)*. Asia Pac J Clin Nutr, 2012. **21**(3): p. 320-6.
260. Momma, K., *Cardiovascular anomalies associated with chromosome 22q11.2 deletion syndrome*. Am J Cardiol, 2010. **105**(11): p. 1617-24.
261. Moon, A.M., et al., *Crkl deficiency disrupts Fgf8 signaling in a mouse model of 22q11 deletion syndromes*. Dev Cell, 2006. **10**(1): p. 71-80.
262. Yagi, H., et al., *Role of TBX1 in human del22q11.2 syndrome*. Lancet, 2003. **362**(9393): p. 1366-73.
263. Mitsui, A., et al., *Overexpression of human thioredoxin in transgenic mice controls oxidative stress and life span*. Antioxid Redox Signal, 2002. **4**(4): p. 693-6.
264. Yan, H., et al., *Revival of glutathione reductase in human cataractous and clear lens extracts by thioredoxin and thioredoxin reductase, in conjunction with alpha-crystallin or thioltransferase*. Curr Eye Res, 2007. **32**(5): p. 455-63.
265. Calabrese, V., et al., *Nitrosative stress, cellular stress response, and thiol homeostasis in patients with Alzheimer's disease*. Antioxid Redox Signal, 2006. **8**(11-12): p. 1975-86.
266. Meplan, C., et al., *Polymorphisms in thioredoxin reductase and selenoprotein K genes and selenium status modulate risk of prostate cancer*. PLoS One, 2012. **7**(11): p. e48709.
267. Slattery, M.L., et al., *Genetic variation in selenoprotein genes, lifestyle, and risk of colon and rectal cancer*. PLoS One, 2012. **7**(5): p. e37312.
268. Hanschmann, E.M., et al., *Thioredoxins, glutaredoxins, and peroxiredoxins--molecular mechanisms and health significance: from cofactors to antioxidants to redox signaling*. Antioxid Redox Signal, 2013. **19**(13): p. 1539-605.
269. Trivedi, M.V., J.S. Laurence, and T.J. Siahaan, *The role of thiols and disulfides on protein stability*. Curr Protein Pept Sci, 2009. **10**(6): p. 614-25.

270. Holmgren, A. and M. Bjornstedt, *Thioredoxin and thioredoxin reductase*. Methods Enzymol, 1995. **252**: p. 199-208.
271. Lee, S.R., et al., *Molecular cloning and characterization of a mitochondrial selenocysteine-containing thioredoxin reductase from rat liver*. J Biol Chem, 1999. **274**(8): p. 4722-34.
272. Gasdaska, P.Y., et al., *Cloning and sequencing of a human thioredoxin reductase*. FEBS Lett, 1995. **373**(1): p. 5-9.
273. Sun, Q.A., et al., *Selenoprotein oxidoreductase with specificity for thioredoxin and glutathione systems*. Proc Natl Acad Sci U S A, 2001. **98**(7): p. 3673-8.
274. Turanov, A.A., D. Su, and V.N. Gladyshev, *Characterization of alternative cytosolic forms and cellular targets of mouse mitochondrial thioredoxin reductase*. J Biol Chem, 2006. **281**(32): p. 22953-63.
275. Biterova, E.I., et al., *Crystal structures of oxidized and reduced mitochondrial thioredoxin reductase provide molecular details of the reaction mechanism*. Proc Natl Acad Sci U S A, 2005. **102**(42): p. 15018-23.
276. Godoy, J.R., et al., *Redox atlas of the mouse. Immunohistochemical detection of glutaredoxin-, peroxiredoxin-, and thioredoxin-family proteins in various tissues of the laboratory mouse*. Biochim Biophys Acta, 2011. **1810**(1): p. 2-92.
277. Schomburg, L. and U. Schweizer, *Hierarchical regulation of selenoprotein expression and sex-specific effects of selenium*. Biochim Biophys Acta, 2009. **1790**(11): p. 1453-62.
278. Rigobello, M.P., et al., *Purification of mitochondrial thioredoxin reductase and its involvement in the redox regulation of membrane permeability*. Free Radic Biol Med, 1998. **24**(2): p. 370-6.
279. Gromer, S., et al., *Active sites of thioredoxin reductases: why selenoproteins?* Proc Natl Acad Sci U S A, 2003. **100**(22): p. 12618-23.

280. Lothrop, A.P., et al., *Selenium as an electron acceptor during the catalytic mechanism of thioredoxin reductase*. *Biochemistry*, 2014. **53**(4): p. 654-63.
281. Nalvarte, I., A.E. Damdimopoulos, and G. Spyrou, *Human mitochondrial thioredoxin reductase reduces cytochrome c and confers resistance to complex III inhibition*. *Free Radic Biol Med*, 2004. **36**(10): p. 1270-8.
282. Nordberg, J. and E.S. Arner, *Reactive oxygen species, antioxidants, and the mammalian thioredoxin system*. *Free Radic Biol Med*, 2001. **31**(11): p. 1287-312.
283. Xia, L., et al., *The mammalian cytosolic selenoenzyme thioredoxin reductase reduces ubiquinone. A novel mechanism for defense against oxidative stress*. *J Biol Chem*, 2003. **278**(4): p. 2141-6.
284. Spyrou, G., et al., *Cloning and expression of a novel mammalian thioredoxin*. *J Biol Chem*, 1997. **272**(5): p. 2936-41.
285. Arner, E.S. and A. Holmgren, *Physiological functions of thioredoxin and thioredoxin reductase*. *Eur J Biochem*, 2000. **267**(20): p. 6102-9.
286. Holmgren, A. and J. Lu, *Thioredoxin and thioredoxin reductase: current research with special reference to human disease*. *Biochem Biophys Res Commun*, 2010. **396**(1): p. 120-4.
287. Lillig, C.H. and A. Holmgren, *Thioredoxin and related molecules--from biology to health and disease*. *Antioxid Redox Signal*, 2007. **9**(1): p. 25-47.
288. Kim, H.Y. and J.R. Kim, *Thioredoxin as a reducing agent for mammalian methionine sulfoxide reductases B lacking resolving cysteine*. *Biochem Biophys Res Commun*, 2008. **371**(3): p. 490-4.
289. Cox, A.G., et al., *Redox potential and peroxide reactivity of human peroxiredoxin 3*. *Biochemistry*, 2009. **48**(27): p. 6495-501.

290. Shelton, M.D., P.B. Chock, and J.J. Mieyal, *Glutaredoxin: role in reversible protein s-glutathionylation and regulation of redox signal transduction and protein translocation*. *Antioxid Redox Signal*, 2005. **7**(3-4): p. 348-66.
291. Chang, T.S., et al., *Characterization of mammalian sulfiredoxin and its reactivation of hyperoxidized peroxiredoxin through reduction of cysteine sulfinic acid in the active site to cysteine*. *J Biol Chem*, 2004. **279**(49): p. 50994-1001.
292. Noh, Y.H., et al., *Sulfiredoxin Translocation into Mitochondria Plays a Crucial Role in Reducing Hyperoxidized Peroxiredoxin III*. *J Biol Chem*, 2009. **284**(13): p. 8470-7.
293. Watson, W.H., et al., *Thioredoxin reductase-1 knock down does not result in thioredoxin-1 oxidation*. *Biochem Biophys Res Commun*, 2008. **368**(3): p. 832-6.
294. Rundlof, A.K., et al., *Evidence for intriguingly complex transcription of human thioredoxin reductase 1*. *Free Radic Biol Med*, 2004. **36**(5): p. 641-56.
295. Kil, I.S., S.H. Bae, and S.G. Rhee, *Study of the signaling function of sulfiredoxin and peroxiredoxin III in isolated adrenal gland: unsuitability of clonal and primary adrenocortical cells*. *Methods Enzymol*, 2013. **527**: p. 169-81.
296. van Roermund, C.W., et al., *The human peroxisomal ABC half transporter ALDP functions as a homodimer and accepts acyl-CoA esters*. *FASEB J*, 2008. **22**(12): p. 4201-8.
297. Hoftberger, R., et al., *Distribution and cellular localization of adrenoleukodystrophy protein in human tissues: implications for X-linked adrenoleukodystrophy*. *Neurobiol Dis*, 2007. **28**(2): p. 165-74.
298. Powers, J.M., et al., *Adreno-leukodystrophy: oxidative stress of mice and men*. *J Neuropathol Exp Neurol*, 2005. **64**(12): p. 1067-79.
299. Fourcade, S., et al., *Early oxidative damage underlying neurodegeneration in X-adrenoleukodystrophy*. *Hum Mol Genet*, 2008. **17**(12): p. 1762-73.

300. Khan, M., J. Singh, and I. Singh, *Plasmalogen deficiency in cerebral adrenoleukodystrophy and its modulation by lovastatin*. J Neurochem, 2008. **106**(4): p. 1766-79.
301. Brites, P., et al., *Plasmalogens participate in very-long-chain fatty acid-induced pathology*. Brain, 2009. **132**(Pt 2): p. 482-92.
302. Hayashi, H. and M. Oohashi, *Incorporation of acetyl-CoA generated from peroxisomal beta-oxidation into ethanolamine plasmalogen of rat liver*. Biochim Biophys Acta, 1995. **1254**(3): p. 319-25.
303. Ivashchenko, O., et al., *Intraperoxisomal redox balance in mammalian cells: oxidative stress and interorganellar cross-talk*. Mol Biol Cell, 2011. **22**(9): p. 1440-51.
304. Forss-Petter, S., et al., *Targeted inactivation of the X-linked adrenoleukodystrophy gene in mice*. J Neurosci Res, 1997. **50**(5): p. 829-43.
305. Galea, E., et al., *Oxidative stress underlying axonal degeneration in adrenoleukodystrophy: a paradigm for multifactorial neurodegenerative diseases?* Biochim Biophys Acta, 2012. **1822**(9): p. 1475-88.
306. Lu, J.F., et al., *The role of peroxisomal ABC transporters in the mouse adrenal gland: the loss of Abcd2 (ALDR), Not Abcd1 (ALD), causes oxidative damage*. Lab Invest, 2007. **87**(3): p. 261-72.
307. Pujol, A., et al., *Late onset neurological phenotype of the X-ALD gene inactivation in mice: a mouse model for adrenomyeloneuropathy*. Hum Mol Genet, 2002. **11**(5): p. 499-505.
308. Pujol, A., et al., *Functional overlap between ABCD1 (ALD) and ABCD2 (ALDR) transporters: a therapeutic target for X-adrenoleukodystrophy*. Hum Mol Genet, 2004. **13**(23): p. 2997-3006.
309. Go, Y.M., et al., *Selective protection of nuclear thioredoxin-1 and glutathione redox systems against oxidation during glucose and glutamine deficiency in human colonic epithelial cells*. Free Radic Biol Med, 2007. **42**(3): p. 363-70.

310. Sandstrom, B.E. and S.L. Marklund, *Effects of variation in glutathione peroxidase activity on DNA damage and cell survival in human cells exposed to hydrogen peroxide and t-butyl hydroperoxide*. *Biochem J*, 1990. **271**(1): p. 17-23.
311. Sen, C.K. and L. Packer, *Antioxidant and redox regulation of gene transcription*. *FASEB J*, 1996. **10**(7): p. 709-20.
312. De Capoa, A., et al., *Silver staining of the nucleolus organizer regions (NOR) requires clusters of sulfhydryl groups*. *J Histochem Cytochem*, 1982. **30**(9): p. 908-11.
313. Dijkwel, P.A. and P.W. Wenink, *Structural integrity of the nuclear matrix: differential effects of thiol agents and metal chelators*. *J Cell Sci*, 1986. **84**: p. 53-67.
314. Pujari, G., et al., *Influence of glutathione levels on radiation-induced chromosomal DNA damage and repair in human peripheral lymphocytes*. *Mutat Res*, 2009. **675**(1-2): p. 23-8.
315. Garcia-Gimenez, J.L., et al., *Nuclear glutathione*. *Biochim Biophys Acta*, 2013. **1830**(5): p. 3304-16.
316. Allen, R.G. and M. Tresini, *Oxidative stress and gene regulation*. *Free Radic Biol Med*, 2000. **28**(3): p. 463-99.
317. Hirota, K., et al., *AP-1 transcriptional activity is regulated by a direct association between thioredoxin and Ref-1*. *Proc Natl Acad Sci U S A*, 1997. **94**(8): p. 3633-8.
318. Spielberger, J.C., A.D. Moody, and W.H. Watson, *Oxidation and nuclear localization of thioredoxin-1 in sparse cell cultures*. *J Cell Biochem*, 2008. **104**(5): p. 1879-89.
319. Picard, M., et al., *Mitochondria: isolation, structure and function*. *J Physiol*, 2011. **589**(Pt 18): p. 4413-21.
320. Picard, M., et al., *Mitochondrial structure and function are disrupted by standard isolation methods*. *PLoS One*, 2011. **6**(3): p. e18317.
321. Salabei, J.K., A.A. Gibb, and B.G. Hill, *Comprehensive measurement of respiratory activity in permeabilized cells using extracellular flux analysis*. *Nat Protoc*, 2014. **9**(2): p. 421-38.

322. Lievens, S., et al., *ArrayMAPPIT: a screening platform for human protein interactome analysis*. *Methods Mol Biol*, 2012. **812**: p. 283-94.
323. Lievens, S., et al., *Array MAPPIT: high-throughput interactome analysis in mammalian cells*. *J Proteome Res*, 2009. **8**(2): p. 877-86.
324. Boisvert, F.M., et al., *A quantitative proteomics analysis of subcellular proteome localization and changes induced by DNA damage*. *Mol Cell Proteomics*, 2010. **9**(3): p. 457-70.
325. Sudmant, P.H., et al., *Diversity of human copy number variation and multicopy genes*. *Science*, 2010. **330**(6004): p. 641-6.
326. Sonoyama, T., et al., *Differentiation of human embryonic stem cells and human induced pluripotent stem cells into steroid-producing cells*. *Endocrinology*, 2012. **153**(9): p. 4336-45.
327. Buaas, F.W., et al., *In vivo evidence for the crucial role of SF1 in steroid-producing cells of the testis, ovary and adrenal gland*. *Development*, 2012. **139**(24): p. 4561-70.
328. Goncharova, N.D. and B.A. Lapin, *Age-related endocrine dysfunction in nonhuman primates*. *Ann N Y Acad Sci*, 2004. **1019**: p. 321-5.
329. Ferrari, E., et al., *Age-related changes of the hypothalamic-pituitary-adrenal axis: pathophysiological correlates*. *Eur J Endocrinol*, 2001. **144**(4): p. 319-29.
330. Goncharova, N.D., V.Y. Marenin, and T.N. Bogatyrenko, *Stress, aging and reliability of antioxidant enzyme defense*. *Curr Aging Sci*, 2008. **1**(1): p. 22-9.
331. Goncharova, N.D., V.Y. Marenin, and A.A. Vengerin, *Age-related changes in the reliability of antioxidant enzyme defense in monkeys with different types of adaptive behavior*. *Curr Aging Sci*, 2012.
332. Goncharova, N.D., et al., *Circadian and age-related changes in stress responsiveness of the adrenal cortex and erythrocyte antioxidant enzymes in female rhesus monkeys*. *J Med Primatol*, 2008. **37**(5): p. 229-38.

333. Tokarz, J., et al., *Zebrafish and steroids: What do we know and what do we need to know?* J Steroid Biochem Mol Biol, 2013.
334. Lohr, H. and M. Hammerschmidt, *Zebrafish in endocrine systems: recent advances and implications for human disease*. Annu Rev Physiol, 2011. **73**: p. 183-211.
335. Chai, C., Y.W. Liu, and W.K. Chan, *Ff1b is required for the development of steroidogenic component of the zebrafish interrenal organ*. Dev Biol, 2003. **260**(1): p. 226-44.
336. Liu, C., et al., *Effects of prochloraz or propylthiouracil on the cross-talk between the HPG, HPA, and HPT axes in zebrafish*. Environ Sci Technol, 2011. **45**(2): p. 769-75.
337. Parajes, S., et al., *Redefining the initiation and maintenance of zebrafish interrenal steroidogenesis by characterizing the key enzyme cyp11a2*. Endocrinology, 2013. **154**(8): p. 2702-11.
338. Alsop, D. and M.M. Vijayan, *Development of the corticosteroid stress axis and receptor expression in zebrafish*. Am J Physiol Regul Integr Comp Physiol, 2008. **294**(3): p. R711-9.
339. Alsop, D. and M.M. Vijayan, *Molecular programming of the corticosteroid stress axis during zebrafish development*. Comp Biochem Physiol A Mol Integr Physiol, 2009. **153**(1): p. 49-54.
340. Dickmeis, T., et al., *Glucocorticoids play a key role in circadian cell cycle rhythms*. PLoS Biol, 2007. **5**(4): p. e78.
341. Cachat, J., et al., *Measuring behavioral and endocrine responses to novelty stress in adult zebrafish*. Nat Protoc, 2010. **5**(11): p. 1786-99.
342. Felix, A.S., et al., *Noninvasive measurement of steroid hormones in zebrafish holding-water*. Zebrafish, 2013. **10**(1): p. 110-5.
343. Fuzzen, M.L., G. Van Der Kraak, and N.J. Bernier, *Stirring up new ideas about the regulation of the hypothalamic-pituitary-interrenal axis in zebrafish (Danio rerio)*. Zebrafish, 2010. **7**(4): p. 349-58.

344. Kobayashi, M., et al., *Identification of the interactive interface and phylogenetic conservation of the Nrf2-Keap1 system*. Genes Cells, 2002. **7**(8): p. 807-20.
345. Van Tiem, L.A. and R.T. Di Giulio, *AHR2 knockdown prevents PAH-mediated cardiac toxicity and XRE- and ARE-associated gene induction in zebrafish (Danio rerio)*. Toxicol Appl Pharmacol, 2011. **254**(3): p. 280-7.
346. Lin, C.T., et al., *Characterization, molecular modelling and developmental expression of zebrafish manganese superoxide dismutase*. Fish Shellfish Immunol, 2009. **27**(2): p. 318-24.
347. Gerhard, G.S., E.J. Kauffman, and M.A. Grundy, *Molecular cloning and sequence analysis of the Danio rerio catalase gene*. Comp Biochem Physiol B Biochem Mol Biol, 2000. **127**(4): p. 447-57.
348. Ken, C.F., et al., *Cloning and expression of a cDNA coding for catalase from zebrafish (Danio rerio)*. J Agric Food Chem, 2000. **48**(6): p. 2092-6.
349. Ding, F., et al., *Oxidative stress and structure-activity relationship in the zebrafish (Danio rerio) under exposure to paclobutrazol*. J Environ Sci Health B, 2009. **44**(1): p. 44-50.
350. Jin, Y., et al., *Oxidative stress response and gene expression with atrazine exposure in adult female zebrafish (Danio rerio)*. Chemosphere, 2010. **78**(7): p. 846-52.
351. Walker, S.L., et al., *Automated reporter quantification in vivo: high-throughput screening method for reporter-based assays in zebrafish*. PLoS One, 2012. **7**(1): p. e29916.
352. Hermann, A.C., et al., *Development of a respiratory burst assay using zebrafish kidneys and embryos*. J Immunol Methods, 2004. **292**(1-2): p. 119-29.
353. Belousov, V.V., et al., *Genetically encoded fluorescent indicator for intracellular hydrogen peroxide*. Nat Methods, 2006. **3**(4): p. 281-6.
354. Meyer, A.J. and T.P. Dick, *Fluorescent protein-based redox probes*. Antioxid Redox Signal, 2010. **13**(5): p. 621-50.

355. Niethammer, P., et al., *A tissue-scale gradient of hydrogen peroxide mediates rapid wound detection in zebrafish*. *Nature*, 2009. **459**(7249): p. 996-9.

APPENDIX 1**cDNA Primer Sequences**

Name	Sequence (5' to 3')	Amplicon (bp)
AAAS1 for	GCCAGCAGCACCATAGTC	190 bp
AAAS1 rev	CAGGGTGAGACAGCACTTG	
AAAS2 for	GAGCCACTGATTTACTCCCTG	167 bp
AAAS2 rev	CCAGACCATGGAGTGAGC	
GAPDH for	GAAGGTGAAGGTCTGGAGTC	206 bp
GAPDH rev	GAAGATGGTGATGGGATTTTC	
StAR 1 for	GACATTCAAGCTGTGCGCTG	191 bp
StAR 1 rev	TGTAGAGAGTCTCTTCTAGCCGA	
TXNRD2 cDNA for	TTGAGGTCTATCACGCC	
TXNRD2 cDNA rev	CTTGAGTAACTTCGCCTGC	

APPENDIX 2

Genomic DNA Primer Sequences

Name	Sequence (5' to 3')
TXNRD2 EX1 for	AGTGTTCCACCCTAGGTCTGA
TXNRD2 EX1 rev	GGTATGTGGACACCCCC
TXNRD2 EX2 for	AATGGAGTGTCCAATCCTG
TXNRD2 EX2 rev	GCTCATGGACGTTTTCTG
TXNRD2 EX3 for	TCACAAGCCCTGAGGAG
TXNRD2 EX3 rev	CTGAAGGACTTTGGTGTCAG
TXNRD2 EX4 for	TGTCAGCTGGTCTGTGTTAG
TXNRD2 EX4 rev	GCTGAGAAACCCATCCTAC
TXNRD2 EX5 for	CCATTGAATCTAATAGTCCATC
TXNRD2 EX5 rev	CATGCTCTGCACAGTAAGTAAG

TXNRD2 EX6 for	TCCCTTTTACCAGTGTTC
TXNRD2 EX6 rev	TTACTAAGAACAGCACCCAG
TXNRD2 EX7 for	GGTCTGTGGTGCTCAGG
TXNRD2 EX7 rev	AAAGGGTGTGCAAGCTG
TXNRD2 EX8 for	GGAAAGCTCTGCTTGATTC
TXNRD2 EX8 rev	CACCAGCACAGGCTCTAAG
TXNRD2 EX9 for	TTGAACAGTAACCTTGAGC
TXNRD2 EX9 rev	AGTAAGTGCCGATCTGAGG
TXNRD2 EX10 for	GTCTTGAGTTGGGAGCC
TXNRD2 EX10 rev	CATCCAATTCAAGGGTTATC
TXNRD2 EX11 for	CTTCATTGAGGCCTTCG
TXNRD2 EX11 rev	GAGGTGACAGGAAGTGGG
TXNRD2 EX12 for	CGGTCTCTAAGTGGACATTC

TXNRD2 EX12 rev	CTCCTACAGGACGGCAG
TXNRD2 EX13&14 for	GAGGGCAAAGGGTGATG
TXNRD2 EX13&14 rev	CTGGAAAGGAGAGACCTTG
TXNRD2 EX15&16 for	GCAGCACTGATCCAGGGTT
TXNRD2 EX15&16 rev	CGCATCGCAGCCTGCATTCC
TXNRD2 EX17 for	CTGAGGCCCTCCTCTTC
TXNRD2 EX17 rev	GTAGCCTTGCTGTACACCTG

APPENDIX 3

AAAS shRNA sequences (Sigma- Aldrich)

Name	Sequence (5' to 3')	Product code
shRNA 22	CCGGCCAAGGGTACAGGATGGTAAACTCGAGTTTACCATCC TGTACCCTTGTTTTTG	TRCN0000118922
shRNA 23	CCGGCCGACTGCTGTTCACTGTATTCTCGAGAATACAGTGAA CAGCAGTCGGTTTTTG	TRCN0000118923
shRNA 24	CCGGGCGAAGATCTGATCGCTGAATCTCGAGATTCAGCGAT CAGATCTTCGCTTTTTG	TRCN0000118924
shRNA 25	CCGGTGCATCAACATTTGGCGTGATCTCGAGATCACGCCAAA TGTTGATGCATTTTTG	TRCN0000118925
shRNA 26	CCGGCGAAGATCTGATCGCTGAATTCTCGAGAATTCAGCGA TCAGATCTTCGTTTTTG	TRCN0000118926

A combination of shRNA 24 and 26 (TRCN0000118924, TRCN0000118926) was used in the study as it achieved best AAAS-knockdown in the H295R cells and SH-SY5Y cells.

TXNRD2 shRNA sequences (Openbiosystems)

Name	Sequence (5' to 3')	Product code
shRNA 171	ACATTGTCGTAGTCCATCA (Exon 13)	V3LHS_354171
shRNA 173	TACATAAACTGGGATGCA (Exon 15)	V3LHS_354173
shRNA 174	TTTTGAACAGCTTCTGCCA (Exon 5)	V3LHS_354174
shRNA 603	TTGCATTGCAGAAATGCC (Exon 18)	V2LHS_63603
shRNA 607	TTACATAAACTGGGATGC (Exon 15)	V2LHS_63607

shRNA 173 (V3LHS_354173) was used in the study as it achieved best *TXNRD2*-knockdown in the H295R cells.

APPENDIX 4

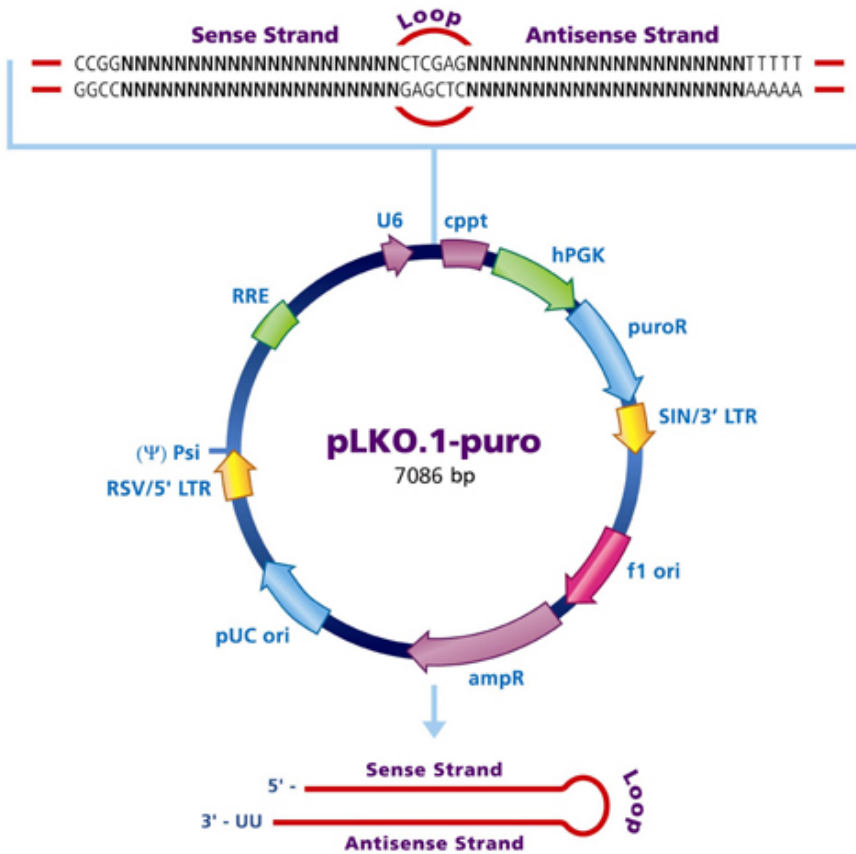
Vector Maps

Sigma pLKO.1 puro lentiviral shRNA vector used for AAAS-knockdown and scrambled control

Vector element	Utility
Cppt	Central polypurine tract
hPGK	Human phosphoglycerate kinase eukaryotic promoter
puroR	Puromycin resistance gene for mammalian selection
SIN/LTR	3' self-inactivating long terminal repeat
f1 ori	f1 origin of replication
ampR	Ampicillin resistance gene for bacterial selection
pUC ori	pUC origin of replication
5' LTR	5' long terminal repeat
Psi	RNA packaging signal
RRE	Rev response element

Sigma pLKO.1 puro lentiviral shRNA vector used for AAAS-knockdown and scrambled control

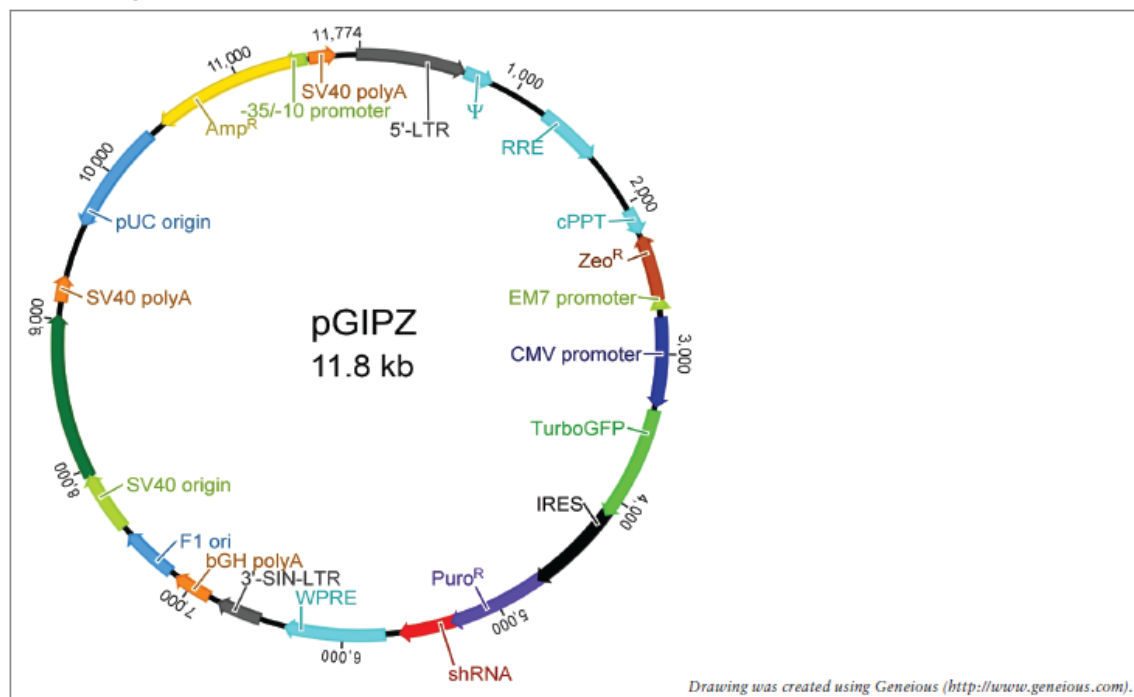
(cont)



Openbiosystems GIPZ Lentiviral shRNA vector used for *TXNRD2*-knockdown and scrambled control

Vector Element	Utility
hCMV	Human cytomegalovirus promoter drives strong transgene expression
tGFP	TurboGFP reporter for visual tracking of transduction and expression
Puro ^R	Puromycin resistance permits antibiotic-selective pressure and propagation of stable integrants
IRES	Internal ribosomal entry site allows expression of TurboGFP and puromycin resistance genes in a single transcript
shRNA	microRNA-adapted shRNA (based on miR-30) for gene knockdown
5' LTR	5' long terminal repeat
3' SIN LTR	3' self-inactivating long terminal repeat for increased lentivirus safety
Ψ	Psi packaging sequence allows viral genome packaging using lentiviral packaging systems
RRE	Rev response element enhances titer by increasing packaging efficiency of full-length viral genomes
WPRE	Woodchuck hepatitis posttranscriptional regulatory element enhances transgene expression in the target cells

Vector Map



APPENDIX 5

Details of antibodies used in western blotting

Name of antibody	Peptide/ Protein Target	Manufacturer, catalogue #	Species raised in; monoclonal or polyclonal	Dilution used
Anti-Adracalin antibody	Recombinant fragment, corresponding to amino acids 1-101 of Human Adracalin	Abcam, #ab56384	Mouse; monoclonal	1 in 500
Anti-GAPDH antibody	Rabbit muscle GAPDH	Abcam, #ab8245	Mouse; monoclonal	1 in 5000
Anti-GAPDH antibody	Full length native protein from human erythrocytes	Abcam, #ab9485	Rabbit; polyclonal	1 in 5000
Anti- STAR antibody	Recombinant fragment, corresponding to amino acids 81-180 of Human StAR	Abcam, #ab58013	Mouse; monoclonal	1 in 1000
PARP antibody	Synthetic peptide corresponding to the caspase	Cell Signalling, #9542	Rabbit; polyclonal	1 in 1000

	cleavage site in PARP			
Polyclonal Anti-CYP11B1	CYP11B1 full length human protein	Sigma, #SAB1401106	Rabbit; polyclonal	1 in 200
Anti-CYP11A1	Cytochrome P450 11A1, mitochondrial precursor recombinant protein epitope signature tag (PrEST)	Sigma, #HPA016436	Rabbit; polyclonal	1 in 500
Anti-TXNRD2 antibody	Immunogen incorporating amino acid sequence 203 to 353 of TXNRD2	Sigma, #HPA003323	Rabbit; polyclonal	1:500
Anti-TXNRD1 antibody	Human recombinant full length protein	Abcam, #ab16840	Rabbit; polyclonal	1:500
Anti-Peroxiredoxin III antibody	Human peptide	Proteintech, #55087-1-AP	Rabbit polyclonal	1:400

APPENDIX 6

Details of the candidate variants remaining following the penultimate filtration step applied to my WES data; i.e homozygous variants common to all 3 individuals, with a MAF <0.01 in dbSNP

#chrom	left	right	ref Seq	var Seq	Gene Name	Where In Gene	Most Disruptive Change
chr1	247978545	247978546	a	-	OR14A16	CDS	UNKNOWN
chr1	247978546	247978547	g	-	OR14A16	CDS	UNKNOWN
chr1	248801607	248801607		ca	OR2T35	CDS	FRAMESHIFT
chr1	248801951	248801952	g	-	OR2T35	CDS	UNKNOWN
chr1	248801952	248801953	c	-	OR2T35	CDS	UNKNOWN
chr1	248801953	248801954	a	-	OR2T35	CDS	UNKNOWN
chr1	248801954	248801955	g	-	OR2T35	CDS	UNKNOWN
chr1	248801955	248801956	c	-	OR2T35	CDS	UNKNOWN
chr1	248801956	248801957	a	-	OR2T35	CDS	UNKNOWN
chr2	95847048	95847049	c	-	ZNF2	CDS	UNKNOWN
chr2	95847049	95847050	g	-	ZNF2	CDS	UNKNOWN
chr3	195512107	195512108	t	a	MUC4	CDS	NONSYNONYMOUS
chr3	195512186	195512187	t	c	MUC4	CDS	NONSYNONYMOUS
chr4	155244426	155244427	t	-	DCHS2	CDS	UNKNOWN
chr4	155244427	155244428	t	-	DCHS2	CDS	UNKNOWN
chr4	155244428	155244429	t	-	DCHS2	CDS	UNKNOWN
chr4	177605088	177605089	t	-	VEGFC	CDS	UNKNOWN

Where #Chrom (Chromosome), left (refers to position on the left of the variant), right (refers to position on the right of the variant), ref Seq (the base in the reference sequence), var Seq (the variant base seen in our 3 individuals in homozygosity), CDS (coding sequence). The final column indicates the anticipated disruptive change.

Details of the candidate variants remaining following the penultimate filtration step applied to my WES data (cont)

chr6	32632637	32632639	tc	ga	HLA-DQB1	CDS	NONSYNONYMOUS
chr9	97080949	97080950	g	-	FAM22F	CDS	UNKNOWN
chr9	138836947	138836948	t	-	UBAC1	CDS	UNKNOWN
chr9	138836948	138836949	c	-	UBAC1	CDS	UNKNOWN
chr11	48285987	48285988	t	-	OR4X1	CDS	UNKNOWN
chr15	93198687	93198688	g	-	FAM174B	CDS	UNKNOWN
chr15	93198688	93198689	a	-	FAM174B	CDS	UNKNOWN
chr15	93198689	93198690	g	-	FAM174B	CDS	UNKNOWN
chr15	93198690	93198691	c	-	FAM174B	CDS	UNKNOWN
chr15	93198691	93198692	t	-	FAM174B	CDS	UNKNOWN
chr15	93198692	93198693	g	-	FAM174B	CDS	UNKNOWN
chr17	44144993	44144994	c	g	KIAA1267	CDS	NONSYNONYMOUS
chr17	79614938	79614939	a	-	TSPAN10	CDS	UNKNOWN
chr17	79614939	79614940	a	-	TSPAN10	CDS	UNKNOWN
chr17	79614940	79614941	c	-	TSPAN10	CDS	UNKNOWN
chr17	79614941	79614942	t	-	TSPAN10	CDS	UNKNOWN
chr22	19865895	19865896	a	c	TXNRD2	CDS	STOPGAIN
chrX	8138170	8138172	ct	gc	VCX2	CDS	NONSYNONYMOUS

Appendix 7

Details of candidate variants following the final filtration step applied to WES data

Variants in the 3 affected members of the kindred, filtering for non-synonymous coding variants, splice variants and indels only; variants with a MAF

>0.01 in GO-ESP were also excluded.

chrom	left	right	ref_seq	var_type	zygosity	var_seq1	var_seq2	coverage	gene_name	transcript_name	where_in_transcript	change type
chr1	248801607	248801607		INS	Hom	ca	ca	19	OR2T35	NM_001001827	CDS	Frameshift
chr22	19865895	19865896	a	SNP	Hom	c	c	28	TXNRD2	NM_006440	CDS	Stop Gain
chr3	195512107	195512108	t	SNP	Hom	a	a	335	MUC4	NM_018406	CDS	Non-Synonymous
chr3	195512186	195512187	t	SNP	Hom	c	c	265	MUC4	NM_018406	CDS	Non-Synonymous

Where Chrom (Chromosome), left (refers to position on the left of the variant), right (refers to position on the right of the variant), ref Seq (the base in the reference sequence), Var type (type of variation), INS (insertion), SNP (single nucleotide polymorphism), Hom (variant seen in homozygosity), var Seq 1 (the variant base in allele 1), var Seq 2 (the variant base in allele 2), coverage (refers to the read coverage in the WES data), CDS (coding sequence). The final column refers to the anticipated disruptive change.

APPENDIX 8

GENERAL BUFFERS AND SOLUTIONS

The following buffers/ solutions were prepared for general laboratory use:

Buffer/ Solution	Formulation
BS ³ conjugation buffer	For 5mM solution 2mg Bis(sulfosuccinimidyl)suberate (BS3)(#21580, Thermo Fisher Scientific) was dissolved in 700 µl dH ₂ O
dNTPs	Sequencing grade dNTPs [100mM] (Promega) were combined in a 1:1:1:1 ratio (dATP:dCTP:dGTP:dTTP) in dH ₂ O to produce a 10mM stock solution dNTP mix which was stored at -20C
LB Agar	10g Agar (#A1296, Sigma), 10g LB Broth (# L3022, Sigma) in 500ml dH ₂ O
LB Broth	10g LB Broth in 500ml dH ₂ O
MOPS running buffer [1x]	50 ml MOPS SDS Running buffer [20x] (#NP0001-02, Invitrogen) in 1L dH ₂ O
PBS	5 tab Phosphate Buffer Saline (#P4417, Sigma) in 1L dH ₂ O
PBS Tween	5 tab Phosphate Buffer Saline (#P4417, Sigma) in 1L dH ₂ O, 0.01% Tween (Sigma)
Transfer buffer [1x]	2.42g Tris, 9g glycine, 800 ml dH ₂ O, 200ml methanol
3M Sodium Acetate	Dissolve 40.8g sodium acetate in 80 ml H ₂ O. Adjust pH to 5.2 with glacial acetic acid; make final volume up to 100ml and autoclave

APPENDIX 9

COMMERCIAL ASSAYS USED AND COMPOSITION of REAGENTS

CellTiter96 Aqueous non-radioactive cell proliferation assay (MTS (3-(4,5-dimethylthiazol-2-yl)-5-(3-carboxymethoxyphenyl)-2-(4-sulfophenyl)-2H-tetrazolium) assay) (Promega, Southampton, UK):

DPBS (MTS reagent): 0.2 g KCl; 8.0 g NaCl; 0.2 g KH₂PO₄; 1.15 g Na₂HPO₄; 100 mg MgCl₂*6H₂O; 133 mg CaCl₂*2H₂O (room temperature dH₂O is added to KCl, NaCl, KH₂PO₄ and Na₂HPO₄ to a 1L final volume. pH is adjusted to 7.5 by addition of 1N HCl; MgCl₂*6H₂O and CaCl₂*2H₂O are then added)

Phenazine methosulfate (PMS): 0.92 mg/ml PMS in DPBS

illustra Nucleon Genomic DNA Extraction Kit (GE Healthcare, Buckinghamshire, UK):

Reagent A (lysis agent): 10 mM Tris-HCl; 320 M sucrose; 5 mM MgCl₂; 1%(v/v) Triton X-100; pH 8.0 (pH adjusted using 40%(w/v) NaOH)

Reagent B: *(precise composition is not disclosed by the company)*

5 M Sodium percholate

Nucleon resin: includes potassium hydroxide *(precise composition is not disclosed by the company)*

GSH/GSSG-Glo assay (Promega, Southampton, UK):

GSH-Glo Reagent: Luciferin-NT substrate (100 µl) and Glutathione S-Transferase Solution (100 µl) diluted 1:100 in 10 ml GSH-Glo Reaction Buffer (50mM Tricine (pH 7.9)) (sufficient for a complete 96 well plate)

Luciferin Detection Reagent: Reconstitution Buffer with esterase added to lyophilized Luciferin Detection Reagent

Glutathione 5mM: for standard curve (serial dilutions in water to generate standards ranging from 0 μ M to 5 μ M)

PAXgene Blood RNA kit (Qiagen, Crawley, UK):

Buffer BR1 (Resuspension Buffer): *(precise composition is not disclosed by the company)*

Buffer BR2 (Binding Buffer): contains a guanidine salt *(precise composition is not disclosed by the company)*

Buffer BR3 (Wash Buffer): contains a guanidine salt, as well as ethanol *(precise composition is not disclosed by the company)*

Buffer BR4 (Wash Buffer): ethanol containing *(precise composition is not disclosed by the company)*

Buffer BR5 (Elution Buffer): *(precise composition is not disclosed by the company)*

RNase-Free Water

Proteinase K

DNase I, RNase-Free (lyophilized)

Buffer RDD: allows digestion of DNA also ensures RNA remains bound to the column. *(precise composition is not disclosed by the company)*

Other components of the kit: PAXgene Blood RNA Tube (contains propriety reagent, composition of which protects RNA molecules from degradation by RNases); PAXgene RNA Spin Columns; Processing Tubes (2 ml); Microcentrifuge Tubes (1.5 ml); PAXgene Shredder Spin Columns

Qiagen HI SPEED Plasmid Midi Kit (Qiagen, Crawley, UK):

Buffer P1 (resuspension buffer): 50 mM Tris·Cl; 10 mM EDTA; 100 μ g/ml RNase A

Buffer P2 (lysis buffer): 200 mM NaOH; 1% SDS (w/v)

Buffer P3 (neutralisation buffer): 3.0 M potassium acetate, pH 5.5

Buffer QBT (equilibration buffer): 750 mM NaCl; 50 mM MOPS, pH 7.0; 15% isopropanol (v/v); 0.15% Triton® X-100 (v/v)

Buffer QC (wash buffer): 1.0 M NaCl; 50 mM MOPS, pH 7.0; 15% isopropanol (v/v)

Buffer QF (elution buffer): 1.25 M NaCl; 50 mM Tris·Cl, pH 8.5; 15% isopropanol (v/v)

Other components of the kit: QIAfilter Cartridge; QIAGEN-tip

Qiagen RNeasy mini kit (Qiagen, Crawley, UK):

Buffer RLT (lysis buffer): contains a guanidine salt (*precise composition is not disclosed by the company*)

Buffer RW1 (stringent wash buffer): contains a guanidine salt, as well as ethanol (*precise composition is not disclosed by the company*)

Buffer RPE (mild wash buffer): Ethanol containing (*precise composition is not disclosed by the company*)

Other components of the kit: RNeasy mini spin columns (with silica membrane for RNA binding); Collection tubes (1.5; 2 ml); RNase-free water

Qiagen QIAquick Gel extraction kit (Qiagen, Crawley, UK):

Buffer QG (solubilization and binding buffer, with pH indicator): 5.5 M guanidine thiocyanate, 20 M Tris HCl pH 6.6

Buffer PE (wash buffer): 10 mM Tris-HCl pH 7.5; 80% ethanol

Other components of the kit: QIAquick spin column; Collection tube (2 ml)

Thioredoxin reductase (TXNRD) assay kit (Abcam, Cambridge, UK):

TrxR Assay Buffer: 500 mM potassium phosphate, pH 7.0, containing 500 mM potassium chloride, 10 mM EDTA, and 2 mg/ml BSA (10x prep)

DTNB (lyophilized): 5,5'-dithiobis (2-nitrobenzoic) acid dissolved into 0.9 ml Assay Buffer (sufficient for 100 assays)

NADPH (lyophilized): dissolved with 0.22 ml dH₂O (sufficient for 100 assays)

TNB Standard (2.5 μM; lyophilized): dissolve in 0.5 ml Assay buffer generating 5 mM TNB standard

TrxR Positive control (~ 20 mU; lyophilized): dilute 10 μl TrxR with 90 μl Assay Buffer

TrxR Inhibitor (lyophilized): dissolve into 1.2 ml Assay Buffer (sufficient for 100 assays)

APPENDIX 10

PRESENTATIONS

Oral Communications:

- **Prasad R.**, Chan L.F., Hughes C.R., Kaski J.P., Kowalczyk J., Savage M.O., Peters C.J., Nathwani N., Clark A.J., Storr H.L., Metherell L.A. A mutation in thioredoxin reductase 2 (*TXNRD2*) is associated with familial glucocorticoid deficiency.

ESPE, Milan, *Sep 2013*
- **Prasad R.**, Hughes C.R., Chan L.F., Peters C.J., Nathwani N., Clark A.J., Storr H.L., Metherell L.A. Thioredoxin reductase 2 mutation associated with familial glucocorticoid deficiency.

William Harvey Research Institute, *June 2013; shortlisted for Young Investigator of The Year*
- **Prasad R.**, Hughes C.R., Chan L.F., Peters C.J., Nathwani N., Clark A.J., Storr H.L., Metherell L.A. Thioredoxin reductase 2 mutation associated with familial glucocorticoid deficiency.

ENDO, San Francisco, *June 2013*
- **Prasad R.**, Hughes C.R., Chan L.F., Peters C.J., Nathwani N., Clark A.J., Storr H.L., Metherell L.A. A mutation in thioredoxin reductase 2 (*TXNRD2*) is associated familial glucocorticoid deficiency.

ESPE adrenal development seminar, *Bern, May 2013*
- **Prasad R.**, Hughes C.R., Chan L.F., Peters C.J., Nathwani N., Clark A.J., Storr H.L., Metherell L.A. A mutation in thioredoxin reductase 2 (*TXNRD2*) is associated with a predominantly adrenal phenotype in humans.

British Endocrine Society Meeting, *Harrogate, March 2013*
- **Prasad R.**, Clark A.J.L., Storr H.L. Deficiency of ALADIN, the AAAS gene product, renders human adrenal and neuronal cells susceptible to oxidative stress.

William Harvey Research Institute Annual Research Review, *London, Jul 2012*
- **Prasad R.**, Clark A.J.L., Storr H.L. Deficiency of ALADIN, the AAAS gene product, renders human adrenal and neuronal cells susceptible to oxidative stress.

European Society of Paediatric Endocrinology, *Leipzig, Sep 2012*

- **Prasad R.,** Clark A.J.L., Storr H.L. Deficiency of ALADIN, the triple A syndrome gene product, renders human adrenal cells susceptible to oxidative stress with subsequent impact on steroidogenesis

British Society for Paediatric Endocrinology and Diabetes Annual Meeting, *Leeds, Nov 2012*

Poster Presentations:

- **Prasad R.,** Clark A.J.L., Storr H.L. Oxidative stress in the pathogenesis of Triple A Syndrome.
39th Meeting of the British Society for Paediatric Endocrinology and Diabetes, *London, Nov 2011*
- **Prasad R.,** Clark A.J.L., Storr H.L. Oxidative stress in the pathogenesis of Triple A Syndrome.
British Endocrine Society Meeting, *Harrogate, March 2012*
- **Prasad R.,** Clark A.J.L., Storr H.L. Oxidative stress and the regulation of ALADIN and its interacting protein partner, Ferritin Heavy Chain
Endocrine Society Meeting, *Houston, Jun 2012*
- **Prasad R.,** Clark A.J.L., Storr H.L. Deficiency of ALADIN, the AAAS gene product, renders human adrenal and neuronal cells susceptible to oxidative stress.
Society for Free Radical Research International, *London, Sep 2012*

